

Studies Towards the Synthesis of Graphene Fragments

Mamdouh Basheer Alshammari

This thesis is submitted in fulfilment of the requirements of the degree of Doctor of Philosophy at the University of East Anglia

2026

©This copy of the thesis has been supplied on the condition that anyone who consults it, is understood to recognize that its copyright rests with the author and that no quotation from the thesis, nor any information derived therefrom, may be published without the author's prior written consent.

Declaration

The research described in this thesis is, to the best of my knowledge, original and my own work except where due reference is made.

Mamdouh Alshammari

2026

Abstract

This thesis presents a bottom-up synthetic strategy for constructing extended graphene fragments starting from readily available naphthalene derivatives. The core approach employs iterative cascade annulation processes to systematically elongate π-conjugation and construct larger fused aromatic frameworks.

Key obstacles involved activation of the ortho and para positions of 1-naphthol and intramolecular cyclization. These were addressed and alkyne precursors were synthesized for cyclization handles.

Screening of cyclization conditions for the intermediate alkynes revealed competition between two regiochemical pathways: 6-endo-dig mode delivering spirocyclic products in excellent yield, and a 7-endo-dig pathway leading to seven-membered rings. Although the spiro isomer gave an excellent yield, an effective isomerization protocol successfully converted the spiro compound into the seven-membered ring system featuring an alcohol group.

Despite these advances, complete cyclization to the target graphene fragment proved elusive, primarily due to persistent regioselectivity challenges and competing cyclization modes. Nevertheless, the high-yielding spirocyclization and effective isomerization sequences provide valuable synthetic tools and mechanistic understanding for regioselective π-extension, paving the way for future elaboration into soluble, larger graphene nanoribbon analogs.

Access Condition and Agreement

Each deposit in UEA Digital Repository is protected by copyright and other intellectual property rights, and duplication or sale of all or part of any of the Data Collections is not permitted, except that material may be duplicated by you for your research use or for educational purposes in electronic or print form. You must obtain permission from the copyright holder, usually the author, for any other use. Exceptions only apply where a deposit may be explicitly provided under a stated license, such as a Creative Commons license or Open Government license.

Electronic or print copies may not be offered, whether for sale or otherwise to anyone, unless explicitly stated under a Creative Commons or Open Government license. Unauthorized reproduction, editing or reformatting for resale purposes is explicitly prohibited (except where approved by the copyright holder themselves) and UEA reserves the right to take immediate ‘take down’ action on behalf of the copyright and/or rights holder if this Access condition of the UEA Digital Repository is breached. Any material in this database has been supplied on the understanding that it is copyright material and that no quotation from the material may be published without proper acknowledgement.

This work is dedicated to my parents

Acknowledgements

I would like to express my sincere gratitude to my supervisor, Professor Andrew Cammidge, for his continuous guidance, encouragement, and unwavering support throughout my PhD. His valuable advice and the freedom he gave me to explore my research ideas. I am truly thankful for everything I have learned from him.

I am also deeply grateful to Dr. Isabelle Fernandes for her constant support and willingness to engage in discussions whenever needed. Her insightful feedback greatly enhanced my work. I would like to thank Dr. David Hughes for his valuable assistance with the X-ray crystallography service.

My deepest appreciation goes to my parents, sisters, and brothers, thank you for your endless love and belief in me. This thesis would not have been possible without their constant support and encouragement.

I would also like to thank all my colleagues in Lab 3.08, past and present, for their friendship and support. Special thanks to my friends in Labs 3.17 and 3.10 for the wonderful memories we shared. I am grateful to the entire School of Chemistry for providing such a supportive environment.

Finally, I extend my sincere thanks to Hail University for this outstanding opportunity to study in the United Kingdom, and to the Saudi Arabian Cultural Bureau in London for their generous support throughout my studies.

Abbreviations

APEX	Annulative π-extension
aq.	Aqueous
Ar	aromatic/ aryl
BINAP	2,2'-bis(diphenylphosphino)-1,1'-binaphthyl
d	doublet
dd	doublet of doublets
DBU	1,8-Diazabicyclo[5.4.0]undec-7-ene
DMF	N,N-Dimethylformamide
DCM	Dichloromethane
DDQ	2,3-dichloro-5,6-dicyano-1,4-benzoquinone
DMF	Dimethylformamide
DME	Dimethoxyethane
E	Energy gap
eV	Electronvolt
Eq.	Equivalent
GO	Graphite oxide
GNRs	Graphene Nanoribbons
HOMO	Highest occupied molecular orbital
HPLC	High-Performance Liquid Chromatography
IR	Infrared
J	Coupling constant in NMR spectroscopy
LUMO	Lowest unoccupied molecular orbital
m	Multiplet
MALDI	Matrix assisted laser desorption ionisation
M	Molarity
m.p.	Melting point
MS	mass spectrometry
MW	Microwave
NBS	*N*-Bromosuccinimide
NGs	Nanographenes
NMR	Nuclear magnetic resonance
Pet.ether	Petroleum ether

PAHs	polycyclic aromatic hydrocarbons
PTLC	Preparative thin-layer chromatography
ppm	parts per million
rt	room temperature
TFA	Trifluoroacetic acid
TLC	Thin-layer chromatography
PTLC	Preparative thin-layer chromatography
s	singlet
t	Triplet
Temp.	Temperature
THF	Tetrahydrofuran
UV	Ultraviolet
Vis	Visible spectroscopy
λ	Lambda (wavelength)
δ	chemical shift in parts per million (ppm)

Table of Contents

Abbreviations vi
List of Schemes xii
List of Figures xiv
List of Tables xvi
1. Introduction 1
1.1 Polycyclic Aromatic Hydrocarbons (PAHs) 2
1.1.1 Classification of Nanographene 4
1.1.2 The structure's edge of PAHs 5
1.1.3 Stability of PAHs 6
1.2 Synthetic strategy of nanographene 8
1.2.1 C-H activation in cross-coupling 9
1.2.2 Directing Group-Assisted C-H Arylation of Functionalized Arenes 11
1.2.3 π-Extension of PAHs via Intramolecular C–H Arylation 13
1.2.3.1 Palladium migration in Intramolecular C-H activation 14
1.2.4 C–H arylation of non-functionalized PAHs 15
1.2.4.1 Annulative π-extension of PAHs at the bay region 16
1.2.4.2 Annulative π-extension (APEX) at K- and L- regions of PAHs. 18
1.2.2 π-extension of PAHs via Scholl reaction(Intramolecularly) 19
1.2.2.1 π-extension of Coronene 22
1.2.2.2 π-extension of Perylene 23
1.2.2.3 π-extension of Chrysene 24
1.2.2.4 π-extension of Corannulene 25
1.2.2.5 π-extension of naphthalene 26
1.3 Application of Nanographene 27
2. Results and Discussion 29
2.1. Aim 30
2.2 Preparation of 8-(*p*-methoxyphenyl)-1-naphthol. [80] 32
2.3 Synthesis and reactivity investigation of 8-(*p*-methoxyphenyl)-1-naphthol 35
2.3.1 Triflation of 8-(*p*-Methoxyphenyl)-1-naphthol 35
2.3.1.1 Reactivity investigation of **2.7** 36
2.3.2 Reactivity test of **2.7** toward bromination 42
2.4 Synthesis of **2.9** by using Sonogashira coupling reaction 44
2.4.1 The intramolecular cyclization in Sonogashira coupling 44
2.4.2 Overcome intramolecular cyclization 46

2.4.3 Synthesis of TMS acetylene derivatives 46
2.4.4 Deprotection of TMS acetylene derivatives 47
2.4.5 Sonogashira coupling between terminal alkyne and aryl iodide derivatives 50
2.5 Cyclization investigation of alkyne 52
2.5.1 Attempts for cyclization of **2.9** 53
2.5.2 Cyclization reaction by TFA 54
2.5.2.1 Investigation of benzanthrone **2.40** formation 57
2.5.2.2 Reactivity of compound **2.38** toward Scholl reaction 60
2.5.3 Cyclization reaction by ICl 63
2.5.3.1 Testing the methoxy effectiveness on the cyclization outcome 65
2.5.3.2 The isomerization of the spiro compound 66
2.5.4 Optical Properties of Seven-, Six-membered rings, and Spiro compounds. 68
2.6 The second model of extension of PAHs 70
2.6.1 The X-ray structure of **2.34** 70
2.6.2 Sonogashira coupling of **2.28** 71
2.6.3 Demethylation of **2.28** 71
2.7 Conclusion 75
2.8 Future work 77
3. Experimental 78
General Methods 79
3.1 C-H arylation of 1-naphtol derivatives 80
3.1.1 Synthesis of 8-(p-Methoxyphenyl)-1-naphthol **2.7** [80] 80
3.1.2 Synthesis of 8-[p-(tert-Butyl)phenyl]-1-naphthol **2.13** 81
3.2 Triflation of arylated 1-naphthols 82
3.2.1 Method A by using Pyridine 82
3.2.2 Method B by using 2,4-lutidine 82
3.2.3 Method C by using 2,4,6-collidine 82
3.2.4 Synthesis of triflate **2.8** 83
3.2.5 Side products resulting from using method A 84
3.2.6 Synthesis of triflate **2.17** 88
3.3 Bromination of 8-(*p*-Methoxyphenyl)-1-naphthol **2.7** 89
3.3.1 Synthesis of 4-bromo-8-(p-methoxyphenyl)-1-naphthol **2.21** 89

3.3.2 Synthesis of 2-bromo-8-(3-bromo-4-methoxyphenyl)-1,4-naphthalenedione **2.22** 90
3.4 Synthesis of TMS acetylene derivatives 91
3.4.1 Synthesis of **2.27** 91
3.4.2 Synthesis of **2.29** 92
3.4 Deprotection of TMS acetylene derivatives 93
3.4.1 Synthesis of 8-(p-Methoxyphenyl)-1-naphthyl ethyne **2.28** 93
3.4.2 Synthesis of 8-[p-(tert-Butyl) phenyl]-1-naphthyl ethyne **2.30** 94
3.5 Synthesis of Sonogashira coupled products from **2.28** 95
3.5.1 Synthesis of **2.9** 95
3.5.2 Synthesis of 8-Methoxyfluoranthene **2.25** 97
3.5.3 Synthesis of 2-[8-(p-Methoxyphenyl)-1-naphthyl]-1-[p-(tert-butyl) phenyl] ethyne **2.31** 98
3.5.4 Synthesis of Homocouplied **2.34** 99
3.6 Acid Cyclization products of **2.9** 100
3.6.1 Route A by utilizing TFA 100
3.6.2 Route B by utilizing $HNTf_2$ 100
3.6.1 Synthesis of cyclized products from **2.9** 101
3.6.1.1 Synthesis of Seven-membered ring **2.38** 102
3.6.1.2 Synthesis of Spiro compound **2.39** 103
3.6.1.3 Synthesis of 9-(methoxy)-7H-benzo[de]anthracen-7-one **2.40**. [87]. 104
3.7 Scholl reaction products of **2.9** 105
3.7.1 Synthesis of 10-methoxy-7H-benzo[de]anthracen-7-one **2.41**.[87] 105
3.7.2 Synthesis of 10-Methoxy-7H-benzo[de]anthracen-7-one **2.42** 106
3.8 ICl cyclization products of **2.9** 107
3.8.1 Synthesis of spiro compound **2.49** 107
3.8.2 Synthesis of compound **2.51** 108
3.8.3 Synthesis of spiro compound **2.50** 109
3.8.4 Synthesis of spiro-seven membered compound **2.53** 110
3.9 Isomerization of spiro compound **2.49** into seven-membered ring by acid and alcohol. 111
3.9.1 Synthesis of compound **2.56** 111
3.9.2 Synthesis of compound **2.57** 112
3.9.3 Synthesis of compound **2.58** 113

3.10 Synthesis of compound **2.61** 114
References 115
5.0. Appendix 120
2.8 121
2.9 124
2.34 127
2.18 131
2.41 134
2.44 138
2.49 141
2.16 144
2.20 147
2.21 150
2.22 153
2.51 156
2.31 159
2.61 162

List of Schemes

Scheme 1: Proposed application of the Diels-Alder reaction to chemical synthesis of uniform single-walled nanotubes (SWNTs).[15] 6
Scheme 2: The Clar structures of tribenzo[fg, ij,rst]pentaphene (**1.16**), benzo[qr]naphto[2,1,8,7-fghi]pentacene (**1.17**), and Diels-Alder adduct[24] 8
Scheme 3: Formation of the aryl palladium intermediate and biaryl.[33] 10
Scheme 4: Modern methods for the formation of biaryl compounds..... 10
Scheme 5: The first cyclometallated compound by Kleimann, Dubeck.[36] 11
Scheme 6: The base role in synthesis of pyrene rhodium complex. Rh catalyst = $[RhCl_2(Cp^*)]_2$.[42] 12
Scheme 7: Conditions A) Iodobenzene (1.2 equiv), $Pd(OAc)_2$, Cs_2CO_3 (1.2 equiv), molecular sieves, **1.24** (76%). B) Iodobenzene (4.0 equiv), $PdCl_2$, Cs_2CO_3 (4 equiv), **1.24** (62%), **1.25** (25%).[43] 13
Scheme 8: Intramolecular C–H Activation Reactions. 13
Scheme 9: The formation of benzofluoranthene.[44] 14
Scheme 10:1,4 and 1,5 Pd migration products, Pd cat = $Pd_2(dba)_3$.[48] 15
Scheme 11: π-Extension of the perylene and bisanthene at bay region via the Diels-Alder method.[49,50] 16
Scheme 12: π-extension via bay region of perylene (**1.33)** and 4,11-dimesitybisanthene (**1.37)**. 17
Scheme 13: The C-H arylation with arylboroxine at K-region of phenanthrene and pyrene, and at L- region of fluoranthene.[52,53] 18
Scheme 14: π-extension at K and L region by diiodobiaryls.[54] 19
Scheme 15: General example of Scholl reaction, where an oxidant and an acid (Lewis or Brønsted) results in the formation of an aryl-aryl bond. 19
Scheme 16**:** Mechanisms for the Scholl Reaction of o-Terphenyl Arenium Cation (proton transfer) (A) and Radical Cation (electron transfer) (B). 20
Scheme 17: The rearrangement of substituent by Scholl condition.[58–60] 21
Scheme 18: Products formed under Scholl conditions.[61] 21
Scheme 19:Formation of **1.62** via Scholl reaction of **1.61** formed by [4+2] cycloaddition. 22
Scheme 20: Synthesis of Novel extended perylene by Scholl and Diels-Alder reaction.[64] 23

Scheme 21 : Synthesis of dibenzo chrysene derivative.[14] 24
Scheme 22: Synthesis of distorted nanographene by extending corannulene.[65] 25
Scheme 23: Synthetic pathway towards nanographene.[67] 26
Scheme 24: The synthetic route to staggered fused anthracene units investigated by our group. 30
Scheme 25: Extension of the pi-system in a model staggere unit. 31
Scheme 26: Proposed synthesis of the extended aromatic system. 31
Scheme 27: Synthesis of 8-(p-methoxyphenyl)-1-naphthol. 32
Scheme 28: Possible reaction mechanisms for cross-coupling aryl iodides with 1-naphthol affording arylated product in 8 position. 34
Scheme 29 The chemical equation for the triflation of **2.7**. 35
Scheme 30: The activation of the 4-position of pyridine. 36
Scheme 31: The effect of the bases on triflate **2.15**. 38
Scheme 32: The mechanism of formation of **2.16**. 39
Scheme 33: The proposed formation of **2.20** 40
Scheme 34 Formation of coupling product. 44
Scheme 35: An alternative route for synthesizing **2.9**. 46
Scheme 36: The deprotection of TMS of **2.27** and **2.29** by K_2CO_3 in MeOH. 48
Scheme 37: The proposed formation of the cyclized products. 52
Scheme 38: Pd-Catalyzed hydroarylation of o-alkynyl biaryls. 53
Scheme 39: $InCl_3$ cyclization reaction. 53
Scheme 40: Synthesis of pyrene from four-fold alkyne benzannulation via TFA.[86] .. 54
Scheme 41: The cyclization outcome of the **2.9** reaction by TFA. 54
Scheme 42: Possible pathway for the oxidative fragmentation of the seven membered ring. 57
Scheme 43: The possible pathway for the formation of **2.40**. 58
Scheme 44: The proposed mechanisms for the formation of **2.40**. 59
Scheme 45: Cyclization of alkynes by ICl. 63
Scheme 46: The ICl cyclization of alkyne outcome of **2.9** and **2.31** 63
Scheme 47: The cyclization of **2.34** by ICl. 65
Scheme 48: The isomerization of spiro compound. 66
Scheme 49:The outline route for the extension of **2.34**. 70
Scheme 50: An alternative route to the target di-alkynes. 77

List of Figures

Figure 1: Examples of PAHs compounds to the final series graphene.[3] 2
Figure 2: A representation of the chemical structure of graphene layers, fullerenes (0D), nanotube (1D), graphite (3D).[7] 3
Figure 3: The graphene terminology according to their lateral size (represented with permission) 4
Figure 4: The periphery of PAHs.[12] 5
Figure 5: The cove and fjord region in chrysene and perylene.[14] 5
Figure 6: The Clar structure for Phenanthrene (**1.3**. **1.4**), Pyrene (**1.5**), Triphenylene (**1.6**). 6
Figure 7: The Clar sextet structure for Chrysene and Tetracene. 7
Figure 8: Clar structure of naphthalene and anthracene resonance.[20–23] 7
Figure 9: The graphene presentation which contains nanographene molecules. 9
Figure 10: The directing group in C-H activation of arene, DG= directing group, FG= Functional group 11
Figure 11: The regioselectivity cleavage of C-H bonds by using directing groups, examples with observed C-H cleavage positions.[31,32] 12
Figure 12: Catalytic cycle for the formation of fluoranthene, highlighting the stages where 1,4- or 1,5-Pd migration may occur.[44–47] 14
Figure 13: Examples of activated C-H bond on edge of PAHs. 15
Figure 14: Calculated activation energies for Diels-Alder cycloadditions of acetylene to the bay regions of PAHs.[15] 17
Figure 15: Coronene and hexa-peri-hexabenzocoronene (HBC). 22
Figure 16: Columnar self-assembly of disc-shaped nanographene molecules. 27
Figure 17; The ^{1}H-NMR spectra for **2.7** and **2.13**. 33
Figure 18: Products **2.7** and **2.8** after triflation in Acetone-D. 35
Figure 19: The ^{1}H NMR spectra of **2.8** and **2.15**, **2.16.** 37
Figure 20: The COSY spectrum of **2.15** 38
Figure 21: The x-ray structure of **2.16** and **2.18**. 39
Figure 22: The x-ray structure and HRMS for **2.20**. 40
Figure 23: UV-vis absorption and emission spectra of triflated products **2.8**, **2.15**, **2.16**, **2.18**, **2.20**. 41

Figure 24: The X-ray structure and ^{1}H NMR spectra of a brominated product **2.21**, **2.22**. 43
Figure 25: The X-ray and ^{1}H NMR spectrum of **2.25**. 45
Figure 26: UV-vis absorption and emission spectra of compound **2.25** in DCM. 45
Figure 27: The ^{1}H NMR spectra for **2.27**, **2.30**, **2.28** in Chloroform-D, **2.29** in Acetone-D. 49
Figure 28: The ^{1}H NMR spectra and X-ray of coupled products **2.9**, **2.31**, **2.32**, **2.34**. 51
Figure 29: UV-vis absorption and emission spectra of compound **2.9, 2.30, 2.32, 2.34** in DCM. 52
Figure 30: Monitoring cyclization reaction progress over time by ^{1}H NMR spectroscopy. 55
Figure 31: The ^{1}H NMR spectra and Maldi-tof Ms for **2.38**, **2.39**, **2.40**, and a preliminary x-ray crystallography result of spiro compound **2.39**..... 56
Figure 32: The Maldi-tof Ms for the mixture. 59
Figure 33: The x-ray structure of **2.44**. 61
Figure 34: The ^{1}H NMR spectra for **2.41**, and the x-ray for **2.41** [87] 61
Figure 35: The ^{1}H NMR, Nosey spectra and HRMS for **2.42.** 62
Figure 36: The X-ray structures of **2.49** and **2.51**, and the ^{1}H NMR spectra of **2.49**, **2.50** and **2.51**. 64
Figure 37: The X-ray crystal structure of **2.53**. 65
Figure 38: The X-ray structure of **2.56** and ^{1}H NMR spectrum of **2.56**, **2.57**, **2.58**. . 67
Figure 39: The isomerization mechanisms of **2.49** into seven-membered ring..... 68
Figure 40: UV–vis absorption and emission spectra of spiro compounds. 68
Figure 41: UV-vis absorption and emission spectra of seven-membered compounds..... 69
Figure 42: UV-vis absorption and emission spectra of **2.51**, **2.42**, **2.40**, **2.41**..... 69
Figure 43: The X-ray structure of **2.34**. 70
Figure 44: The ^{1}H NMR and X-ray crystal structure for **2.61**. 73
Figure 45: The Maldi-tof Ms of the mixture. 74
Figure 46: Products formed during the investigation of project. 76

List of Tables

Table 1:Optimization of the synthesis of **2.7** and **2.13**.[a] in glove box. , [b] drying Cs_2CO_3 and reagents. 32
Table 2: The optimized conditions for **2.8** formation. 36
Table 3: Bromination of 1 eq of **2.7** with different equivalents of NBS at room 42
Table 4 Optimization condition for the formation of **2.9**. [a] Microwave condition. 44
Table 5: Optimization conditions for Sonogashira coupling with TMS acetylene. 47
Table 6: Optimization of reaction conditions for the Sonogashira coupling. 50
Table 7: Applying the coupled product **2.9** to routes A and B, and C. [a] microwave irradiation. 53
Table 8: The optimization conditions for TFA cyclization. 55
Table 9: The observation of workups of the **2.28** cyclization reaction. 58
Table 10: The effect of Scholl reaction on **2.38**. 60
Table 11: The isomerization of spiro compound **2.49** into a seven-membered ring. . 66
Table 12: The optimization conditions for synthesis of **2.34**. 71
Table 13: The utilized condition for demethylating methoxy to hydroxy. 72

1. Introduction

1.1 Polycyclic Aromatic Hydrocarbons (PAHs)

Polycyclic aromatic hydrocarbons (PAHs) are a class of organic compounds consisting of two or more fused aromatic rings; examples are shown in Figure 1. They have a conjugated system where the electrons are delocalized, and because of the extension of their π system, they can show longer wavelength absorption and emissions, and π-π interactions. Naturally, PAHs can be formed during the combustion processes, for example, oil, wood, and coal.[1] The final material in a series of PAHs, such as naphthalene, anthracene, coronene, and ovalene, is graphene, which is a layer of carbon atoms that are made from graphite. The term graphene was recommended by Boehm et al. in 1986.[2]

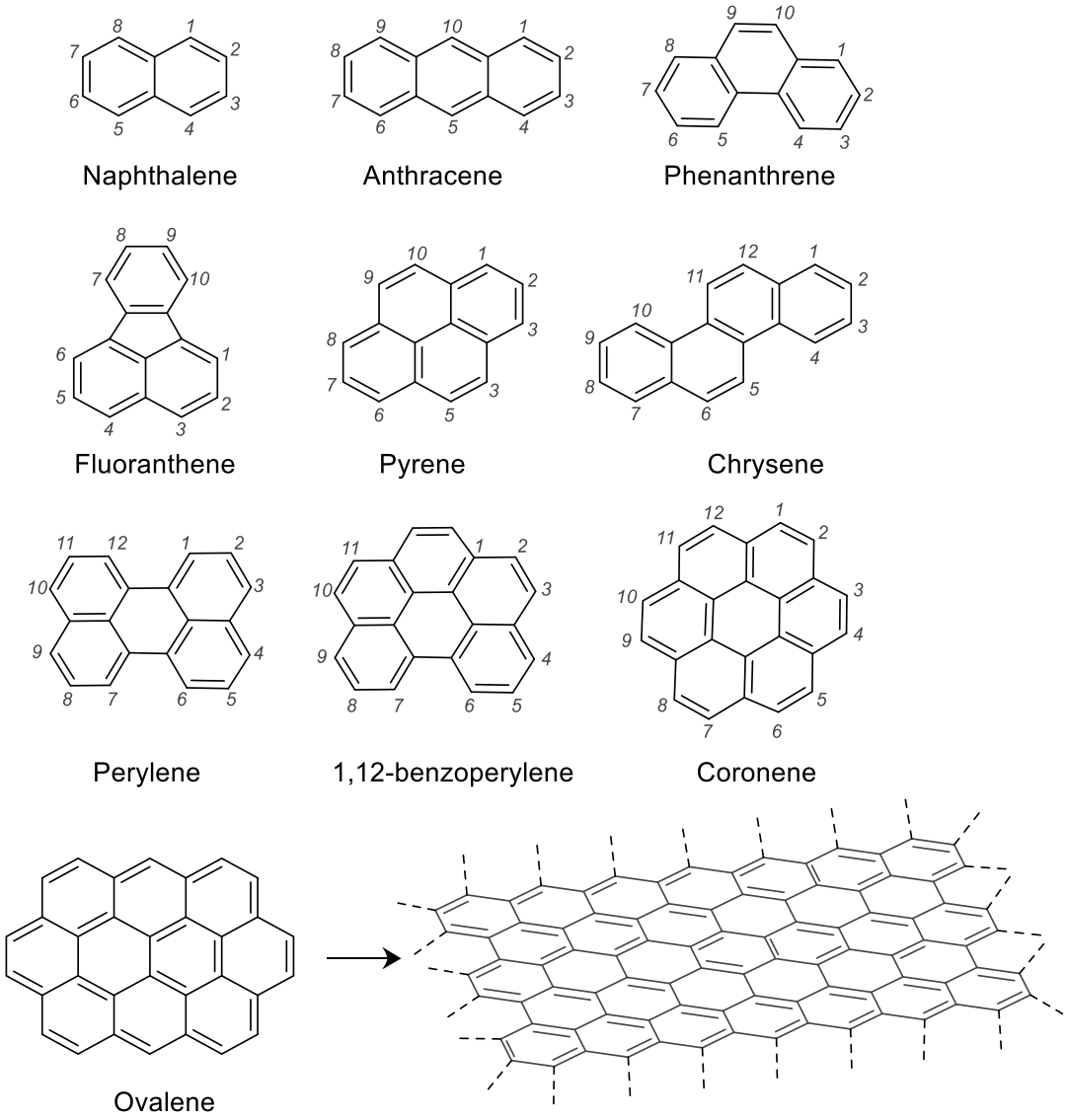

Figure 1: Examples of PAHs compounds to the final series graphene.[3]

The chemistry of graphite began in 1859, and the successful isolation of free-standing carbon nanosheets graphene was in 2004 by Geim and Novoselov.[4,5] Sheet-like graphene is an important material due to the stability of the carbon allotrope, in which sp^2 carbon atoms are arranged in a two-dimensional honeycomb lattice, forming an atomically thin layer. Figure 2 shows that the distance between these layers in graphite is 0.334 nm, and the bond length between neighboring atoms is 0.1418 nm. These layers are held together by van der Waals forces.[6]

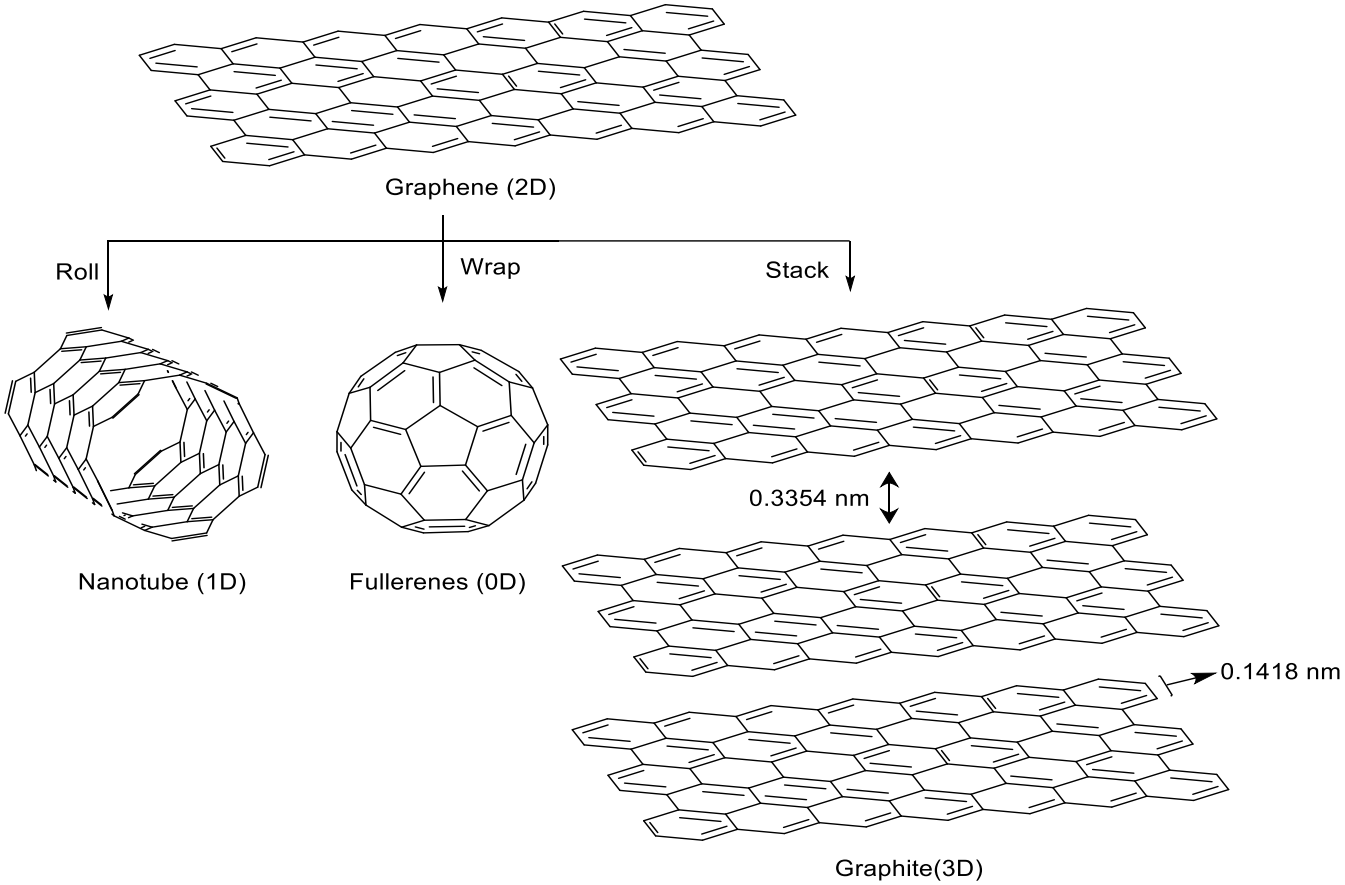

Figure 2: A representation of the chemical structure of graphene layers, fullerenes (0D), nanotube (1D), graphite (3D).[7]

In addition, graphene is considered the backbone of all graphitic materials, regardless of their dimensionality. The wrapped form of graphene , as shown in Figure 2, is called a fullerene (C_{60}) in 0D, rolling it to form a nanotube in 1D, and stacking as layers giving graphite in 3D.[7] This thesis will provide an overview of PAHs, including their sizes, structural edges, aromaticity, and synthetic approaches toward graphene fragments.

1.1.1 Classification of Nanographene

Nanographene molecules are atomically precise fragments of graphene which can be classified by lateral size. Graphene nanoribbons (GNRs) are cut out of graphene sheets into narrow strips, and they can be considered as an intermediate between PAHs and graphene.[8] As shown in Figure 3, the typical width of graphene molecules 1-5 nm, GNRs < 10 nm, whereas the width of graphene quantum dots is more than 10 nm and less than 100 nm. Generally, the nanographene width (graphene fragments) ranges from 1 to 100 nm, and graphene exceeds 100 nm.[9] Graphene has a variety of properties, particularly in electronics, as its high charge-carrier mobility makes it a promising material for field-effect transistors.[10] This property diminishes when the graphene bandgap vanishes (zero bandgap), which means the device stops switching the current on and off. The way to achieve an open bandgap (non-zero bandgap) that significantly enhances the on-off ratio is via geometric confinement, as seen in graphene nanoribbons.[8]

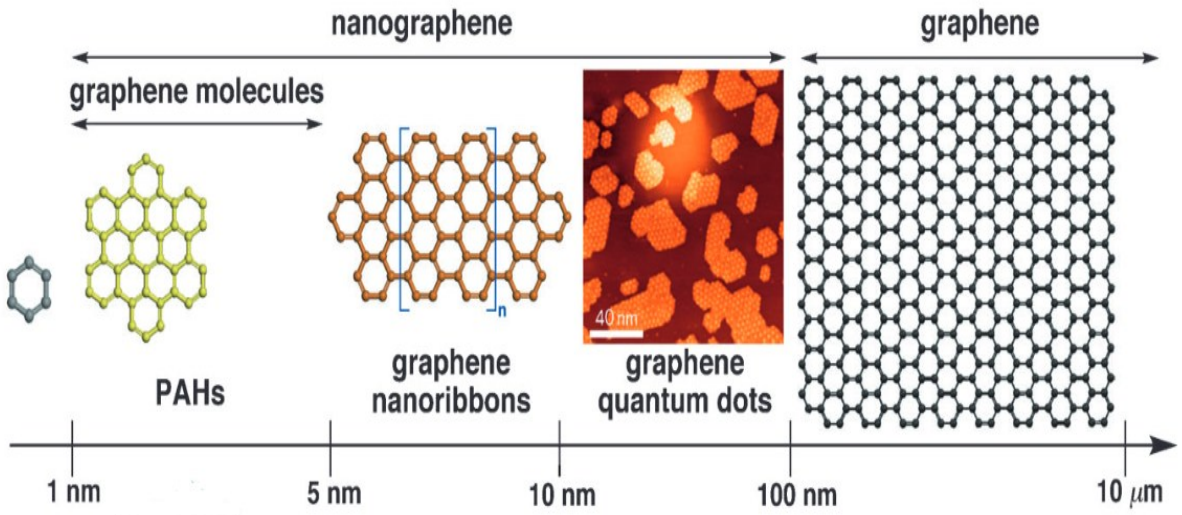

Figure 3: The graphene terminology according to their lateral size (represented with permission)

The extended structures of GNRs show a good balance between high charge-carrier mobility and bandgap, which are important for semiconductor applications.[11] The non-zero bandgap in nanographene is mainly governed by the structures, such as edges and widths, at the atomic level. PAHs typically have edge topologies that influence chemical and physical properties, attracting the attention of different fields in science.

1.1.2 The structure's edge of PAHs

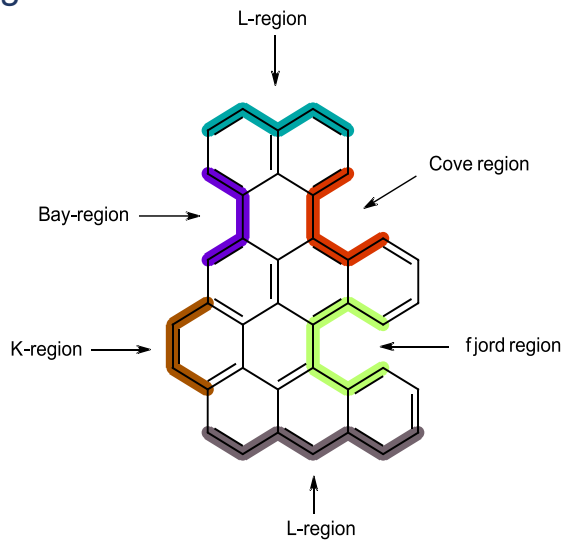

Figure 4: The periphery of PAHs.[12]

The structure's edge of PAHs, as indicated in Figure 4, shows the L-region (zigzag edges), bay region (also known as an armchair edge), cove and fjord regions that are hindered regions, and finally the k-region (carbon-carbon double bond that is not related to the Clar sextet).[12,13] These regions are affecting the structure geometry of the molecule, for example when two aromatic rings are fused in a way that creates cove or fjord region as illustrated in figure 5.[14] This causes steric hindrance which typically distorts the molecule from planarity, resulting in non-planar geometry. The planarity of PAHs has possibility of being beneficial for organic optoelectronic devices because of their strong intermolecular π-π interactions.

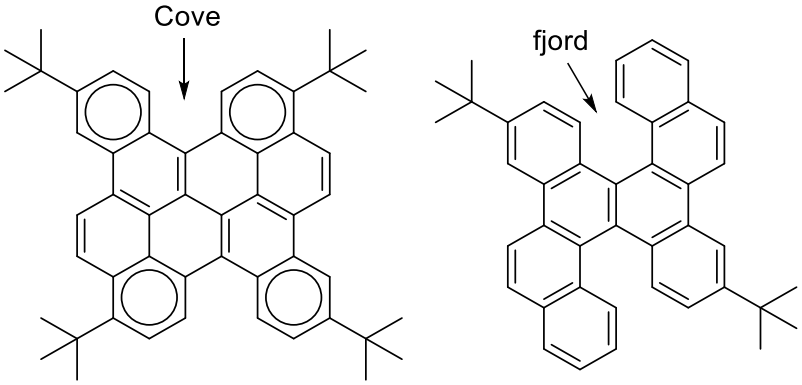

Figure 5: The cove and fjord region in chrysene and perylene.[14]

From a synthetic perspective, the periphery of PAHs is critically important due to potential for π-system expansion. For instance, the Diels-Alder cycloaddition of acetylene to bay regions of nanotube **1.1** in scheme 1 would generate a new benzene ring after dehydrogenation, thereby extending the overall conjugation.[15]

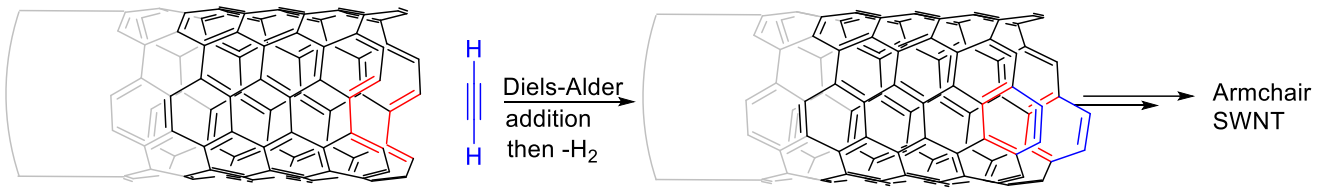

1.1 **1.2**

Scheme 1: Proposed application of the Diels-Alder reaction to chemical synthesis of uniform single-walled nanotubes (SWNTs).[15]

The reactivity of a certain position (edges) in PAHs can be explained by their aromatic characteristics.

1.1.3 Stability of PAHs

The aromaticity in general is associated with Hückel's rule (4n + 2π electrons) which explains the stability of the monocyclic system such as benzene. The stability of multi-ringed species can be explained by the Clar π-sextet rule, providing a better understanding. This rule was established in 1972 by Clar and named Clar's sextet, which suggested the Kekulé resonance structure, with the largest number of disjoint π-sextets are the most important for the characterization of PAHs.[16] Clar's rule is also defined as six π-electrons localized in a single benzene-like ring separated from the adjacent rings by formal C-C single bonds.

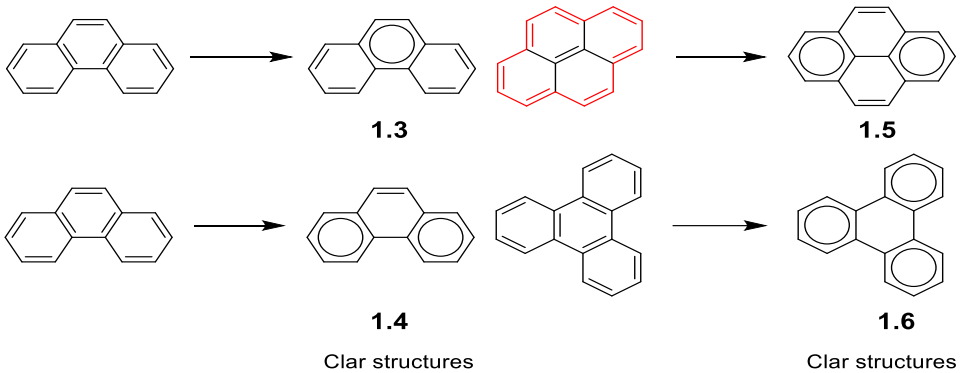

Figure 6: The Clar structure for Phenanthrene (**1.3**. **1.4**), Pyrene (**1.5**), Triphenylene (**1.6**).

This model is useful for prediction of the stability of the PAHs, for example, phenanthrene can be shown by structure **1.3** and **1.4** where **1.4** possesses two aromatic π-sextets in outer rings (circled rings) and **1.3** has only one. The favoured Clar's structure for phenanthrene is **1.4** due to the presence of two aromatic π-sextets that indicate more stability than its form **1.3** with fewer aromatic π-sextets.[17] Clar structure is the resonance representation with the greatest number of disjoint aromatic π-sextets and a closed-shell configuration. Clar structure of pyrene features two disjoint aromatic π-sextets.[18] Pyrene **1.5** is aromatic despite having 16 π-electrons, and the reason for pyrene aromaticity is the 14 π-electrons of its conjugated perimeter of sp^2 hybridized carbon atoms. Accordingly, Platt's ring perimeter model PAHs were divided into the perimeter and

the inner core.[19] Moreover, triphenylene **1.6** is the most stable since it possesses a fully benzenoid species, whereas others have less aromatic π-sextets.[17] Rings with an aromatic π-sextet are "fully benzenoid" whereas those without (typically showing localized double bonds) are "empty rings".

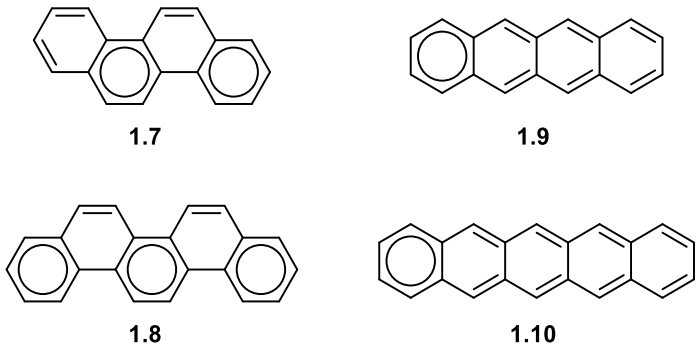

Figure 7: The Clar sextet structure for Chrysene and Tetracene.

Clar's rule effectively accounts for the stability and aromaticity of linear and non-linear polycyclic aromatic hydrocarbons (PAHs). Larger linear acenes, such as tetracene **1.9** and pentacene **1.10**, exhibit lower stability and higher reactivity compared to their angular isomers, Chrysene **1.7** and Picene **1.8,** respectively. This difference arises because tetracene and pentacene possess only a single Clar π-sextet (with a migrating sextet in alternative representations). In contrast, chrysene features two disjoint aromatic π-sextets, and picene features three, conferring greater aromatic stabilization and reduced reactivity.[3]

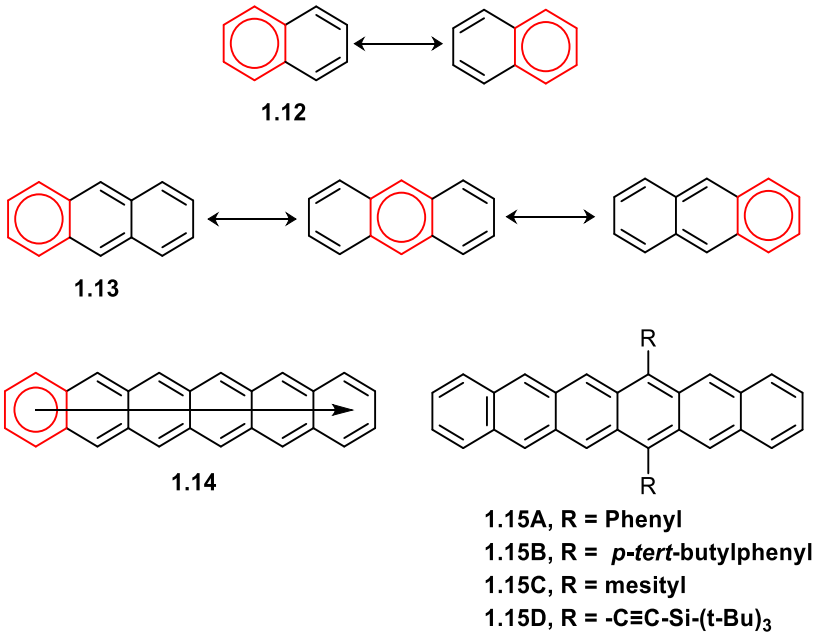

Figure 8: Clar structure of naphthalene and anthracene resonance.[20–23]

The migration of the one π-sextet in naphthalene (**1.12**), and anthracene (**1.13**) is shown, Clar symbolizes this migration in figure 8 by an arrow, as indicated in hexacene (**1.14**).[23] The migration of one sextet in large acenes induces significant aromatic dilution, resulting in the loss of benzenoid character, which overall diminishes aromatic stabilization.[21] Thus, hexacene (**1.14**) is highly reactive and unstable in solution, primarily due to its susceptibility to oxidation, and photochemical dimerization occurs even at very low concentrations.[20] It turns out that even the hexacene derivative substitution **1.15(A,B,C)** could not prevent the decomposition.[20] Substitution with a bulkier alkyne, such as a tri-*tert*-butylsilyl group **1.15D**, enhanced hexacene's stability and solubility, enabling complete spectroscopic characterization.[22]

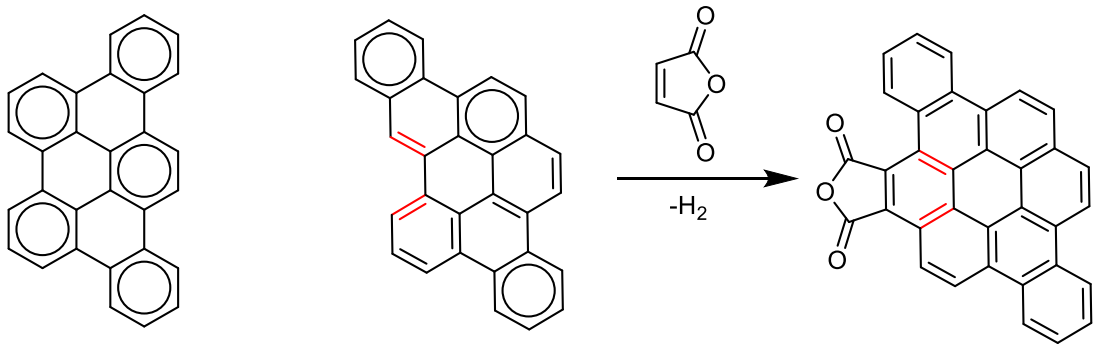

1.16 **1.17** **1.18**

Scheme 2: The Clar structures of tribenzo[fg, ij,rst]pentaphene (**1.16**), benzo[qr]naphto[2,1,8,7-fghi]pentacene (**1.17**), and Diels-Alder adduct[24]

Clar and Zander demonstrated the difference in reactivity between **1.16** and its isomer, benzo[qr]naphto[2,1,8,7-fghi]pentacene **1.17** toward maleic anhydride (scheme 2). They noticed that **1.16** is unreactive toward maleic anhydride, whereas **1.17** can act as a diene, enabling it to undergo a Diels-Alder reaction. The reason is that compound **1.16** is a fully benzenoid hydrocarbon with five aromatic π-sextets, rendering it chemically inert.[24]

1.2 Synthetic strategy of nanographene

The π-extension of polycyclic aromatic hydrocarbons (PAHs) is crucial owing to their diverse applications across various scientific disciplines. However, the extent of π-extension, molecular width, and edge topology profoundly influence the physicochemical properties of nanographenes. Hence, a precise controllable synthesis of a uniform structure of nanographene is highly desirable. There are two methods for the synthesis of graphene or nanographene which are top-down and bottom-up methods. The top-down method means a dimensional reduction from graphite (3D) to graphene (2D) or from graphene (2D) to (1D) or nanographene.[11] In contrast, the bottom-up method entails the reverse process: building up from smaller molecular precursors to achieve controlled dimensionality and well-defined structures. [25]

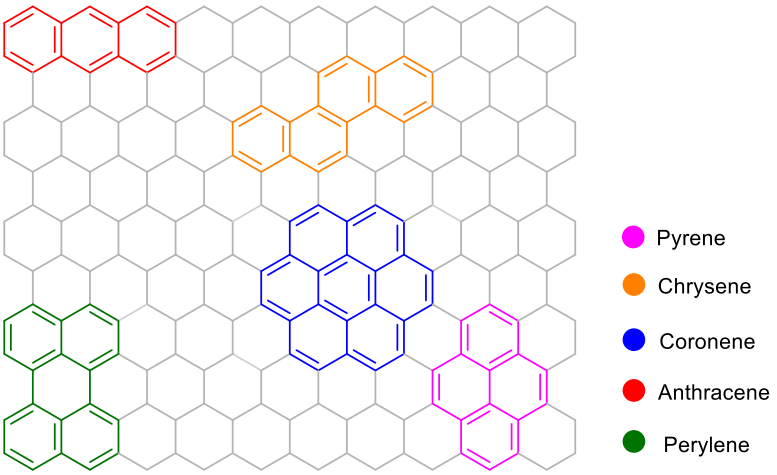

Figure 9: The graphene presentation which contains nanographene molecules.

Figure 9 demonstrates graphene structure which contains known nanographene fragments, for example coronene, anthracene, perylene. This chapter focuses on bottom-up methodologies, particularly the assembly of small π-conjugated components into extended nanographene.

1.2.1 C-H activation in cross-coupling

Generally, palladium-catalyzed cross-coupling reactions have become a fundamental method for forming carbon-carbon bonds between pre-functionalized substrates. Methods such as Stille, Negishi, Suzuki-Miyaura, and Sonogashira couplings enable the extension of conjugation systems in organic synthesis, providing reliable tools for constructing complex molecules from simpler aryl halides and organometallic reagents.[26–30] These traditional approaches often require multi-step pre-activation of substrates, which can be a time consuming and economically inefficient process.[31] In recent decades, C-H activation of arene has emerged as transformative in organic synthesis, thereby broadening substrate scope and enhancing overall synthetic efficiency compared to traditional cross-coupling methods.[31] The cleavage and subsequent functionalization of C-H bond is often described as C-H activation, C-H functionalization, and catalytic direct arylation which represents a powerful strategy for constructing carbon-carbon bonds.[32]

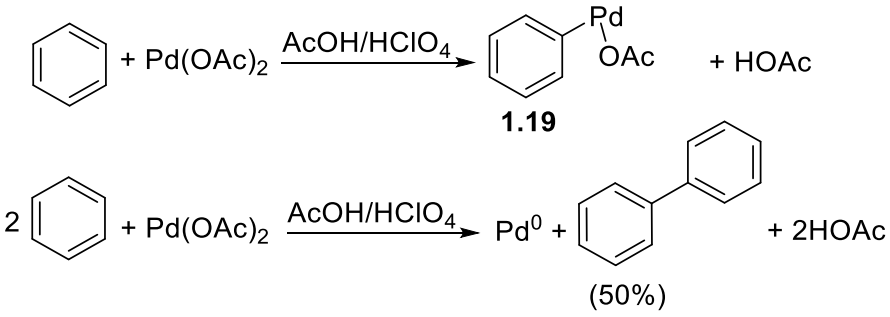

Scheme 3: Formation of the aryl palladium intermediate and biaryl.[33]

The development of direct C–H palladation as a key step in palladium-mediated C–H activation began with the seminal 1968 work of Davidson and Trigg.[33] As shown in scheme 3, they demonstrated that palladium(II) acetate reacts with benzene in acetic acid/perchloric acid via an electrophilic substitution pathway to generate aryl palladium(II) complex (**1.19**). The aryl palladium species were detected by their decomposition to biaryls and by isolation of a purple, explosive complex formulated as $[Pd(C_6H_5)(H_2O)ClO_4]_n$. According to Davidson, transition metal ions capable of reacting with aromatic compounds to form aryl–metal complexes include palladium(II), mercury(II), and rhodium(III). Biaryl motif represents one of the most prevalent structural frameworks in bioactive compounds and pharmaceuticals.[34]

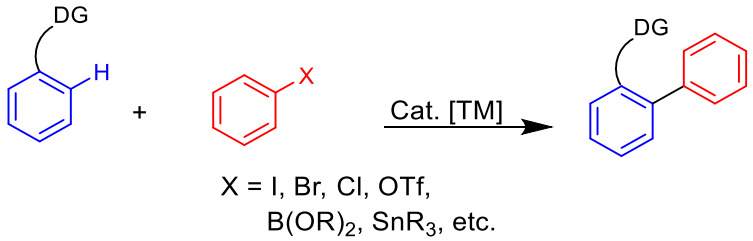

Scheme 4: Modern methods for the formation of biaryl compounds.

Consequently, the direct construction of C–C aryl bond, as shown in scheme 4, is through the coupling of a pre-activated aryl, such as organohalides or organometallic reagents, with unactivated aryl C–H bond and has emerged as a prominent research area. Nevertheless, achieving precise regioselectivity in the C–H activation step remains a significant challenge. The use of directing groups has proven to be an effective strategy to address this issue by controlling the site of C–H activation.[31]

1.2.2 Directing Group-Assisted C-H Arylation of Functionalized Arenes

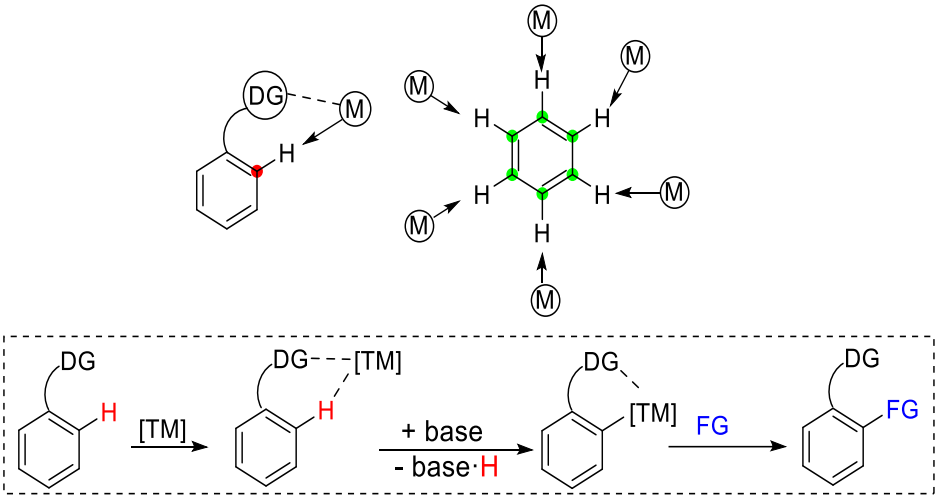

Figure 10: The directing group in C-H activation of arene, DG= directing group, FG= Functional group.

Generally, the presence of directing groups on arenes (figure 10) such as oxygen and nitrogen is essential for the regioselective cleavage of C-H on arene, while their absence causes problems with site selectivity.[35] The concept of utilizing directing groups to govern the regioselectivity during transition-metal insertion into C-H bond was first reported by Kleinman and Dubeck, as shown in scheme 5.[36]

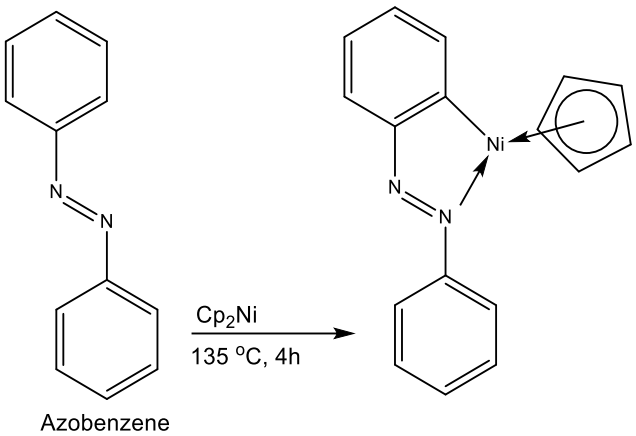

Scheme 5: The first cyclometallated compound by Kleimann, Dubeck.[36]

The assistance of the lone pair of the directing group to the metal enabling an agostic interaction (M···H–C), hence weakens the C-H bond, usually resulting in the formation of a five- or six-membered metallcycle.[35] This cyclometallated species exhibits high reactivity due to its polarized metal–carbon σ-bond, making it invaluable for regioselectivity in organic synthesis and catalytic C–H functionalization.[31],[35] The commonly employed directing groups are presented in figure 11, including phenols[37,38], oxazolines[39], imines[40], pyridines[40,41], and phosphines[42].

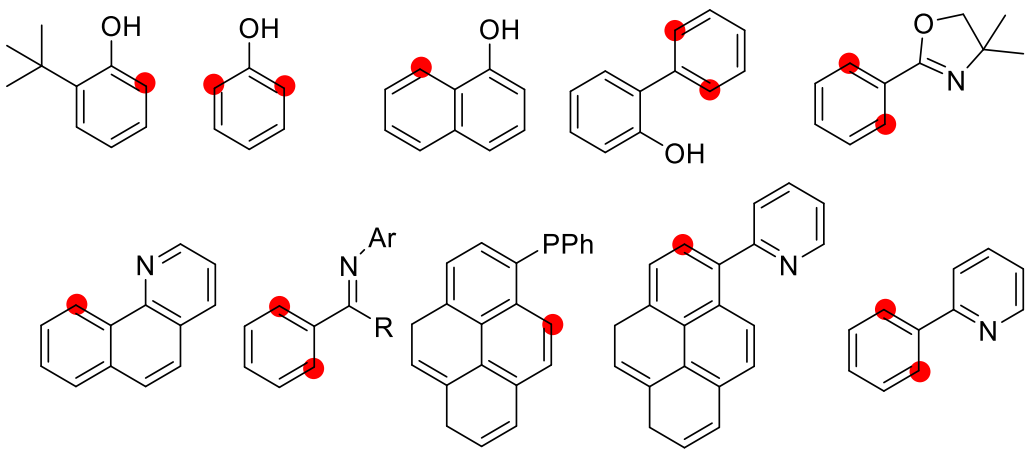

Figure 11: The regioselectivity cleavage of C-H bonds by using directing groups, examples with observed C-H cleavage positions.[31,32]

1.2.2.1 Direct arylation of PAHs with Aryl Halide

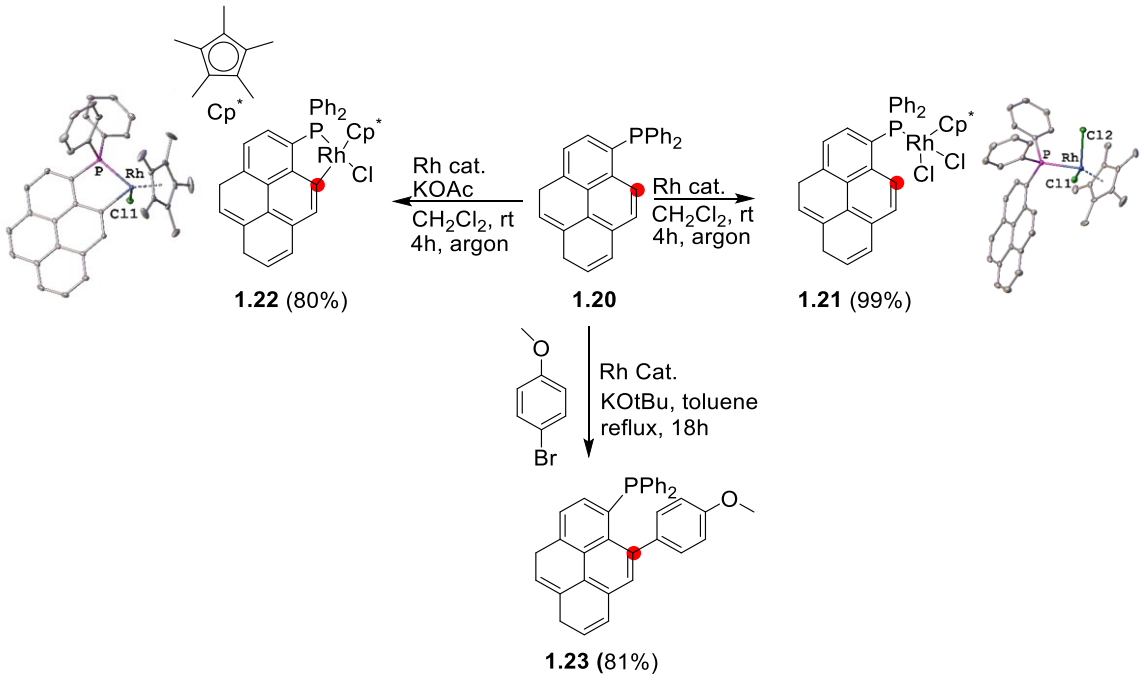

Scheme 6: The base role in synthesis of pyrene rhodium complex. Rh catalyst = $[RhCl_2(Cp^*)]_2$.[42]

Recently, Sire and co-workers (scheme 6) synthesized π-extended pyrene (**1.23**) using a phosphorus directing group.[42] They accomplished selective C–H arylation with 4-bromoanisole using a rhodium catalyst. A key finding was the pivotal role of the base in metallacycle formation, demonstrating the absence of the base leads to P-coordinated Rh(III) complex (**1.21**), while its presence promotes selective C–H activation at the pyrene 10-position to afford the corresponding five-membered rhodacycle (**1.22**). Miura and co-workers (scheme 7) showed that 2-phenylphenol undergoes mono and di arylation at ortho position depending on the stoichiometric amount of aryl

halide and base.[43] Limiting equivalents under condition A favour monoarylation to give (**1.24**), while excess of aryl halide promotes diarylation to afford (**1.24**) and (**1.25**).

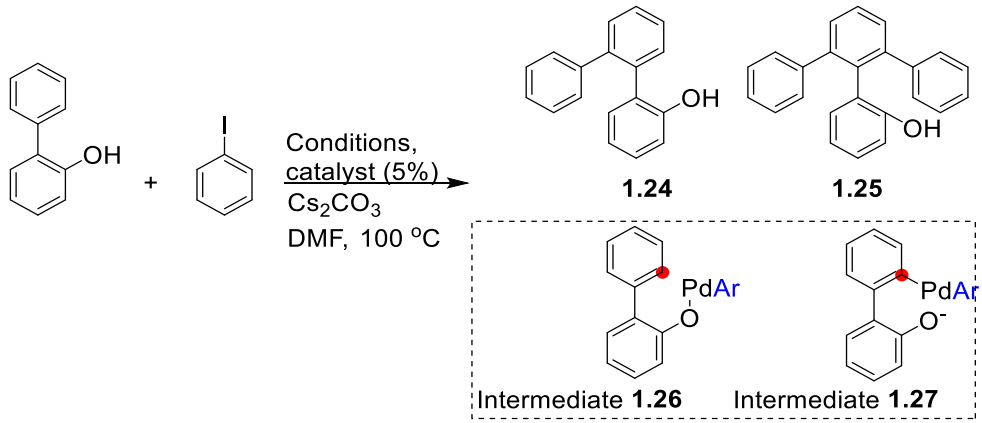

Scheme 7: Conditions A) Iodobenzene (1.2 equiv), $Pd(OAc)_2$, Cs_2CO_3 (1.2 equiv), molecular sieves, **1.24** (76%). B) Iodobenzene (4.0 equiv), $PdCl_2$, Cs_2CO_3 (4 equiv), **1.24** (62%), **1.25** (25%).[43]

The author highlights the importance of the base for achieving efficient reaction performance. The role is believed to be removing the iodide ion from the reaction medium resulting in the enhancement of the formation of intermediate **1.26**. The high solubility of the base in DMF could improve the conversion of **1.26** to **1.27** by assisting the deprotonation which lead upon reductive elimination the arylated product.[43]

1.2.3 π-Extension of PAHs via Intramolecular C–H Arylation

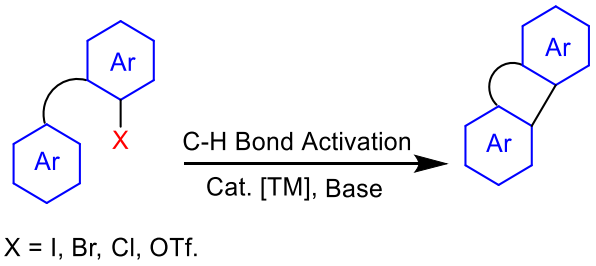

Scheme 8: Intramolecular C–H Activation Reactions.

Intramolecular C–H arylation is a powerful strategy for π-extension of PAHs. It typically involves transition-metal-catalyzed coupling of an aryl halide or pseudohalide with a tethered arene C–H bond in the same molecule, forming a fused ring. Rice and co-workers demonstrated this strategy (scheme 9) by synthesizing benzofluoranthenes from arene-triflate **1.28**.[44]

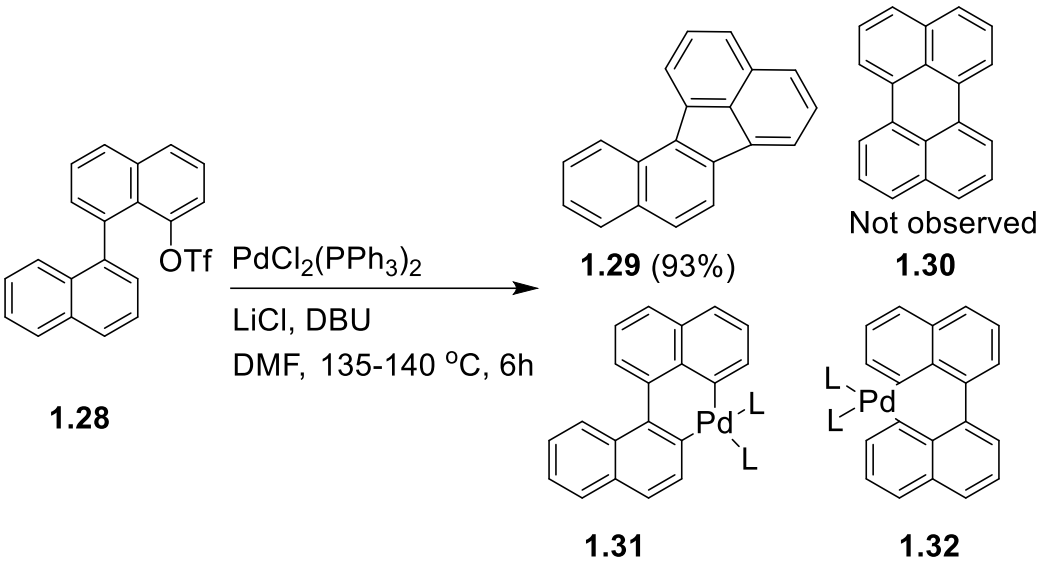

Scheme 9: The formation of benzofluoranthene.[44]

Treatment of aryl triflate **1.28** with $PdCl_2(PPh_3)_2$ and LiCl generates the reactive intermediate $[Pd(PPh_3)_2Ar(Cl)]$. In the presence of DBU, C–H bond cleavage occurs via HCl removal, forming two possible cyclopalladated intermediates (**1.31** and **1.32**). The reaction proceeds through the six-membered palladacycle **1.31**, affording the benzofluoranthene product (**1.29**), while the seven-membered palladacycle **1.32** which would lead to perylene (**1.30**) is not observed. This demonstrates high regioselectivity of favouring the five-membered ring closure.

1.2.3.1 Palladium migration in Intramolecular C-H activation

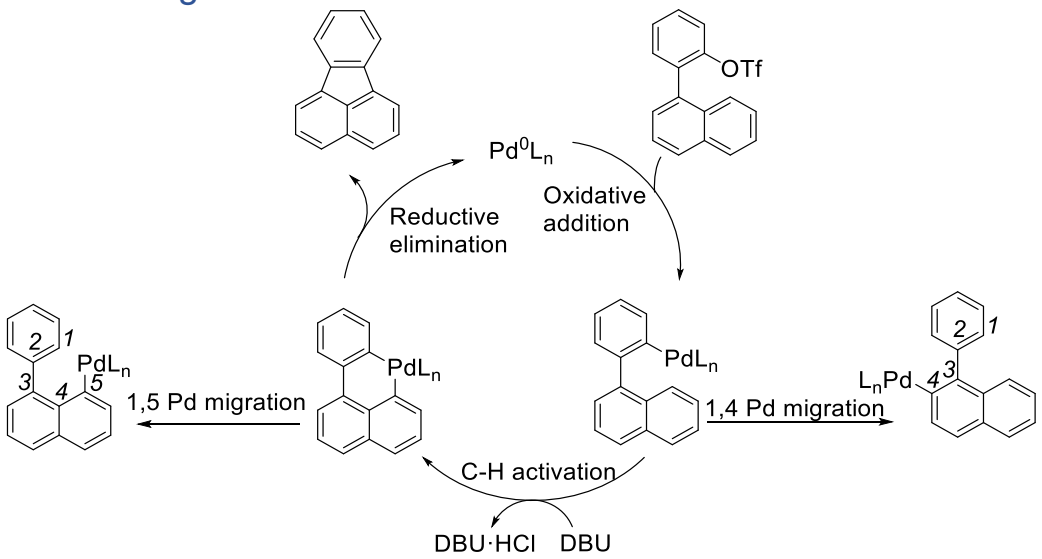

Figure 12: Catalytic cycle for the formation of fluoranthene, highlighting the stages where 1,4- or 1,5-Pd migration may occur.[44–47]

Palladium migration represents an important competing pathway in intramolecular C–H arylation reactions for π-extension of PAHs. The desired cyclized product is obtained when the reaction

proceeds without palladium migration. However, structural rearrangements as shown in figure 12 frequently occur possibly via 1,4- or 1,5-Pd migration processes. These migrations are triggered by C–H activation at different positions on the aromatic framework, ultimately delivering regioisomeric products.[44–46] An illustrative example is presented in Scheme 10, where Mohammad-Pour and co-workers reported the formation of regioisomeric product while synthesizing a series of naphtho-fluoranthenes.[48]

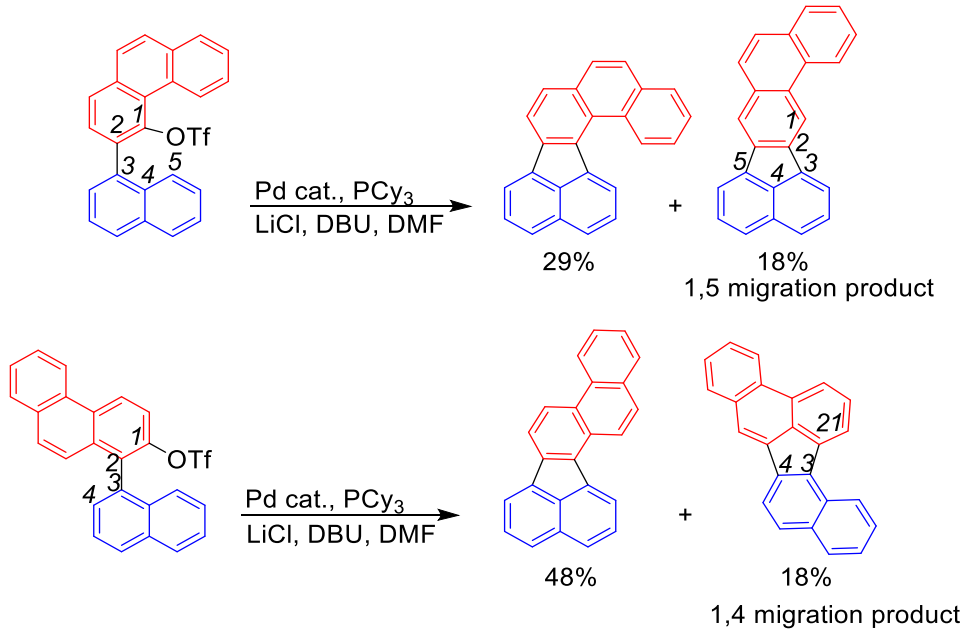

Scheme 10:1,4 and 1,5 Pd migration products, Pd cat = $Pd_2(dba)_3$.[48]

1.2.4 C–H arylation of non-functionalized PAHs

Conventional C–H activation reactions in PAHs have generally relied on the presence of a directing group to achieve site selectivity. An alternative and increasingly explored approach exploits the intrinsic reactivity of PAH peripheral edges to enable directing-group-free functionalization and subsequent extension of the conjugated π-system.

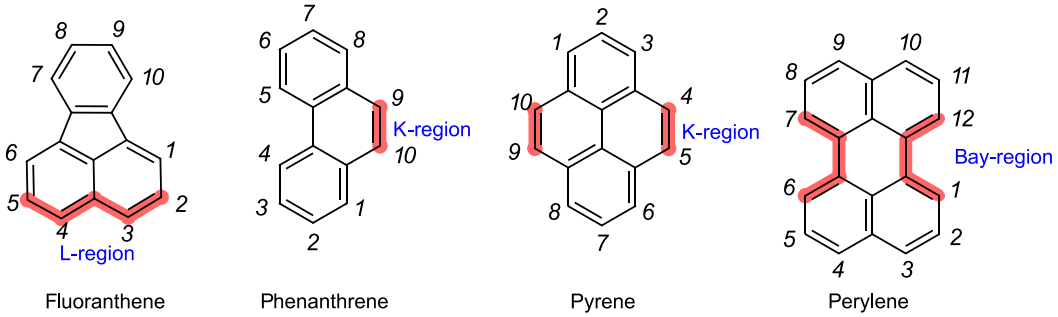

Figure 13: Examples of activated C-H bond on edge of PAHs.

Figure 13 presents selected PAH structures with their characteristic edge designations. For instance, phenanthrene and pyrene shows K-region, fluoranthene exhibits an L-region, and

perylene contains a bay-region. These distinct edge motifs serve as viable sites for C–H activation and π-extension.

1.2.4.1 Annulative π-extension of PAHs at the bay region

Diels-Alder cycloadditions at the bay regions of PAHs with a broad range of dienophiles such as maleic anhydride and acetylene, provide a powerful single-step annulative π-extension (APEX) strategy, delivering π-extended benzoperylene frameworks.

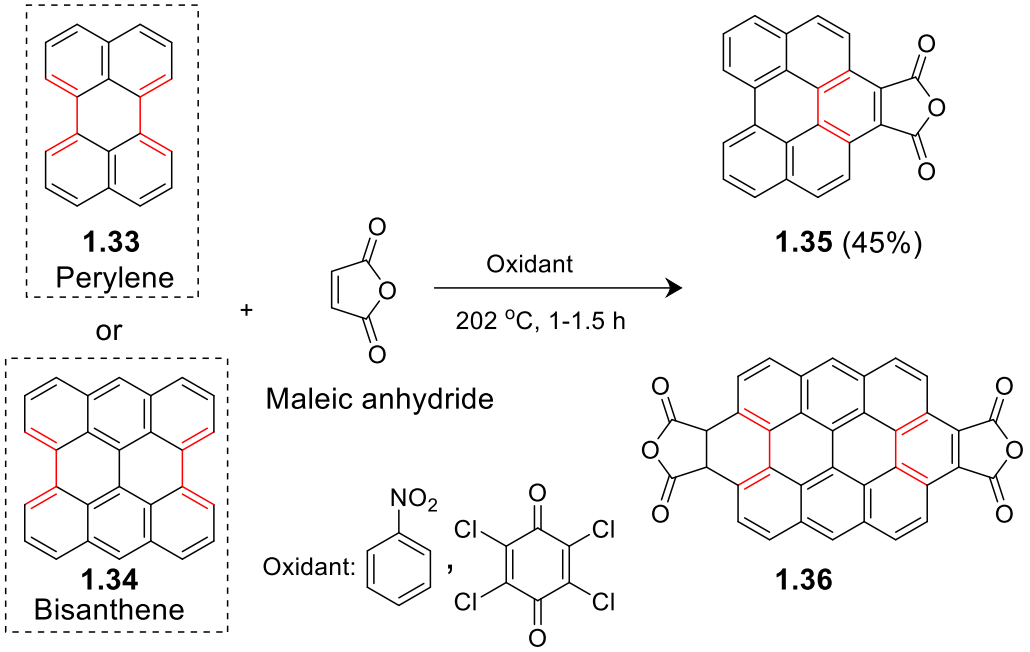

Scheme 11: π-Extension of the perylene and bisanthene at bay region via the Diels-Alder method.[49,50]

The Diels-Alder cycloaddition of maleic anhydride, as shown in Scheme 11, to the bay region of perylene and bisanthene requires heating under reflux in nitrobenzene to furnish the corresponding anhydride adduct.[49,50] When *p*-chloranil is employed in molten maleic anhydride at reflux instead of nitrobenzene, the yield of adduct (**1.35)** rises significantly to 93 % and the reaction time is reduced to 10 min.[51] The extended bisanthene (**1.34)** system exhibits markedly higher reactivity than bare perylene, under the nitrobenzene conditions, cycloaddition occurs readily at both bay regions, furnishing the dianhydride (**1.36**) quantitatively.[50]

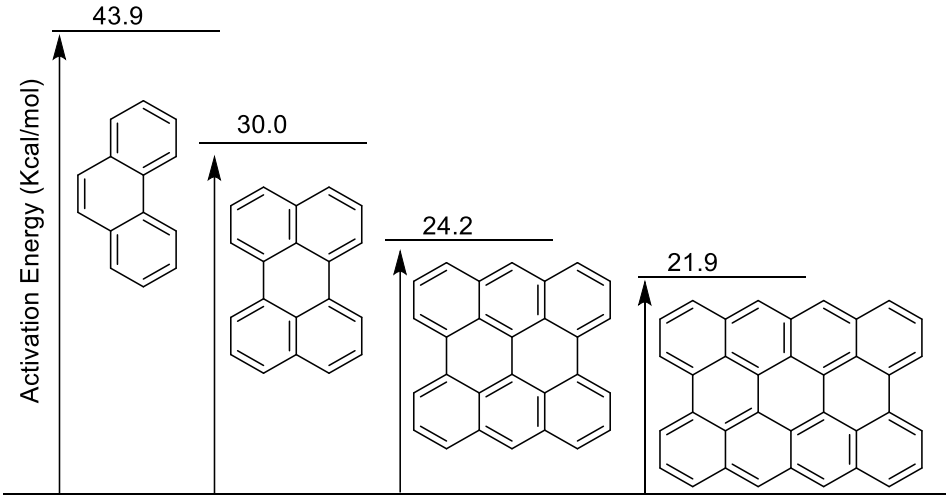

Figure 14: Calculated activation energies for Diels-Alder cycloadditions of acetylene to the bay regions of PAHs.[15]

Fort and co-workers in figure 14 calculated the activation energies for Diels–Alder addition of acetylene to the bay regions of PAHs in the periacene series.[15] This study reveals a clear and continuous decrease in the activation barrier with increasing size of the aromatic framework, showing that extended π-system such as bisanthene (**1.34**) undergo bay-region cycloadditions far more readily than perylene (**1.33**).

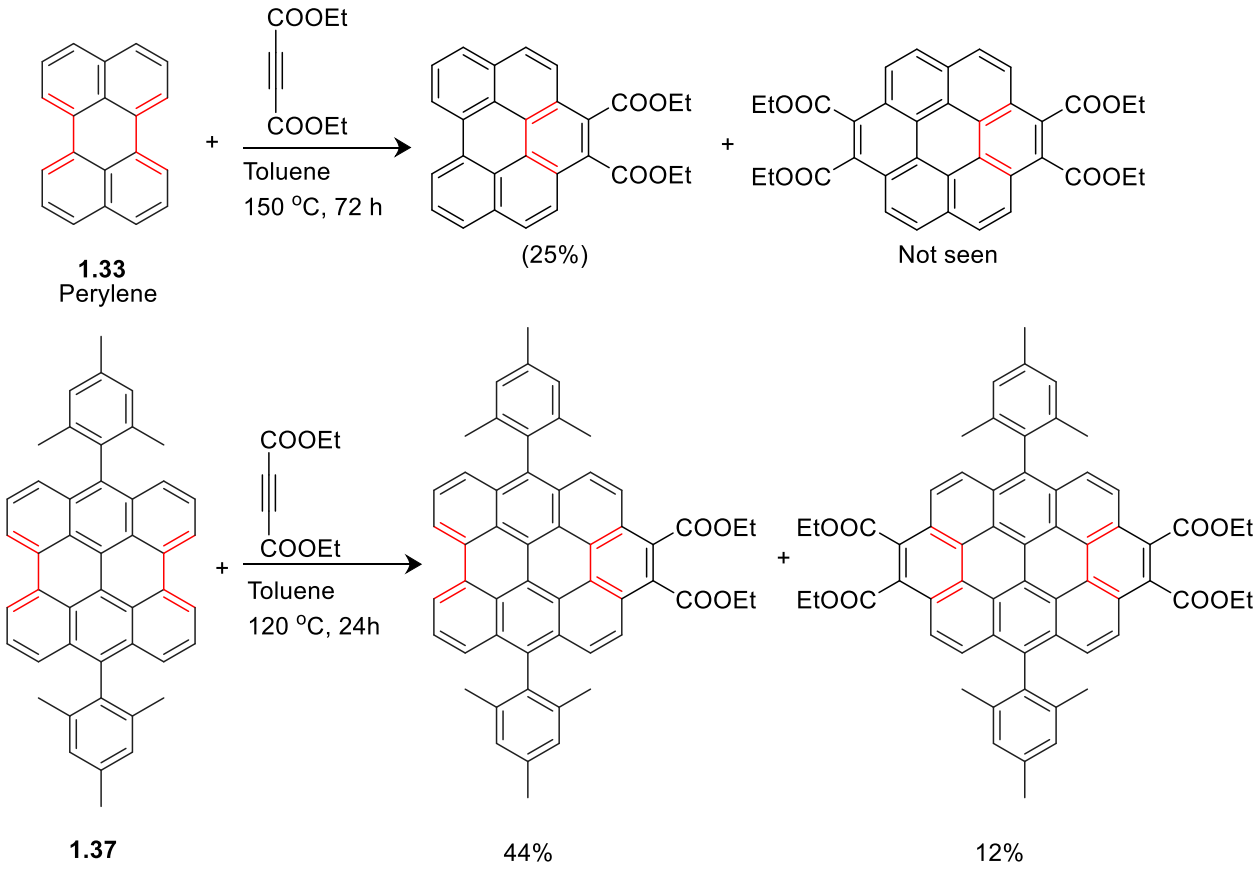

Scheme 12: π-extension via bay region of perylene (**1.33)** and 4,11-dimesitybisanthene (**1.37)**.

Therefore, the cycloaddition with diethyl acetylene occurs at one bay region of perylene whereas extended compound (**1.37)** undergoes mono and di addition.

1.2.4.2 Annulative π-extension (APEX) at K- and L- regions of PAHs.

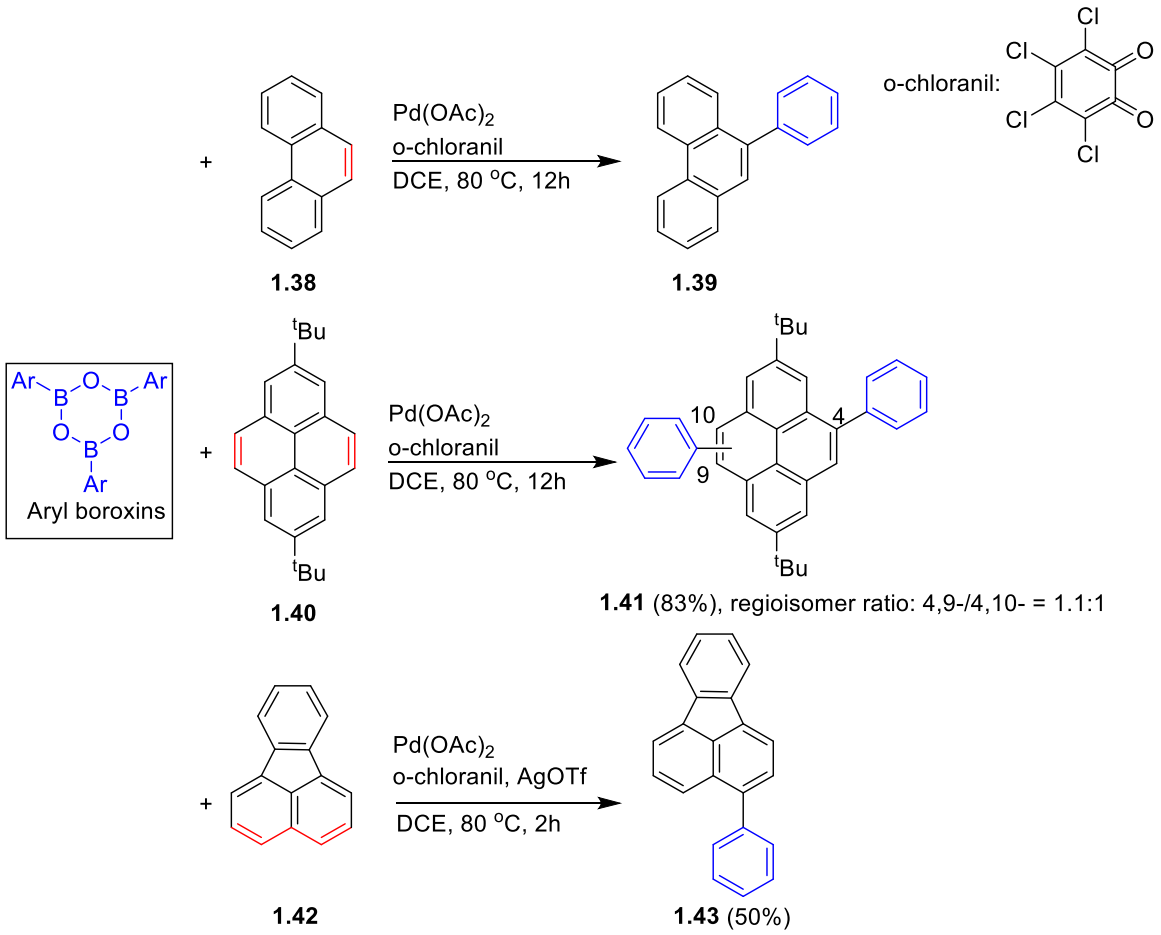

Scheme 13: The C-H arylation with arylboroxine at K-region of phenanthrene and pyrene, and at L- region of fluoranthene.[52,53]

In 2011, Mochida and coworkers (scheme 13) reported a palladium-catalysed direct C-H arylation with phenylboroxin at L-region of fluoranthene (**1.42**), K-regions of phenanthrene (**1.38**) and pyrene (**1.40**).[52,53] This approach utilizes Pd (II), o-chloranil as oxidant, and an arylating agent to provide an efficient platform for synthesizing extended polyarenes and nanographenes. The arylation of **1.38** and **1.42** with phenyl boroxin was straightforward giving mono product. In contrast, the two K-regions of pyrene (**1.40**) under APEX condition gives a mixture of regioisomeric diarylated products at the 9- and 10-positions with essentially no regiocontrol over the second arylation step (C9/C10 ≈1.1:1). The mono- and diarylated products were isolated by preparative thin-layer chromatography (PTLC). Further progress was developed by Matsuoka and coworkers (scheme 14) who introduced one step APEX that enables efficient and rapid construction of one or more new fused aromatic rings by using diiodobiaryls as the arylating agent.[54]

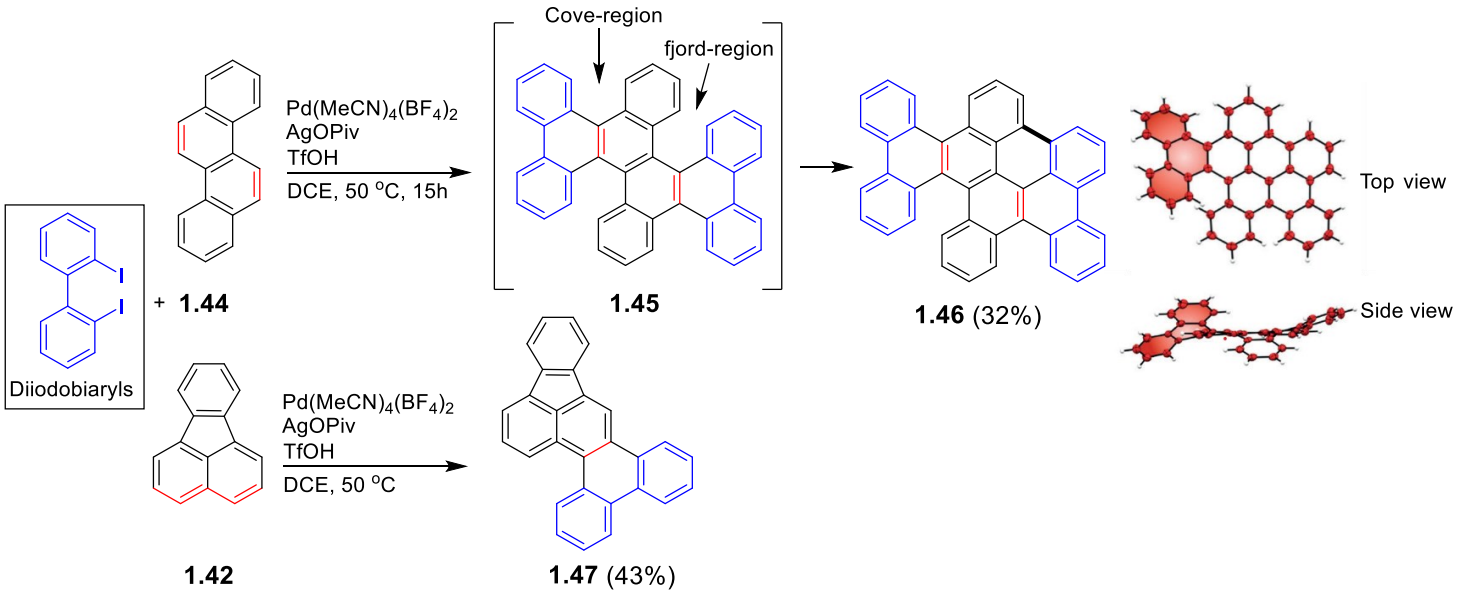

Scheme 14: *π*-extension at K and L region by diiodobiaryls.[54]

The APEX of chrysene **1.44** generates highly fused nanographene **1.46** passing through intermediate **1.45** that undergoes Scholl cyclodehydrogenation at the fjord region. X-ray crystallographic analysis shows that the phenanthrene moiety in **1.46** is significantly twisted due to steric repulsion between the hydrogen atoms located at the fjord and cove regions.

1.2.2 π-extension of PAHs via Scholl reaction(Intramolecularly)

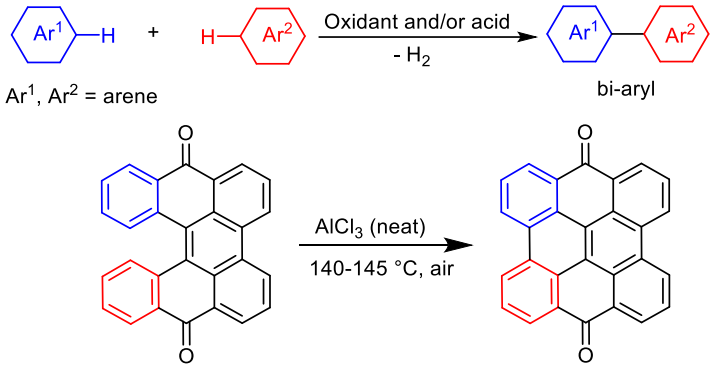

Scheme 15: General example of Scholl reaction, where an oxidant and an acid (Lewis or Brønsted) results in the formation of an aryl-aryl bond.

Scholl reaction is an effective tool for π-extension of PAHs via intramolecular oxidative cyclodehydrogenation which was reported in 1910 by Scholl as shown in scheme 15.[55] Scholl approach remained a vital synthetic tool for over a century to generate fused PAHs by using oxidant and/or acid (Lewis or Brønsted) forming aryl-aryl bond typically in an intramolecular manner. This approach produces defined graphene nanoribbons with the formation of up to

hundreds of C-C bonds in a single step.[56] The carbon-carbon formation proceeds through two primary mechanistic pathways as shown in scheme 16 which are arenium cation and radical cation.[57] In both cases, the catalyst and oxidant drive oxidative cyclodehydrogenation, leading to the elimination of (H_2) and the formation of new aryl–aryl C–C bonds, thereby fusing additional aromatic rings.

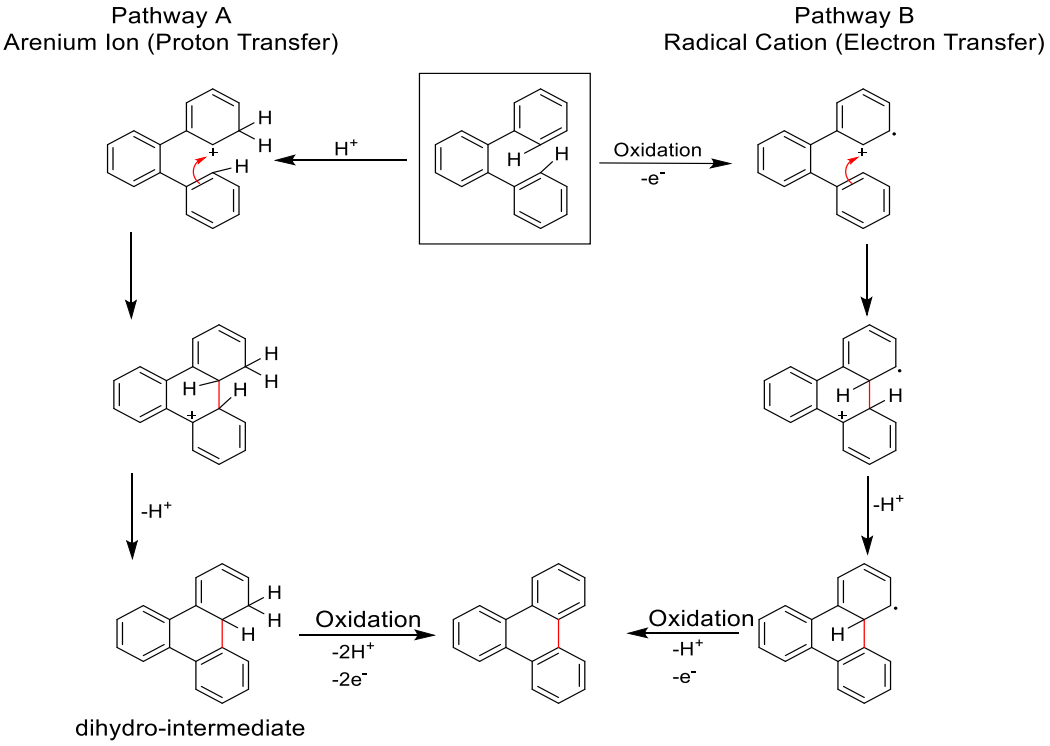

Scheme 16**:** Mechanisms for the Scholl Reaction of *o*-Terphenyl Arenium Cation (proton transfer) (A) and Radical Cation (electron transfer) (B).

Acids in arenium cation mechanisms play a role in activating one aromatic ring by protonation which generates a positive arenium ion (known as σ-complex or Wheland intermediate). The adjacent electron rich aromatic ring attacks this electrophilic species intramolecularly forming a new carbon-carbon bond. Rearrangement follows through deprotonation forming fused ring (dihydro intermediate), then finally oxidative dehydrogenation step by removing two hydrogens affording fused polycyclic aromatic product.[57] This pathway is commonly favoured in acidic conditions with reagents such as $AlCl_3$ or $FeCl_3$. In contrast, the radical cation mechanism initiated by one electron oxidation of an aromatic ring by oxidants such as DDQ producing a radical cation which is attacked by the neighbouring aromatic ring leading to formation of a new carbon-carbon bond. Subsequent steps include further oxidation followed by deprotonation to give fused ring.[55,57] Generally, Scholl reaction is a powerful tool for the π-extension, but the mechanism is still poorly predictable due to the effect of some variables such as the position of substitution and chlorinated products.

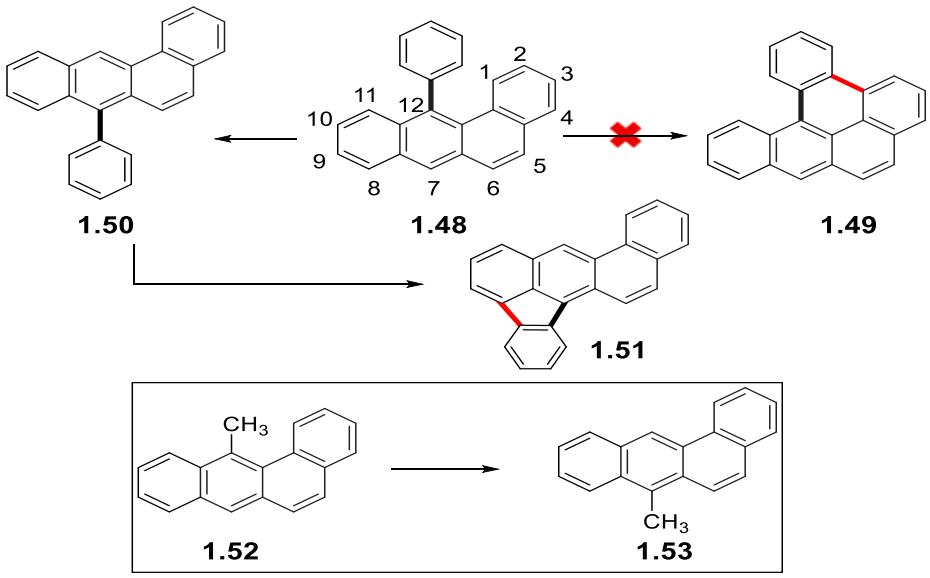

Scheme 17: The rearrangement of substituent by Scholl condition.[58–60]

For example, Clar reported (scheme 17) the attempted synthesis of **1.49** from **1.48** using $AlCl_3$ where the reaction was intended to proceed by direct oxidative cyclodehydrogenation to form a new six-membered ring.[60] However, Buu-Hoi and coworkers proposed that it could be product **1.51** instead of **1.49** due to rearrangement of compound **1.48** to **1.50**; they noted as evidence the similar conversion of **1.52** into **1.53**, although no mechanistic rationale was proposed.[59] This hypothesis was experimentally confirmed in 1967 by Vingiello who showed the rearrangement of **1.48** to **1.50** does indeed occur prior to cyclization forming **1.51** with an embedded five-membered ring.[58]

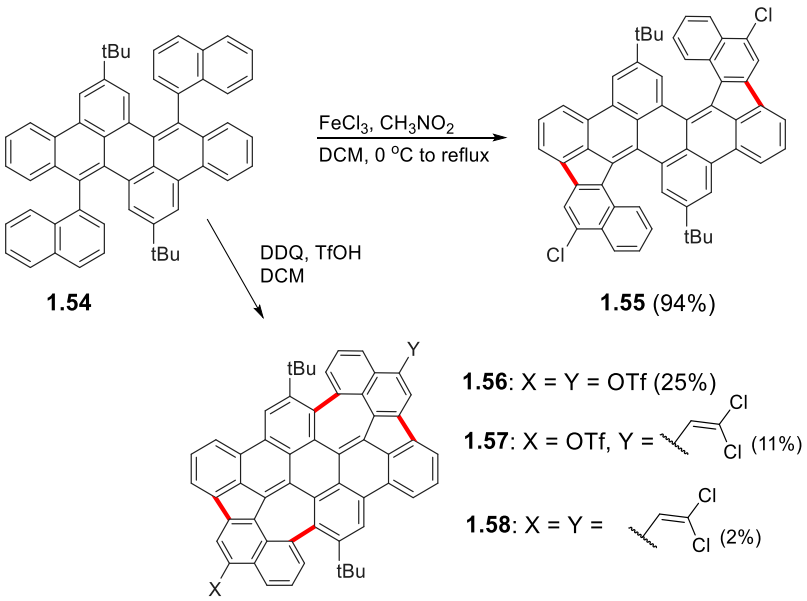

Scheme 18: Products formed under Scholl conditions.[61]

Furthermore, Mastalerz and co-workers (scheme 18) reported an interesting outcome from the treatment of precursor **1.54** under Scholl condition. Employing $FeCl_3$ afforded the chlorinated product **1.55** with formation of a five-membered ring. However, treatment with DDQ and TfOH in CH_2Cl_2 resulted in formation of five- and seven-membered rings. This reaction produced the bis-triflate **1.56** together with compounds **1.57** and **1.58**. The authors suggest that these dichlorovinyl groups originate from the CH_2Cl_2 solvent, although the exact mechanism of this side reaction remains unclear.

1.2.2.1 π-extension of Coronene

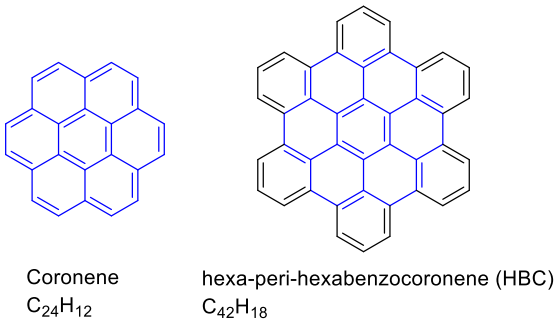

Figure 15: Coronene and hexa-peri-hexabenzocoronene (HBC).

Coronene consists of seven peri-fused benzene rings (figure 15), and the π-extension of coronene leads to large PAH, which involves the addition of a peripheral benzene ring, leading to hexa-peri-hexabenzocoronene (HBC). The unsubstituted HBC exhibits limited solubility, whereas functionalized HBC derivatives offer an enhancement in the solubility.[25,62]

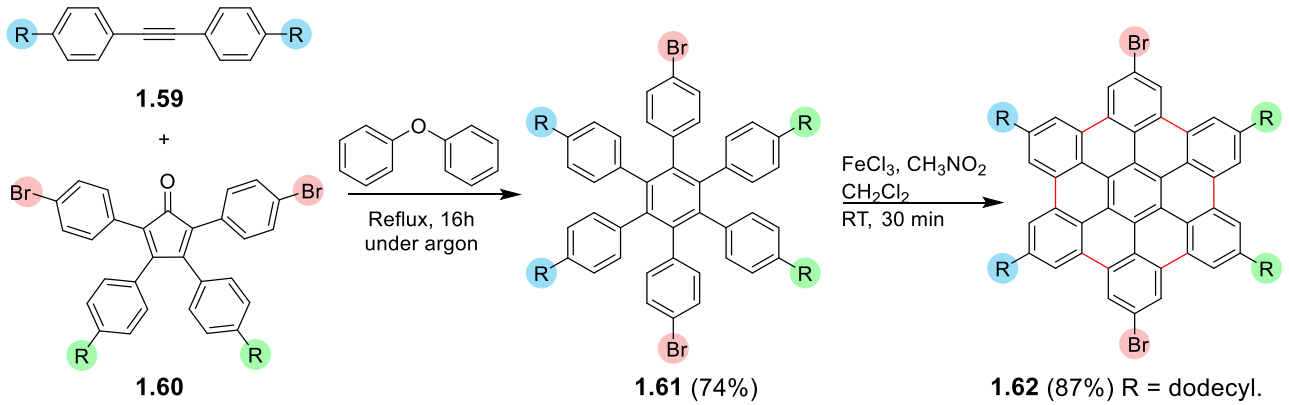

Scheme 19:Formation of **1.62** via Scholl reaction of **1.61** formed by [4+2] cycloaddition.

Ito and co-workers (scheme 19) introduced a novel synthetic strategy for functionalizing HBC derivatives (**1.62**). It is prepared via a Diels-Alder cycloaddition between alkyne (**1.59**) and substituted cyclophentadienone (**1.60**) forming (**1.61**) which undergoes oxidative cyclodehydrogenation obtaining (**1.62**). The bromo substituents serve as versatile handles for Pd-catalyzed couplings, enabling precise electronic tuning while preserving solubility through alkyl

chains.[63] The authors encountered challenges during the Scholl-type cyclodehydrogenation. Formation of chlorinated by-products and inseparable mixtures were observed when adding $FeCl_3$ directly to the precursor solution in DCM. This problem was mitigated by predissolving $FeCl_3$ in nitromethane before addition to the reaction then quenching with methanol to achieve an increase in yield.[63] The solubility of **1.62** in organic solvents at room temperature is relatively low. Hence, the separation was done by column chromatography with hot toluene/petroleum ether.[63]

1.2.2.2 π-extension of Perylene

Building upon substituted cyclopentadienone precursor, Müllen and co-workers (scheme 20) successfully synthesized novel extended perylene (**1.67**) via oxidative cyclodehydrogenation.[64]

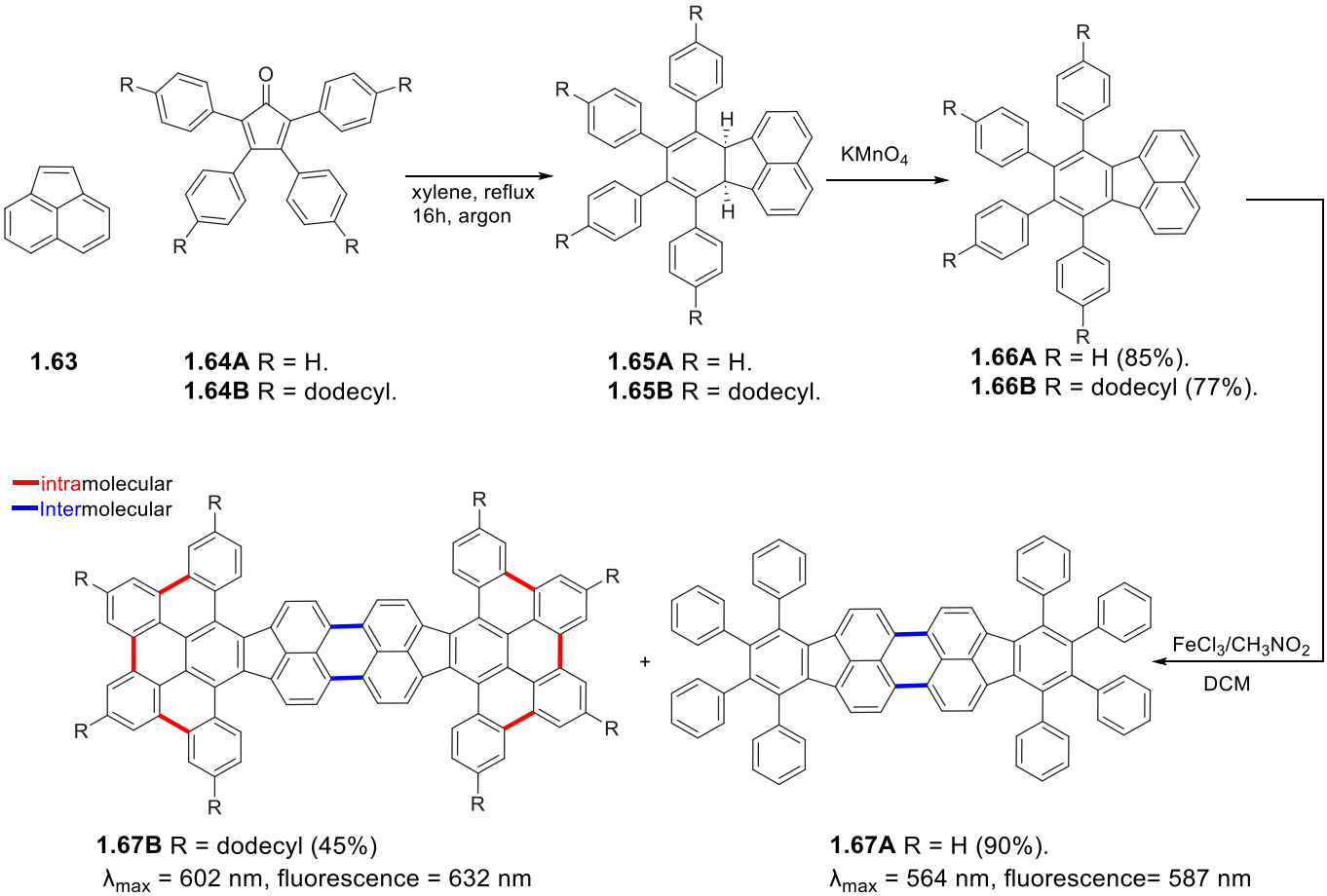

1.63

1.64A R = H.
1.64B R = dodecyl.

1.65A R = H.
1.65B R = dodecyl.

1.66A R = H (85%).
1.66B R = dodecyl (77%).

1.67B R = dodecyl (45%)
λ_{max} = 602 nm, fluorescence = 632 nm

1.67A R = H (90%).
λ_{max} = 564 nm, fluorescence= 587 nm

Scheme 20: Synthesis of Novel extended perylene by Scholl and Diels-Alder reaction.[64]

The precursors (**1.66**) were synthesized by Diels–Alder reaction of substituted cyclopentadienone precursors (**1.64**) with acenaphthylene (**1.63**), followed by $KMnO_4$ to aromatize the ring. The resulting adducts were then subjected to Scholl conditions. The unsubstituted precursor (**1.66A**) underwent intermolecular coupling to give the red dimer (**1.67A**). In contrast, the dodecyl-substituted precursor (**1.66B**) proceeded via both intermolecular and intramolecular cyclodehydrogenation at the peripheral phenyl rings to furnish the dark-green chromophore

(**1.67B**) with a significantly extended planar π-system. A major challenge was unwanted chlorination of the aromatic core under conventional oxidizing conditions. This was suppressed by predissolving $FeCl_3$ in nitromethane and purging the reaction vigorously with argon to remove evolved HCl. The unsubstituted derivatives (**1.67A**) suffered from poor solubility, whereas the dodecyl-substituted analogues (**1.67B**) were readily soluble.

1.2.2.3 π-extension of Chrysene

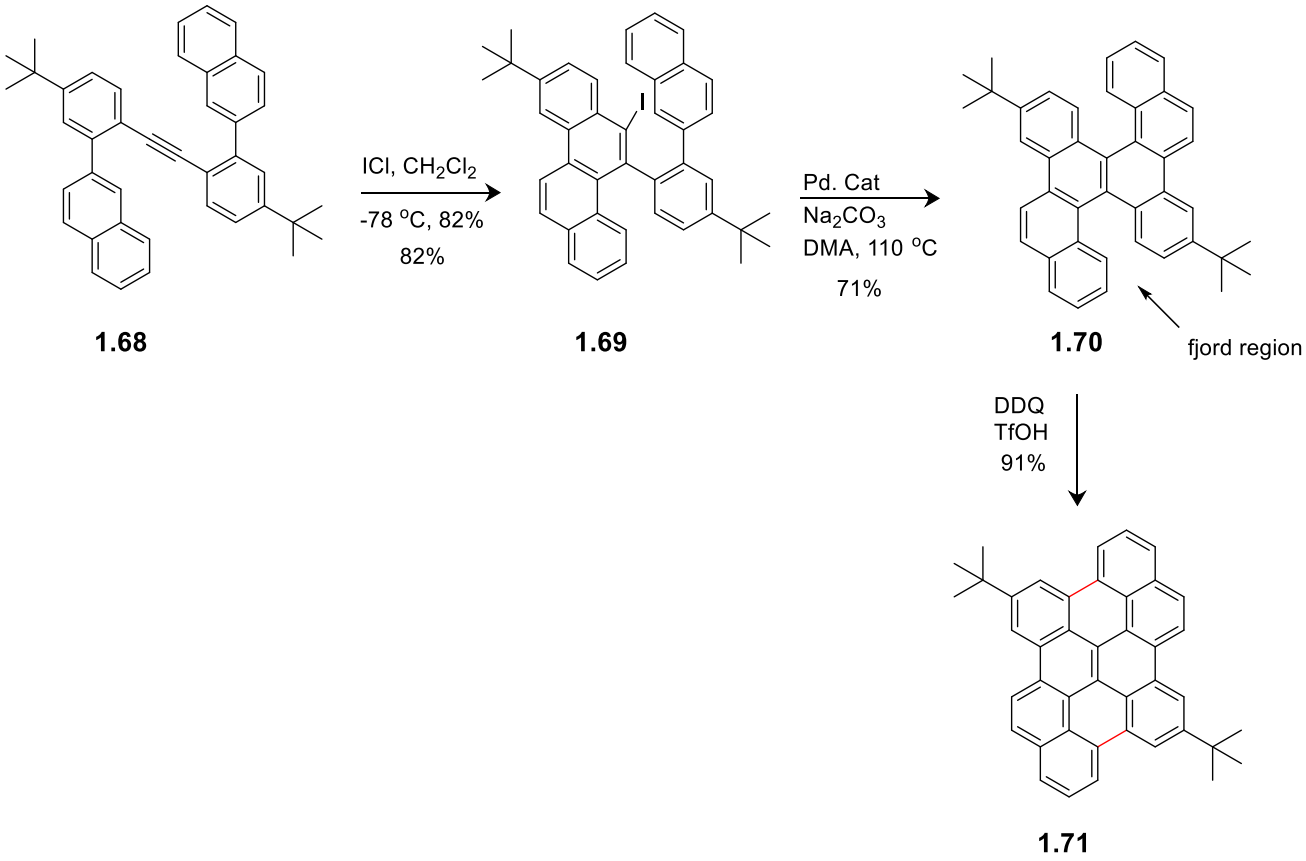

Scheme 21 : Synthesis of dibenzo chrysene derivative.[14]

Chen and Liu developed an efficient synthetic route to access chrysene derivatives as illustrated in scheme 21.[14] The sequence commences with ICl-mediated intramolecular aromatization of bis(biaryl)acetylenes (**1.68**), affording the iodo-substituted intermediate (**1.69)**. This is followed by a palladium-catalyzed Mizoroki–Heck coupling, which involves intramolecular direct arylation via C–H activation under palladium catalysis, furnishing the dibenzo chrysene derivative (**1.70)** in a good yield. The precursor (**1.70)** incorporates two sterically congested fjord regions, resulting in a nonplanar geometry due to significant intramolecular repulsion. However, the non-planarity was resolved by oxidative cyclodehydrogenation of (**1.70)** using DDQ which effects closure of both

fjord regions, delivering the fully planar target PAH (**1.71)** in excellent yield. Photophysical investigations demonstrated significant red shifts upon achieving planarity, the longest absorption maximum shifted from 375 nm in the nonplanar dibenzo chrysene (**1.70)** to 478 nm in the planar PAH **1.71** (Δλ = 103 nm). The reduction in the HOMO–LUMO gap from 2.84 eV (**1.70**) to 2.51 eV (**1.71**), highlights the critical role of molecular flattening in extending effective conjugation and optoelectronic properties.

1.2.2.4 π-extension of Corannulene

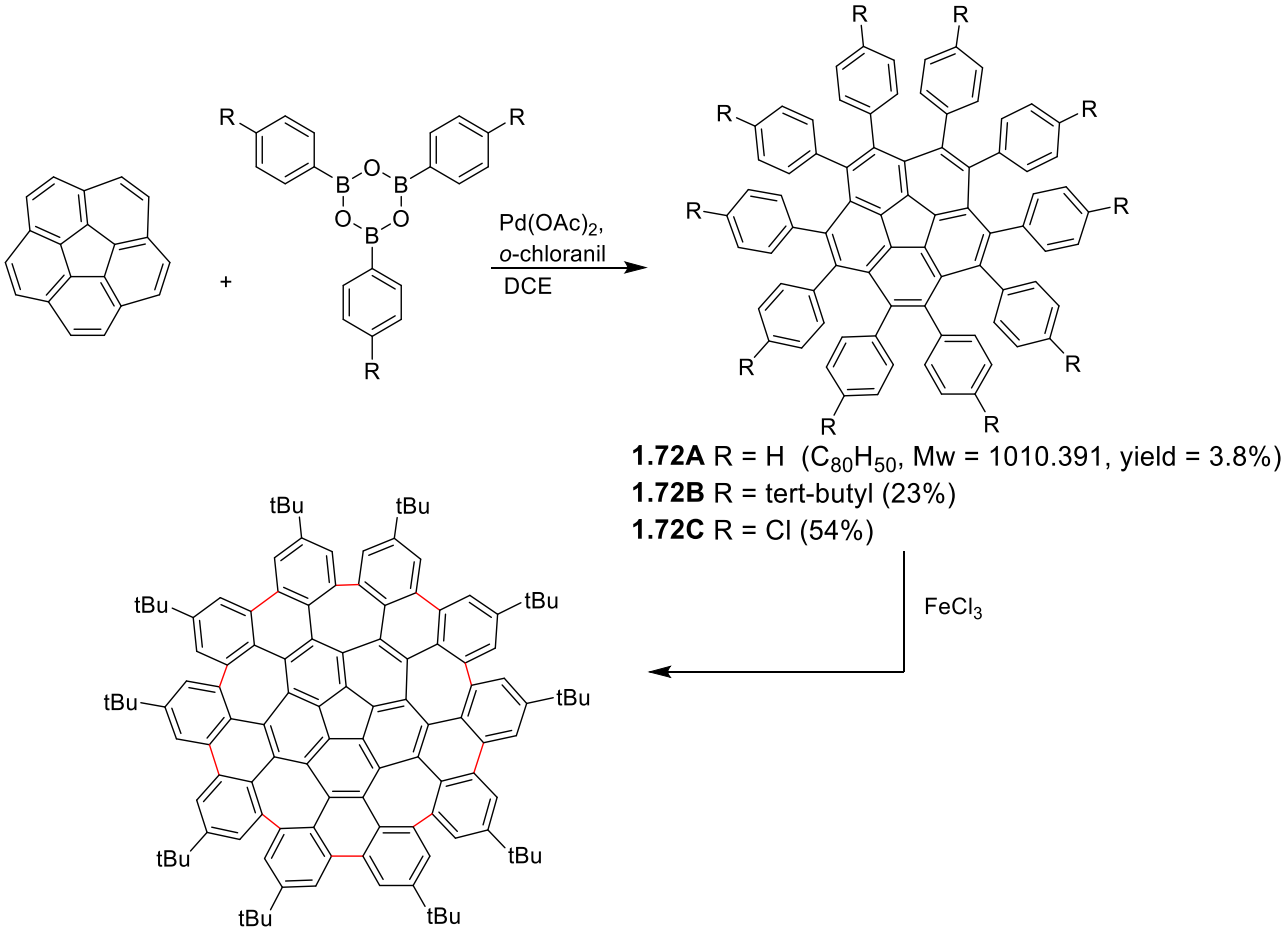
R
R
R

after the second cycle and it only shown with unsubstituted para position of the phenyl group. The over-arylation is suppressed when *tert*-butyl or *p*-chloro substituents are introduced at the para position. Cyclodehydrogenation of the corresponding compound (**1.72B**) with $FeCl_3$ results in the formation of warped nanographenes (**1.73**) in moderate yield.[66] The presence of *tert*-butyl groups on **1.73** further enhances the solubility, rendering the compound even soluble in hexane.

1.2.2.5 π-extension of naphthalene

In 2025, Kivala and co-workers demonstrated (scheme 23) the use of naphthalene as a compact central initiator in the synthesis of a negatively curved nanographene (**1.77**) featuring a Stone–Wales defect.[67]

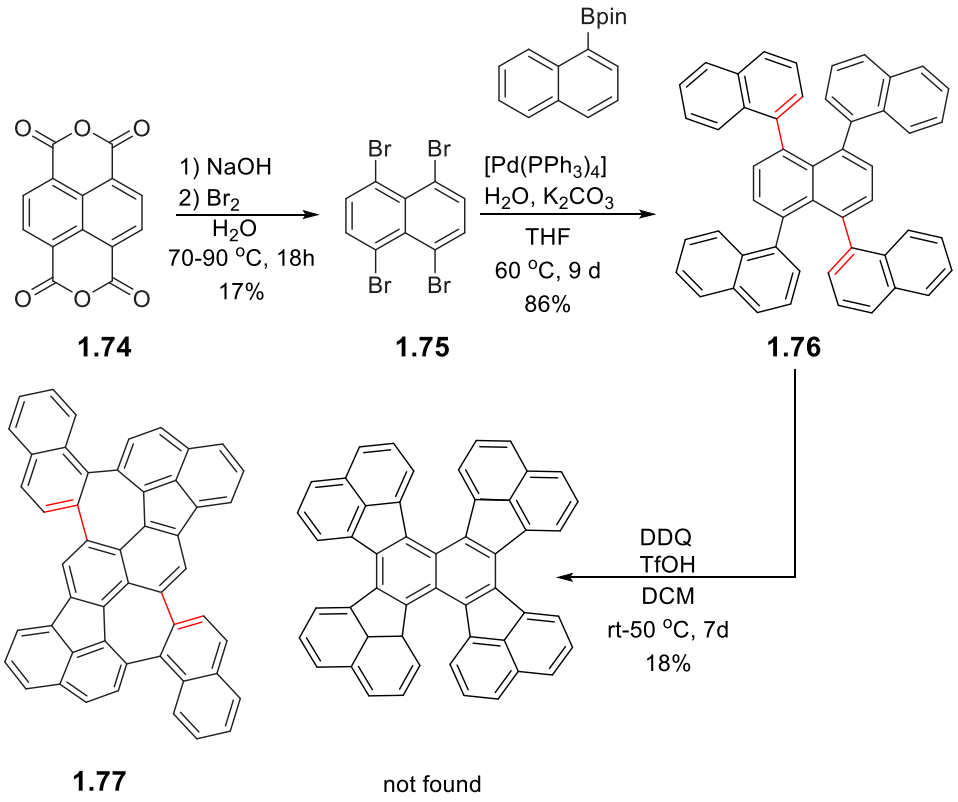

Scheme 23: Synthetic pathway towards nanographene.[67]

Starting from commercially available 1,4,5,8-naphthalenetetracarboxylic dianhydride (**1.74**) it is converted to 1,4,5,8-tetrabromonaphthalene (**1.75**) through a bromodecarboxylation sequence. Fourfold Suzuki–Miyaura cross-coupling of **1.75** with 1-naphthylboronic acid pinacol ester furnished the key precursor tetra(1-naphthyl)naphthalene (**1.76**) in high yield. Subsequent oxidative cyclodehydrogenation of **1.76** under optimized Scholl conditions delivered the target defect nanographene (**1.77**) as a dark-red solid. The authors extensively screened reaction conditions and observed that classical $FeCl_3$-mediated Scholl reactions predominantly produced

chlorinated side products with only traces of the desired compound. In contrast, DDQ/TfOH system at room temperature mainly afforded the 3-fold cyclized intermediate, while heating to 50 °C enabled clean fourfold cyclodehydrogenation. This process was accompanied by naphthyl migration, resulting in the formation of two seven-membered rings. The π-extension is evident from the bathochromic shift in the UV-Vis spectra, with λ_{max} shifting from 335 nm (**1.76**) to 566 nm in the final nanographene (**1.77**).

1.3 Application of Nanographene

Nanographene (NGs) molecules are found in a wide variety of advanced applications. They exhibit a tunable energy bandgap due to quantum confinement which makes them attractive for optoelectronic applications.[68] This effect enables precise control over light absorption and emission colors through adjustment of molecular size and edge geometry. Furthermore, perylene diimide derivatives (PDIs) have been widely investigated as n-type semiconductors in organic field-effect transistors (OFETs), with optimized single-crystal devices achieving electron mobilities as high as 5.0 cm^2/Vs.[69,70] The exceptional photostability and tunable luminescence of nanographene position them as promising candidates for organic light-emitting diodes (OLEDs)[71] and bio-imaging probes[72].

The biological and environmental sectors have also benefited from the unique surface chemistry, high surface area, and excellent photothermal properties of graphene-based nanomaterials, including NGs and graphene quantum dots. In the biomedical field, these materials efficiently convert absorbed near-infrared light into heat, making them promising agents for photothermal therapy (PTT).This approach provides a minimally invasive strategy to selectively target and ablate malignant cancer cells with high spatial precision.[73,74]

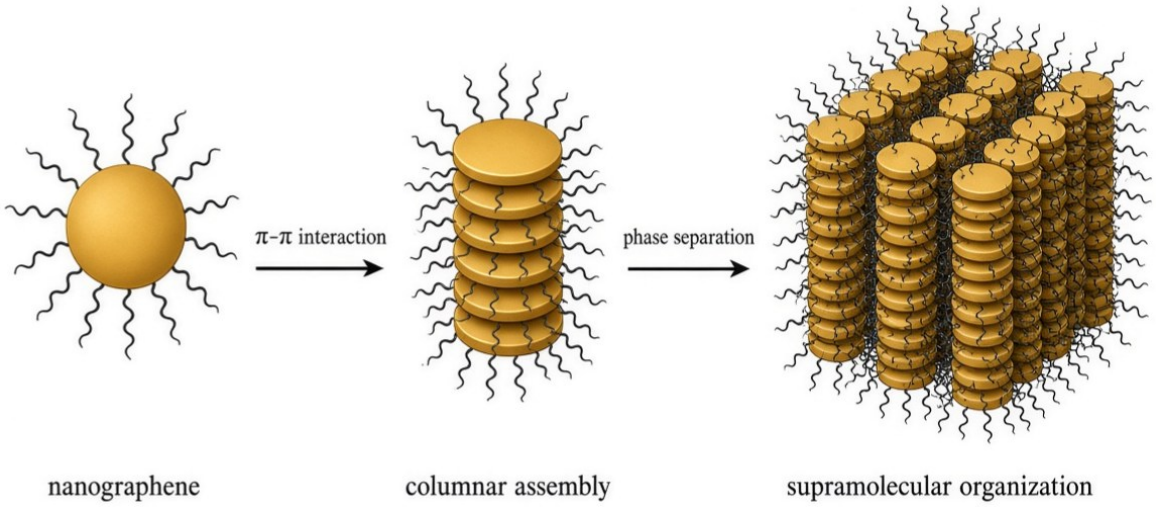

Figure 16: Columnar self-assembly of disc-shaped nanographene molecules.

In the fields of energy storage and quantum technology, NGs have been explored for possible use in high-efficiency devices. The disc-shaped structure of hexa-peri-hexabenzocoronene (HBC) nanographenes, when decorated with alkyl chains, promotes the formation of columnar liquid-crystalline mesophases. These ordered assemblies, as shown in figure 16, create efficient π–π stacking channels that enable one-dimensional charge transport, making HBC derivatives promising materials for organic field-effect transistors (FETs) and photovoltaic devices.[75] They have been investigated as electrode modifiers in lithium-ion batteries and supercapacitors.[76,77] In addition, bottom-up synthesis enables precise doping of these molecules with heteroatoms such as boron or nitrogen.[78] This atomic-level control can modulate the electronic structure and spin states of the NGs. Such structural precision may be relevant for research in spintronics and quantum computing, where open-shell NGs and graphene nanoribbons have been studied as platforms exhibiting magnetic edge states with possible applications as molecular qubits.[79]

2. Results and Discussion

2.1. Aim

As we mentioned, PAHs such as graphene are important in various applications and our group is currently investigating the synthesis of graphene fragments based on staggered anthracene units as illustrated in Scheme 24.

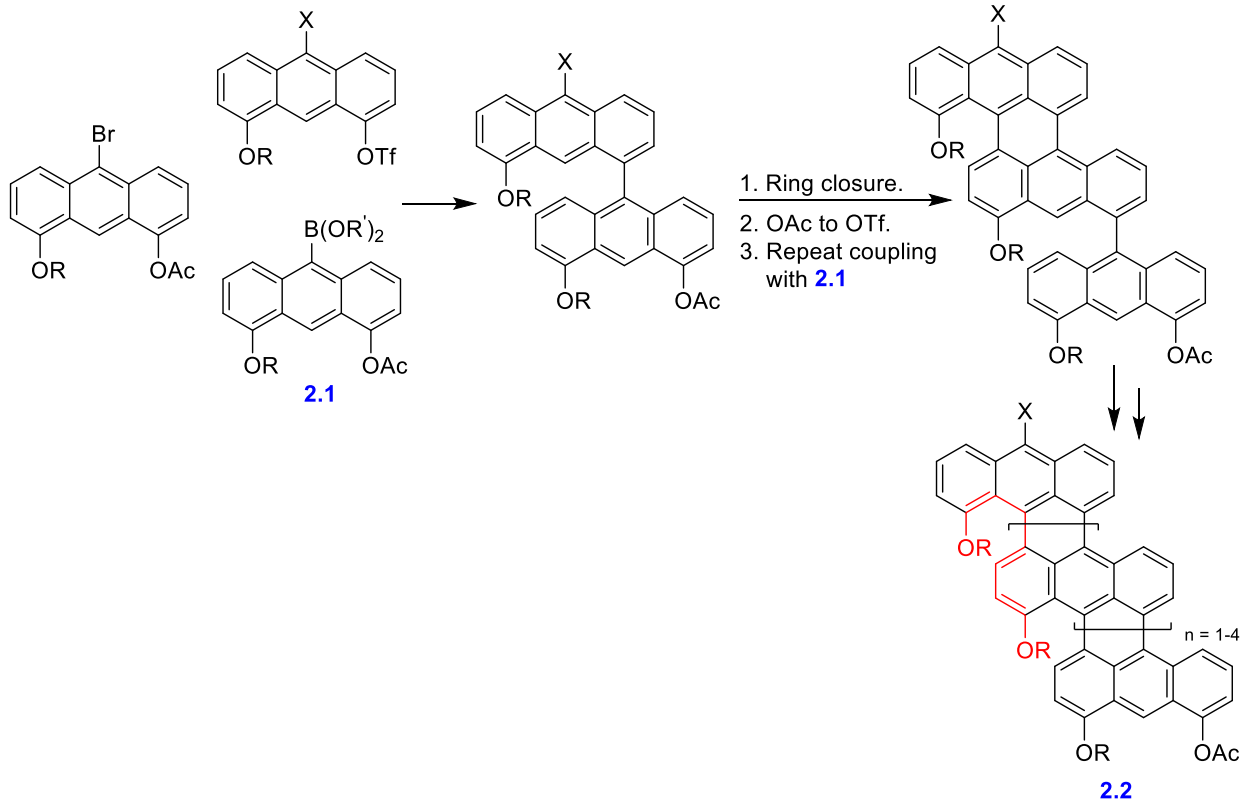

Scheme 24: The synthetic route to staggered fused anthracene units investigated by our group.

The extension of these systems **2.2** (staggered anthracene) in the lateral direction affords sheet-like structures that are single-component graphene fragments. This project aims to assemble such graphene fragments using iterative cascade processes that can be repeated to extend the conjugation as indicated in scheme 25. We will develop the chemistry starting from a small initiator molecule **2.3** which represents the key functionality of **2.2**. Extension will be achieved by using cross-coupling and oxidative cascades as shown in Scheme 25.

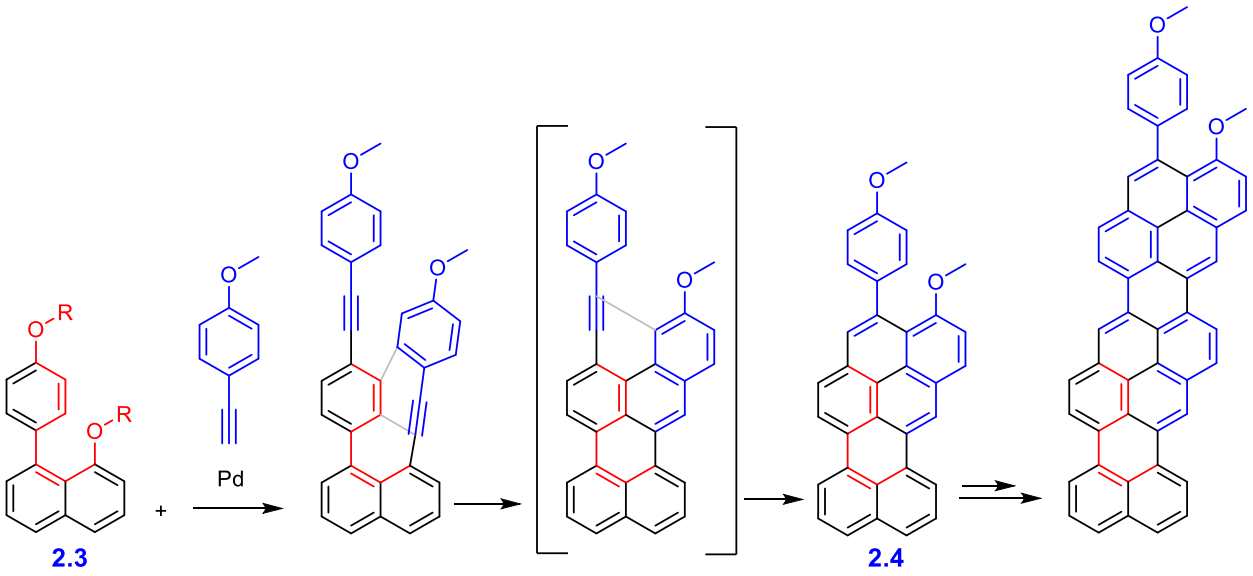

Scheme 25: Extension of the pi-system in a model staggere unit.

The extension approach begins with the proposed pathway outlined in scheme 26. It starts with arylation of 1-naphthol **2.5** at 8-position with 4-iodoanisole **2.6** affording C-8 arylated product **2.7** followed by triflation of the hydroxy group to obtain **2.8**.[80] Coupling between **2.8** and a terminal alkyne will be carried out to give the Sonogashira-coupled product **2.9**. Ring closure will be attempted to cyclize **2.9,** affording **2.10** further reaction aims to produce **2.11**. If the synthesis of **2.11** is achieved, the demethylation of **2.8** by BBr_3 will be carried out followed by triflation (both hydroxyls) and again coupling, hopefully to achieve **2.4**.

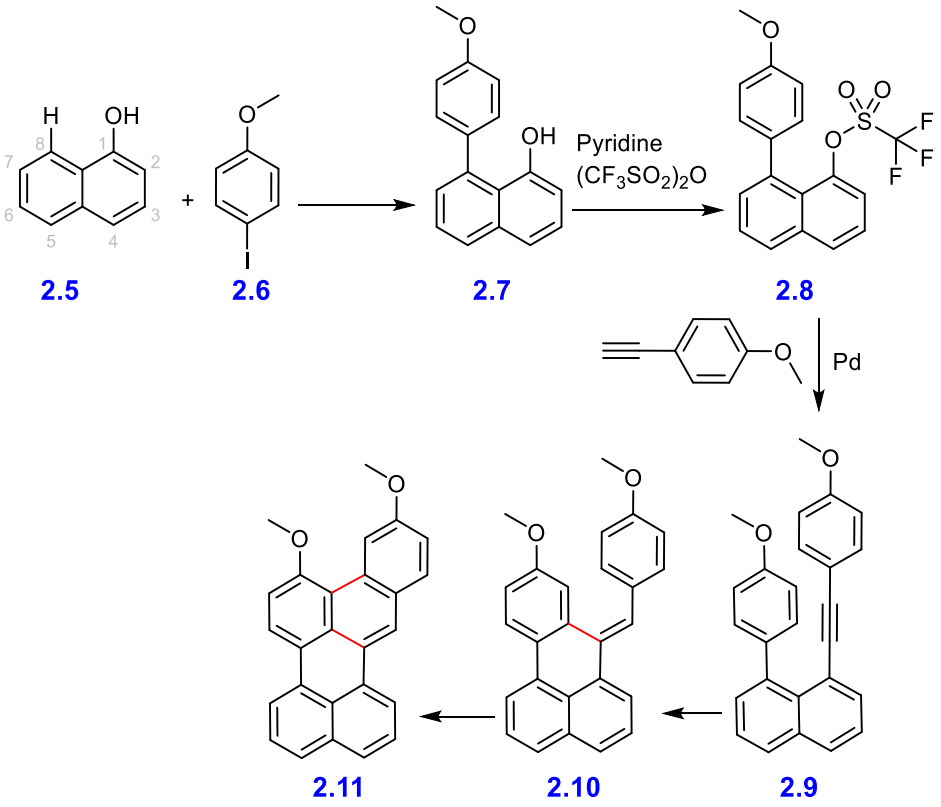

Scheme 26: Proposed synthesis of the extended aromatic system.

2.2 Preparation of 8-(*p*-methoxyphenyl)-1-naphthol. [80]

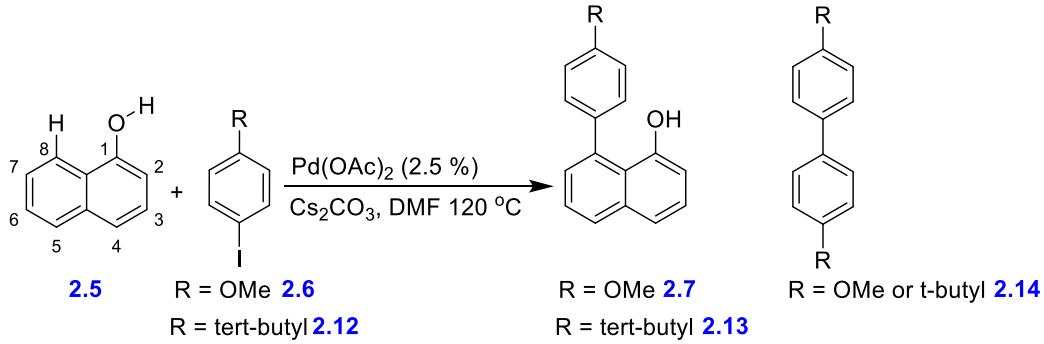

Scheme 27: Synthesis of 8-(p-methoxyphenyl)-1-naphthol.

The project commenced by using reported methodology for arylation of 1-naphthol **2.5** in the 8 position with 4-iodoanisole **2.6** or *p*-iodo(*tert*-butyl) benzene **2.12** as illustrated in scheme 27.[37,80] Consistent with literature reports, the reaction initially afforded a modest yield, and upon repetition, we observed similar results. This modest yield may be attributed to the dryness of Cs_2CO_3, because we observed that when the reaction was executed under dry conditions, the yield increased significantly to 75% and 82% for **2.7** and **2.13** respectively (Entry 4,5, Table 1). Cs_2CO_3 was dried at 100 °C under vacuum for 2 hours, then placed under N_2 and at room temperature. The reagents 4-iodoanisole **2.5**, 1-naphthol **2.4**, and $Pd(OAc)_2$ were added under N_2 then placed under vacuum for 1 hour before the addition of solvent. The product **2.13** is achieved by addition of 4-iodo(*tert*-butyl) benzene **2.12** and solvent after degassing 1-naphthol **2.5**, and $Pd(OAc)_2$. Entries 1,2 were performed without drying whereas entry 3 was conducted in a glovebox.

Entry	2.5 (mmol)	Aryl iodide (mmol)	Base (mmol)	DMF (mL)	Reaction time (h)	Catalyst	Yield (%)	
							2.7	2.13
1	3	2.6 (3.4)	Cs_2CO_3 (5)	5	17	$Pd(OAc)_2$ 5%	6	
2	3	2.6(3.4)	Cs_2CO_3 (5)	5	19	$Pd(PPh_3)_2Cl_2$ 5%	15	
3[a]	3.4	2.6(5)	Cs_2CO_3 (3.4) CH_3COOK (3.4)	5	48	$[Ru(COD)Cl]_2$ 5%	19	
4[b]	3	2.6(4)	Cs_2CO_3 (4)	15	23	$Pd(OAC)_2$ (2.5 %)	75	
5[b]	3	2.12(4)	Cs_2CO_3 (4)	15	26	$Pd(OAC)_2$ (2.5 %)		82

Table 1:Optimization of the synthesis of **2.7** and **2.13**.[a] in glove box. , [b] drying Cs_2CO_3 and reagents.

The ^{1}H NMR spectrum of compound **2.7** (Figure 17) is consistent with the reported literature.[37,80] Spectra of compounds **2.7** and **2.13**, also shown in Figure 4, display the expected number of proton signals, including those corresponding to the methoxy, hydroxy, and *tert*-butyl group.

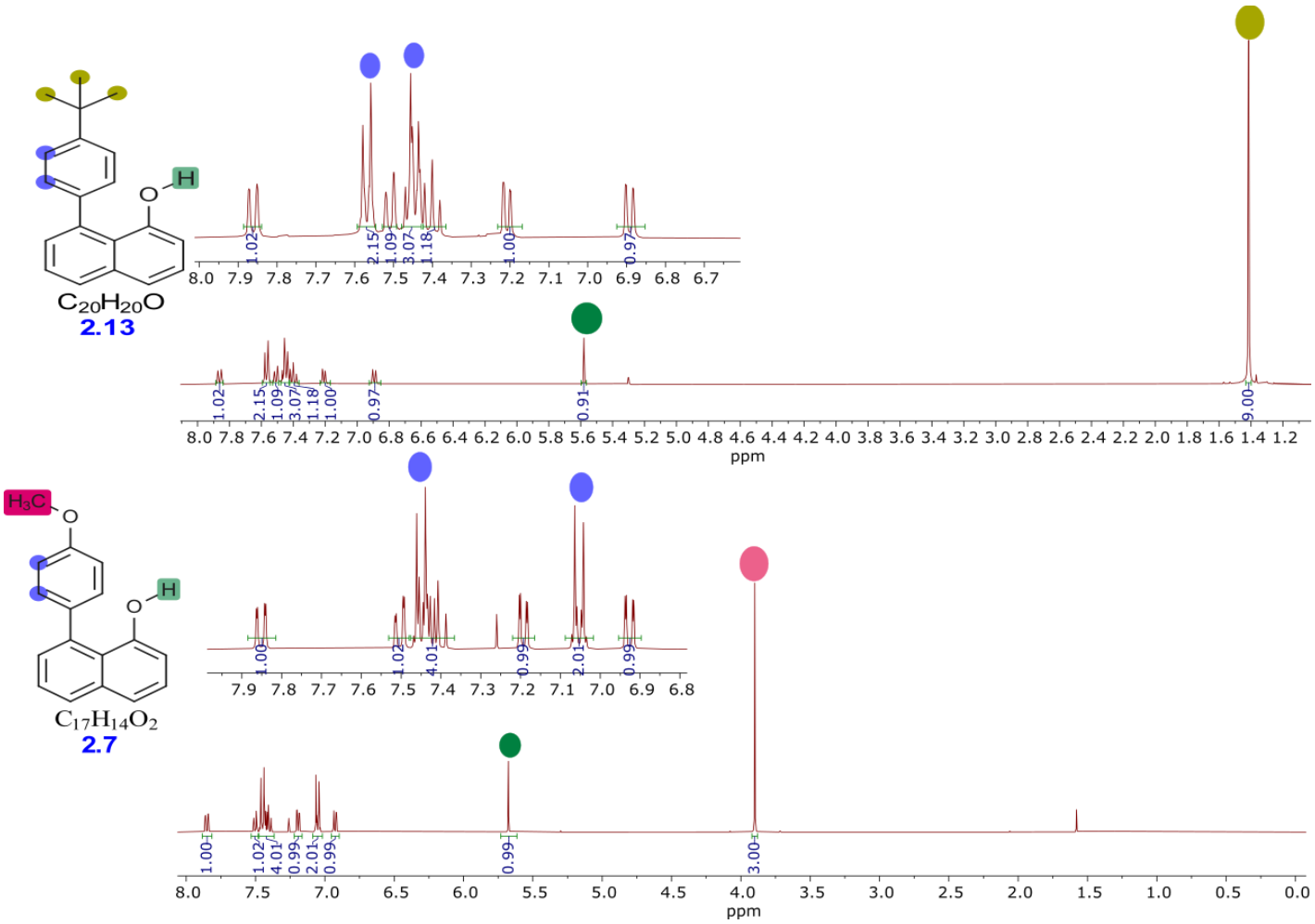

Figure 17; The ^{1}H-NMR spectra for **2.7** and **2.13**.

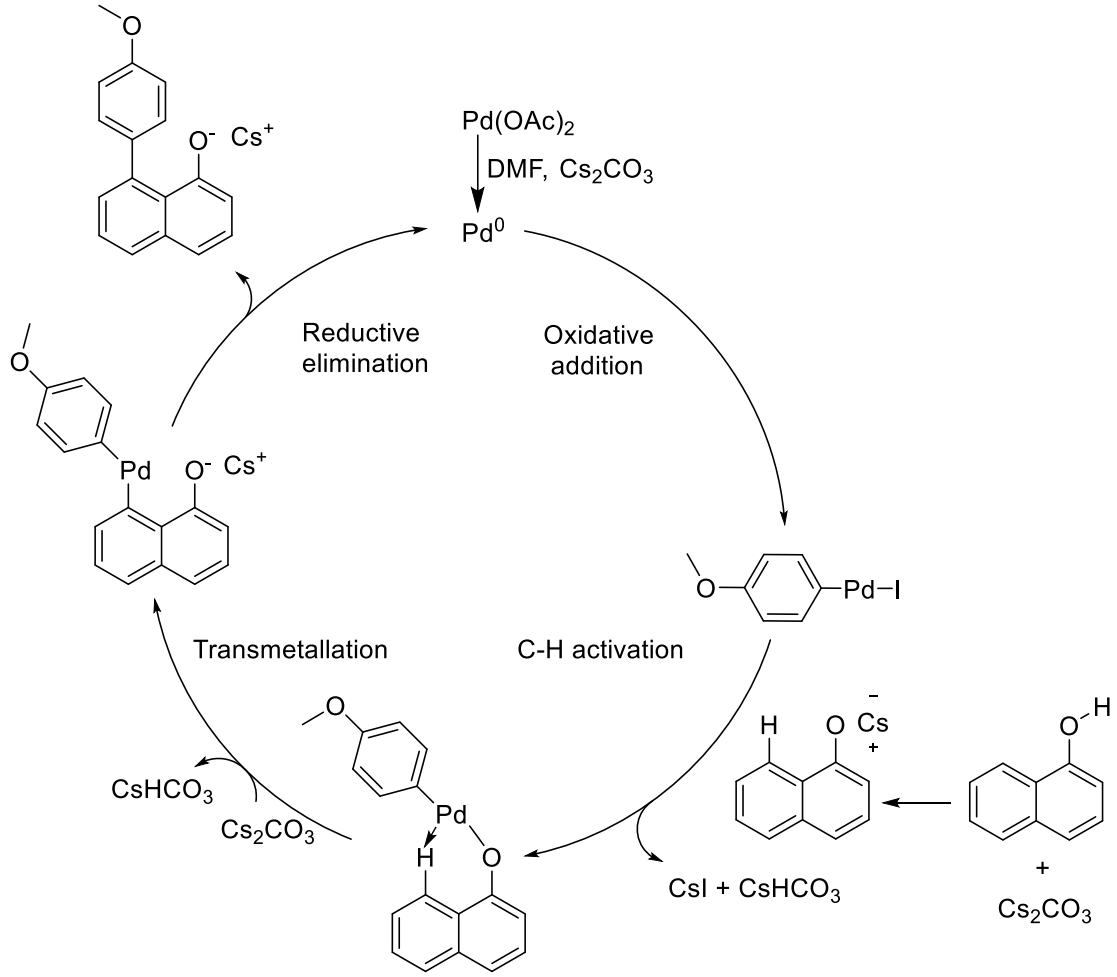

Scheme 28: Possible reaction mechanisms for cross-coupling aryl iodides with 1-naphthol affording arylated product in 8 position.

A postulated mechanism for the formation of arylated product **2.7** in the 8 position is illustrated in scheme 28. The first step is the oxidative addition of the aryl iodide to palladium (0) species, which is generated in situ, followed by a reaction with a 1-naphtholate, forming aryl(1-naphtholoxy) palladium intermediate. Then it may transfer into diary palladium species followed by reductive elimination giving the monoarylated product.

2.3 Synthesis and reactivity investigation of 8-(*p*-methoxyphenyl)-1-naphthol

In this section, we will demonstrate the preparation of **2.8** and investigate the reactivity of **2.7**.

2.3.1 Triflation of 8-(*p*-Methoxyphenyl)-1-naphthol

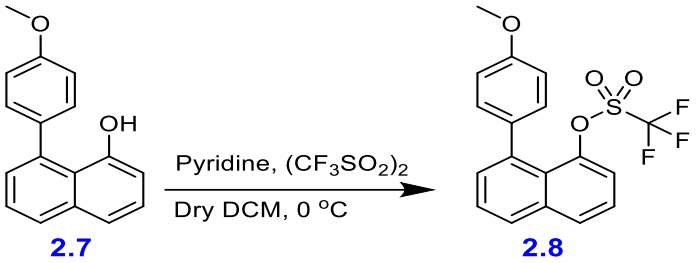

2.7 **2.8**

Scheme 29 The chemical equation for the triflation of **2.7**.

The triflation of **2.7** was achieved by reaction with triflic anhydride in DCM/pyridine at 0 °C. The triflate product **2.8** is formed as a white solid, yielding 52%. Both **2.7** and **2.8** were dissolved in acetone-d_6 for ^{1}H NMR comparison. Figure 18 depicts the x-ray structure of **2.8** and shows the ^{1}H NMR spectrum of **2.7** before and **2.8** after the triflation, which demonstrates the spectra in the aromatic region showing 11 protons, 10 correlate to aromatic protons, and 1 to OH. The OH singlet disappears after triflation. Both **2.7** and **2.8** show methoxy protons around 3.8 ppm.

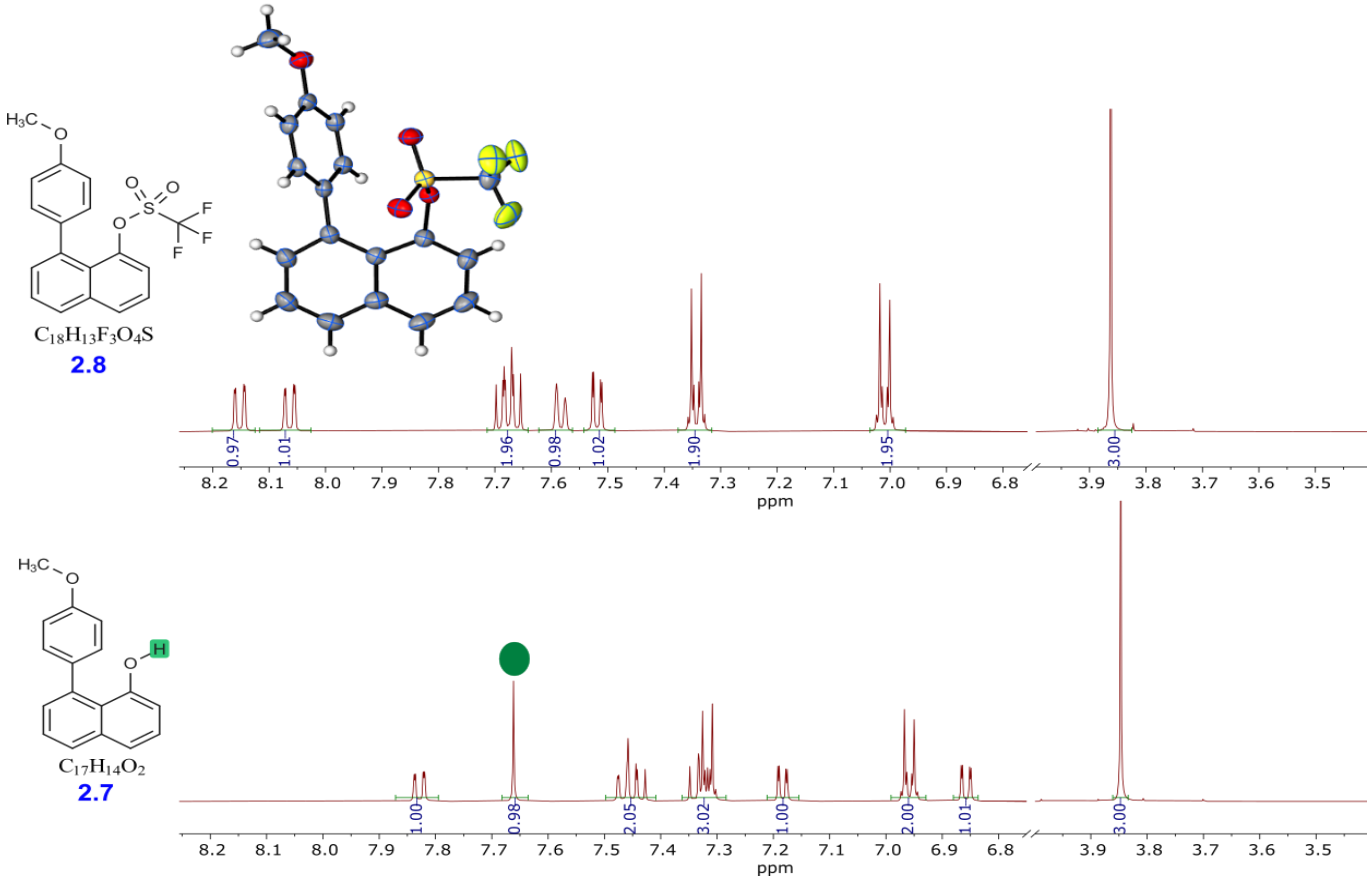

Figure 18: Products **2.7** and **2.8** after triflation in Acetone-D.

2.3.1.1 Reactivity investigation of **2.7**

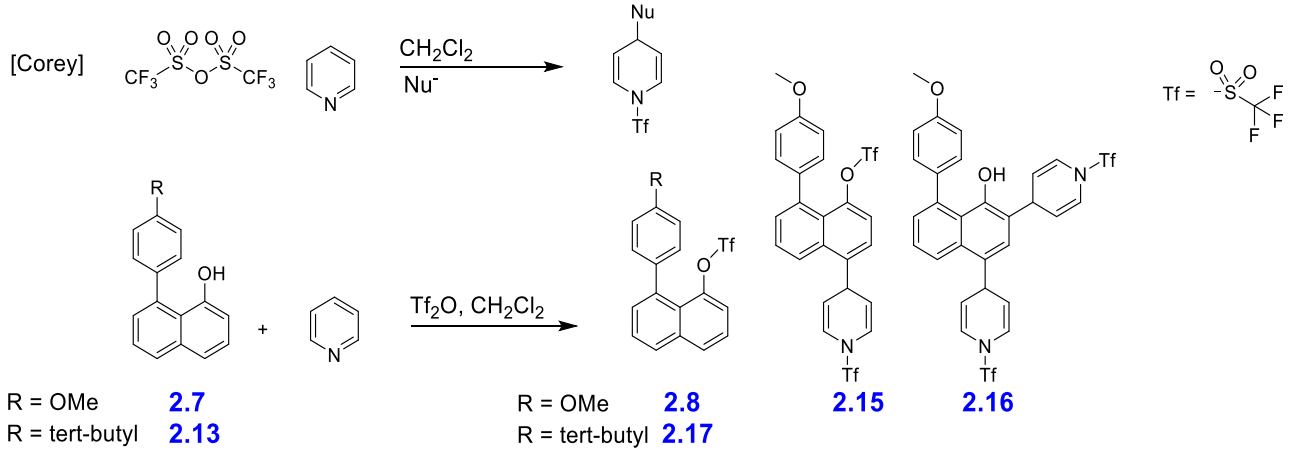

Scheme 30: The activation of the 4-position of pyridine.

The triflation of **2.7** was repeated with different conditions, attempting to increase the yield of **2.8**, which is summarized in Table 2. Under the conditions in entries 1 and 2, three side products were detected by TLC. Generally, the triflation process involves using triflic anhydride and pyridine as a base and nucleophilic catalyst. Pyridine can also react in a separate process as demonstrated by Corey as shown in Scheme 30. The 4-position of pyridine is activated to nucleophilic attack, while positions 2 and 6 are sterically screened by the bulk of the CF_3SO_2 group.[81] Therefore, a nucleophilic attack at the 4-position of pyridine is possible. The two side products result from activation of the ortho and para positions of **2.7** to N-activated pyridine forming **2.15** and **2.16**. Using 2,6-lutidine (Entry 4, Table 2) resulted in a slight increase in the yield of compound **2.8** to 56%, and **2.17** to 28%, whereas more sterically hindered base, 2,4,6-collidine (Entry 5, Table 2), further improved the yield of **2.8** to 62%. However, to drive the reaction to completion if 2,4,6-collidine is used, two sequential additions of 3 equivalents each of 2,4,6-collidine and triflic anhydride were required to drive the reaction to completion.

Entry	2.7	Base (equiv.)	$(CF_3SO_2)_2O$	Yield (%)			
				2.8	**2.15**	**2.16**	**2.17**
1	1 eq	Pyridine (3)	3 eq	52%	6%	7%	
2	1 eq	Pyridine (6)	6 eq	29%	6.5%	1%	
3	1 eq	Et_3N (1.5)	1.5 eq	20%	Mixture	Mixture	
4	1 eq	2,6-lutidine (3)	3 eq	56%			28%
5	1 eq	2,4,6-collidine (3)	3 eq	62%			

Table 2: The optimized conditions for **2.8** formation.

Figure 19 shows a comparison of ^{1}H NMR spectra between **2.8** and **2.15**, **2.16**. The overall integration of compound **2.15** shows 17 protons, 5 of which are attributed to (hydro) pyridine. In contrast, compound **2.16** shows 22 protons, with 10 assigned to hydro pyridine, as indicated by the color annotations.

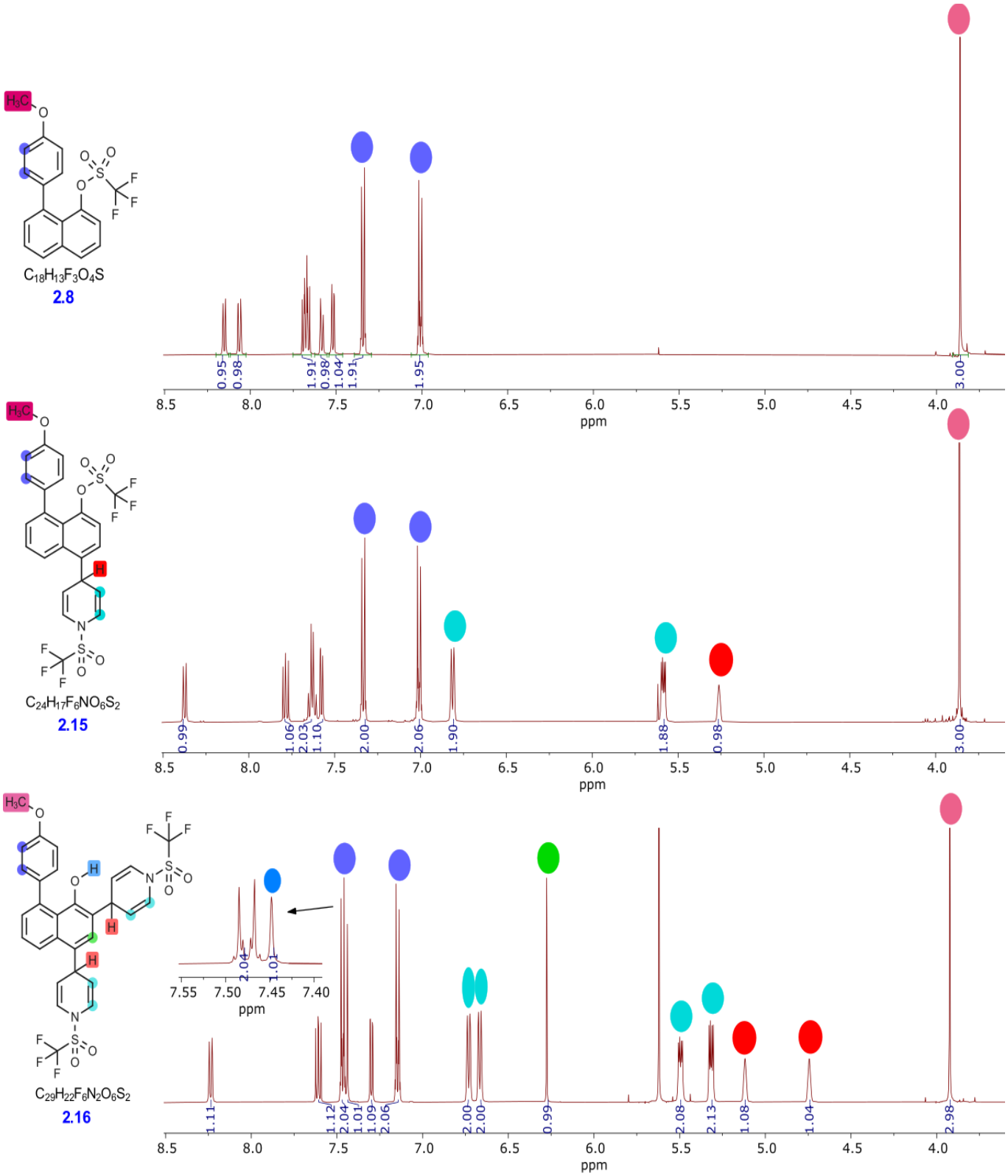

Figure 19: The ^{1}H NMR spectra of **2.8** and **2.15**, **2.16.**

The pyridine derived protons were identified with the assistance of COSY as illustrated in Figure 20.

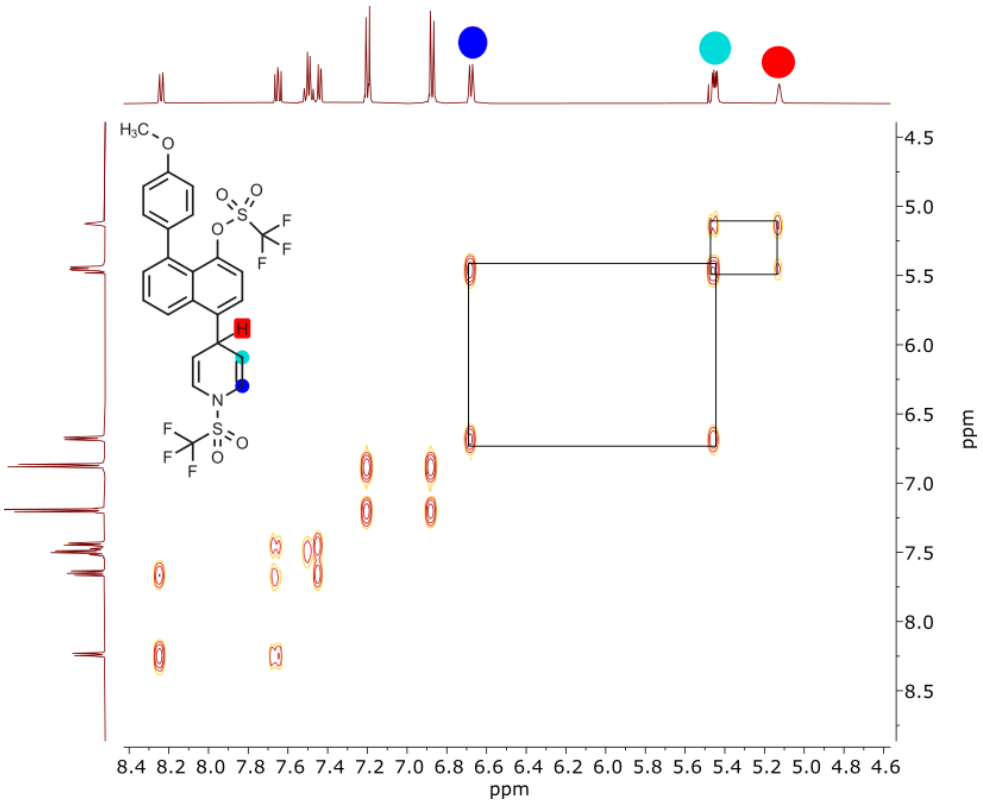

Figure 20: The COSY spectrum of **2.15**.

The conversion of compound **2.15** into **2.18** was investigated using three bases as shown in scheme 31. TLC analysis revealed that treating **2.15** with 2.5 equiv. of DBU in DMF at 120 °C for 30 minutes led to the formation of **2.18**. However, prolonged reaction time resulted in further transformation of **2.18** into compound **2.19**, indicating that the reaction becomes uncontrollable. Treatment with a 1 equiv. of KOtBu in DMSO at room temp. for 10 minutes resulted in the rapid elimination of the triflyl (-Tf) group from N-pyridine and oxygen **2.19**. In contrast, using 5 equiv. of K_2CO_3 in 5 mL of DMF, stirring at room temperature for approximately 36 h, selectively converted **2.15** to **2.18**, yielding 67%.

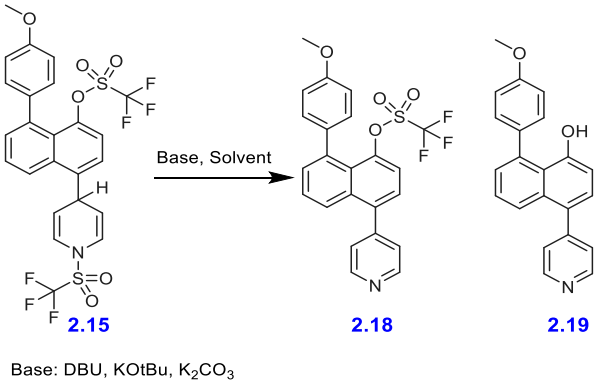

Scheme 31: The effect of the bases on triflate **2.15**.

Compound **2.16** gave suitable crystals for X-ray diffraction analysis (Figure 21). In contrast, product **2.15** formed small, white, needle-like crystals that were too small for such analysis. However, conversion of **2.15** into compound **2.18** produced crystals appropriate for structural analysis (Figure 22), thereby confirming the structure. The X-ray structures of **2.16** and **2.18** were solved by our collaborator Dr David Hughes, and his comments can be found in the appendix.

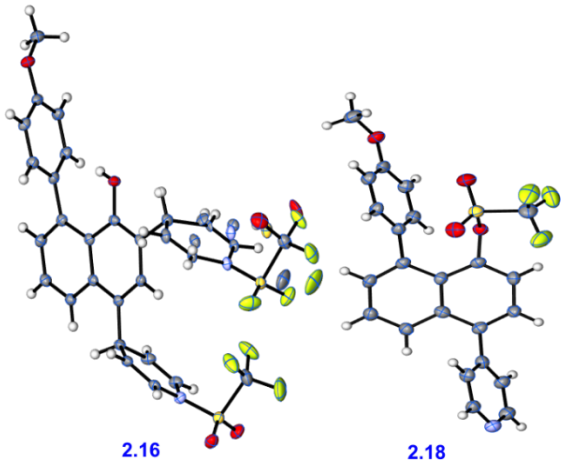

Figure 21: The x-ray structure of **2.16** and **2.18**.

The mechanism of formation of **2.16** is illustrated in scheme 32. After the insertion step of pyridine in the para position, the hydroxy group gets triflated, explaining the formation of **2.16**.

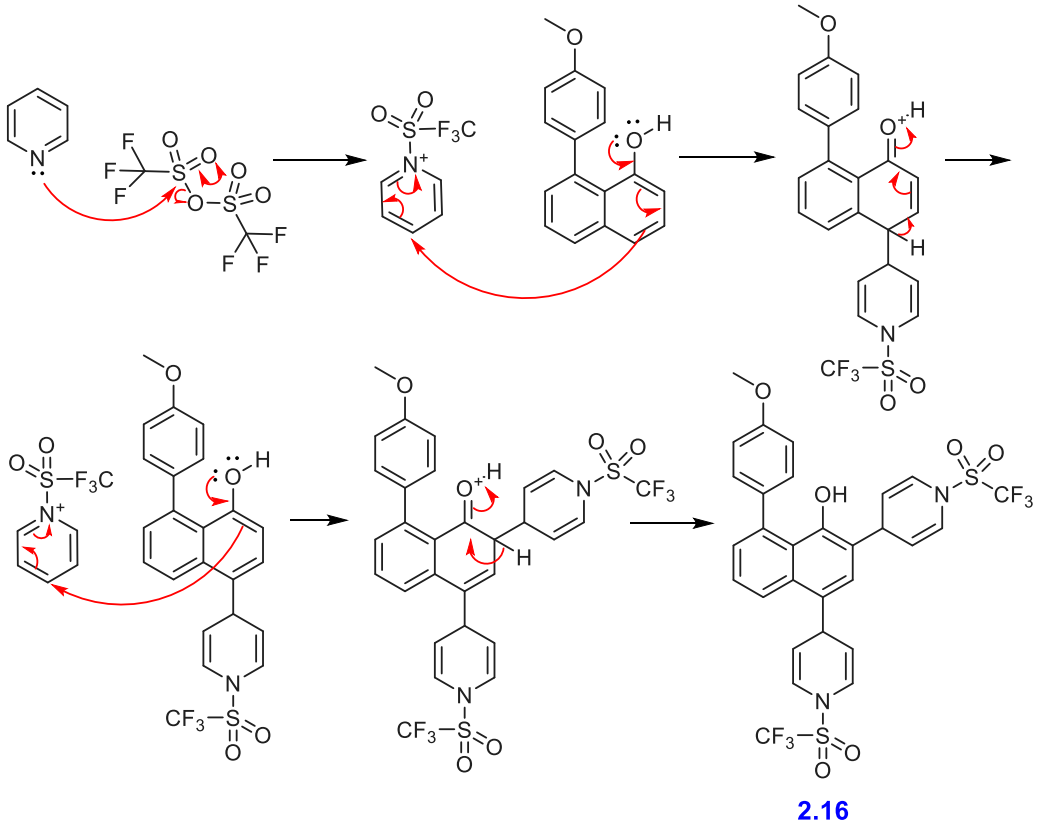

Scheme 32: The mechanism of formation of **2.16**.

Treating pyridine with triflic anhydride not only causes the N-activated pyridine to undergo a nucleophile attack but also forms an azatriene intermediate "Zincke imine," which comes from a ring opening of pyridine.[82] These intermediates are polarized alkenes that undergo electrophilic substitution reactions. We separated a trace amount of this third side product due to its pink colour. Figure 22 demonstrates the identification of **2.20** by assistance of X-ray crystallography, and HRMS confirms its molecular ion peak at 500.1155 corresponding to [M+H].

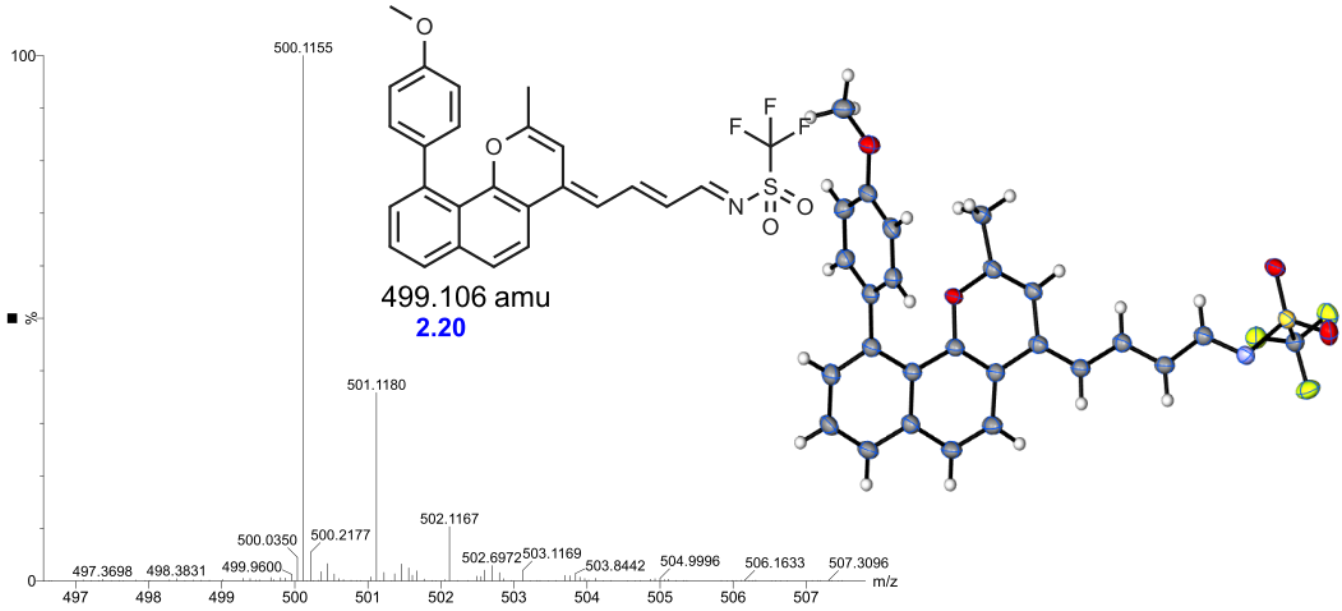

Figure 22: The x-ray structure and HRMS for **2.20**.

The extra carbons and hydrogen could come from a trace of acetone during work-up, as it forms an enol in an acidic environment. The enol form may attack the polarized alkenes of pyridine, causing the formation of pyran **2.20**. The proposed formation of **2.20** is illustrated in Scheme 33.

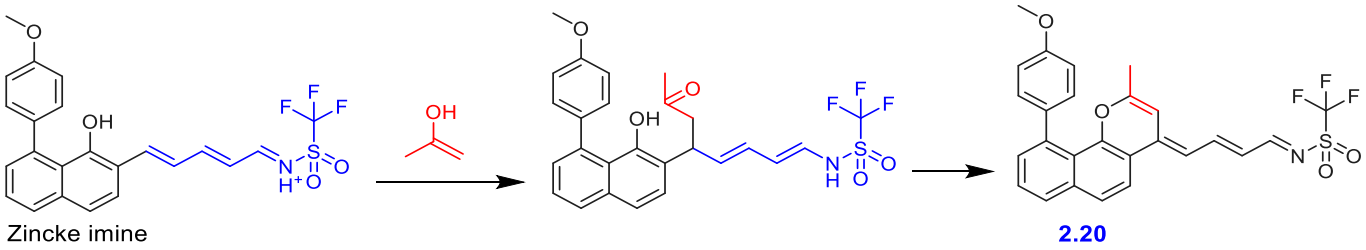

Scheme 33: The proposed formation of **2.20**.

The addition of 5 mL of dry acetone dropwise to reaction mixture prior to work-up lead to formation of compound **2.20**. The direct isolation of compound **2.20** after the work-up forms a traceable amount while stirring for 21 h increased the yield to 4%. Product **2.20** was crystallized from DCM, forming a red needle that was filtered cold. Compound **2.20** is unstable in alcohols, and it decomposes (losing the pink colour). Figure 23 presents the absorption spectra of the arylated product **2.7** and the triflation products (**2.8**, **2.15**, **2.16**, **2.18**), which exhibit absorption bands primarily in the 300–350 nm range, characteristic of moderately conjugated naphthol-based

systems. In contrast, compound **2.20** displays a markedly red-shifted absorption extending up to 546 nm. Fluorescence emission from **2.20** occurs at ~597 nm, whereas the others (**2.7, 2.8**, **2.15**, **2.16**, **2.18**) emit in the 380–450 nm range, consistent with the blue-shifted fluorescence typically observed in less conjugated naphthol derivatives.

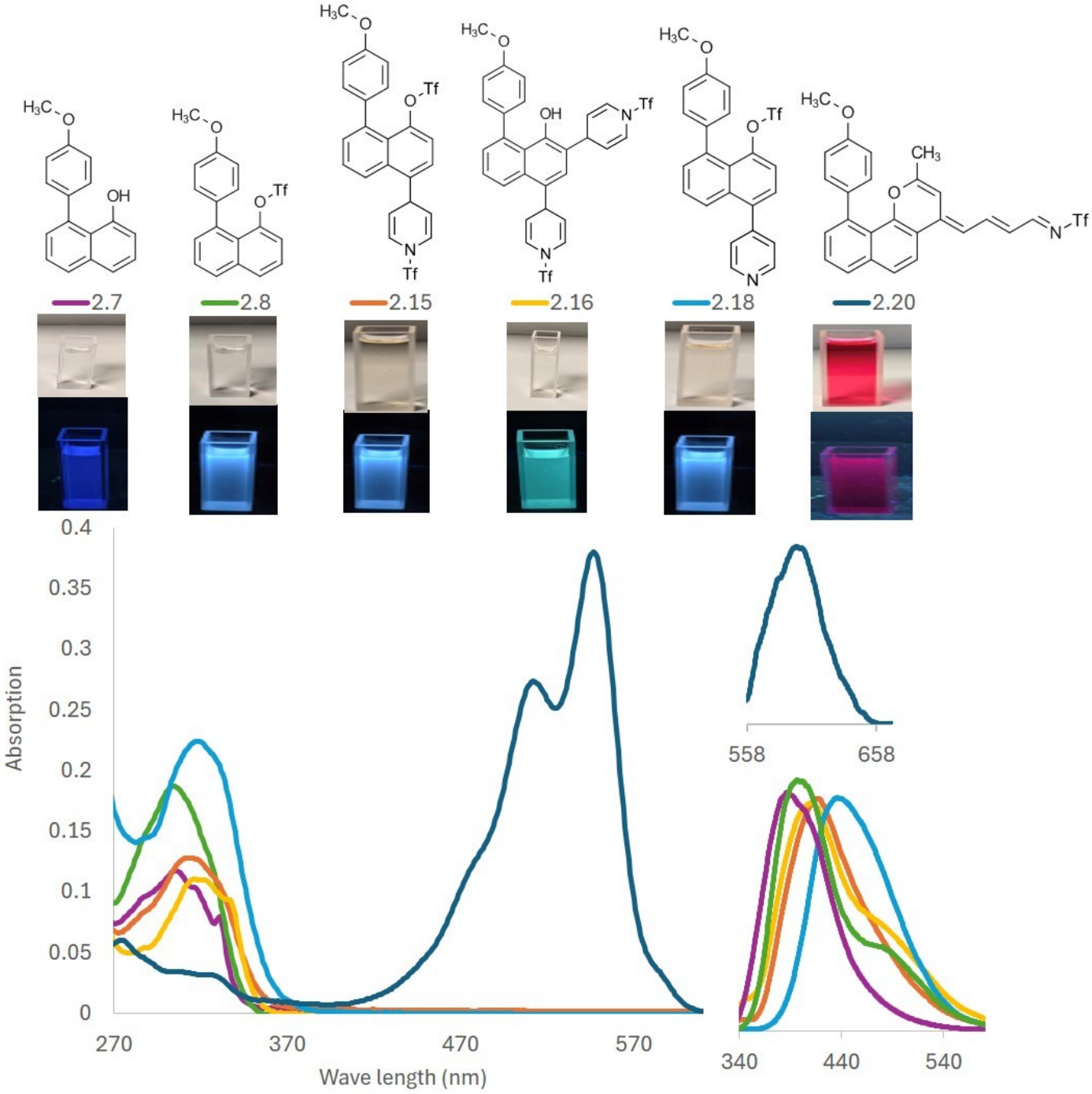

Figure 23: UV-vis absorption and emission spectra of triflated products **2.8**, **2.15**, **2.16**, **2.18**, **2.20**.

2.3.2 Reactivity test of **2.7** toward bromination

In the previous triflation process, we observed the activation of the ortho and para positions of **2.7** toward electrophilic attack. Since the project focuses on bottom-up synthesis from one direction, the para position of **2.7** is useful if bromine is introduced because extension from two directions is possible. Bromination of **2.7** at the para position is straightforward, whereas the ortho position is challenging. The bromination of the para position was successfully achieved under N_2, using 1.1 equivalent of NBS, affording **2.21** in 54% yield (Entry 1, Table 3). In contrast, employing 4 equivalents of NBS (entry 3) to brominate the ortho position, resulted in the formation of a complex mixture. When the reaction was conducted under air, compound **2.22** was obtained as the major product 24%. ^{1}H NMR spectra and X-ray analysis (Figure 24) confirm the structure of **2.21** and **2.22**.

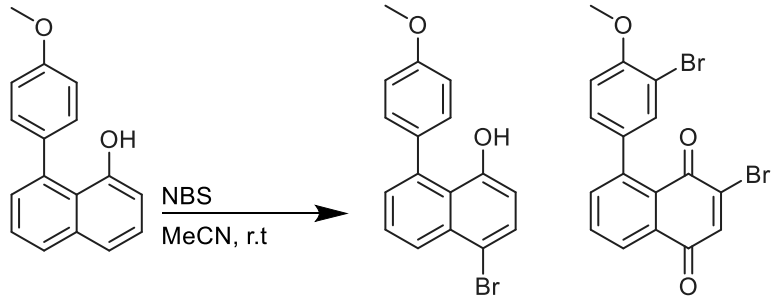

2.7 **2.21** **2.22**

Entry	NBS (equiv)	Condition	Yield	
			2.21	**2.22**
1	(1.1)	under N_2	52%	
2	(4)	under air		24%
3	(4)	under N_2	Mixture	

Table 3: Bromination of 1 eq of **2.7** with different equivalents of NBS at room temperature for 21h.

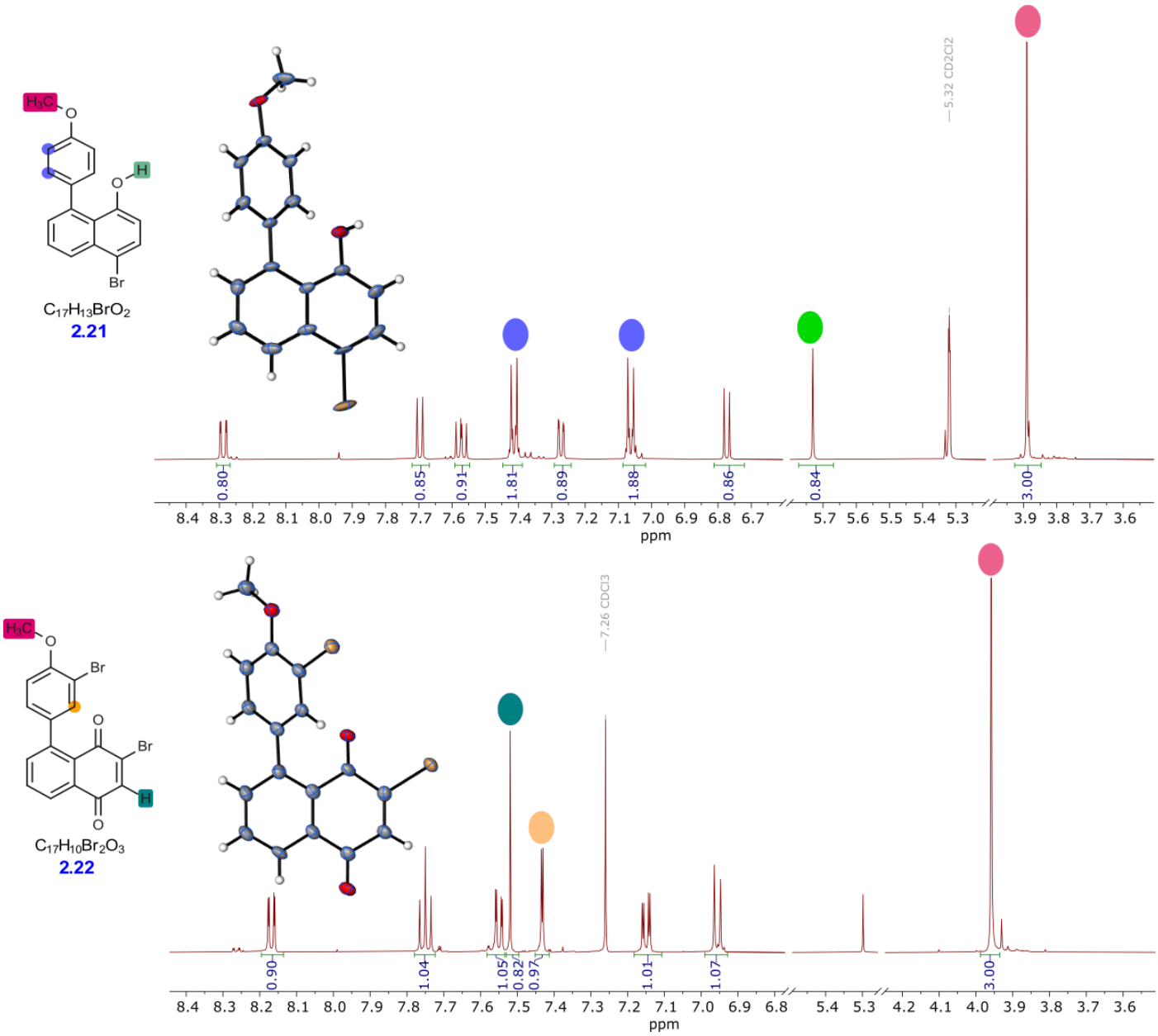

Figure 24: The X-ray structure and ^{1}H NMR spectra of a brominated product **2.21**, **2.22**.

2.4 Synthesis of **2.9** by using Sonogashira coupling reaction

2.4.1 The intramolecular cyclization in Sonogashira coupling

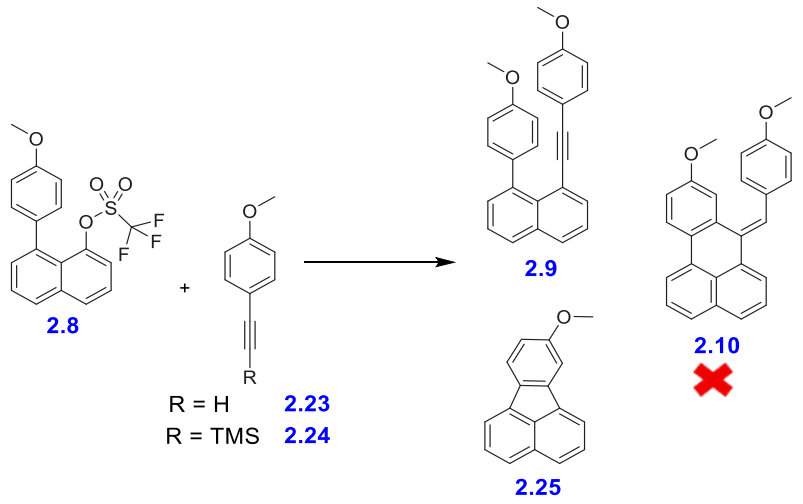

Scheme 34 Formation of coupling product.

Sonogashira cross coupling reaction as illustrated in Scheme 34 is the next preformed step between triflate **2.8** and a terminal alkyne.

Entry	2.8	Alkyne (eq)	Base (eq.)	Catalyst	Temp.	Yield		
						2.9	**2.10**	**2.25**
1[a]	1 eq	**2.23** (2.6)	2.5 eq (DBU)	$Pd(MeCN)_2Cl_2$ (2%) BINAP (4%)	120 °C	9%		62%
2	1 eq	**2.24** (2)	2.5 eq (DBU)	$Pd(MeCN)_2Cl_2$ (2%) BINAP (4%)	80 °C	2%		85%
3	1 eq	**2.23** (2.5)	6 mL (Et_3N)	$Pd(PPh_3)_2Cl_2$ (7%) CuI (14%)	r.t => 80 °C	30%		

Table 4 Optimization condition for the formation of **2.9**. [a] Microwave condition.

Table 4 shows the conditions used to perform the coupling between **2.8** and **2.23** or **2.24**. Entry 1 was initiated by charging a microwave vial with 1 equivalent of **2.8** along with the other reagents. The reaction mixture was purged with nitrogen and irradiated at 120 °C for 4h, TLC analysis indicated complete consumption of the alkyne **2.23**, while a significant amount of unreacted **2.8** remained. To drive the reaction to completion, an additional 0.5 equivalent of **2.23** was added, and the mixture was subjected to 3 h irradiation. TLC monitoring showed the consumption of **2.8**. After the work-up and purification, the intramolecular product **2.25** (62%) and **2.9** (19%) were formed

whereas **2.10** was not observed. According to TLC, the fluoranthene product **2.25** formed after the first 1h of irradiation. The ^{1}H-NMR spectra of **2.25,** as shown in Figure 25, matches the reported spectrum, and we confirmed its molecular structure by x-ray analysis.[80]

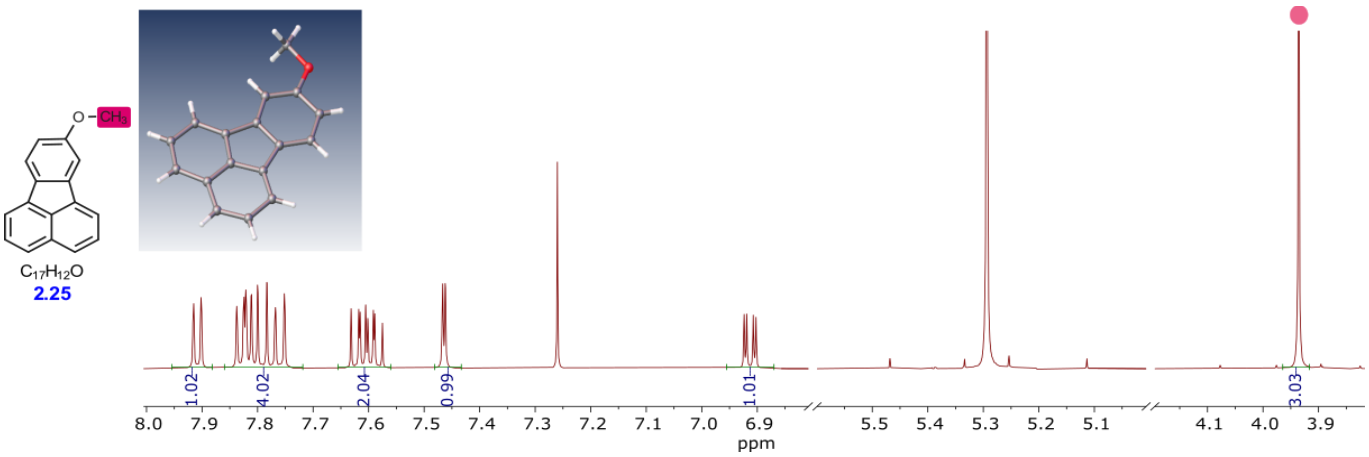

Figure 25: The X-ray and ^{1}H NMR spectrum of **2.25**.

Fluoranthene **2.25** exhibits bright fluorescence under UV irradiation. As shown in Figure 26, it displays a maximum absorption peak at λ ≈ 360 nm and emits at 485 nm.

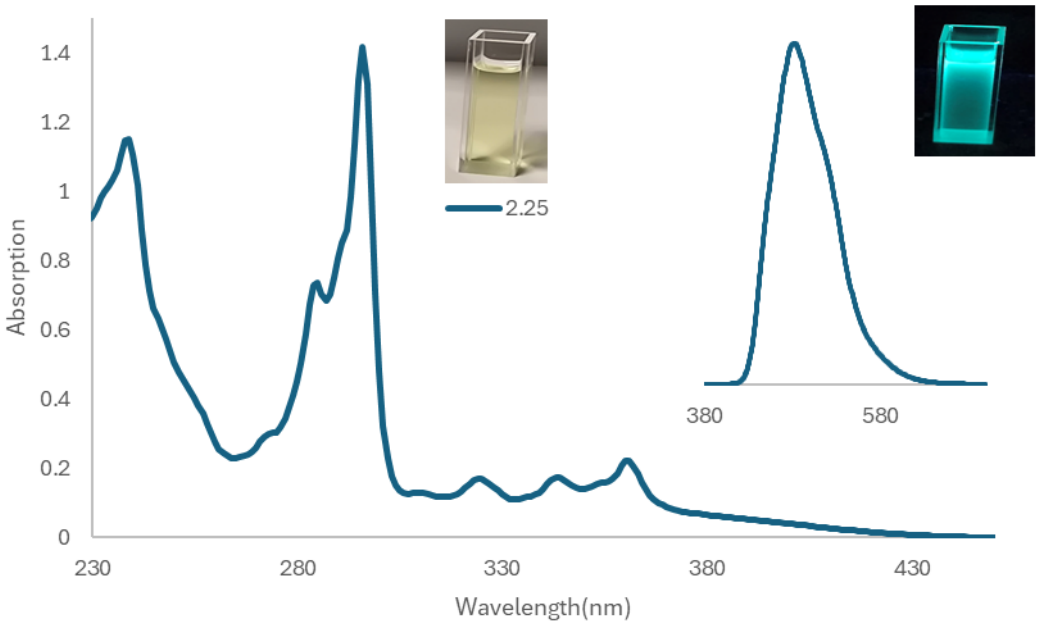

Figure 26: UV-vis absorption and emission spectra of compound **2.25** in DCM.

There are two challenges causing the low yield of **2.9**. The high percentage yield of **2.25** indicates the formation of intramolecular cyclization product is faster than forming **2.9**. The second challenge is the separation of **2.9** by column chromatography due to formation of homocoupling of terminal alkyne. The reaction was repeated without DBU to evaluate its impact. TLC analysis revealed presence of only starting materials, indicating the importance of DBU to undergo deprotonation of **2.23**, and also facilitate the formation of **2.25**. We repeated the reaction (entry 2) in a preheated oil bath at 80 ºC to investigate whether cyclization of **2.25** occurs at that

temperature. We also exchanged **2.23** to a less reactive **2.24,** attempting to avoid homocoupling. The reaction finished in 17h, and the triflate **2.8** was consumed, but **2.24** remained. After the work-up and separation, the yield of **2.25** increased to 85%, and **2.9** decreased to 2%. These two entries (Entry 1,2) favour the formation of fluoranthenes, and it seems that the **2.23** is required due to the reactivity to undergo the coupling faster before the formation of intramolecular product **2.25**. Another utilization is from reported literature, their reported methodology is coupling at r.t. in THF, which in our case may help to avoid the formation of **2.25**.[83] After adding the reagents (entry 3) and stirring for 94h (approx. 4 days) in DMF at r.t the **2.23** was consumed, and the TLC shows the remaining **2.8;** therefore 2.5 eq of **2.23** was added, and the temperature increased to 80 °C for 96h (approx. 4 days). The triflate **2.8** was still not consumed, so the reaction stopped, and after the work-up and purification, the yield of **2.9** rose to 30%, and **2.25** did not form.

2.4.2 Overcome intramolecular cyclization

Due to insufficient yield in the previous approach for synthesizing **2.9,** and formation of intramolecular cyclization and homocoupling that make the purification difficult, we proceeded with a different route for synthesizing **2.9**.

2.4.3 Synthesis of TMS acetylene derivatives

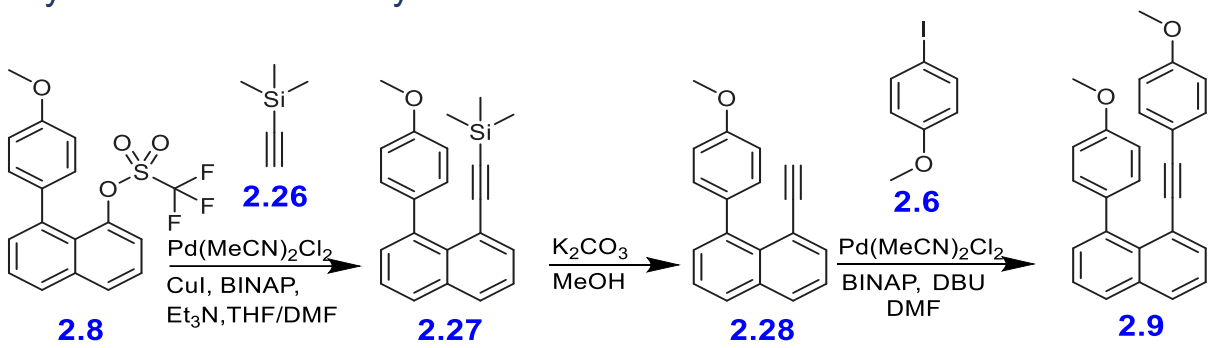

Scheme 35: An alternative route for synthesizing **2.9**.

As indicated in scheme 35, firstly, coupling **2.8** with 10 equivalents of TMS acetylene **2.26** affords the coupled product **2.27**, solving the homocoupling separation problem. Table 5 shows the optimization of **2.27** and **2.29** and the best yield is entries 4 and 5 for **2.27** and **2.29,** respectively. The reaction requires a solution of 10 equivalents of TMS acetylene **2.26** and Et_3N, and after 24 h, an additional 10 equivalent of TMS acetylene **2.26** and Et_3N were added and left for approx. 18 h for **2.29** and 48 h for **2.27**, yielding 88% and 73%, respectively.

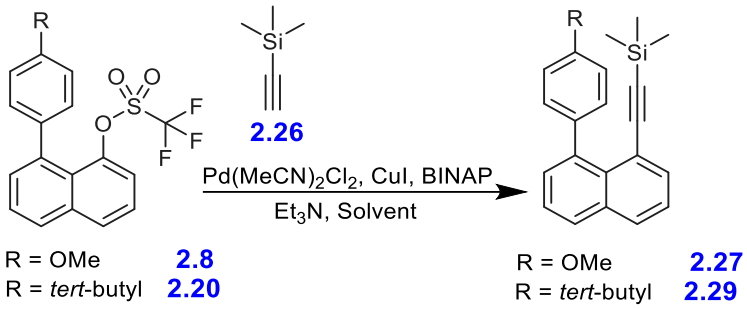

Entry	Triflate	TMS (eq)	Solvent	Temp/°C (time/h)	Catalyst	Yield (%)	
						2.27	**2.29**
1	**2.8**	10	Benzene/dioxane	60 (61)	$Pd(MeCN)_2Cl_2$ (2%) CuI (2%) BINAP (4%)	47%	
2	**2.8**	10	THF (3 ml)	60 (21)	$Pd(MeCN)_2Cl_2$ (2%) CuI (2%) BINAP (4%)	33%	
3	**2.8**	10	THF (3 ml)	52 (72)	$Pd(MeCN)_2Cl_2$ (2%) CuI (4%) BINAP (6%)	55%	
4	**2.8**	10 then 10 after 24h	THF (3 ml) + DMF (1 ml)	52 (72)	$Pd(MeCN)_2Cl_2$ (2%) CuI (4%) BINAP (6%)	73%	
5	**2.20**	10 then 10 after 24h	THF (3 ml) + DMF (1 ml)	52 (42)	$Pd(MeCN)_2Cl_2$ (2%) CuI (4%) BINAP (6%)		88%

Table 5: Optimization conditions for Sonogashira coupling with TMS acetylene.

2.4.4 Deprotection of TMS acetylene derivatives

The deprotection of **2.27** to terminal alkyne **2.28** is required prior to the coupling with aryl iodide. We have attempted direct cross coupling **2.27** with 4-iodoanisole **2.6** resulting in the formation of homocoupling of aryl iodide and unreacted TMS **2.27** remained in solution. Therefore, scheme 36 shows the deprotection of the TMS-protected acetylenes **2.27** and **2.29** to the corresponding terminal alkynes **2.28** and **2.30**, it was carried out using K_2CO_3 in MeOH. Treatment of **2.27** with 5 equivalents of K_2CO_3 furnished **2.28** in 39% yield.

Increasing the base loading to 10 equivalents significantly improved the outcome, delivering **2.28** in 67% yield and **2.30** in 49% yield, respectively.

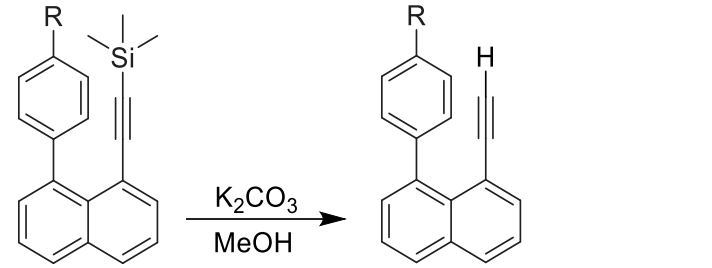

R = OMe **2.27**
R = *tert*-butyl **2.29**

R = OMe **2.28** (67%)
R = *tert*-butyl **2.30** (49%)

Scheme 36: The deprotection of TMS of **2.27** and **2.29** by K_2CO_3 in MeOH.

The product **2.30** was purified by precipitation from hexane. The resulting solid was collected by filtration and washed with small portions of hexane to remove residual oily starting material **2.29**, affording pure **2.30**. However, **2.28** is oily and was isolated by column chromatography using 1:10 DCM/petroleum ether. The ^{1}H NMR spectra for **2.27** and **2.29** as well as their deprotected adducts **2.28** and **2.30** are depicted in Figure 27, which shows the TMS protons peak at 0 ppm and terminal alkyne proton around 2.6 ppm.

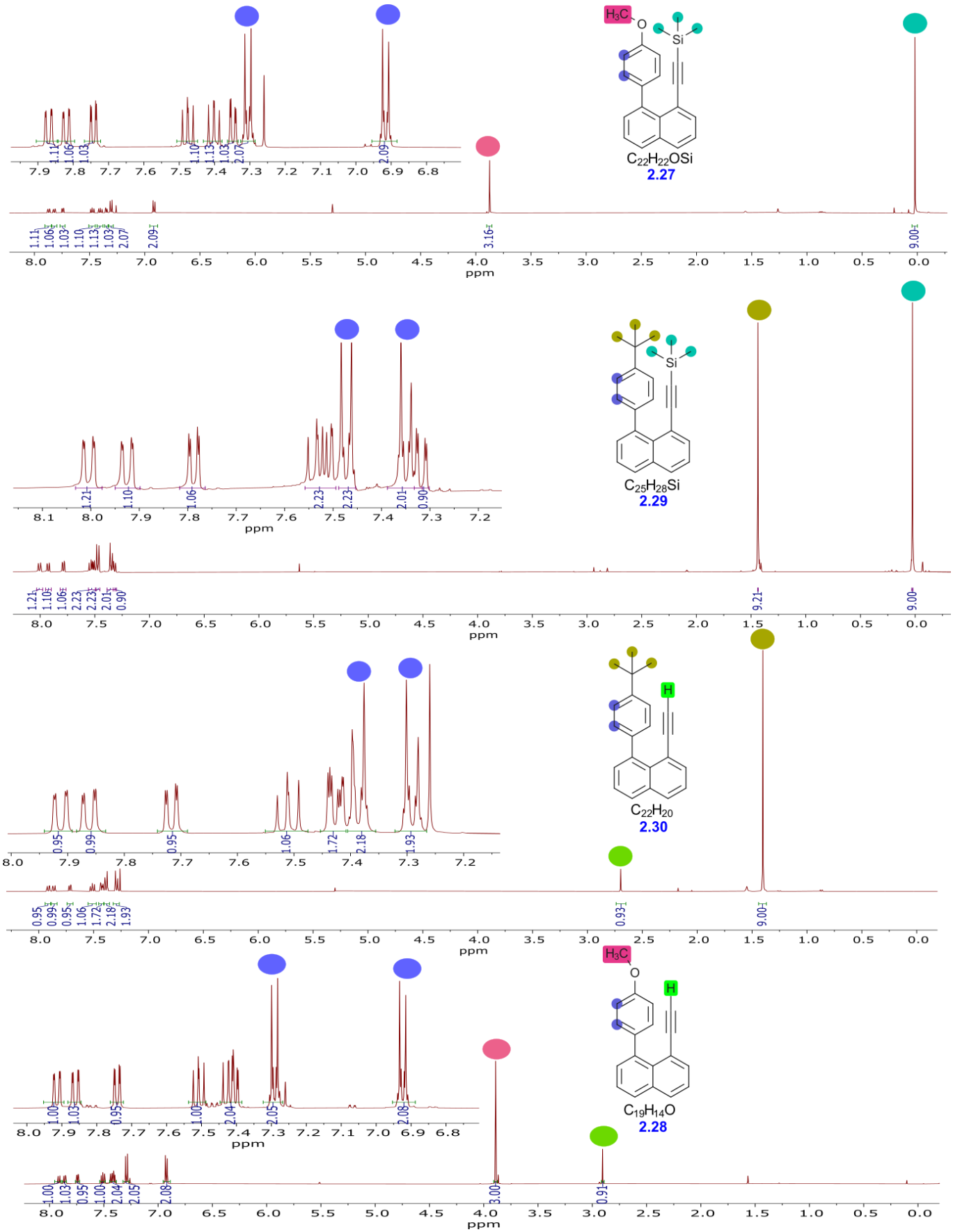

Figure 27: The ^{1}H NMR spectra for **2.27**, **2.30**, **2.28** in Chloroform-D, **2.29** in Acetone-D.

2.4.5 Sonogashira coupling between terminal alkyne and aryl iodide derivatives

Compound **2.9** was synthesized in moderate yield under microwave conditions. Table 6 presents the results of Sonogashira cross-coupling reactions between terminal alkynes **2.28** or **2.30** and substituted aryl iodides **2.6** or **2.12**. The reaction of terminal alkyne **2.28** with 4-iodoanisole **2.6** under microwave irradiation afforded **2.9** in 45% yield, along with a side product, **2.32**, in 9% yield (Entry 1). The diminished yield of **2.9** is likely attributable to the concurrent formation of **2.32** as an unexpected byproduct. In contrast, coupling terminal alkyne **2.28** with 4-*tert*-butyliodobenzene **2.12** provided the corresponding product **2.31** in 87% yield (Entry 2). When the methoxy-substituted alkyne **2.28** was replaced with the *tert*-butyl analogue **2.30** and reacted with 4-iodoanisole **2.6** under microwave irradiation, a mixture was formed, and it was difficult to separate. The conventional method decreases the yield of **2.9** and **2.31** to 38% and 48% respectively (Entry 4,5, Table 6). X-ray diffraction of the coupled products confirms the structure as illustrated in Figure 28, along with ^{1}H NMR spectra which shows four doublets for phenyl AB protons correlating to **2.9**, **2.31,** and two doublets corresponding to **2.32** and **2.34**.

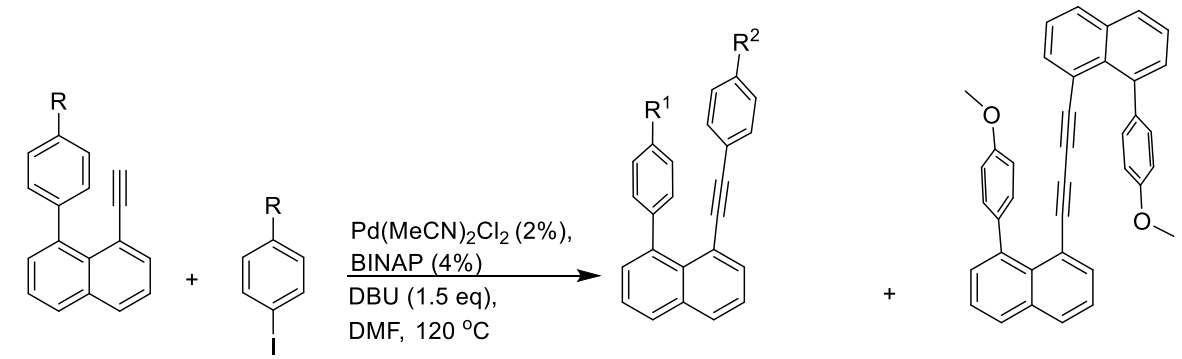

R = OMe **2.28**
R = *tert*-butyl **2.30**

R = OMe **2.6**
R = *tert*-butyl **2.12**

R^1 = R^2 = OMe **2.9**
R^1 = OMe, R^2 = *tert*-butyl **2.31**
R^1 = OMe, R^2 = H **2.32**
R^1 = *tert*-butyl, R^2 = OMe **2.33**

2.34

Entry	Alkyne	Aryl Iodide (equiv)	Time	Yield (%)
1[a]	**2.28**	**2.6** (3)	4h	**2.9** (45%), **2.32** (9%)
2[a]	**2.28**	**2.12** (3)	6h	**2.31** (87%)
3[a]	**2.30**	**2.6** (3)	5h	Mixture
4[b]	**2.28**	**2.12** (3)	51h	**2.31** (48%), **2.34** (7%)
5[b]	**2.28**	**2.6** (3)	46h	**2.9** (38%), **2.32** (12%), **2.34** (4%)

Table 6: Optimization of reaction conditions for the Sonogashira coupling.
[a] Microwave condition, [b] Oil bath condition.

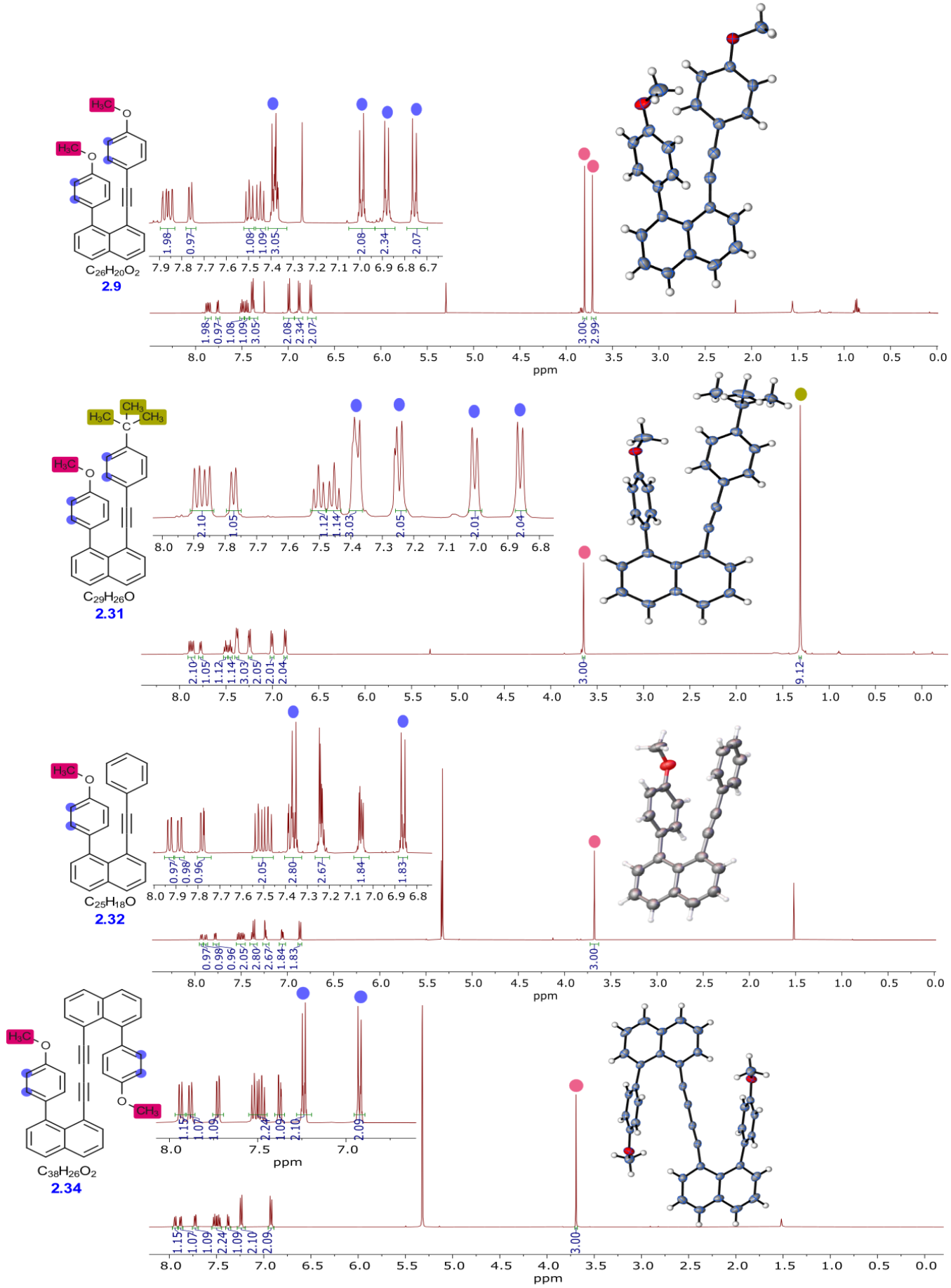

Figure 28: The ^{1}H NMR spectra and X-ray of coupled products **2.9**, **2.31**, **2.32**, **2.34**.

The UV–vis spectra of terminal alkyne **2.30** in Figure 29 shows an absorption maximum at ~316 nm, whereas the internal alkynes (**2.9**, **2.32, 2.31)** display at ~350 nm. The corresponding homo coupled diyne **2.34** exhibits a bathochromic shift to ~390 nm, consistent with increased conjugation across the diyne bridge. These compounds emit in the 380-432 nm range.

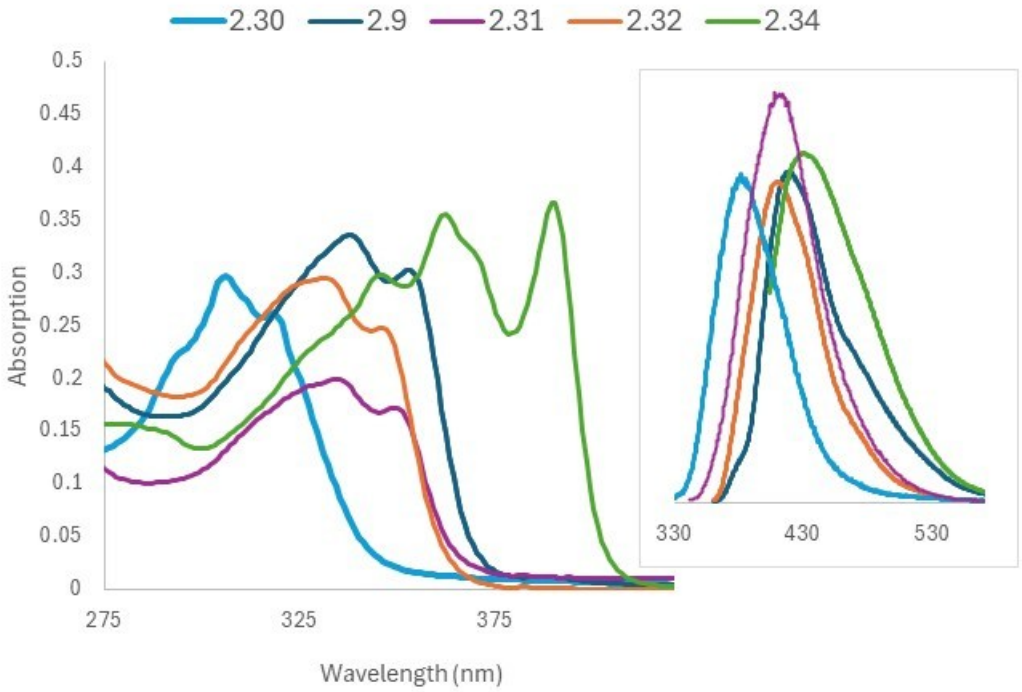

Figure 29: UV-vis absorption and emission spectra of compound **2.9, 2.30, 2.32, 2.34** in DCM.

2.5 Cyclization investigation of alkyne

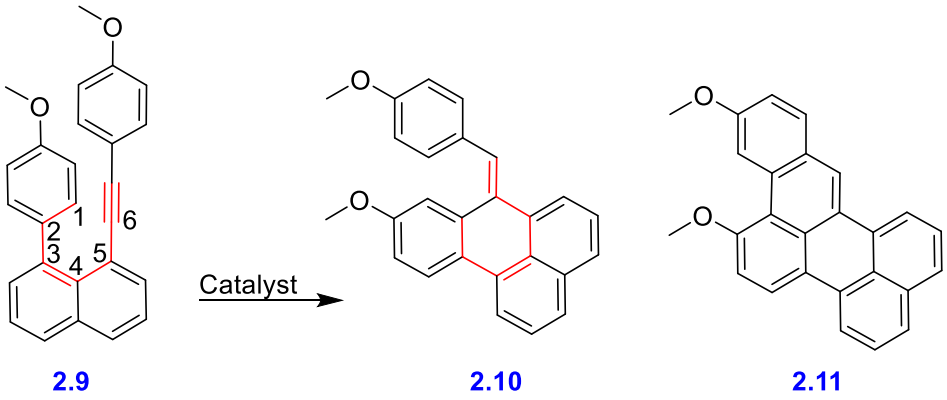

Scheme 37: The proposed formation of the cyclized products.

In this section, we will demonstrate the conditions explored for the cyclization of compound **2.9** and their respective outcomes. According to Baldwin's rules for ring closure, exo-dig cyclization is favoured from 5 to 7, theoretically allowing **2.9** to undergo a 6-exo-dig cyclization to form **2.10**.

2.5.1 Attempts for cyclization of **2.9**

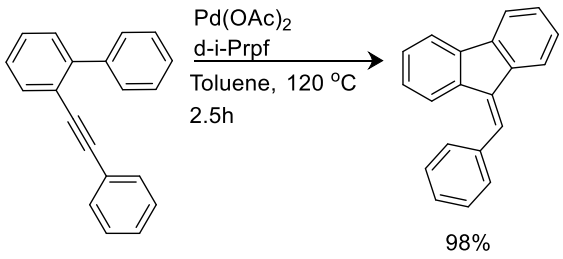

Scheme 38: Pd-Catalyzed hydroarylation of *o*-alkynyl biaryls.

Palladium acetate as seen in scheme 38 has been used to cyclize alkyne via 5-exo-dig.[84] The initial catalytic condition (Entry 1, Table 7) involved a palladium source under microwave irradiation at 120 °C for 8 h. Thes reaction showed no progress (monitored by ^{1}H NMR spectroscopy). Further heating at 140 °C for an additional hour also failed to induce cyclization. Similarly, conventional heating (Entry 2) did not lead to cyclization. Copper iodide failed to perform cyclization under microwave irradiation at 120 °C (Entry 4, Table 7).

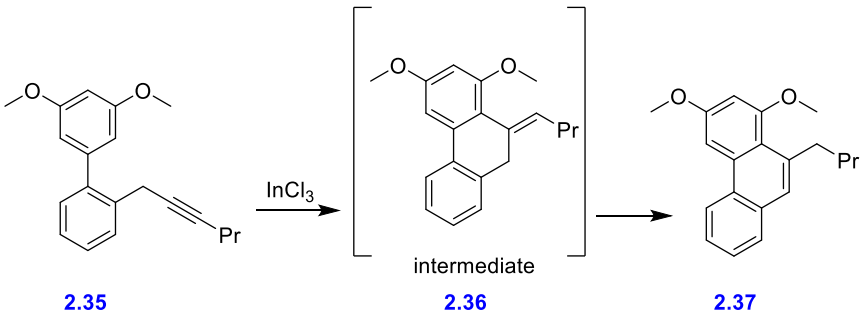

Scheme 39: $InCl_3$ cyclization reaction.

Indium trichloride ($InCl_3$) has been shown in scheme 39 to promote 6-exo-dig cyclization.[85] Kwon and coworkers cyclized compounds **2.35** to **2.37** using 10 mol% $InCl_3$ in toluene at 80 °C. The intermediate **3.36** formed when the temperature was lowered to 50 °C, or the catalyst loading decreased to 5 mol%. The isolation of **2.36** is by HPLC, which gradually converted to phenanthrene **2.37** upon heating with $InCl_3$. We attempted their method (Entries 5, 6, Table 7), and TLC revealed a complex mixture.

Entry	Catalysts	Solvent	Temp/°C	Time	Yield
1[a]	$Pd(MeCN)_2Cl_2$ 7%	DMF	120 – 140	9h	No reaction
2	$Pd(OAc)_2$ (5%)	DMF	120	4 days	No reaction
4	CuI (20%)	DMF	120		No reaction
5	$InCl_3$ (10 %)	Toluene	80		Mixture
6	$InCl_3$ (5 %)	Toluene	80		Mixture

Table 7: Applying the coupled product **2.9** to routes A and B, and C. [a] microwave irradiation.

2.5.2 Cyclization reaction by TFA

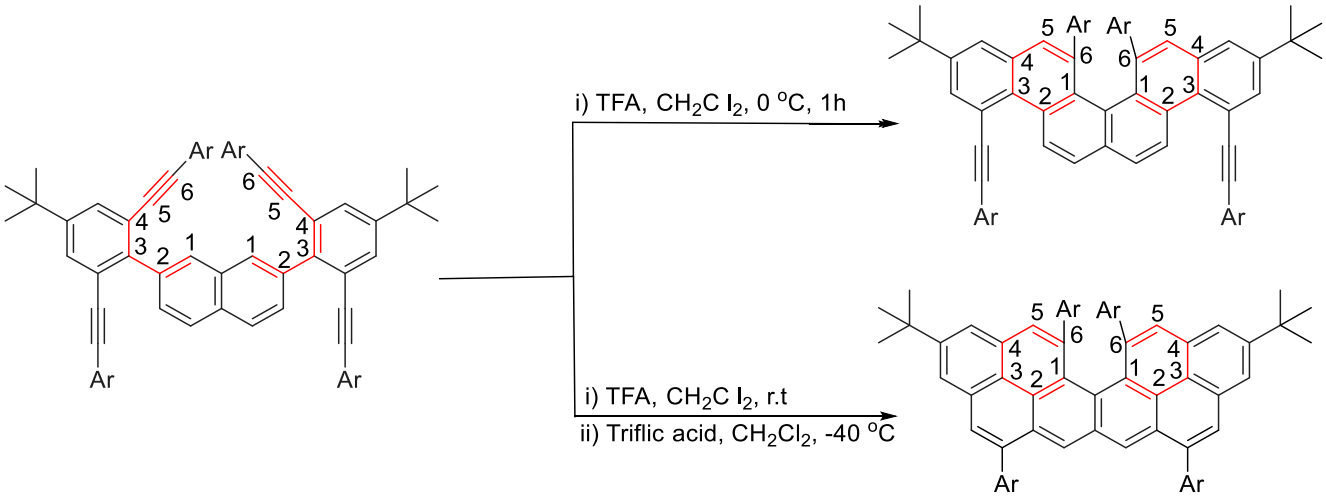

Scheme 40: Synthesis of pyrene from four-fold alkyne benzannulation via TFA.[86]

Trifluoroacetic acid (TFA) is a Brønsted acid that is used to cyclize an alkyne. Redha and coworkers, as shown in Scheme 40, utilized TFA and triflic acid to achieve a four-fold alkyne benzannulation.[86] In their study, the presence of four alkyne units enabled TFA to facilitate the cyclization of two alkynes. The combination of TFA and triflic acid (TfOH) was required to drive the reaction to completion, promoting the cyclization of all four alkyne moieties.

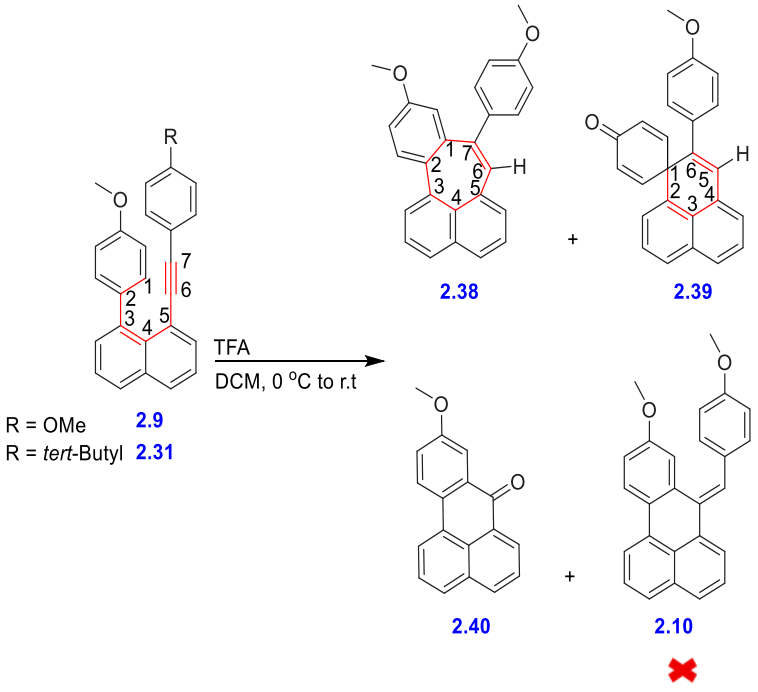

Scheme 41: The cyclization outcome of the **2.9** reaction by TFA.

We were inspired to attempt the cyclization of **2.9** by using TFA, as illustrated in Scheme 41, which led to the formation of the seven-membered ring **2.38**, spiro compound **2.39**, and benzanthrone **2.40**. Figure 30 shows the reaction progress monitored by the ^{1}H NMR spectra over time, showing the formation of **2.38** and **2.39**.

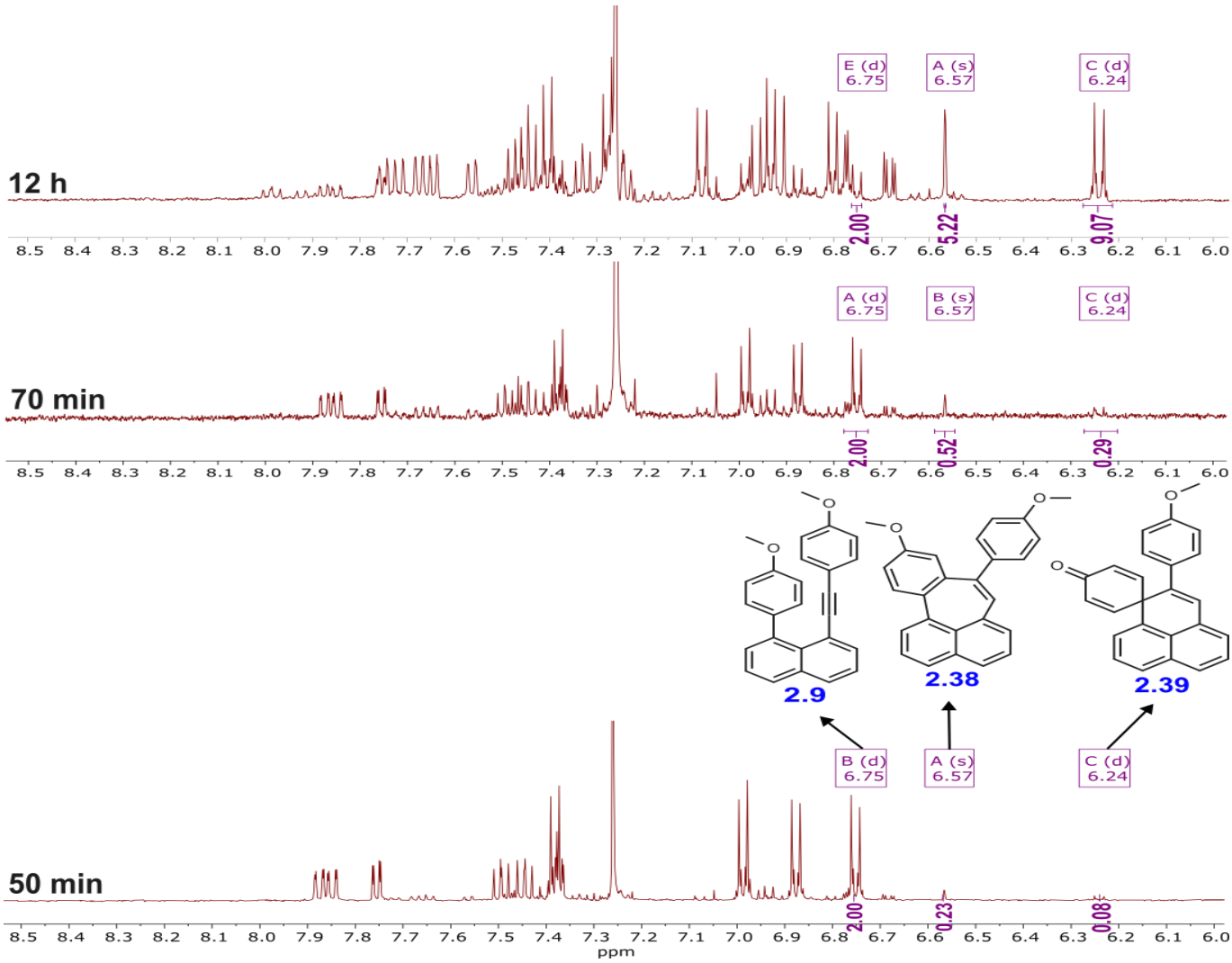

Figure 30: Monitoring cyclization reaction progress over time by ^{1}H NMR spectroscopy.

Benzanthrone **2.39** appears on TLC clearly after the work-up with $NaHCO_3$, showing a clear yellow spot **2.40**, whereas work-up under Et_3N exhibits only a trace amount. We observed that the percentage yield of products is affected by the work-up, as shown in Table 8.

Entry	Acid (eq)	Work-up	Time	Yield[a] 2.38/2.39/2.40
1	TFA 3 mL, (50 eq)	$NaHCO_3$	15 - 20 h (15h)	50% /13%/ 32%
2	TFA 3 mL, (50 eq)	Et_3N then Aluminum oxide	15 - 20 h (19h)	86% / 17%/ trace
3	$HNTf_2$ (5 drops)	Et_3N then Aluminum oxide	24 h	76%/ 22% / trace

Table 8: The optimization conditions for TFA cyclization.

The ^{1}H NMR spectra in Figure 31 highlight the C-H proton as a singlet for **2.39** and **2.38**, phenyl protons as four doublets for **2.39** and two doublets for **2.38**. The methoxy protons for **2.38** show two sets of singlets, whereas **2.39** and **2.40** depict one singlet. The spectrum for compound **2.40**

matches that reported in the literature.[87] The spiro system in compound **2.38** was proven by analysis of its crystal structure.

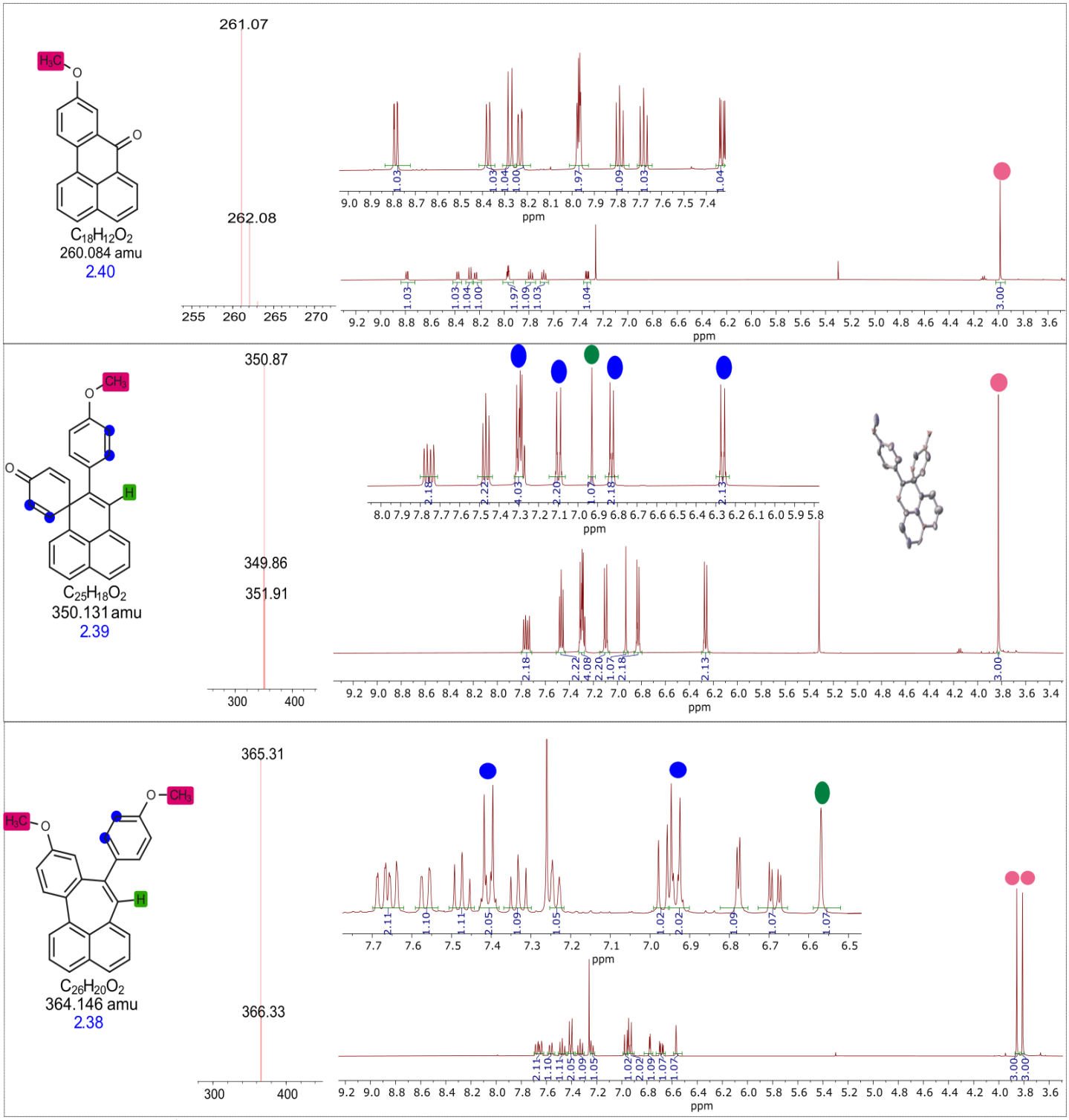

Figure 31: The ^{1}H NMR spectra and Maldi-tof Ms for **2.38**, **2.39**, **2.40**, and a preliminary x-ray crystallography result of spiro compound **2.39**.

2.5.2.1 Investigation of benzanthrone **2.40** formation

TFA promotes two cyclization pathways, 7-endo-dig for **2.38** and 6-endo-dig for **2.39**, while **2.10** was not formed. The unexpected product, benzanthrone **2.40**, formed regardless of whether TFA is introduced to **2.9** or **2.31**. Cyclization of **2.31** yielded a mixture that proved difficult to separate by TLC, even after using preparative TLC. We observed on TLC the formation of benzanthrone **2.40**, and it was isolated after two successive column chromatographies, confirming its formation by ^{1}H NMR spectroscopy. Yan and coworkers, as shown in Scheme 42, introduced the seven-membered ring to the Scholl condition. Instead of achieving the dehydrogenative C-C coupling between the aryl-substituted or aryl substituent and the naphthalene core, oxidative fragmentation and ring contraction occurred, forming anthracene-4-one. They stated that "Further exploration of transformations of the present heptagon compounds is underway" and proposed a mechanism for the formation of anthracene-4-one as illustrated below.[88]

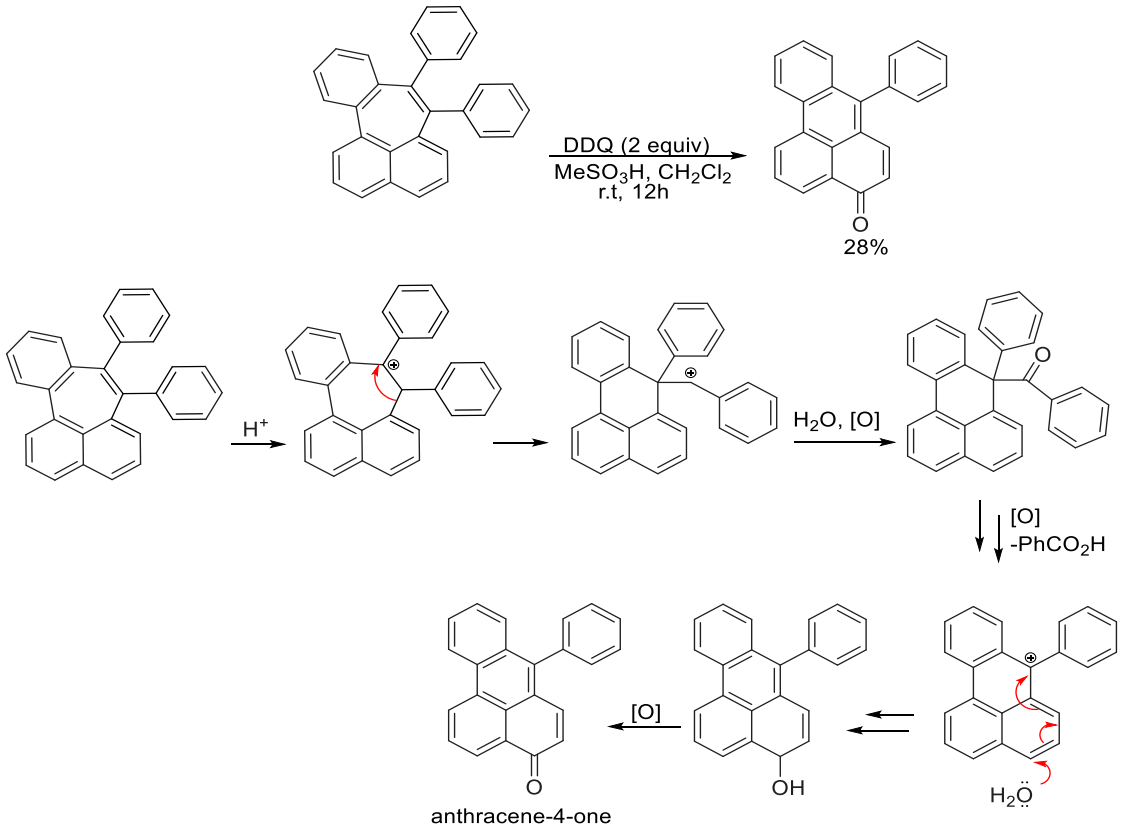

Scheme 42: Possible pathway for the oxidative fragmentation of the seven membered ring.

The formation of benzanthrone **2.40** could originate from the oxidation of seven-membered ring **2.38** passing through similar mechanisms as proposed in Scheme 43. This mechanism explains the presence of the **2.40** regardless of the attached phenyl substituent, whether methoxy or tert-butyl.

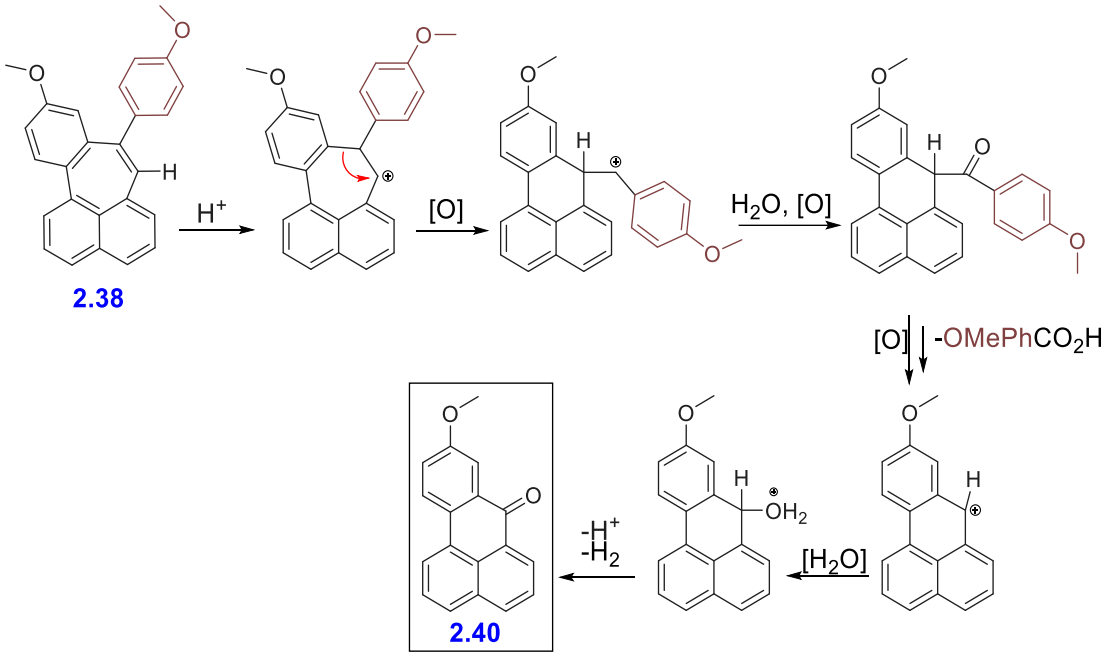

Scheme 43: The possible pathway for the formation of **2.40**.

Accordingly, treatment of compound **2.28** with TFA is expected to afford **2.40**. To test this transformation, we conducted further experiments by reacting **2.28** with TFA. The reaction completed after 17h and TLC revealed the products are unstable and sensitive to work-up. Table 9 indicates that the work-up with $HNaCO_{3\,(aq)}$ shows decomposition of the products while moving on TLC, whereas Et_3N and methanol gives an inseparable product (mixture) that are difficult to separate by column chromatography.

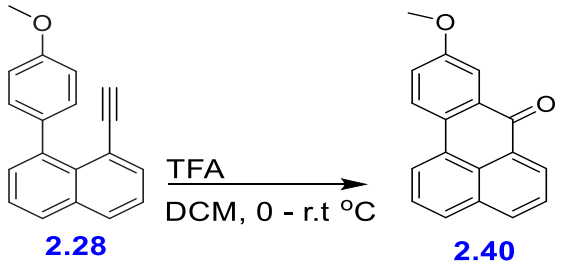

Entry	Work-up	TLC observation
1	$HNaCO_3$	Decomposition, unstable products
2	Et_3N	Difficult separation (mixture)
3	MeOH	Difficult separation (mixture)

Table 9: The observation of workups of the **2.28** cyclization reaction.

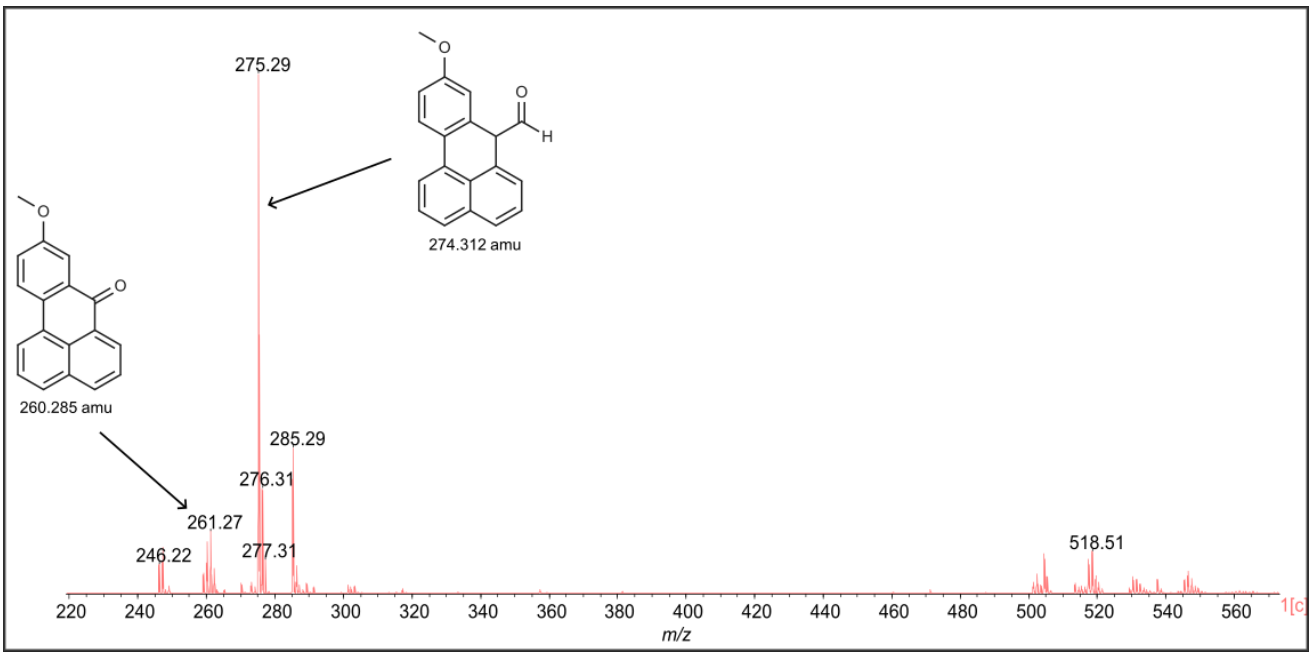

Figure 32: The Maldi-tof Ms for the mixture.

A sample of the reaction mixture, followed by work-up with methanol, was analyzed by TLC and MALDI-MS. Both techniques confirmed the presence of Benzanthrone **2.40**. As shown in Figure 32, MALDI-MS revealed a molecular ion peak at m/z 261, corresponding to the $[M+H]^+$ ion of compound **2.40**. The cyclization of **2.28** should pass through an aldehyde species because mechanism as shown in scheme 44 demonstrates the molecular weight of the aldehyde 274 which may correspond to molecular ion peak at 275 (M+H) in figure 33.[89]

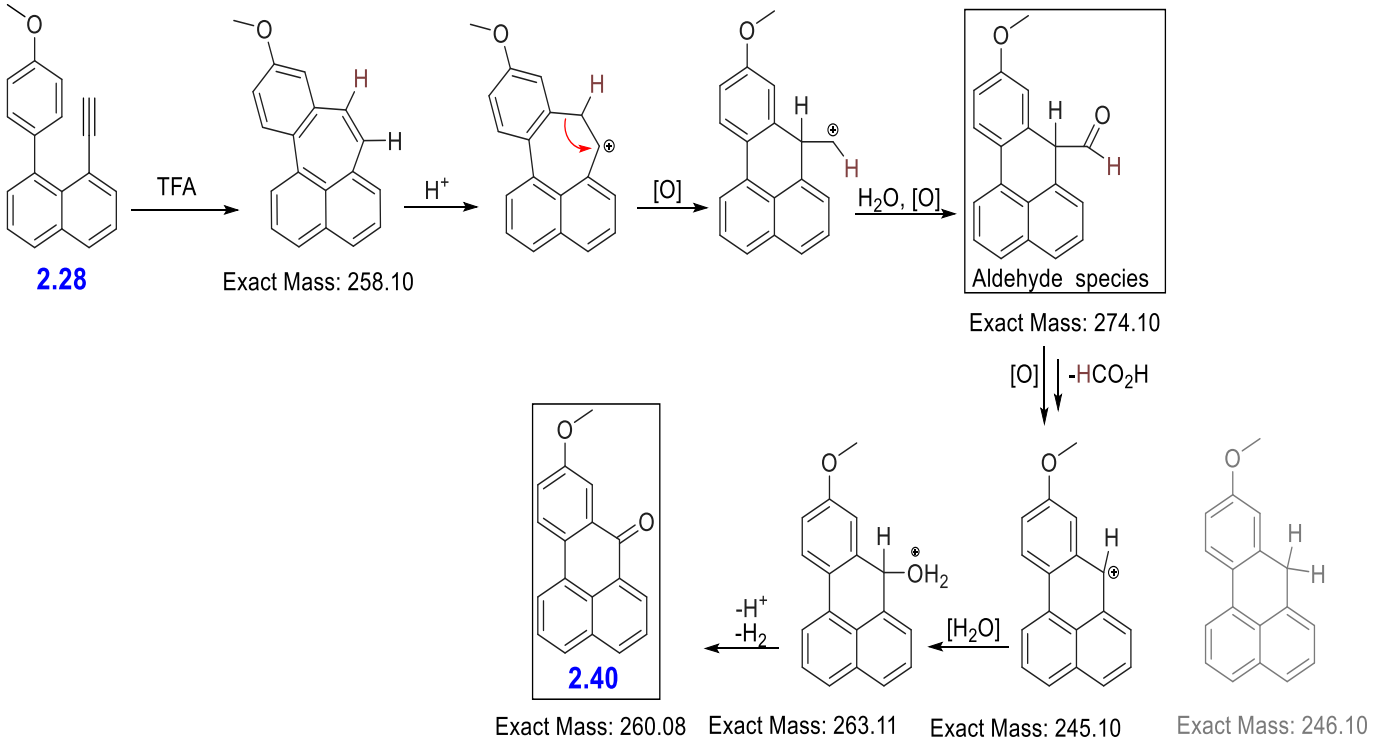

Scheme 44: The proposed mechanisms for the formation of **2.40**.

2.5.2.2 Reactivity of compound **2.38** toward Scholl reaction

The **2.38** species is a noteworthy intermediate, attracting attention due to its distinctive reactivity. Upon oxidative fragmentation, the seven-membered ring intermediate yields a six-membered ring, providing valuable insights into bottom-up synthesis strategies. To explore this transformation, we investigated the effect of Scholl conditions, specifically the use of DDQ as a strong oxidizing agent on **2.38**.

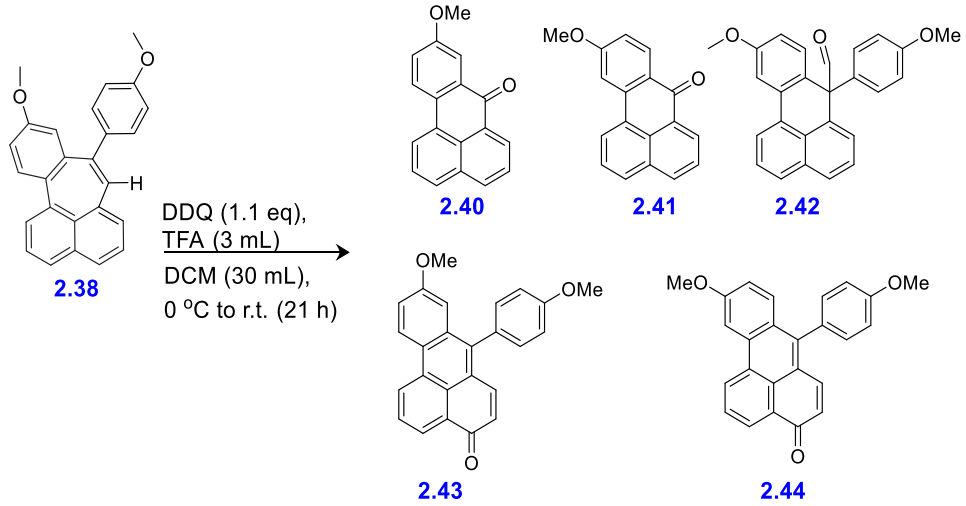

Entry	Work-up	Yield (%)
1	$NaHCO_3$	Mixtures, unstable products
2	$MeOH/NaHCO_3$	**2.44** trace
3	$MeOH(6h)/NaHCO_3$	**2.41** (16%), **2.40** (7%)
4	Et_3N/ Aluminum oxide	**2.42** (21%), **2.40** Trace, unstable product

Table 10: The effect of Scholl reaction on **2.38**.

We noticed the reaction outcome of **2.38** under Scholl conditions is affected by the work-up, hence a direct quenching with $HNaCO_3$ (entry 1, Table10) gives mixture and unstable products. However, quenching with MeOH followed by $NaHCO_{3(aq)}$, gives a trace amount of compound **2.44** which was isolated by column chromatography (Entry 2, Table 10). The X-ray structure of **2.44** is shown in Figure 33 which depicts unexpected "migration" of the methoxy group from the para to the meta position. The structure was resolved by our collaborator, Dr David Hughes, and his comments on the details of the structure can be found in the appendix. We repeated the reaction under the same conditions, but we could not obtain **2.44**. We hypothesized that the reason could be a need to prolong the stirring time in MeOH.

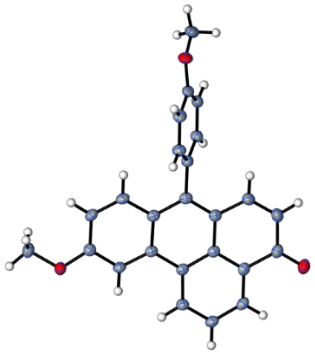

Figure 33: The x-ray structure of **2.44**.

To test this, 8 mL of MeOH was added, and the mixture was stirred for 6 hours prior to quenching with aqueous $NaHCO_3$. TLC showed a complex mixture due to formation of several products, making the separation difficult. Nevertheless, compound **2.41** was isolated by column chromatography (DCM/acetone/petroleum ether, 20:5:200), and the ^1H NMR spectrum and for **2.41** is shown in figure 34 which matched with reported literature.[87] X-ray structural analysis also confirms the chemical structure.

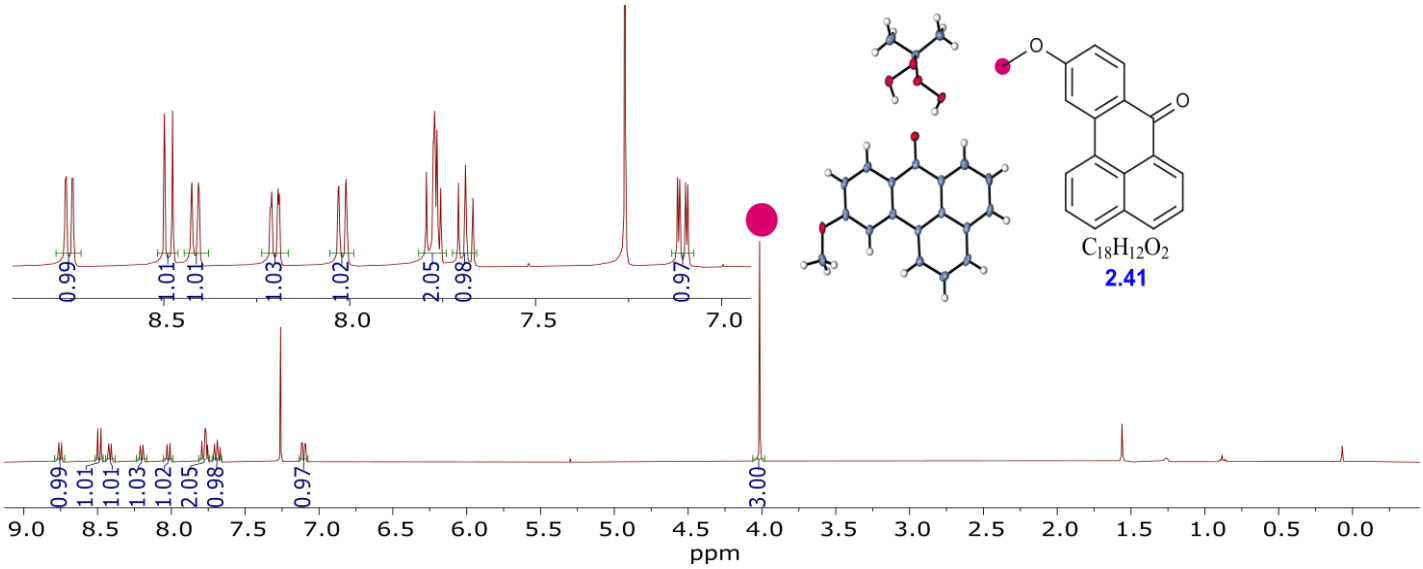

Figure 34: The ^1H NMR spectra for **2.41**, and the x-ray for **2.41** [87]

These preliminary results suggest that the addition of alcohols such as methanol might cause insertion at the meta position, generating new products and complicating separation. However, work-up with Et_3N (Entry 4), enabled the isolation of compound **2.42** (21%). The ^1H NMR spectra in figure 35 for compound **2.42** shows the AB phenyl protons and the aldehyde proton at 9.8 ppm and two methoxies at 3.9 and 3.8 ppm. The expanded region of the ^1H–^1H NOESY spectrum showing the NOE cross-peak between the aromatic protons (blue highlighted). This correlation confirms the meta positioning of the methoxy group. Also, HRMS analysis confirmed the molecular ion peak $[M+H]^+$ (required: 381.1491, found 381.1495).

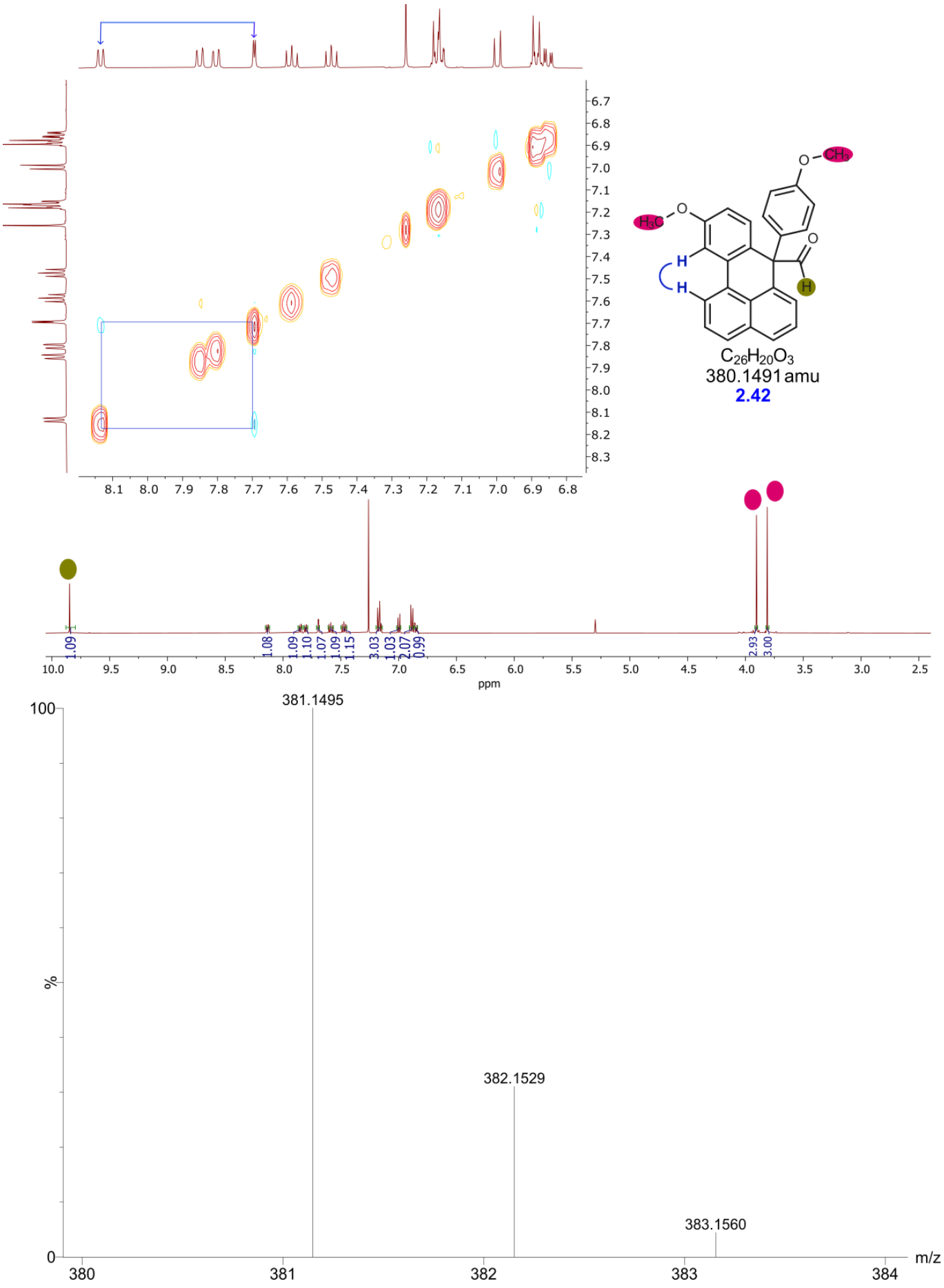

Figure 35: The ^{1}H NMR, Nosey spectra and HRMS for **2.42.**

2.5.3 Cyclization reaction by ICl

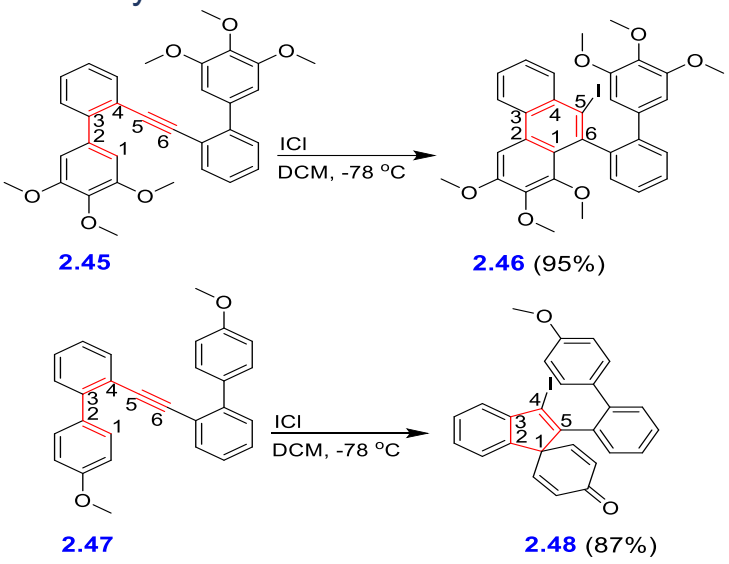

Scheme 45: Cyclization of alkynes by ICl.

Iodine monochloride has been reported to induce intramolecular acetylene cyclization, forming alkenyl iodides.[90] Chia-Wen and colleagues as shown in scheme 45 used ICl to cyclize bis(biaryl)acetylenes **2.45**, affording iodophenanthrene derivatives **2.46**. The substitution position on the phenyl affects cyclization, when tri-methoxy-substituted **2.45** is present, favoring **2.46**, whereas one methoxy-substituted **2.47** favors spiro compound **2.48** via 5-endo-dig cyclization.

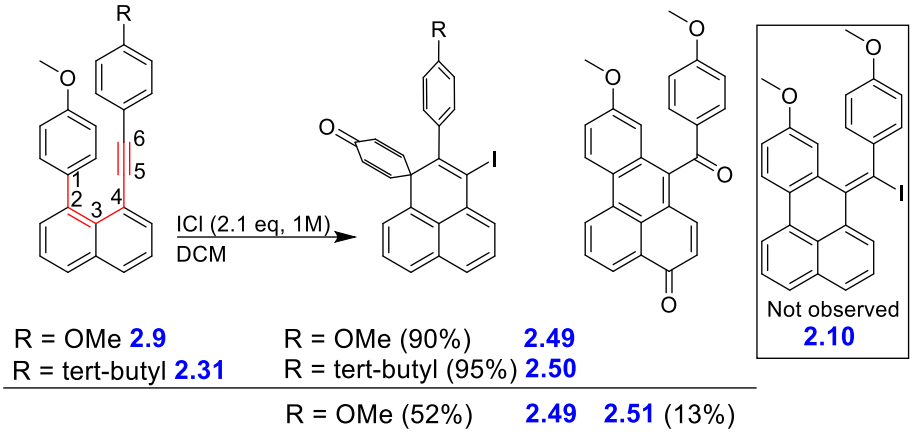

Scheme 46: The ICl cyclization of alkyne outcome of **2.9** and **2.31**.

Herein, scheme 46 demonstrates the use of ICl dropwise at -78 °C using a dry ice/acetone bath to cyclize **2.9** and **2.31,** resulting in the formation of spiro compounds **2.49** and **2.50,** yielding 90% and 95% respectively. The reaction was completed after 2.5 hours, yielding one spiro product. When the temperature increased to 0 °C before the addition of ICl to **2.9,** the yield of **2.49** decreased to 52% and a new product benzanthracene **2.51** formed**,** yielding 13%. In both sets of condition, the desired product **2.10** was not formed. The x-ray structures of **2.49** and **2.51**, as well as the ^{1}H NMR spectra for **2.49**, **2.50**, and **2.51** are depicted in Figure 36. The highlighted blue

colour indicates the four doublets for **2.49** and **2.50** corresponding to phenyl and spiro protons, whereas **2.51** shows two doublets, one of which broadens due to the effect of the carbonyl.

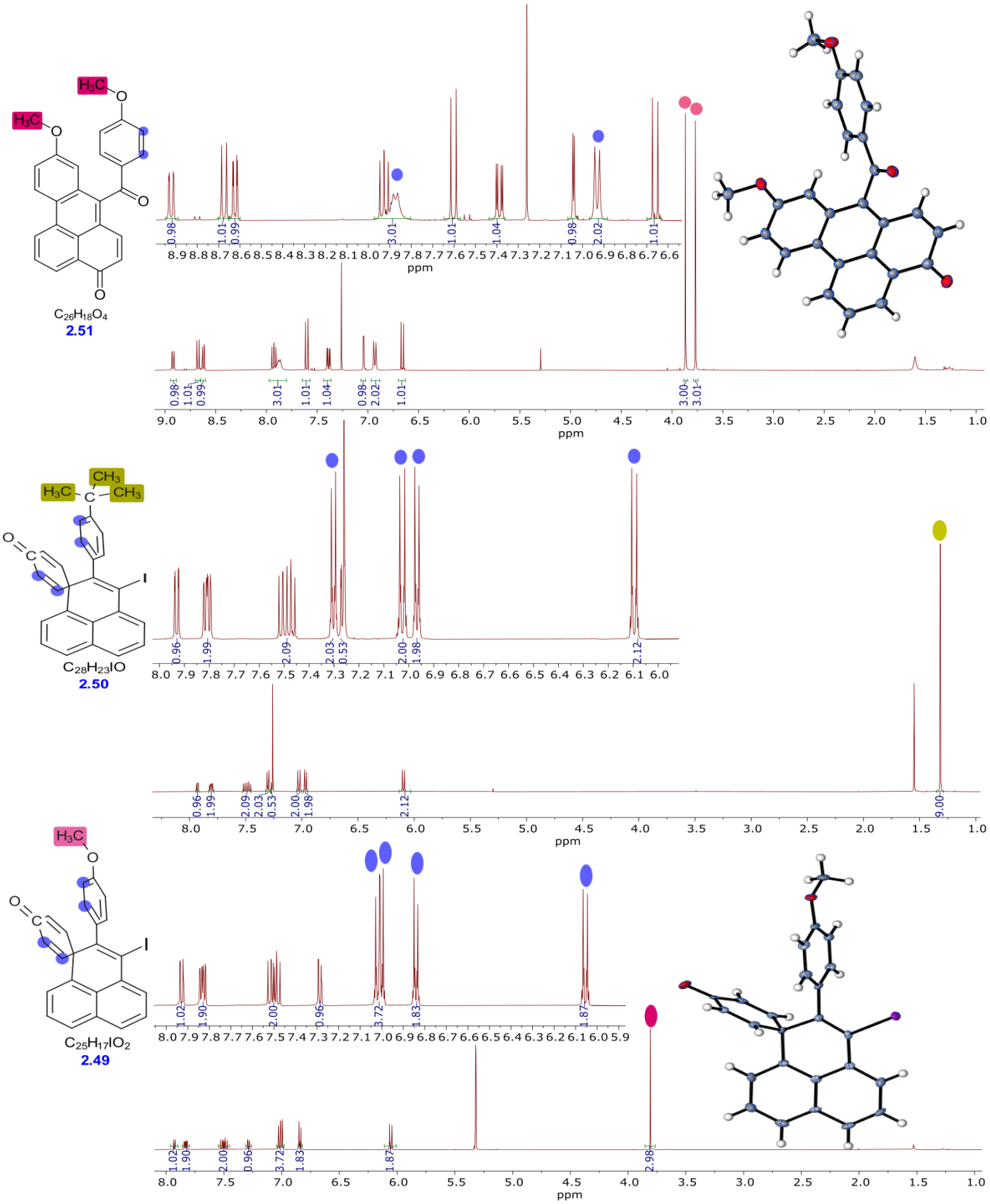

Figure 36: The X-ray structures of **2.49** and **2.51**, and the ^{1}H NMR spectra of **2.49**, **2.50** and **2.51**.

2.5.3.1 Testing the methoxy effectiveness on the cyclization outcome

The electron-donating group on phenyl-methoxy **2.9** or the electron-neutral group on phenyl tert-butyl **2.31** does not affect the cyclization path. However, the methoxy group on the para position of the phenyl ring on the naphthalene core directly contributes to favouring 6-endo-dig cyclization.

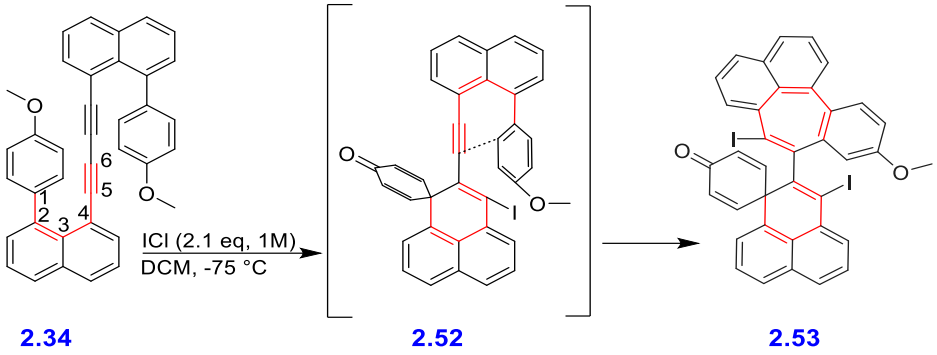

Scheme 47: The cyclization of **2.34** by ICl.

This cyclization path is favourable if one alkyne is present in the compound. When the symmetrical di-alkyne **2.34** was subjected to ICl conditions, as shown in Scheme 47, the expected path for the second cyclization of **2.52** is the 6-endo-dig. However, the second cyclization passes through 7-endo-dig ultimately forming spiro-seven-membered compound **2.53,** yielding 84%. Compound **2.34** is consumed after approximately 30 min, cyclizing **2.34** to form **2.52**. The reaction was left for a further 2h to allow for the possibility of the second cyclization of **2.52**. The ICl cyclization outcome favors the spiro compound via 6-endo-dig and seven-membered ring through 7-endo-dig. This implies the formation of **2.10** under ICl conditions is not favorable. The result of favouring this cyclization path is aligned with the TFA outcome. The chemical structure of **2.53** is confirmed by X-ray as shown in Figure 37 which shows two views for spiro and seven membered rings and it was resolved by our collaborator, Dr David Hughes, and his comments on the details of the structure can be found in the appendix.

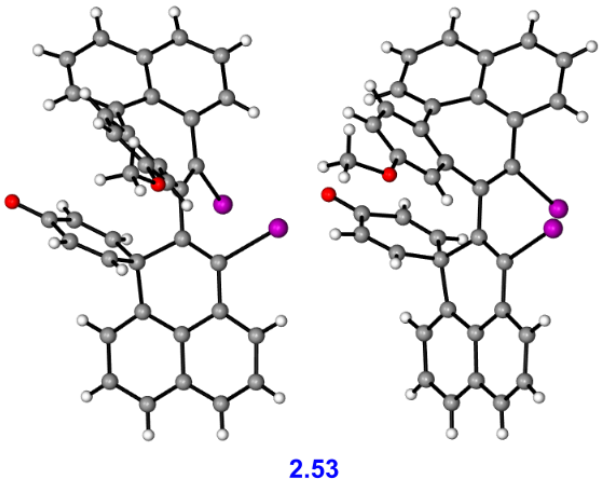

Figure 37: The X-ray crystal structure of **2.53**.

2.5.3.2 The isomerization of the spiro compound

In this part, we will demonstrate the isomerization of the spiro compound. Chia-Wen and colleagues reported the isomerization of spiro compound **2.54** into **2.55** resulting in forming six-membered ring as illustrated in Scheme 48.[90] They used 2 equivalents of H_2SO_4 and stirring at room temperature in a 1:1 ratio of DCM:MeOH. We attempted their method to isomerize **2.49** into **2.56**, resulting in only starting materials.

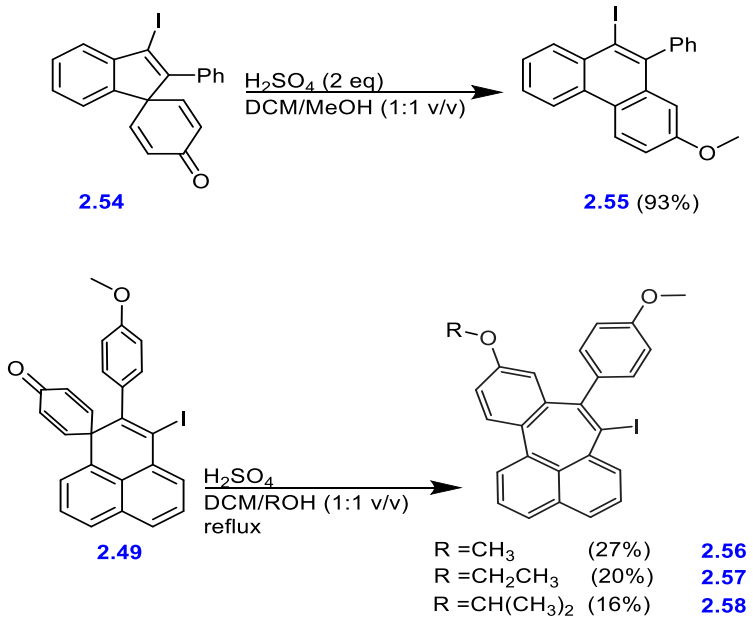

Scheme 48: The isomerization of spiro compound.

However, heating to reflux in 1:1 mixture of DCM with primary or secondary alcohol in the presence of H_2SO_4 promotes isomerization of spiro compounds into a seven-membered ring. Under these conditions, methanol and ethanol afforded 27% and 20% yields of compounds **2.56** and **2.57**, respectively (Entries 1 and 2, Table 11), while isopropanol gave a 16% yield of compound **2.58** (Entry 3). We noticed while monitoring the isomerization of **2.49** by TLC, the starting materials were present in the reaction but in isopropanol compound **2.49** precipitates.

Entry	ROH	Temp.	Time	Yield	
				2.49[a]	Seven-membered ring
1	Methanol	65 °C	71h	56%	**2.56** (27%)
2	Ethanol	80 °C	96h	61%	**2.57** (20%)
3	Isopropanol	84 °C	96h	53%	**2.58** (16%)

[a] Recovered starting materials.

Table 11: The isomerization of spiro compound **2.49** into a seven-membered ring.

Compound **2.56** was successfully crystallized in the dark using a mixture of DCM/hexane. Notably, exposure to light during crystallization led to decomposition. The X-ray structure of **2.56** and the ^1H NMR spectra of **2.56**, **2.57**, and **2.58** are illustrated in Figure 38 showing the phenyl

proton (blue highlighting) as a broadness peak due to the iodine atom's effect on the phenyl's rotation.

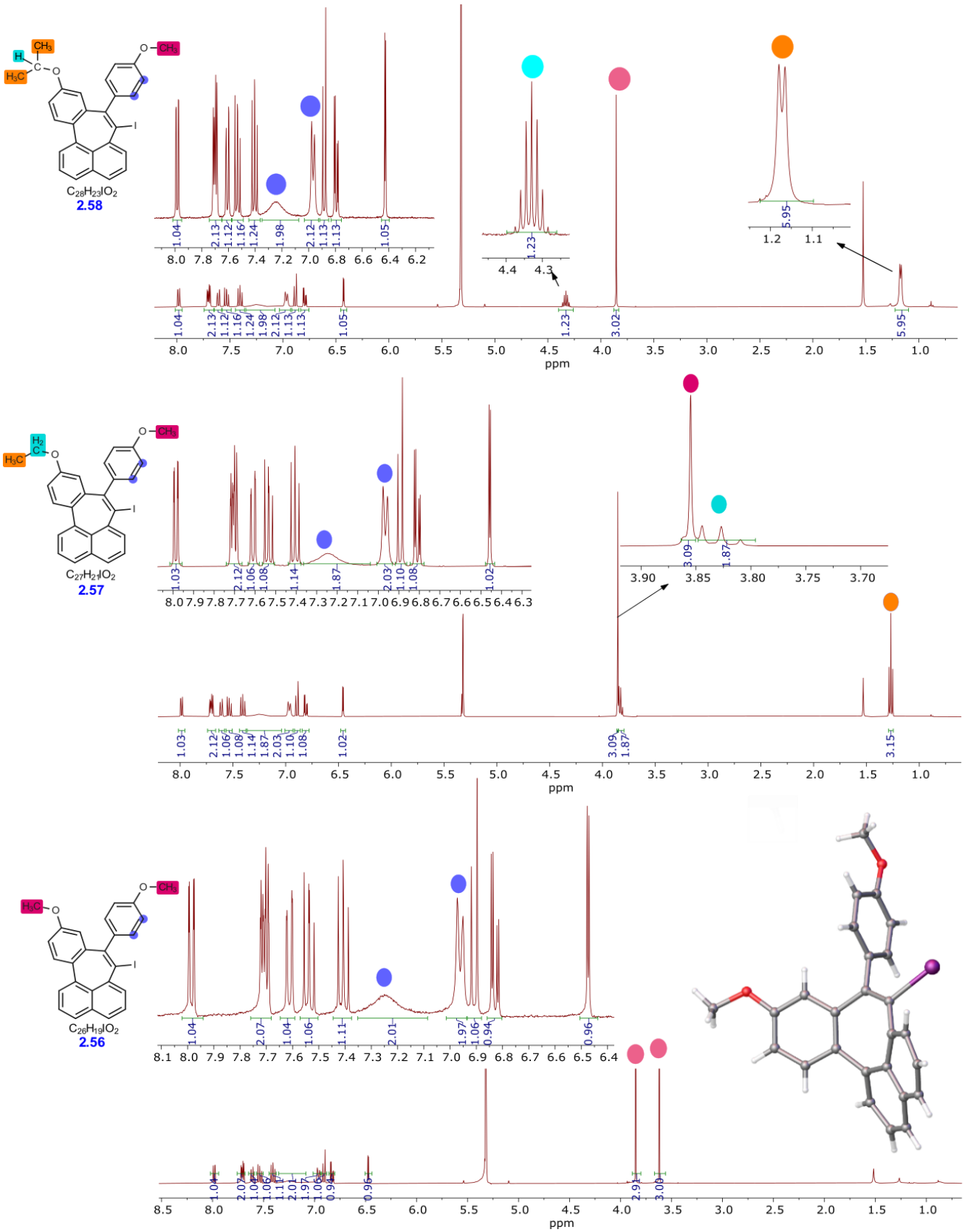

Figure 38: The X-ray structure of **2.56** and ^{1}H NMR spectrum of **2.56**, **2.57**, **2.58**.

The proposed isomerization mechanism is depicted in figure 39.

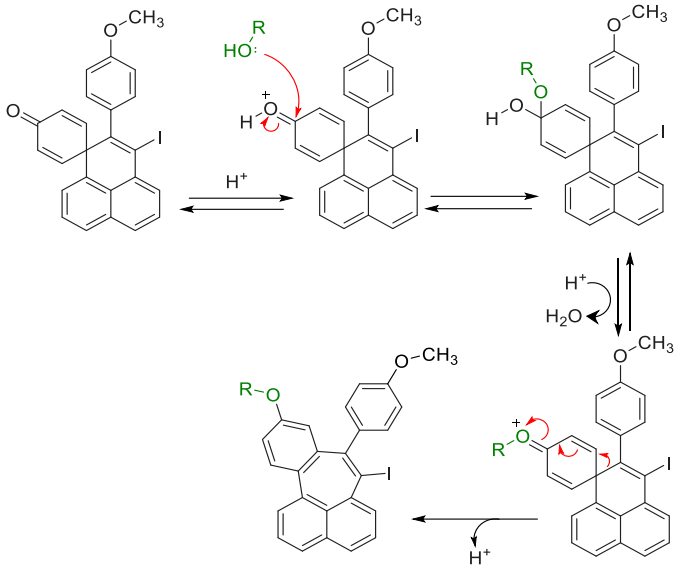

Figure 39: The isomerization mechanisms of **2.49** into seven-membered ring.

2.5.4 Optical Properties of Seven-, Six-membered rings, and Spiro compounds.

The photophysical properties (UV–Vis absorption and fluorescence emission) of the seven-, six-membered and spiro rings were investigated. The spiro compounds (**2.50** and **2.49**) in Figure 40 display three distinct absorption peaks at approximately λ ~ 317, 330, and 350 nm. Product **2.53** shows a similar progression but with a slight red shift (λ = 323, 340, 359 nm). Compound **2.39** exhibits two absorption bands at 332 and 348 nm. These compounds emit in the 468–498 nm range.

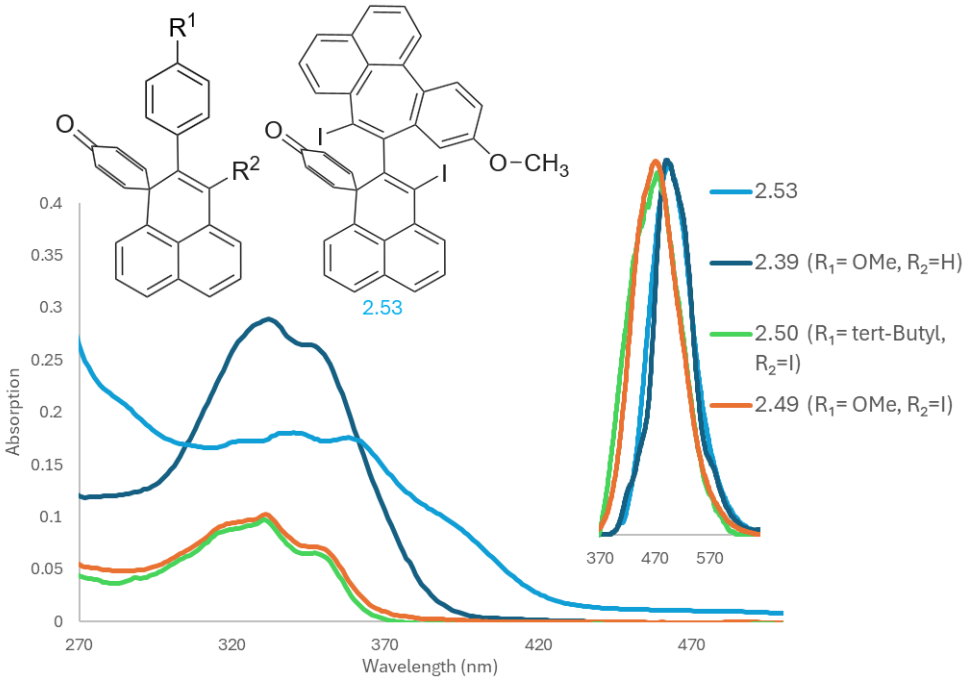

Figure 40: UV–vis absorption and emission spectra of spiro compounds.

Compared to the spiro systems, the seven-membered ring derivatives in Figure 41 feature a single maximum absorption band around ~373 nm. Their emission covers a broader range (472–491 nm).

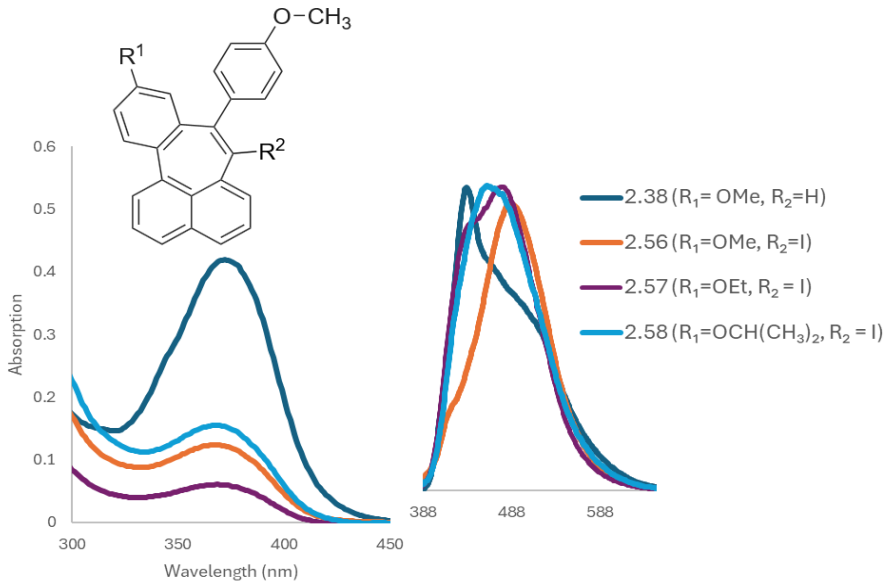

Figure 41: UV-vis absorption and emission spectra of seven-membered compounds.

The benzanthrone absorbs (figure 42) at 413 nm (**2.40**), and 378 nm (**2.41**). Compound **2.41** emits at 504 nm (upon excitation at 378 nm), while **2.40** emits at 491 nm (upon excitation at 413 nm). Additionally, compound **2.51** shows two absorption peaks at λ = 298 and 384 nm, with emission at 513 nm (excitation at 384 nm). The aldehyde **2.42** exhibits a maximum absorption at λ = 349 nm and emits at 471 nm.

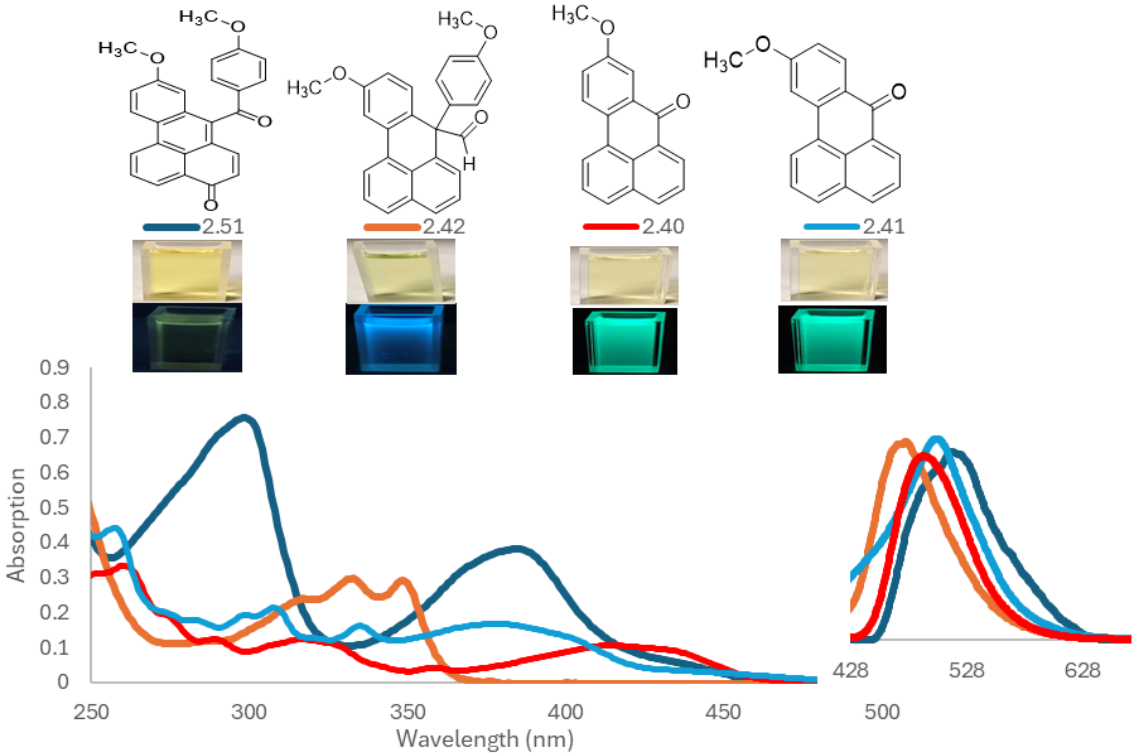

Figure 42: UV-vis absorption and emission spectra of **2.51**, **2.42**, **2.40**, **2.41**.

2.6 The second model of extension of PAHs

2.6.1 The X-ray structure of **2.34**

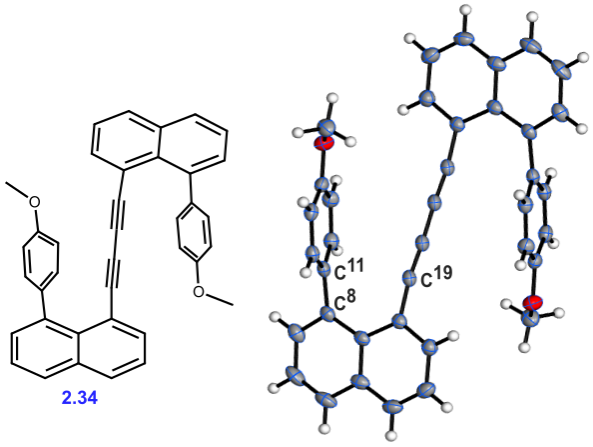

Figure 43: The X-ray structure of **2.34**.

The X-ray structure of **2.34** in figure 43 inspired us to exploit the conjugation extension. In addition, this inspiration is due to the rotation of the phenyl ring and our collaborator Dr David Hughes states that the two naphthalene rings are parallel and bent only slightly from coplanarity. The phenyl rings are rotated *ca* 67° about the C(8)-C(11) bond, away from the naphthalene rings and lie close on either side of the di-ynyl chain, with the C(11)…C(19) contact distances at 2.820 Å. This forced π-π overlap can be seen qualitatively from the crystal structure. Intriguingly, this illustrates face to face communication between the phenyl groups via the alkyne. The proposed pathway for the extension of compound **2.34** is illustrated in Scheme 49. The sequence begins with optimizing yield of **2.34**, followed by demethylation of its methoxy groups, triflation, and finally a Suzuki coupling.

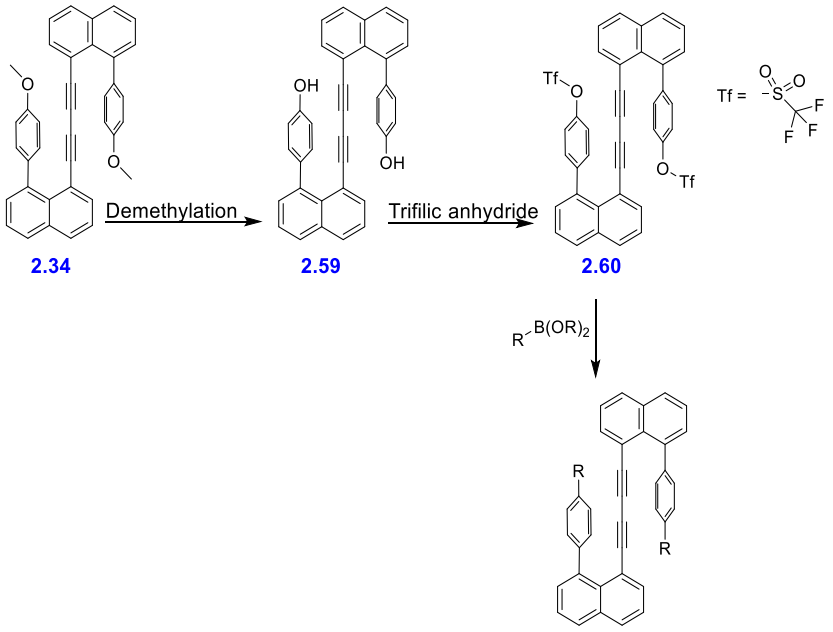

Scheme 49:The outline route for the extension of **2.34**.

2.6.2 Sonogashira coupling of **2.28**

The homo-coupling of compound **2.28** to yield **2.34** was optimized, as summarized in Table 12. When palladium was used as the catalyst (Entry 1, Table 12), the yield of **2.34** was low. In contrast, using CuI or CuCl (Entries 2, 3, and 4) resulted in the precipitation of **2.34** from the reaction mixture. The solid product was collected by filtration, washed with water and then hexane, affording pure **2.34**. Although some amount of **2.34** remained in solution, attempts to isolate it by crystallization were unsuccessful due to impurities; it was subsequently purified by column chromatography using petroleum ether/ethyl acetate (100:15). In Entries 1 and 2, TLC analysis indicated incomplete consumption of starting material **2.28**, therefore we switched to CuI in entry 3,4 leading to only a trace amount of starting material **2.28** and increase in the yield of **2.34**.

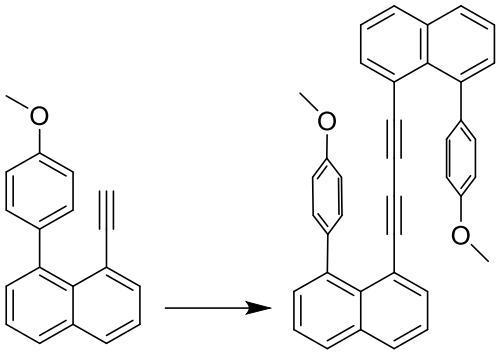

2.28 **2.34**

Entry	Cat.(%)	Ligand(%) /Base(equiv.)	DMF (mL)	Temp/°C (time/h)	Yield 2.34 (%)	
					Precipitation	Column
1	$Pd(MeCN)_2Cl_2$ (2%)	BINAP (4%) /DBU (6 eq)	4	120 (43)	-	16%
2	CuCl (4%)		2	60 (45)	33%	6%
3	CuI (4%)		2	60 (92)	41%	7%
4	CuI (7%)		2	60 (89)	47%	12%

Table 12: The optimization conditions for synthesis of **2.34**.

2.6.3 Demethylation of **2.28**

Boron tribromide (BBr_3) is commonly used for methoxy group demethylation, however it was avoided in our case **2.34** due to the presence of an alkyne group, which raises concerns about undesired cyclization reactions. Lithium iodide (LiI) has been reported to cleave alkyl aryl ethers.[91] For example, Harris demonstrated that refluxing 8-methoxynaphthalene with LiI in dry 2,4,6-collidine under nitrogen for 10 hours, followed by acidification, yielded 2-naphthol. However, this method failed to cleave hexadecylmethyl ether, highlighting its selectivity. To test lithium iodide effect, we introduced compound **2.34** (Entry 1, Table 13) into DME as a solvent that contains LiI

and stirred at room temperature for 2 hours, TLC analysis showed no reaction. Increasing the temperature to 60 °C for 23 hours also resulted in no conversion, only starting materials present. Entry 2 started by using LiI with 2,4,6-collidine and **2.34** at 130 °C for 7 hours resulting in no conversion. Heating at 160 °C for 18 hours, similarly showed no demethylation, as only starting materials were recovered.

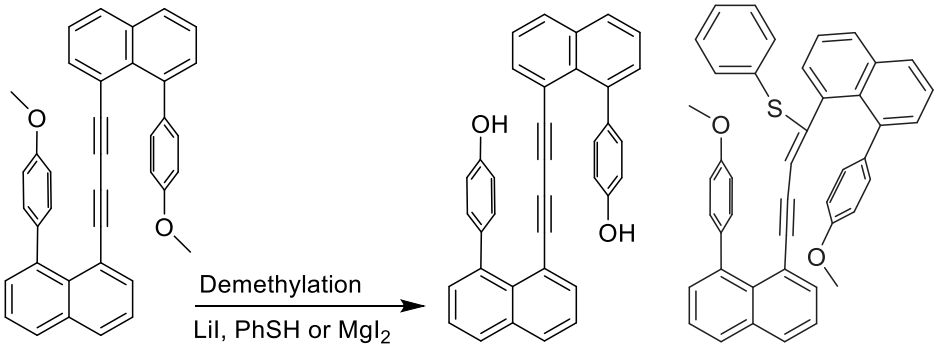

2.34 **2.59** **2.61**

Entry	Demethylating agent (eq)	Base (Eqiv.)	Solvent (mL)	Temp/°C (time/h)	Yield (%)
1	LiI (4)		DME	r.t - 60 (25)	No reaction
2	LiI (4)	2,4,6-trimethyl pyridine		130 - 160 (25)	No reaction
3[a]	Thiophenol (6)	K_2CO_3(5)	DMF (6)	120 (23)	**2.61 (**54%**)**
4[b]	MgI_2 (10)		Toluene (3)	170 (28)	Mixture, decomposes

Table 13: The utilized condition for demethylating methoxy to hydroxy. [a]Microwave vial, [b] Sealed tube.

Another well-known demethylation agent is thiophenol and we attempted to use this reagent to demethylate **2.34** (Entry 3).[92] However, instead of converting methoxy to hydroxy we ended up in conversion of alkyne to alkene resulting in breaking down the symmetry of **2.34** due to the addition of thiophenol **2.61**.[93] The ^{1}H NMR spectra (figure 44) of compound **2.61** displays the expected number of protons, with two sets of signals corresponding to the methoxy groups (pink highlight) and the alkene signal for C–H proton (green highlight). Additionally, X-ray crystallographic analysis confirms the structure and unambiguously demonstrates the addition of thiophenol.

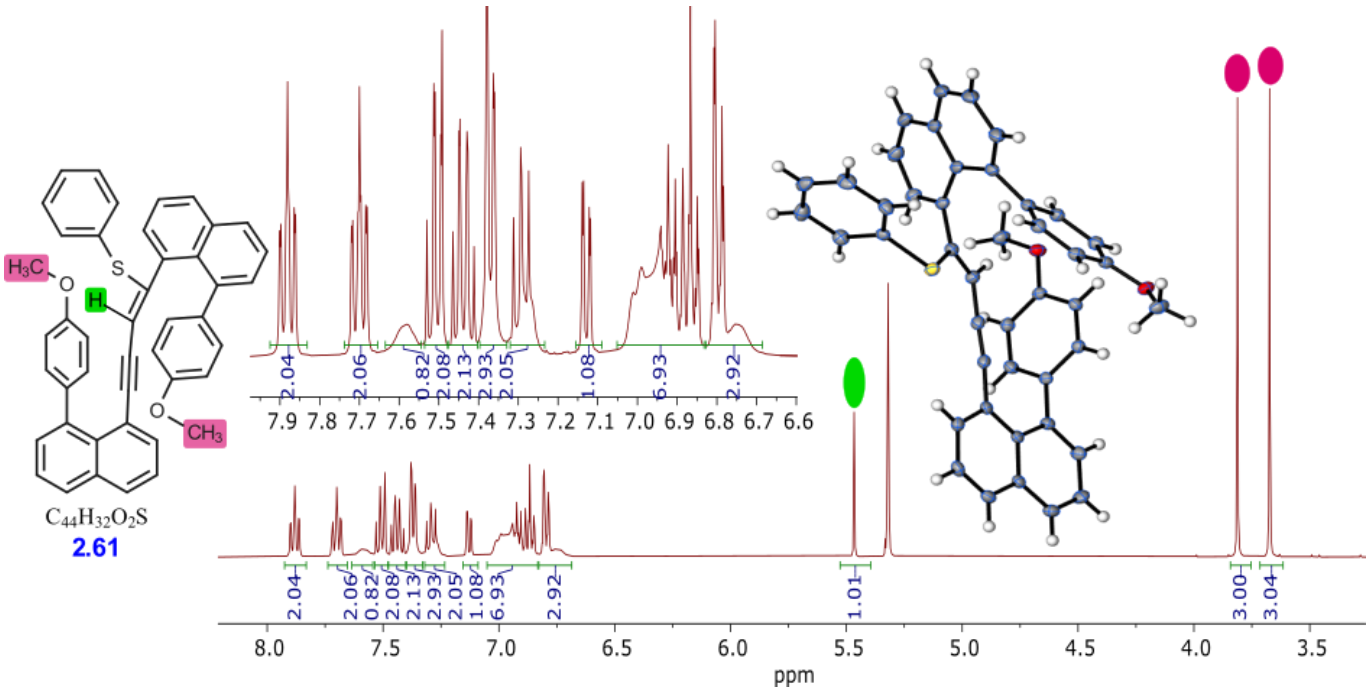

Figure 44: The ^{1}H NMR and X-ray crystal structure for **2.61**.

Another attempt to demethylate was made by using magnesium iodide, which is reported for conversion of the methoxy group.[94] We performed the experiment in entry 4 in a sealed tube, under N_2 at 170 °C for 28h. The starting materials **2.34** on TLC show a traceable amount (shadow). We added 15 ml of MeOH and stirred for 10 minutes then removed the solvent. A sample of the reaction mixture was analyzed by TLC, which indicated the presence of mixture and unstable compounds. MALDI-MS analysis, as shown in Figure 45, revealed peaks corresponding to the starting material **2.34** at m/z 515 [M+H], a monodemethylated product at m/z 501 [M+H], and a didemethylated species **2.59** at m/z 487 [M+H]. However, the product appears to undergo decomposition.

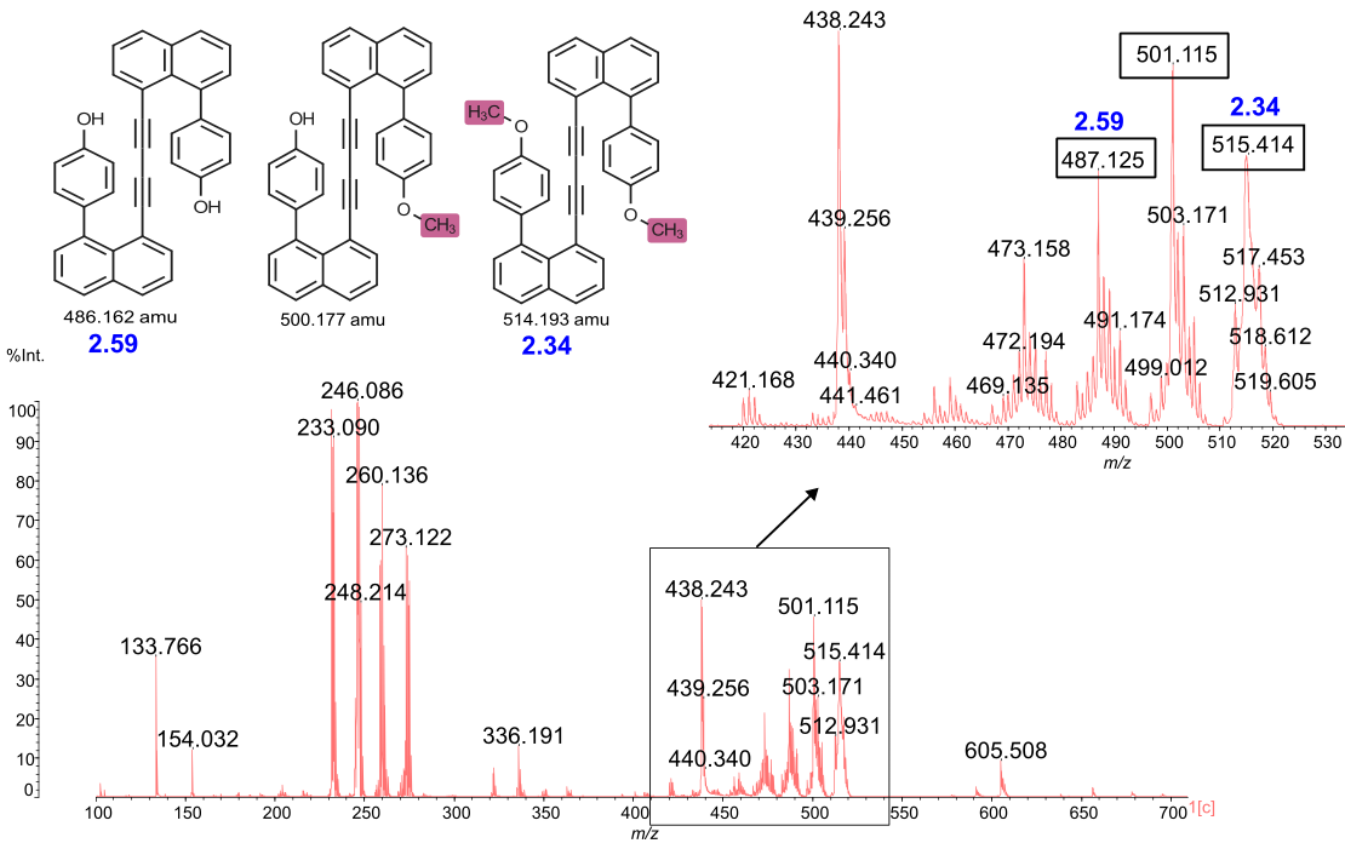

Figure 45: The Maldi-tof Ms of the mixture.

The demethylation of **2.34** was not successful due to presence of alkyne in the molecule which is easily affected by the demethylating reagents such as thiophenol.

2.7 Conclusion

Our project resulted in studying the challenging of bottom-up synthesis toward our target product from a small building block **2.7** which was prepared by using C-H activation cross coupling. The project commenced by optimizing the yield of **2.7,** then triflation led to activation of ortho and para position of **2.7** due to using pyridine which causes the insertion of pyridinium-triflate (in ortho and para position) and formation of Zincke imine**.** Replacing pyridine with 2,6-lutidine or 2,4,6-collidine led to overcoming the formation of side products. In addition, we exploit these positions toward electrophiles such as bromination. A new problem arises when coupling triflate **2.8** with terminal alkyne, and results in formation of fluoranthene **2.25** intramolecularly. The difficulty was resolved and ultimately, we were able to synthesize the coupled product **2.9** in reasonable yield. Cyclization of alkyne was attempted using a variety of catalysts Pd, Cu, where no cyclization was observed. Introducing acids such as TFA to **2.9** have shown to favour the formation of spiro compound **2.39** via 6-endo-dig and seven-member ring **2.38** ring via 7-endo-dig. Introducing TFA to **2.9** or **2.31** yields Benzanthrone and it's formation was investigated. Another attempt at cyclizing alkyne **2.9** or **2.31** by using ICl at -75 °C which was shown to favor 6-endo-dig path with a good yield 90-95%. Cyclization of homocoupling product **2.34** using ICl yields **2.53** which can be formed via two cyclization paths 6-endo-dig and 7-endo-dig. The required 6-exo-dig cyclization mode leading to obtain **2.10** was not observed. In addition, we have successfully isomerized the spiro compound into seven-membered ring by using refluxing in an acidic mixture of DCM and primary alcohol such as methanol, ethanol, and secondary alcohol for example isopropanol. We explored the possibility of extending the conjugation system of **2.34** from demethylated methoxies which proven to be challenging due to the presence of alkyne in a position that is easily cyclized or affected. We have attempted known demethylation reagents, some have no effect, or product decomposes, and others result in reaction of alkyne.

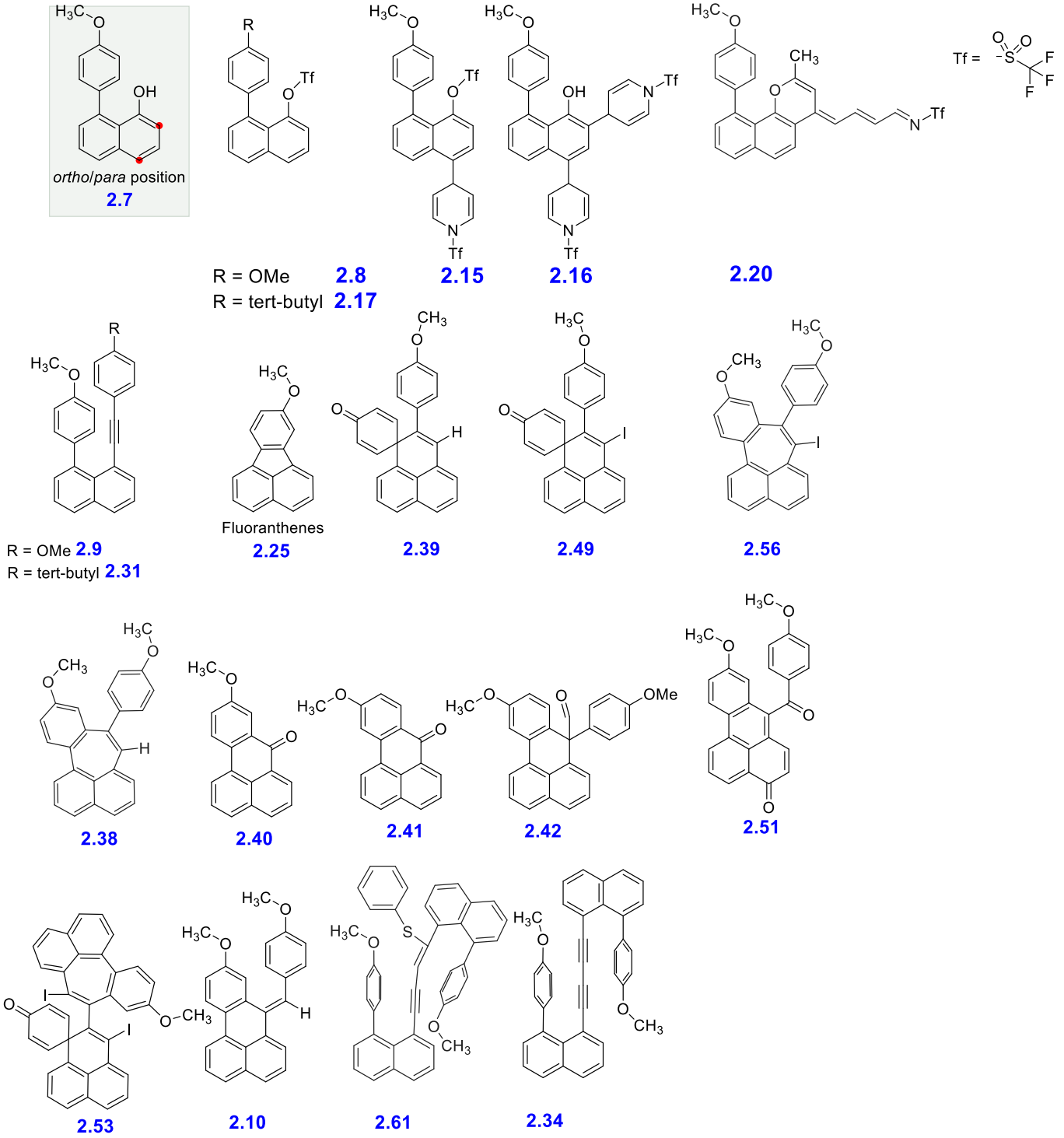

Figure 46: Products formed during the investigation of project.

2.8 Future work

The direct demethylation of the homocoupled product **2.34** under the previously discussed conditions was unsuccessful. Future work could investigate an alternative route (Scheme 50) beginning with an aryl iodide (or bromide, triflate) already functionalized with the extended aryl fragment. This sequence couples the intermediate with 1-naphthol, via similar C–H-activation. The approach installs different substituents at the 8-position of the naphthalene core and thereby provides access to symmetrical di-alkynes bearing varied groups at that position.

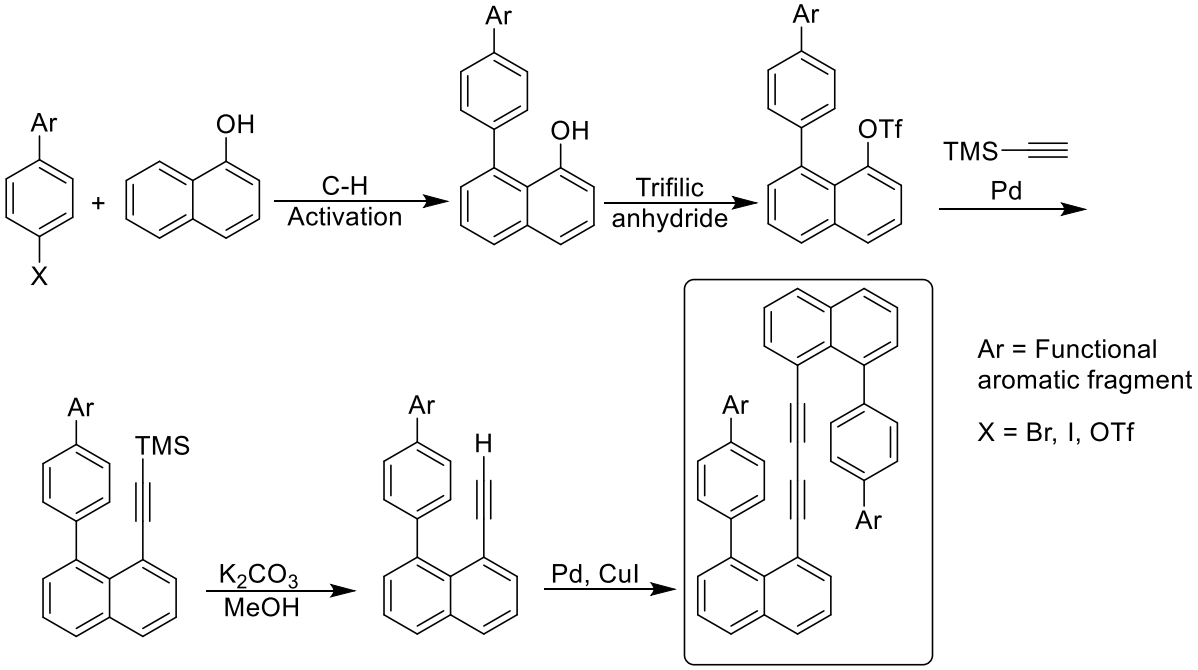

Scheme 50: An alternative route to the target di-alkynes.

3. Experimental

General Methods

Reagents and solvents were purchased from commercial suppliers and used without further purification unless otherwise specified. Reactions sensitive to moisture or oxygen were conducted under an inert nitrogen atmosphere. The term brine refers to a saturated aqueous solution of sodium chloride. Liquid–liquid extractions were performed using distilled water or saturated aqueous sodium hydrogen carbonate, and organic layers were dried over magnesium sulfate monohydrate. A Büchi rotary evaporator was used to remove solvents under reduced pressure.

Thin-layer chromatography (TLC) was performed on silica gel 60 F_{254} aluminum sheets (Alugram® Sil G/UV_{254}). Column chromatography was carried out using silica gel (60 Å, 70–230 mesh). Column chromatography was performed at ambient temperature, and the solvent ratios were calculated based on volume (v:v).

^{1}H NMR, ^{13}C NMR, and ^{19}F NMR spectra, as well as COSY and NOESY experiments, were recorded on a Bruker Avance 500 MHz spectrometer or on a Ultrashield PlusTM 400 spectrometer using 5 mm diameter tubes. Deuterated (i.e., acetone, chloroform, DCM) were used as solvents. ^{1}H and ^{13}C NMR chemical shifts are reported in ppm, with coupling constants (J) given in Hz. Spectra were recorded at room temperature unless otherwise specified.

UV–Vis absorption spectra were recorded on a Hitachi U-3310 spectrophotometer, and molar absorption coefficients (ε) were calculated from solutions of known concentration (M). Molecular masses were determined by MALDI-TOF mass spectrometry or/and HRMS using a Shimadzu AXIMA Performance instrument or/and MassLynx software. Melting points were determined using a Reichert Thermovar microscope equipped with a thermocouple-based temperature controller. Microwave-assisted reactions were performed in a Biotage Initiator microwave reactor.

3.1 C-H arylation of 1-naphtol derivatives

3.1.1 Synthesis of 8-(*p*-Methoxyphenyl)-1-naphthol **2.7** [80]

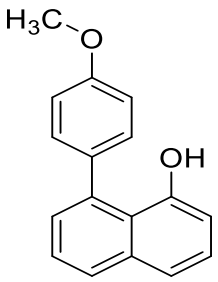

2.7

Cs_2CO_3 (1.3 g, 4 mmol) was added to a 25 ml two-neck round-bottom flask equipped with a coil condenser and heated to 105 °C under vacuum for 3 h. After cooling to r.t and purging with N_2, 1-naphthol (0.432 g, 3 mmol), 4-iodoanisole (0.936 g, 4 mmol), and $Pd(OAc)_2$ (0.016 g, 0.075 mmol, 2.5%) were added and the mixture subjected to vacuum for 2h. DMF (15 ml) was added under N_2, the temp. increased to 110 °C and the reaction stirred for 23 h. After cooling, the mixture was diluted with EtOAc (50 ml), washed with 1M HCl (30 ml), H_2O, and brine (30 ml). It was dried over $MgSO_4$, concentrated under vacuum, and subjected to column chromatography (Petroleum ether/ethyl acetate, 100:3) yielding **2.7** as a yellow solid (0.315 g, 75%).

m.p.112.9-115.2 °C.

Rf: 0.7 (Hexane/Ethyl acetate, 9:1).

^{1}H NMR (400 MHz, $CDCl_3$) δ 7.85 (dd, J = 8.4, 1.3 Hz, 1H), 7.50 (dd, J = 8.2, 1.3 Hz, 1H), 7.47 – 7.38 (m, 4H), 7.19 (dd, J = 7.0, 1.3 Hz, 1H), 7.05 (d, J = 8.7 Hz, 2H), 6.93 (dd, J = 7.5, 1.3 Hz, 1H), 5.68 (s, 1H), 3.90 (s, 3H).

^{13}C NMR (126 MHz, $CDCl_3$) δ 159.90, 153.24, 135.79, 135.73, 133.01, 130.75, 128.75, 128.54, 126.84, 124.87, 121.52, 120.88, 114.42, 111.62, 55.43.

MS (MALDI-TOF): m/z = 250.4 $[M]^+$

Chemical formula and molecular weight : $C_{17}H_{14}O_2$, 250.10 $g.mol^{-1}$.

UV-Vis (DCM): λ max (nm) (Ɛ ($M^{-1}.cm^{-1}$)) = 330 ($3.71\cdot10^3$), 305 ($5.71\cdot10^3$), 234 ($2.28\cdot10^4$).

Fluorescence (CH_2Cl_2, Excitation at 305 nm): 388 nm.

3.1.2 Synthesis of 8-[*p*-(tert-Butyl)phenyl]-1-naphthol **2.13**

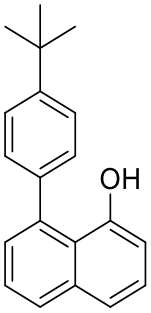

2.13

Cs_2CO_3 (1.3 g, 4 mmol) was added to a 25 ml two-neck round-bottom flask and equipped with a coil condenser and heated to 105 °C under vacuum for 3 h. After cooling to r.t and purging with N_2,1-naphthol (0.432 g, 3 mmol), $Pd(OAc)_2$ (0.016 g, 0.075 mmol, 2.5%) were added and the mixture subjected to vacuum for 2h. DMF (15 ml) and 4-tert-butyliodobenzene (0.53 ml, 3 mmol) were added under N_2 and temperature increased to 110 °C and the reaction stirred for 26 h. After cooling, the mixture was diluted with EtOAc (50 ml), washed with 1M HCl (30 ml), H_2O, and brine (30 ml). It was dried over $MgSO_4$, concentrated under vacuum, and subjected to column (Petroleum ether/ethyl acetate, 100:1-10) yielding **2.13** as yellow solid (0.679 g, 82%).

m.p.128.6-131.6 °C.

Rf: 0.5 (ethyl acetate/petroleum ether, 1:9).

^{1}H NMR (400 MHz, $CDCl_3$) δ 7.86 (dd, J = 8.3, 1.3 Hz, 1H), 7.60 – 7.54 (m, 2H), 7.51 (dd, J = 8.0, 1.4 Hz, 1H), 7.48 – 7.43 (m, 3H), 7.40 (t, J = 7.9 Hz, 1H), 7.21 (dd, J = 7.1, 1.3 Hz, 1H), 6.89 (dd, J = 7.7, 1.3 Hz, 1H), 5.58 (s, 1H), 1.42 (s, 9H).

^{13}C NMR (101 MHz, $CDCl_3$) δ 155.20, 153.78, 140.11, 138.20, 137.72, 131.05, 130.49, 130.39, 128.71, 127.91, 126.86, 123.35, 122.77, 113.45, 36.60, 33.02.

MS (MALDI-TOF): m/z = 275.53 [M-1].

Chemical formula and molecular weight : $C_{20}H_{20}O$, 276.15 g.mol^{-1}.

3.2 Triflation of arylated 1-naphthols

3.2.1 Method A by using Pyridine

8-Arylated-1-naphthol derivatives (1 eq) were placed in 50 ml two neck-round-bottom flask followed by dry DCM 10 ml and stirred for 10 min under N_2. Pyridine (3 eq) was added and stirred for 10 min at room temperature followed by the slow addition of a solution of triflic anhydride in DCM (0.28 M, 3 eq). The mixture was left to stir overnight at room temperature then transferred to separating funnel, and washed with water (30 ml), dried over $MgSO_4$, concentrated, and subjected to column chromatography yielding the desired product.

3.2.2 Method B by using 2,4-lutidine

8-Arylated-1-naphthol derivatives (1 eq) were placed in 50 ml two neck-round-bottom flask followed by dry DCM 10 ml and stirred for 10 min under N_2. 2,6-Lutidine (3 eq) was added to the flask and stirred for 10 min at room temperature followed by the slow addition of a solution of triflic anhydride in DCM (0.28 M, 3 eq). The mixture was left to stir overnight at room temperature then transferred to a separating funnel and washed with 1M HCl (20 ml), water (30 ml x3) and brine (30 ml). It was dried over $MgSO_4$, concentrated, and subjected to column chromatography yielding the desired product.

3.2.3 Method C by using 2,4,6-collidine

8-Arylated-1-naphthol derivatives (1 eq) were placed in 50 ml two neck-round-bottom flask followed by dry DCM 10 ml and stirred for 10 min under N_2. 2,4,6-collidine (3 eq) was added to the flask and stirred for another 10 min at room temperature followed by the slow addition of triflic anhydride in DCM (0.28 M, 3 eq). The mixture was left to stir at room temperature overnight and more 2,4,6-collidine (3 eq) and triflic anhydride in DCM (0.28 M, 3 eq), were introduced in the same sequential manner. The reaction was left to stir at room temperature for 19 h then transferred to separating funnel and washed with 1M HCl (10 ml), water (10 ml x3) and brine (30 ml). It was dried over $MgSO_4$, concentrated, and subjected to column chromatography yielding the desired compound.

3.2.4 Synthesis of triflate **2.8**

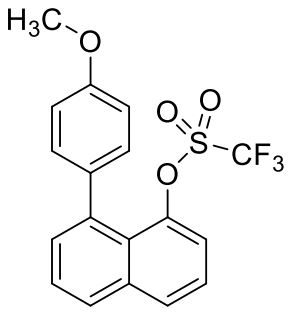

2.8

Method A

8-p-Methoxyphenyl-1-naphthol **2.7** (0.296 g, 1.184 mmol, 1 eq), pyridine (0.28 ml, 3.552 mmol, 3 eq), triflic anhydride (0.596 ml, 0.28 M, 3 eq). The product isolated by column chromatography (Petroleum ether/ethyl acetate, 100/5) as white solid (0.236 g, 52%).

Method B

8-p-Methoxyphenyl-1-naphthol **2.7** (0.11 g, 0.28 mmol, 1 eq), 2,6-lutidine (0.15 ml, 1.32 mmol, 3 eq), triflic anhydride (0.56 ml, 0.28 M, 3 eq). The product isolated by column chromatography (Petroleum ether/ethyl acetate, 100/10) as white solid (0.056 g, 56%).

Method C

8-p-Methoxyphenyl-1-naphthol **2.7** (0.289 g, 1.12 mmol, 1 eq), 2,4,6-collidine (0.4 ml, 3.36 mmol, 3 eq), triflic anhydride (0.56 ml, 0.28 M, 3 eq). The product is isolated by column chromatography (Petroleum ether/ethyl acetate, 100/10) as white solid (0.266 g, 62%).

2.8

m.p.131.4-132.6 °C.

Rf: 0.8 (Hexane/Ethyl acetate, 9:1).

^{1}H NMR (500 MHz, $(CD_3)_2CO$) δ 8.18 (dd, J = 8.2, 1.2 Hz, 1H), 8.09 (dd, J = 8.2, 1.2 Hz, 1H), 7.73 – 7.68 (m, 2H), 7.61 (dt, J = 7.7, 1.0 Hz, 1H), 7.55 (dd, J = 7.2, 1.2 Hz, 1H), 7.37 (d, J = 8.8 Hz, 2H), 7.04 (d, J = 8.7 Hz, 2H), 3.89 (s, 3H).

^{13}C NMR (126 MHz, $(CD_3)_2CO$) δ 159.54, 145.66, 137.05, 136.60, 133.89, 132.05, 130.75, 130.01, 127.79, 126.75, 125.35, 124.38, 119.96, 119.78, 117.23, 113.34, 54.74.

^{19}F (471 MHz, $(CD_3)_2CO$) δ -72.60.

HRMS (ESI^+-TOF) m/z: $[M+H]^+$ calcd for $C_{18}H_{14}F_3O_4S$ 383.0565, found 383.0573.

UV-Vis (DCM): λ max (nm) (Ɛ ($M^{-1}.cm^{-1}$)) = 304 ($8.26\cdot10^3$), 226 ($4.0\cdot10^4$).

Fluorescence (CH_2Cl_2, Excitation at 304 nm): 397 nm.

3.2.5 Side products resulting from using method A

3.2.5.1 Synthesis of **2.15**

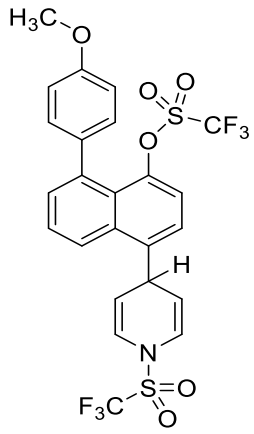

2.15

This compound was obtained as white crystals (0.04 g, 6%).

m.p.112.3-114.5 °C.

Rf: 0.5 (Hexane/ethyl acetate, 2:8).

^{1}H NMR (500 MHz, $(CD_3)_2CO$) δ 8.39 (dt, J = 8.4, 0.9 Hz, 1H), 7.80 (dd, J = 8.6, 7.2 Hz, 1H), 7.69 – 7.61 (m, 2H), 7.59 (dd, J = 7.2, 1.1 Hz, 1H), 7.35 (d, J = 8.8 Hz, 1H), 7.02 (d, J = 8.7 Hz, 1H), 6.87 – 6.79 (m, 2H), 5.62 – 5.56 (m, 2H), 5.27 (s, 1H), 3.87 (s, 3H).

^{13}C NMR (126 MHz, $(CD_3)_2CO$) δ 159.58, 144.84, 141.60, 138.01, 134.12, 133.35, 132.08, 130.68, 127.38, 126.09, 124.79, 122.60, 121.37, 121.07, 119.83, 119.76, 118.49, 117.21, 113.41, 112.78, 54.75, 33.64.

^{19}F (471 MHz, $(CD_3)_2CO$) δ -73.69, -75.60.

HRMS (ESI-TOF) m/z: $[M]^+$ calcd for $C_{24}H_{17}F_6NO_6S_2$ 593.040, found 593.0406.

UV-Vis (DCM): λ max (nm) (Ɛ ($M^{-1}.cm^{-1}$)) = 314 ($4.63\cdot10^4$), 230 ($1.18\cdot10^4$).

Fluorescence (CH_2Cl_2, Excitation at 314 nm): 413 nm.

3.2.5.2 Synthesis of **2.16**

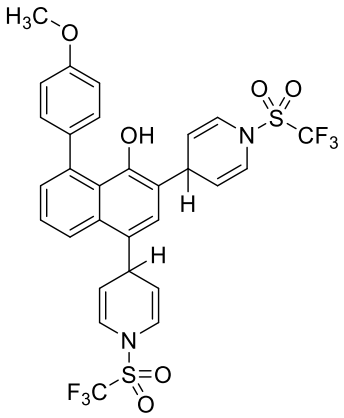

2.16

This compound was crystalized by DCM/MeOH yielding the titled compound as colorless crystals (0.054 g, 7%).

m.p.166.4-168.1 °C.

Rf: 0.38 (Hexane/ethyl acetate, 2:8).

^{1}H NMR (500 MHz, $(CD_3)_2CO$) δ 8.27 – 8.22 (m, 1H), 7.62 (dd, J = 8.6, 7.0 Hz, 1H), 7.48 (d, J = 8.6 Hz, 1H), 7.45 (s, 1H), 7.31 (dd, J = 7.0, 1.2 Hz, 1H), 7.16 (d, J = 8.7 Hz, 1H), 6.77 – 6.71 (m, 2H), 6.70 – 6.65 (m, 2H), 6.29 (s, 1H), 5.53 – 5.47 (m, 2H), 5.36 – 5.29 (m, 2H), 5.13 (s, 1H), 4.75 (s, 1H), 3.93 (s, 3H).

^{19}F (471 MHz, $(CD_3)_2CO$) δ -75.47.

HRMS (ESI-TOF) m/z: $[M]^+$ calcd for $C_{29}H_{22}F_6N_2O_6S_2$ 672.0823, found 672.0819.

UV-Vis (DCM): λ max (nm) (Ɛ ($M^{-1}.cm^{-1}$)) = 316 ($1.10\cdot10^4$), 337 ($9.36\cdot10^3$), 246 ($4.3\cdot10^4$).

Fluorescence (CH_2Cl_2, Excitation at 316 nm): 410 nm.

3.2.5.3 Synthesis of **2.20**

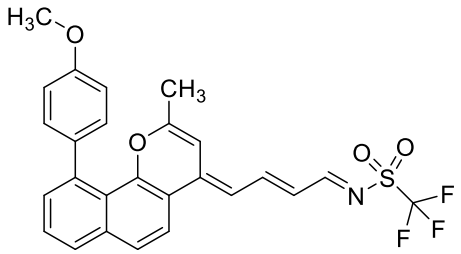

2.20

Modified Method A

Before work-up, acetone was added dropwise (6 ml) and stirred for 24 h, product **2.16** was isolated by column chromatography (Petroleum ether/ethyl acetate, 7:3), crystalized from DCM and filtered while cold producing red crystals, yielding (0.023 g , 4%).

m.p.>350 °C.

Rf: 0.4 (hexane: ethyl acetate, 7:3).

^{1}H NMR (500 MHz, $(CD_3)_2CO$) δ 8.65 (d, J = 10.6 Hz, 1H), 8.57 (t, J = 13.1 Hz, 1H), 8.20 (d, J = 9.1 Hz, 1H), 8.10 (dd, J = 8.2, 1.3 Hz, 1H), 8.05 (d, J = 9.1 Hz, 1H), 7.81 (dd, J = 8.1, 7.2 Hz, 1H), 7.55 (dd, J = 7.2, 1.3 Hz, 1H), 7.38 – 7.33 (m, 2H), 7.24 (s, 1H), 7.12 – 7.06 (m, 3H), 6.60 (dd, J = 13.4, 10.6 Hz, 1H), 3.93 (s, 3H), 1.81 (s, 3H).

^{19}F (376 MHz, $(CD_3)_2CO$) δ -79.08.

HRMS (ESI) m/z: $[M+H]^+$ calcd for $C_{26}H_{21}F_3NO_4S$ 500.1143, found 500.1155.

UV-Vis (DCM): λ max (nm) (Ɛ ($M^{-1}.cm^{-1}$)) = 546 ($7.60\cdot10^3$), 512 ($5.4\cdot10^3$), 232 ($2.8\cdot10^3$).

Fluorescence (CH_2Cl_2, Excitation at 546 nm): 597 nm.

3.2.5.4 Synthesis of triflate pyridine **2.18**

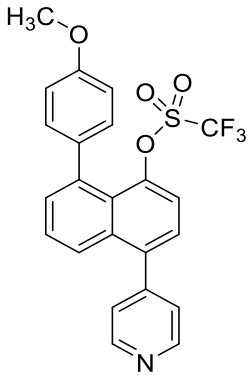

2.18

Compound **2.15** (0.127g, 0.214 mmol, 1 eq), and K_2CO_3 (0.147 g, 1.07 mmol, 5 eq) were mixed in a 50 ml two neck-round-bottom flask followed by dry DMF 5 ml. The reaction mixture stirred at room temperature under N_2 for 36h, and diluted with EtOAc and transferred to separating funnel, washed with water (30 ml), dried over $MgSO_4$, and concentrated under vacuum. Purification by column chromatography (DCM/ethyl acetate, 1:1) yielded the title compound as a white solid (0.066 g, 67%).
m.p.114.2-115.3 °C.
Rf: 0.5 (ethyl acetate).
^{1}H NMR (500 MHz, $(CD_3)_2CO$) δ 8.67 (d, J = 5.0 Hz, 2H), 7.75 (dd, J = 8.5, 1.2 Hz, 1H), 7.59 – 7.51 (m, 3H), 7.49 – 7.43 (m, 3H), 7.25 (d, J = 8.7 Hz, 2H), 6.90 (d, J = 8.9 Hz, 2H), 3.75 (s, 3H).
^{13}C NMR (126 MHz, $(CD_3)_2CO$) δ 159.65, 149.59, 147.81, 145.77, 139.15, 137.64, 133.94, 133.80, 132.33, 130.74, 128.76, 127.35, 126.51, 125.19, 125.08, 124.72, 119.49, 113.45, 54.77.
^{19}F (471 MHz, $(CD_3)_2CO$) δ -73.67.
HRMS (ESI$^+$-TOF) m/z: $[M+H]^+$ calcd for $C_{23}H_{17}F_3NO_4S$ 460.083, 460.084.
UV-Vis (DCM): λ max (nm) (Ɛ ($M^{-1}.cm^{-1}$)) = 318 ($1.05\cdot10^4$), 228 ($4.43\cdot10^4$).
Fluorescence (CH_2Cl_2, Excitation at 318 nm): 440 nm.

3.2.6 Synthesis of triflate **2.17**

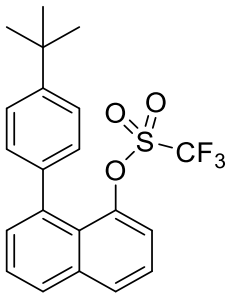

2.17

Method B

8-[p-(tert-Butyl)phenyl]-1-naphthol **2.13** (0.52 g, 1.88 mmol, 1 eq), 2,6-lutidine (0.65 ml, 5.6 mmol, 3 eq), subjected to column chromatography (Pet.ether/DCM, 100/10) yielding **2.17** as white solid (0.21g, 28%).

m.p.104.8-106.7 °C.

Rf: 0.6 (ethyl acetate/petroleum ether, 1:9).

1H NMR (500 MHz, Acetone-d6) δ 8.20 (d, J = 8.3 Hz, 1H), 8.11 (d, J = 8.9 Hz, 1H), 7.77 – 7.67 (m, 2H), 7.62 (d, J = 7.7 Hz, 1H), 7.58 (d, J = 7.2 Hz, 1H), 7.52 (d, J = 7.0 Hz, 2H), 7.38 (d, J = 7.0 Hz, 2H), 1.42 (s, 9H).

^{13}C NMR (126 MHz, Acetone) δ 150.19, 145.45, 138.66, 137.29, 136.58, 131.93, 129.98, 129.27, 127.98, 126.74, 125.38, 124.66, 124.30, 119.97, 119.72, 117.17, 34.20, 30.77.

^{19}F (471 MHz, Acetone-d_6) δ -73.80.

HRMS (ESI$^+$-TOF) m/z: $[M+H]^+$ calcd for $C_{21}H_{20}F_3O_3S$ 408.1007, found 408.0933.

3.3 Bromination of 8-(*p*-Methoxyphenyl)-1-naphthol **2.7**

3.3.1 Synthesis of 4-bromo-8-(*p*-methoxyphenyl)-1-naphthol **2.21**

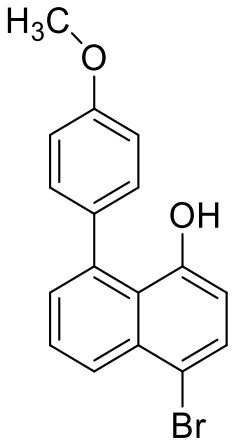

2.21

Compound **2.7** (0.2 g, 0.8 mmol, 1 eq) and NBS (0.16 g, 0.9 mmol, 1.1 eq) were introduced into a two-neck round-bottom flask, followed by MeCN (20 ml). The reaction was stirred for 20h under N_2, then stopped and transferred into a separating funnel, and the organic layer extracted with DCM, followed by brine. The organic layer was dried over Na_2SO_4, the solvent evaporated, and the title product purified with column chromatography (Petroleum ether/ethyl acetate, 200/8) yielding the title compound as off-white solid (0.144 g, 54%).

m.p.124.3-127.8 °C.

Rf: 0.5 (ethyl acetate/petroleum ether, 1:4).

^{1}H NMR (500 MHz, CD_2Cl_2) δ 8.32 – 8.25 (m, 1H), 7.70 (d, J = 8.2 Hz, 1H), 7.57 (dd, J = 8.6, 7.0 Hz, 1H), 7.41 (d, J = 8.7 Hz, 2H), 7.27 (dd, J = 7.0, 1.3 Hz, 1H), 7.06 (d, J = 8.7 Hz, 2H), 6.77 (d, J = 8.2 Hz, 1H), 5.73 (s, 1H), 3.89 (s, 3H).

^{13}C NMR (126 MHz, CD_2Cl_2) δ 160.21, 153.37, 136.53, 133.20, 132.01, 130.77, 130.76, 129.75, 127.59, 126.37, 122.78, 114.47, 113.00, 112.05, 55.43.

MS (MALDI-TOF): m/z = 329.07 ($[M + H]^+$, ^{79}Br), 331.06 ($[M + H]^+$, ^{81}Br) (calcd 329.0177 and 331.0158 for $C_{17}H_{14}BrO_2$).

HRMS (ESI^+-TOF) m/z 329.0187 ($[M + H]^+$, ^{79}Br), 331.0171 ($[M + H]^+$, ^{81}Br) (calcd 329.0177 and 331.0158 for $C_{17}H_{14}BrO_2$).

UV-Vis (DCM) : λ max (nm) (Ɛ ($M^{-1}.cm^{-1}$)) = 315 ($1.03 \cdot 10^4$).

3.3.2 Synthesis of 2-bromo-8-(3-bromo-4-methoxyphenyl)-1,4-naphthalenedione **2.22**

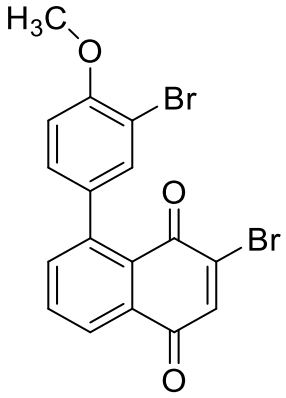

2.22

Compound **2.7** (0.2 g, 0.8 mmol, 1 eq) and NBS (0.28 g, 1.6 mmol, 4 eq) were introduced into a two-neck round-bottom flask, followed by MeCN (20 ml). The reaction was stirred for 17h under N_2, then stopped and transferred into a separating funnel, and the organic layer was extracted with DCM, followed by brine. The organic layer was dried over Na_2SO_4, and the solvent evaporated, and the title product purified with column chromatography (Petroleum ether/ethyl acetate, 100:10) yielding the title compound as a off-white solid (0.04 g, 24%).

m.p.203-206 °C.

Rf: 0.3 (ethyl acetate/petroleum ether, 2:8).

^{1}H NMR (500 MHz, $CDCl_3$) δ 8.17 (dd, J = 7.8, 1.4 Hz, 1H), 7.75 (t, J = 7.7 Hz, 1H), 7.55 (dd, J = 7.7, 1.4 Hz, 1H), 7.52 (s, 1H), 7.43 (d, J = 2.2 Hz, 1H), 7.15 (dd, J = 8.4, 2.2 Hz, 1H), 6.96 (d, J = 8.5 Hz, 1H), 3.96 (s, 3H).

^{13}C NMR (126 MHz, $CDCl_3$) δ 182.42, 177.73, 155.45, 143.07, 141.70, 139.17, 137.89, 134.15, 133.40, 133.09, 132.75, 128.41, 128.02, 127.12, 111.50, 111.40, 56.29.

HRMS (ESI$^+$-TOF) m/z 420.9073 ([M + H]$^+$, $^{79}Br_2$), 422.9056 ([M + H]$^+$, $^{79}Br^{81}Br$), 424.9042 ([M + H]$^+$, $^{81}Br_2$) (calcd 420.9075, 422.9054 and 424.9037 for $C_{17}H_{11}Br_2O_3$).

UV-Vis (DCM) : λ max (nm) (Ɛ ($M^{-1}.cm^{-1}$)) = 280 ($1.63 \cdot 10^5$).

3.4 Synthesis of TMS acetylene derivatives

3.4.1 Synthesis of **2.27**

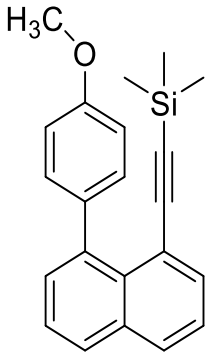

2.27

To a 10 mL microwave vial were added compound **2.8** (0.36 g, 0.94 mmol, 1 eq) and $Pd(MeCN)_2Cl_2$ (0.005 g, 0.0188 mmol, 2%), BINAP (0.035 g, 0.0564 mmol, 6%), and CuI (0.007 g, 0.0376 mmol, 4%). The vial was sealed, followed with addition of THF/DMF (3:1, 4 mL) under N_2 and the resulting mixture was stirred for 10 min. A solution of trimethylsilyl acetylene (1.3 ml, 9.4 mmol, 10 eq) and Et_3N (1.3 ml, 9.4 mmol, 10 eq) in glass vial were added to the microwave vial which was placed in the oil bath at 52 °C for 24h. Another solution of trimethylsilyl ethylene (1.3 ml, 9.4 mmol, 10 eq) and Et_3N (1.3 ml, 9.4 mmol, 10 eq) in glass vial were added to the microwave vial and left the reaction for another 48h. After cooling, the mixture was dissolved with ethyl acetate 30 ml and transferred to separatory funnel, quenched with 1M HCl (10 ml), brine 20 ml, then H_2O. The organic layer dried over $MgSO_4$, concentrated, and subjected to column chromatography (petroleum ether/DCM, 100:1) yielding the titled compound **2.27** as yellow oil (0.227 g, 73%).

Rf: 0.9 (Hexane/Ethyl acetate, 9:1).

^{1}H NMR (500 MHz, $CDCl_3$) δ 7.87 (dd, J = 8.2, 1.4 Hz, 1H), 7.82 (dd, J = 8.2, 1.4 Hz, 1H), 7.74 (dd, J = 7.2, 1.4 Hz, 1H), 7.47 (dd, J = 8.2, 7.0 Hz, 1H), 7.40 (dd, J = 8.2, 7.2 Hz, 1H), 7.35 (dd, J = 7.0, 1.4 Hz, 1H), 7.30 (d, J = 8.7 Hz, 2H), 6.91 (d, J = 8.7 Hz, 2H), 3.87 (s, 3H), 0.02 (s, 9H).

^{13}C NMR (126 MHz, $CDCl_3$) δ 159.09, 140.43, 136.08, 135.57, 134.59, 131.50, 131.32, 130.32, 129.85, 128.33, 125.53, 125.15, 120.77, 112.99, 104.68, 102.68, 55.19, 0.00.

MS (MALDI-TOF) : m/z = 330.10 $[M]^+$

Chemical formula and molecular weight : $C_{22}H_{22}OSi$, 330.14 $g.mol^{-1}$.

3.4.2 Synthesis of **2.29**

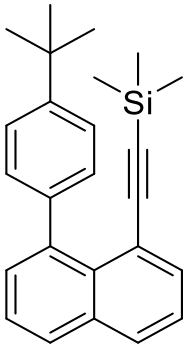

2.29

To a microwave vial were added compound **2.13** (0.46 g, 1.13 mmol, 1eq) and $Pd(MeCN)_2Cl_2$ (0.006 g, 0.026 mmol, 2%), BINAP (0.04 g, 0.067 mmol, 6%), and CuI (0.0085 g, 0.0045 mmol, 4%), The vial was sealed, followed with addition of THF/DMF (3:1, 4 mL) under N_2 and the resulting mixture was stirred for 10 min. A solution of trimethylsilyl acetylene (1.6 ml, 11.27 mmol, 10 eq) and Et_3N (1.5 ml, 11.27 mmol, 10 eq) in glass vial were added to the microwave vial which was placed in the oil bath at 52 °C for 24h. Another solution of trimethylsilyl ethylene (1.6 ml, 11.27 mmol, 10 eq) and Et_3N (1.5 ml, 11.27 mmol, 10 eq) in glass vial were added to the microwave vial and the reaction left for 20h. The reaction mixture was dissolved with ethyl acetate 30 ml and transferred to a separatory funnel, and the organic layer was quenched with 1M HCl (10 ml), H_2O (30 ml), and brine (30 ml). The organic layer was dried over $MgSO_4$, concentrated, and subjected to column chromatography (petroleum ether/DCM, 200:15) yielding compound **2.29** as a yellow oil (0.356 g, 88%).

^{1}H NMR (400 MHz, $(CD_3)_2CO$) δ 8.00 (dd, J = 8.2, 1.4 Hz, 1H), 7.93 (dd, J = 8.2, 1.4 Hz, 1H), 7.79 (dd, J = 7.2, 1.4 Hz, 1H), 7.56 – 7.49 (m, 2H), 7.47 (d, J = 8.4 Hz, 2H), 7.35 (d, J = 8.3 Hz, 2H), 7.32 (dd, J = 7.1, 1.4 Hz, 1H), 1.44 (s, 9H), 0.02 (s, 9H).

^{13}C NMR (101 MHz, $(CD_3)_2CO$) δ 150.36, 141.63, 141.27, 136.79, 135.87, 132.26, 131.42, 131.05, 130.97, 129.46, 126.73, 126.28, 125.50, 121.70, 106.15, 103.63, 35.44, 32.27, 0.59.

MS (MALDI-TOF) : m/z = 357.45 $[M+H]^+$.

Chemical formula and molecular weight : $C_{25}H_{28}Si$, 356.196 $g.mol^{-1}$.

3.4 Deprotection of TMS acetylene derivatives

3.4.1 Synthesis of 8-(p-Methoxyphenyl)-1-naphthyl ethyne **2.28**

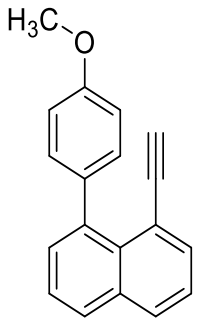

2.28

Compound **2.27** (0.372 g, 1.13 mmol, 1 eq) was added to 50 ml one neck-round bottom flask followed by K_2CO_3 (1.6 g, 11.3 mmol, 10 eq) then 30 ml methanol. The reaction was stirred overnight then quenched with H_2O, transferred into a separatory funnel, then extracted with 30 ml DCM. The organic layer was dried over $MgSO_4$, concentrated, and subjected to column chromatography (petroleum ether/DCM, 100/10) yielding the title compound as a yellow oil (0.202 g, 67%).

^{1}H NMR (500 MHz, $CDCl_3$) δ 7.91 (dd, *J* = 8.2, 1.4 Hz, 1H), 7.86 (dd, *J* = 8.2, 1.4 Hz, 1H), 7.74 (dd, *J* = 7.1, 1.4 Hz, 1H), 7.51 (dd, *J* = 8.2, 7.0 Hz, 1H), 7.45 – 7.37 (m, 2H), 7.29 (d, *J* = 8.7 Hz, 2H), 6.92 (d, *J* = 8.6 Hz, 2H), 3.89 (s, 3H), 2.91 (s, 1H).

^{13}C NMR (126 MHz, $CDCl_3$) δ 160.63, 141.57, 136.99, 136.60, 135.72, 133.41, 132.98, 131.37, 131.28, 129.76, 126.81, 126.35, 120.95, 113.91, 85.30, 84.44, 56.77.

MS (MALDI-TOF): m/z = 259.15 $[M+H]^+$.

Chemical formula and molecular weight : $C_{19}H_{14}O$, 258.10 $g.mol^{-1}$.

3.4.2 Synthesis of 8-[p-(tert-Butyl) phenyl]-1-naphthyl ethyne **2.30**

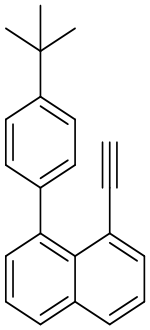

2.30

Compound **2.29** (0.439 g, 1.23 mmol, 1 eq) was added to 50 ml one-neck-round bottom flask followed by K_2CO_3 (1.7 g, 12.33 mmol, 10 eq), then methanol (30 ml). The reaction was stirred for 6h, quenched with H_2O, and transferred into a separatory funnel, followed by DCM (30 ml). The organic layer was separated and dried over $MgSO_4$, concentrated, resulting in formation of **2.30** as solid. The resulting solid was collected by filtration and washed with small portions of hexane to remove residual oily starting material **2.29**, yielding **2.30** as a white solid (0.156 g, 49%).

m.p.84.6 – 86.8 °C.

Rf: 0.7 (ethyl acetate/petroleum ether, 1:9).

^{1}H NMR (400 MHz, $CDCl_3$) δ 7.91 (dd, J = 8.3, 1.4 Hz, 1H), 7.86 (dd, J = 8.2, 1.5 Hz, 1H), 7.72 (dd, J = 7.2, 1.4 Hz, 1H), 7.51 (dd, J = 8.1, 7.0 Hz, 1H), 7.44 – 7.43 (m, 1H), 7.42 (dd, *J* = 2.8, 1.2 Hz, 1H), 7.40 – 7.37 (m, 2H), 7.29 (d, J = 8.5 Hz, 2H), 2.70 (s, 1H), 1.40 (s, 9H).

^{13}C NMR (101 MHz, $CDCl_3$) δ 150.45, 140.51, 140.00, 135.16, 134.29, 131.89, 130.20, 129.98, 129.57, 128.37, 125.39, 124.92, 123.94, 119.53, 83.27, 82.87, 34.62, 31.61.

MS (MALDI-TOF): m/z = 285.12 $[M+H]^+$.

HRMS (ESI^+-TOF) m/z: $[M+H]^+$ calcd for $C_{22}H_{21}$ 285.1643, found 285.1674.

UV-Vis (DCM): λ max (nm) (Ɛ ($M^{-1}.cm^{-1}$)) = 319 ($5.18\cdot10^3$), 305 ($4.00\cdot10^3$), 234 ($2.18\cdot10^4$).

Fluorescence (CH_2Cl_2, Excitation at 305 nm): 380 nm.

3.5 Synthesis of Sonogashira coupled products from **2.28**

3.5.1 Synthesis of **2.9**

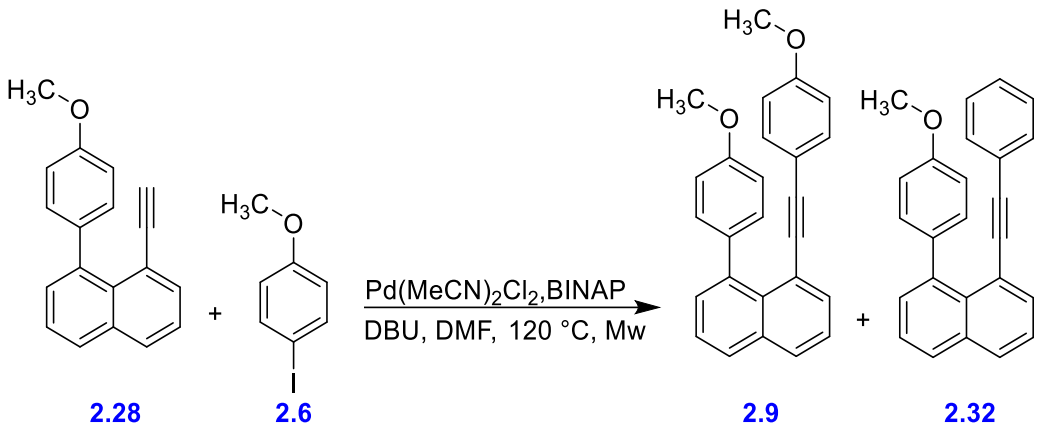

A mixture of [8-(*p*-methoxyphenyl)-1-naphthyl]ethyne **2.28** (0.16 g, 0.62 mmol, 1 eq), 4-iodoanisole (0.43 ml, 1.8 mmol, 3 eq), $Pd(MeCN)_2Cl_2$ (0.003 g, 0.0124 mmol, 2 mol%), BINAP (0.0154 g, 0.025 mmol, 4 mol%), DBU (0.14 ml, 0.93 mmol, 1.5 eq) were placed in microwave vial and stirred in DMF (4 ml) under N_2 for 10 min. Then the vial was placed in a microwave for 4 h at 120 °C. After cooling, the reaction was dissolved with ethyl acetate (30 ml) and washed with $NaHCO_3$, H_2O, dried over $MgSO_4$ and filtered, concentrated, and subjected to column chromatography (petroleum ether/ethyl acetate, 200:5) yielding **2.9** as a brown solid (0.1g, 45%), **2.32** (0.018 g, 9%).

2.9

m.p.123.7-126.8 °C.

Rf: 0.4 (ethyl acetate/petroleum ether, 1:9).

^{1}H NMR (500 MHz, $CDCl_3$) δ 7.86 (ddd, J = 13.3, 8.2, 1.4 Hz, 2H), 7.76 (dd, J = 7.2, 1.4 Hz, 1H), 7.49 (dd, J = 8.2, 7.0 Hz, 1H), 7.45 (dd, J = 8.2, 7.2 Hz, 1H), 7.40 – 7.35 (m, 3H), 6.99 (d, J = 8.9 Hz, 2H), 6.88 (d, J = 8.6 Hz, 2H), 6.76 (d, J = 8.8 Hz, 2H), 3.80 (s, 3H), 3.72 (s, 3H).

^{13}C NMR (126 MHz, $CDCl_3$) δ 159.14, 158.89, 140.30,135.33, 134.56, 134.53, 133.06, 131.28, 130.80, 130.14, 129.18, 128.29, 125.33,125.11, 120.98, 115.99, 113.37, 112.87, 97.79, 88.92, 55.28, 55.12.

MS (MALDI-TOF): m/z = 365.64 $[M+H]^+$.

HRMS (ESI^+-TOF) m/z: $[M+H]^+$ calcd for $C_{26}H_{21}O_2$ 365.1541, found 365.1544.

UV-Vis (DCM): λ max (nm) (Ɛ ($M^{-1}.cm^{-1}$)) = 352 ($1.66\cdot10^4$), 337 ($1.88\cdot10^4$), 240 ($3.31\cdot10^4$).

Fluorescence (CH_2Cl_2, Excitation at 352 nm): 414 nm.

2.32

m.p.105.2-108.6 °C

Rf: 0.5 (ethyl acetate/petroleum ether, 1:9).

^{1}H NMR (500 MHz, CD_2Cl_2) δ 7.93 (dd, J = 8.2, 1.4 Hz, 1H), 7.88 (dd, J = 8.3, 1.4 Hz, 1H), 7.78 (dd, J = 7.2, 1.4 Hz, 1H), 7.52 (dd, J = 8.2, 7.0 Hz, 1H), 7.48 (dd, J = 8.2, 7.2 Hz, 1H), 7.41 – 7.33 (m, 3H), 7.28 – 7.19 (m, 3H), 7.09 – 7.02 (m, 2H), 6.86 (d, J = 8.7 Hz, 2H), 3.68 (s, 3H).

^{13}C NMR (126 MHz, CD_2Cl_2) δ 159.02, 140.27, 135.11, 134.69, 134.56, 131.46, 131.22, 130.79, 130.19, 129.52, 128.24, 127.77, 127.65, 125.41, 125.08, 124.84, 123.68, 120.53, 112.89, 97.50, 90.05, 55.00.

MS (MALDI-TOF): m/z = 335.45 $[M+H]^+$.

HRMS (ESI^+-TOF) m/z: $[M+H]^+$ calcd for $C_{25}H_{19}O$ 335.1436, found 335.1446.

UV-Vis (DCM): λ max (nm) (Ɛ ($M^{-1}.cm^{-1}$)) = 346 ($1.23\cdot10^4$), 331 ($1.47\cdot10^4$), 242 ($3.23\cdot10^4$).

Fluorescence (CH_2Cl_2, Excitation at 346 nm): 412 nm.

3.5.2 Synthesis of 8-Methoxyfluoranthene **2.25**

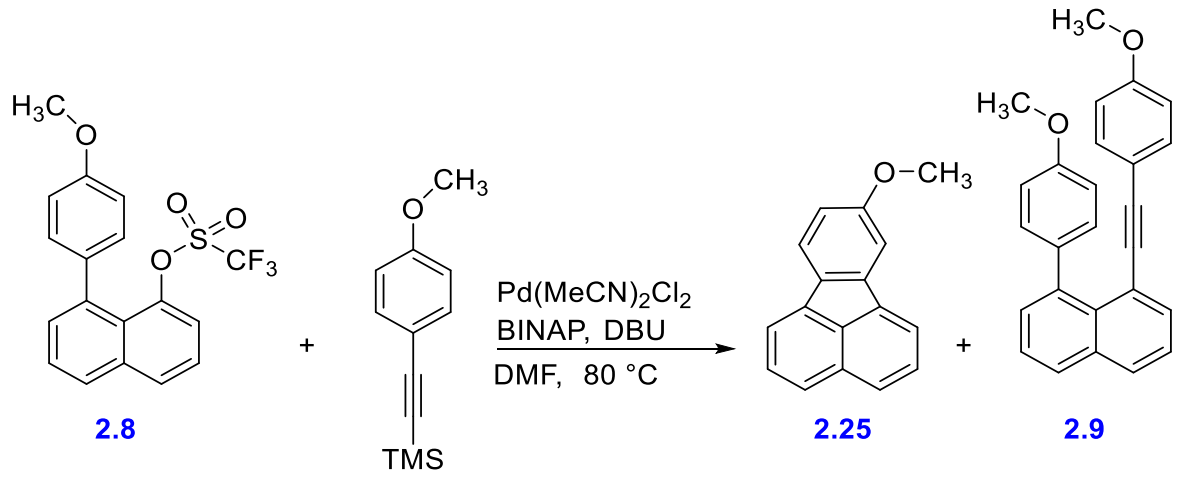

A mixture of **2.8** (0.2 g, 0.52 mmol, 1eq), ((4-methoxyphenyl)ethynyl)trimethylsilane (0.25 ml, 1.05 mmol, 2 eq), $PdCl_2(MeCN)_2$ (0.003 g, 0.0104 mmol, 2%), DBU (0.2 ml, 1.3 mmol, 2.5 eq) were placed in microwave vial followed with DMF (2 ml). The mixture stirred for 10 min under argon then placed in oil path at 80 °C for 17h. After cooling, the reaction was dissolved with ethyl acetate (30 ml) and washed with $NaHCO_3$, dried over $MgSO_4$ and filtrated, concentrated, and subjected to column chromatography by using (petroleum ether/ethyl acetate, 50:1) yielding **2.25** as yellow solid (0.08 g, 85%), **2.9** (0.005 g, 2%).

2.25 [80]

m.p.119.5-123.2 °C.

Rf: 0.6 (ethyl acetate/petroleum ether, 1:9).

^{1}H NMR (500 MHz, $CDCl_3$) δ 7.91 (dd, J = 6.9, 0.7 Hz, 1H), 7.84 – 7.75 (m, 4H), 7.60 (ddd, J = 13.1, 8.2, 6.9 Hz, 2H), 7.46 (d, J = 2.4 Hz, 1H), 6.91 (dd, J = 8.3, 2.4 Hz, 1H), 3.94 (s, 3H).

^{13}C NMR (126 MHz, $CDCl_3$) δ 159.98, 141.27, 136.99, 136.85, 132.88, 132.46, 129.96, 128.06, 127.77, 126.91, 125.47, 122.22, 119.95, 118.99, 112.86, 107.71, 55.65.

MS (MALDI-TOF): m/z = 233.49 $[M+H]^+$.

HRMS (ESI^+-TOF) m/z: $[M+H]^+$ calcd for $C_{17}H_{13}O$ 233.0966, found 233.0978.

UV-Vis (DCM): λ max (nm) (Ɛ ($M^{-1}.cm^{-1}$)) = 360 ($7.33\cdot10^3$), 343 ($5.66\cdot10^3$), 324 ($5.66\cdot10^3$), 296 ($4.73\cdot10^4$), 285 ($2.46\cdot10^4$), 239 ($3.83\cdot10^4$).

Fluorescence (CH_2Cl_2, Excitation at 360 nm): 485 nm.

3.5.3 Synthesis of 2-[8-(*p*-Methoxyphenyl)-1-naphthyl]-1-[*p*-(tert-butyl) phenyl] ethyne **2.31**

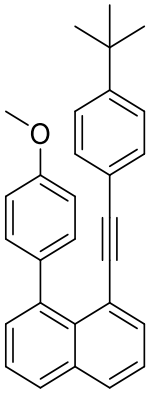

2.31

A mixture of [8-(*p*-(tert-butyl))-1-naphthyl]ethyne **2.30** (0.1 g, 0.38 mmol, 1 eq), 4-tert-butyliodobenzene (0.3 ml, 1.14 mmol, 4.5 eq), $Pd(MeCN)_2Cl_2$ (0.0018 g, 0.007 mmol, 2%), BINAP (0.009 g, 0.0.0152 mmol, 4%), and DBU (0.08 ml, 0.57 mmol, 1.5 eq) were placed in microwave vial and stirred in DMF (4 ml) under N_2 for 10 min. Then the vial placed in microwave for 6h at 120 ˚C. After cooling, the reaction was dissolved with EtOAc (30 ml) and washed with $NaHCO_3$, and H_2O and dried over $MgSO_4$ and filtrated, concentrated, and subjected to column chromatography (petroleum ether/ethyl acetate, 200:3) yielding **2.31** as colorless solid (0.13 g, 87%).

m.p.127.5-129.7 °C.

Rf: 0.5 (ethyl acetate/petroleum ether, 1:10).

^{1}H NMR (500 MHz, Chloroform-d) δ 7.89 (d, J = 8.1 Hz, 1H), 7.86 (d, J = 8.1 Hz, 1H), 7.77 (d, J = 7.1 Hz, 1H), 7.50 (t, J = 7.6 Hz, 1H), 7.45 (t, J = 7.7 Hz, 1H), 7.38 (dd, J = 7.8, 4.1 Hz, 3H), 7.25 (d, J = 8.1 Hz, 2H), 7.01 (d, J = 7.9 Hz, 2H), 6.86 (d, J = 8.1 Hz, 2H), 3.65 (s, 3H), 1.31 (s, 9H).

^{13}C NMR (126 MHz, $CDCl_3$) δ 158.86, 150.78, 140.35, 135.23, 134.67, 134.54, 131.29, 131.27, 130.93, 130.09, 129.34, 128.29, 127.73, 125.35, 125.09, 124.70, 120.90 , 120.80, 113.14, 112.95, 97.83 , 89.47, 55.06, 34.70, 31.22.

MS (MALDI-TOF): m/z = 391.155 $[M+H]^+$.

Chemical formula and molecular weight : $C_{29}H_{26}O$, 390.198 $g.mol^{-1}$.

UV-Vis (DCM): λ max (nm) (Ɛ ($M^{-1}.cm^{-1}$)) = 334 ($2.0\cdot10^4$), 240 ($3.8\cdot10^4$), 350 ($1.7\cdot10^4$).

Fluorescence (CH_2Cl_2, Excitation at 334 nm): 413 nm.

3.5.4 Synthesis of Homocouplied **2.34**

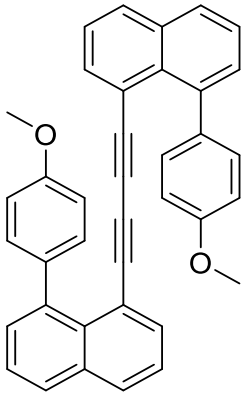

2.34

Compound **2.28** (0.3 g, 1.16 mmol, 1 eq), and CuI (0.015 g, 0.0813 mmol, 7%) were placed in microwave vial followed with addition of DMF (2 ml) under N_2. The mixture is heated in an oil bath for 89h at 60 °C. After cooling, the precipitate was filtered and washed with H_2O and hexane yielding **2.34** (0.28 g, 47%). The remaining filtrate was diluted with ethyl acetate (EtOAc, 30 mL) and transferred to a separatory funnel. The organic layer was washed with water (2 × 15 mL), dried over anhydrous $MgSO_4$, filtered, and concentrated under reduced pressure, and subjected to column chromatography (petroleum ether/ethyl acetate, 100:10) yielding **2.34** (0.071 g, 12%). Combined yield of **2.34** (59%).

m.p.249-251 °C.

Rf: 0.5 (ethyl acetate/petroleum ether, 2:8).

^{1}H NMR (500 MHz, CD_2Cl_2) δ 7.93 (dd, J = 8.2, 1.4 Hz, 1H), 7.88 (dd, J = 8.2, 1.4 Hz, 1H), 7.72 (dd, J = 7.2, 1.4 Hz, 1H), 7.52 (dd, J = 8.2, 6.9 Hz, 1H), 7.48 (dd, J = 8.2, 7.2 Hz, 1H), 7.37 (dd, J = 7.0, 1.4 Hz, 1H), 7.24 (d, J = 8.6 Hz, 2H), 6.92 (d, J = 8.6 Hz, 2H), 3.69 (s, 3H).

^{13}C NMR (126 MHz, CD_2Cl_2) δ 159.52, 140.44, 135.65, 134.75, 134.41, 132.12, 131.39, 130.13, 129.74, 128.47, 125.66, 125.16, 119.72, 112.94, 83.76, 81.21, 55.15.

HRMS (ESI$^+$-TOF) m/z: $[M+H]^+$ calcd for $C_{38}H_{27}O_2$ 515.2011, found 515.2016.

UV-Vis (DCM): λ max (nm) (Ɛ ($M^{-1}.cm^{-1}$)) = 390 ($2.64\cdot10^4$), 362 ($2.57\cdot10^4$), 345 ($2.14\cdot10^4$).

Fluorescence (CH_2Cl_2, Excitation at 390 nm): 432 nm.

3.6 Acid Cyclization products of **2.9**

3.6.1 Route A by utilizing TFA

To a two-neck round bottom flask **2.9** (1 eq) and dry DCM (30 ml) were added under N_2. The reaction temperature was decreased to 0 ^oC by ice bath followed by the addition of TFA (50 eq) dropwise, and the reaction was left to stir for 19h at room temperature.

3.6.1.1 work-up with Et_3N

Et_3N (1ml) added dropwise and the mixture stirred at room temperature for 5 min. It was filtrated through Aluminum oxide with approximately 50 ml DCM followed by 30 ml EtOAc, dried over $MgSO_4$, concentrated, and subjected to column chromatography by using (petroleum ether/ethyl acetate, 100:3) to afford cyclized products.

3.6.1.2 Work-up with $NaHCO_3$

The mixture was transferred to separating funnel and washed with $NaHCO_3$, and H_2O and dried over $MgSO_4$ and filtrated, concentrated, and subjected to column chromatography using (petroleum ether/ethyl acetate, 100:3) to afford cyclized products.

3.6.2 Route B by utilizing $HNTf_2$

To a two-neck round-bottom flask, **2.9** (1 eq) and dry DCM (30 mL) were added under N_2 then cooled to 0 °C using an ice bath followed by addition of $HNTf_2$ (5 drops) dropwise. The reaction was left to stir for at room temperature for 19 h then Et_3N (1 mL) was added dropwise followed by filtration through aluminum oxide using 30 ml EtOAc. The mixture was dried over $MgSO_4$, concentrated under reduced pressure, and purified by column chromatography (petroleum ether/ethyl acetate, 200:5) to afford cyclized products.

3.6.1 Synthesis of cyclized products from **2.9**

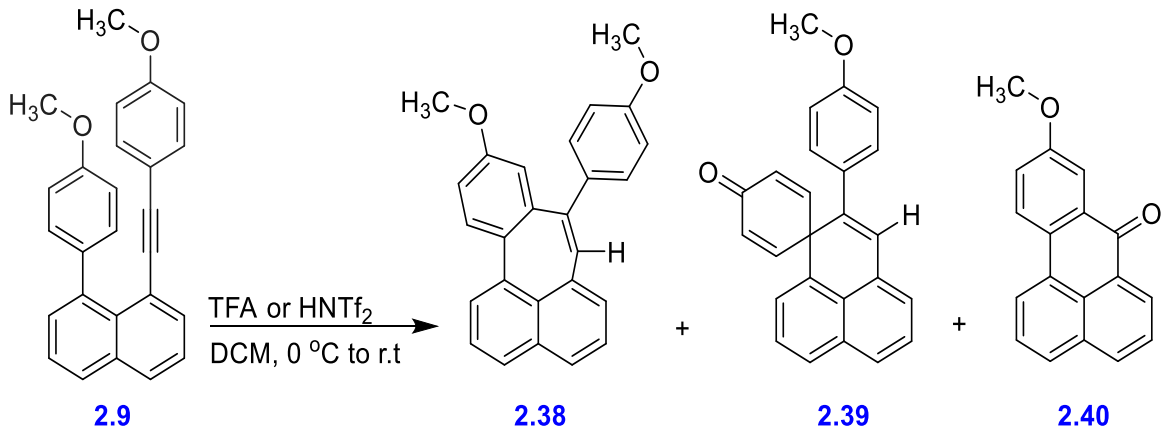

Route A - workup with Et_3N

2.9 (0.3 g, 0.824 mmol, 1 eq) , TFA (3.2 ml, 50 eq) compound **2.38** appeared as yellow oil which solidified under vacuum yielding a yellow solid (0.26 g, 86%), compound **2.39** formed as a brownish solid (0.038 g, 38%), and **2.40** as a yellow solid (trace).

Route A - workup with $NaHCO_3$

2.9 (0.14 g, 0.38 mmol, 1 eq), TFA (1.46 ml, 50 eq), yielding compound **2.38** (0.07 g, 50%), **2.39** (0.0175 g, 13%), and **2.40** (0.32 g, 32%).

Route B

2.9 (0.11 g, 0.302 mmol, 1 eq), $HNTf_2$ (5 drops), yielding compound **2.38** (0.084 g, 76%), **2.39** (0.024 g, 22%), and **2.40** (trace).

3.6.1.1 Synthesis of Seven-membered ring **2.38**

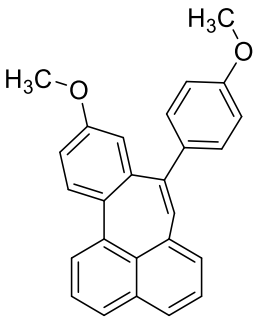

2.38

m.p.decomposes.

Rf: 0.5 (ethyl acetate/petroleum ether, 1:9).

^{1}H NMR (500 MHz, $CDCl_3$) δ 7.68 (dd, J = 8.0, 1.3 Hz, 1H), 7.65 (dd, J = 7.4, 1.3 Hz, 1H), 7.57 (dd, J = 8.2, 1.3 Hz, 1H), 7.47 (dd, J = 8.0, 7.4 Hz, 1H), 7.41 (d, J = 8.7 Hz, 2H), 7.33 (dd, J = 8.1, 7.1 Hz, 1H), 7.24 (dt, J = 7.1, 1.1 Hz, 1H), 6.97 (d, J = 8.8 Hz, 1H), 6.94 (d, J = 8.7 Hz, 2H), 6.78 (d, J = 2.8 Hz, 1H), 6.69 (dd, J = 8.7, 2.7 Hz, 1H), 6.57 (d, J = 0.9 Hz, 1H), 3.86 (s, 3H), 3.81 (s, 3H).

^{13}C NMR (126 MHz, $CDCl_3$) δ 160.90, 158.84, 143.08, 141.17, 138.97, 137.91, 137.17, 135.02, 134.51, 133.66, 131.89, 131.46, 130.01, 129.10, 128.15, 128.10, 126.44, 126.20, 125.71, 119.26, 113.73, 112.31,55.36, 55.34.

MS (MALDI-TOF): m/z = 365.3079 $[M+H]^{+\cdot}$

HRMS (ESI^+-TOF) m/z: $[M+H]^+$ calcd for $C_{26}H_{21}O_2$ 365.1541, found 365.1550.

UV-Vis (DCM): λ max (nm) (Ɛ ($M^{-1}.cm^{-1}$)) = 372 ($2.8\cdot10^4$), 255 ($8.5\cdot10^4$).

Fluorescence (CH_2Cl_2, Excitation at 372 nm): 442 nm.

3.6.1.2 Synthesis of Spiro compound **2.39**

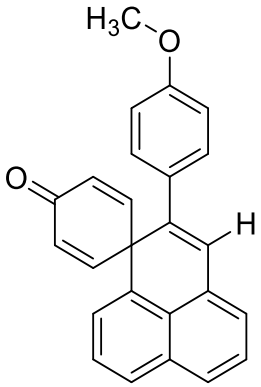

2.39

m.p.196.4-199.6 °C.

Rf: 0.6 (petroleum ether/ethyl acetate, 7:3).

^{1}H NMR (500 MHz, CD_2Cl_2) δ 7.76 (dd, J = 8.1, 1.1 Hz, 1H), 7.73 (dd, J = 8.4, 1.1 Hz, 1H), 7.45 (dd, J = 8.2, 7.2 Hz, 2H), 7.31 – 7.26 (m, 4H), 7.08 – 7.06 (m, 2H), 6.91 (s, 1H), 6.83 – 6.80 (m, 2H), 6.18 (d, J = 10.0 Hz, 2H), 3.79 (s, 3H).

^{13}C NMR (126 MHz, CD_2Cl_2) δ 186.20, 160.17, 153.58, 138.20, 134.22, 133.27, 132.80, 130.84, 130.07, 129.00, 128.35, 127.99, 127.31, 127.27, 127.20, 127.17, 126.94, 124.92, 113.84, 55.85, 52.45.

MS (MALDI-TOF): m/z = 350.87 $[M]^+$.

HRMS (ESI^+-TOF) m/z: $[M+H]^+$ calcd for $C_{25}H_{19}O_2$ 351.1385, found 351.1396.

UV-Vis (DCM): λ max (nm) (Ɛ ($M^{-1}.cm^{-1}$)) = 348 ($1.18\cdot10^4$), 332 ($1.31\cdot10^4$), 239 ($4.51\cdot10^4$).

Fluorescence (CH_2Cl_2, Excitation at 348 nm): 490 nm.

3.6.1.3 Synthesis of 9-(methoxy)-7H-benzo[de]anthracen-7-one **2.40**. [87]

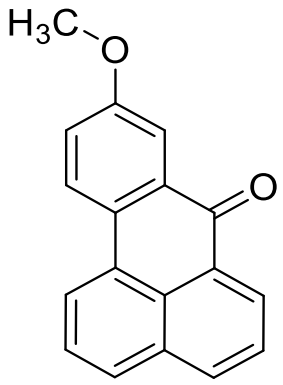

2.40

m.p.147.9-149.8 °C.

Rf: :0.5 (Hexane/DCM/Acetone, 8:1:1).

^{1}H NMR (500 MHz, $CDCl_3$) δ 8.79 (dd, J = 7.3, 1.3 Hz, 1H), 8.38 (dd, J = 7.6, 1.0 Hz, 1H), 8.31 – 8.21 (m, 2H), 8.00 – 7.94 (m, 2H), 7.79 (dd, J = 8.0, 7.3 Hz, 1H), 7.68 (dd, J = 8.2, 7.4 Hz, 1H), 7.33 (dd, J = 8.8, 3.0 Hz, 1H), 3.99 (s, 3H).

^{13}C NMR (126 MHz, $CDCl_3$) δ 182.75, 158.79, 134.27, 131.96, 131.45, 128.94, 128.65, 128.28, 127.52, 126.20, 125.98, 125.63, 125.51, 123.84, 122.46, 121.32, 108.20, 54.66.

IR (thin film) ν (cm^{-1}): 2929, 1649, 1605, 1576, 1305, 1267, 778.

MS (MALDI-TOF): m/z = 261.07 $[M+H]^+$.

HRMS (ESI-TOF) m/z: $[M+H]^+$ calcd for $C_{18}H_{12}O_2$ 261.0916, found 261.0930.

UV-Vis (DCM): λ max (nm) (Ɛ ($M^{-1}.cm^{-1}$)) = 413 ($8.27\cdot10^3$), 316 ($9.02\cdot10^3$), 260 ($2.48\cdot10^4$), 231 ($3.30\cdot10^4$).

Fluorescence (CH_2Cl_2, Excitation at 413 nm): 491 nm.

3.7 Scholl reaction products of **2.9**

3.7.1 Synthesis of 10-methoxy-7H-benzo[de]anthracen-7-one **2.41**.[87]

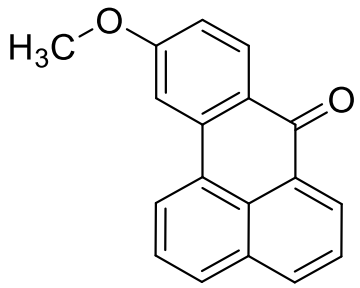

2.41

Compound **2.38** (0.1 g, 0.27 mmol, 1.0 eq) and DDQ (0.068 g, 0.3 mmol, 1.1 eq) were placed in a two-neck round-bottom flask and dissolved in DCM (30 mL) under N_2. The solution was cooled to 0 °C by ice path prior to the dropwise addition of TFA (3 mL). The reaction mixture was left to stir at room temperature for 17 hours followed by addition of methanol (10 mL) then stirring for another 6 hours. The solution transferred to a separatory funnel, diluted with DCM (30 mL), and quenched with $NaHCO_{3(aq)}$ (30 ml). The organic layer was separated, dried over $MgSO_4$, filtered, and concentrated under reduced pressure. The crude residue was purified by column chromatography (DCM/acetone/petroleum ether, 4:1:40) to afford **2.41** (0.011 g, 16%) as a yellow solid.

m.p.159.8-161.7 °C.

Rf: :0.4 (Hexane/DCM/Acetone, 8:1:1).

^{1}H NMR (400 MHz, $CDCl_3$) δ 8.75 (dd, J = 7.3, 1.3 Hz, 1H), 8.49 (d, J = 8.8 Hz, 1H), 8.42 (dd, J = 7.5, 1.1 Hz, 1H), 8.20 (dd, J = 8.2, 1.4 Hz, 1H), 8.02 (dd, J = 8.2, 1.0 Hz, 1H), 7.80 – 7.75 (m, 2H), 7.69 (dd, J = 8.2, 7.4 Hz, 1H), 7.10 (dd, J = 8.8, 2.4 Hz, 1H), 4.02 (s, 3H).

^{13}C NMR (101 MHz, $CDCl_3$) δ 182.90, 163.88, 138.35, 134.68, 132.99, 130.69, 130.42, 129.60, 128.68, 128.30, 126.90, 126.60, 126.41, 125.25, 124.05, 114.84, 107.28, 55.61.

IR (thin film) ν (cm^{-1}): 2923, 1645, 1597, 1581, 1292, 1242,773.

MS (MALDI-TOF): m/z = 261.42 $[M+H]^+$.

HRMS (ESI-TOF) m/z: $[M+H]^+$ calcd for $C_{18}H_{13}O_2$ 261.0938, found 261.0916.

UV-Vis (DCM): λ max (nm) (Ɛ ($M^{-1}.cm^{-1}$)) = 378 ($7.72\cdot10^3$), 334 ($7.27\cdot10^3$), 307 ($9.54\cdot10^3$), 258 ($2.00\cdot10^4$).

Fluorescence (CH_2Cl_2, Excitation at 378 nm): 504 nm.

3.7.2 Synthesis of 10-Methoxy-7H-benzo[de]anthracen-7-one **2.42**

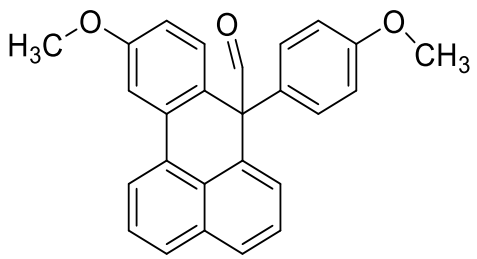

2.42

Compound **2.38** (0.11 g, 0.3 mmol, 1 eq) and DDQ (0.075 g, 0.33 mmol, 1.1 eq) were placed in a two-neck round-bottom flask and dissolved in dry DCM (30 mL) under N_2. The solution was cooled to 0 °C by ice path prior to the dropwise addition of TFA (3 mL). The reaction mixture was left to stir at room temperature for 17 hours then Et_3N (0.8 ml) added dropwise and stirred for 2 min then filtered through Aluminum oxide with approximately 50 ml DCM followed by 30 ml ethyl acetate. Then the mixture dried over $MgSO_4$, concentrated, and subjected to column chromatography using (DCM), to afford **2.42** as sticky product (0.024 g, 21%).

Rf: 0.5 (DCM, eluent).

^{1}H NMR (500 MHz, $CDCl_3$) δ 9.85 (s, 1H), 8.13 (dd, J = 7.5, 1.1 Hz, 1H), 7.85 (dd, J = 8.2, 1.1 Hz, 1H), 7.80 (dd, J = 8.1, 1.2 Hz, 1H), 7.69 (d, J = 2.6 Hz, 1H), 7.59 (dd, J = 8.2, 7.4 Hz, 1H), 7.47 (dd, J = 8.1, 7.3 Hz, 1H), 7.21 – 7.12 (m, 3H), 7.00 (d, J = 8.7 Hz, 1H), 6.89 (d, J = 8.9 Hz, 2H), 6.85 (dd, J = 8.7, 2.6 Hz, 1H), 3.90 (s, 3H), 3.81 (s, 3H).

^{13}C NMR (126 MHz, $CDCl_3$) δ 195.70, 159.40, 158.53, 137.63, 133.80, 133.73, 133.23, 132.54, 130.33, 128.94, 128.68, 128.53, 127.67, 127.60, 126.99, 126.37, 126.14, 120.02, 114.23, 114.11, 108.48, 64.34, 55.36, 55.27.

HRMS (ESI-TOF) m/z: $[M+H]^+$ calcd for $C_{26}H_{21}O_3$ 381.1491, found 381.1495.

UV-Vis (DCM): λ max (nm) (Ɛ ($M^{-1}.cm^{-1}$)) = 349 ($8.02\cdot10^3$), 333 ($8.02\cdot10^3$), 227 ($3.44\cdot10^3$).

Fluorescence (CH_2Cl_2, Excitation at 349 nm): 471 nm.

3.8 ICl cyclization products of **2.9**

3.8.1 Synthesis of spiro compound **2.49**

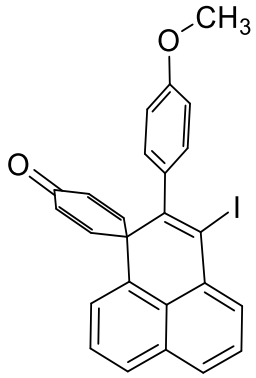

2.49

Compound **2.9** (0.113 g, 0.31 mmol, 1.0 eq) was placed in a two-neck round-bottom flask and dissolved in dry DCM (20 mL) under N_2. The reaction mixture was cooled to –78 °C using an acetone/dry ice bath, and ICl (0.63 mL, 0.65 mmol, 2.1 eq, 1 M) was added dropwise by addition funnel. The mixture was stirred for 2 h, then quenched with saturated aqueous sodium thiosulfate solution and allowed to warm to room temperature. The reaction mixture was extracted with CH_2Cl_2 (2 × 20 mL), washed with brine, dried over $MgSO_4$, filtered, and concentrated under reduced pressure. Purification by column chromatography (ethyl acetate/petroleum ether, 1:20) afforded the compound **2.49** (0.132 g, 90%) as a yellow solid.

m.p.207-210 °C.

Rf: 0.2 (ethyl acetate/petroleum ether, 2:8).

^{1}H NMR (500 MHz, $CDCl_3$) δ 7.93 (dd, *J* = 7.4, 1.1 Hz, 1H), 7.84 – 7.78 (m, 2H), 7.49 (quintet, J = 7.7 Hz, 2H), 7.29 – 7.24 (m, 1H), 7.01 (d, *J* = 10.0 Hz, 2H), 6.97 (d, *J* = 8.6 Hz, 2H), 6.82 (d, *J* = 8.6 Hz, 2H), 6.11 (d, *J* = 9.8 Hz, 2H), 3.81 (s, 3H).

^{13}C NMR (126 MHz, $CDCl_3$) δ 185.40, 159.28, 151.21, 143.04, 136.59, 133.37, 132.37, 130.90, 130.47, 130.07, 129.51,127.72 ,126.70, 126.64, 126.61, 126.44, 125.97, 113.10, 109.07, 55.16, 54.04.

IR (thin film) ν (cm^{-1}): 2954, 1656, 1505, 1230, 856, 827, 771.

HRMS (ESI-TOF) m/z: $[M+H]^+$ calcd for $C_{25}H_{18}IO_2$ 477.0352, found 477.0354.

UV-Vis (DCM): λ max (nm) (Ɛ ($M^{-1}.cm^{-1}$)) = 351 ($6.79\cdot10^3$), 332 ($1.01\cdot10^4$), 317 ($9.21\cdot10^3$), 232 ($4.69\cdot10^4$).

Fluorescence (CH_2Cl_2, Excitation at 351 nm): 469 nm.

3.8.2 Synthesis of compound **2.51**

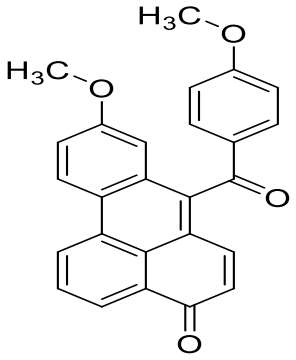

2.51

Compound **2.9** (0.177 g, 0.488 mmol, 1.0 eq) was placed in a two-neck round-bottom flask and dissolved in dry DCM (20 mL) under N_2. The reaction mixture was cooled to 0 °C using an ice bath, and ICl (1.02 mL, 1.02 mmol, 2.1 eq, 1 M) was added dropwise by additional funnel. The mixture was stirred for 2 h and 30 min, then quenched with saturated aqueous sodium thiosulfate solution and allowed to warm to room temperature. The reaction mixture was extracted with DCM (2 × 20 mL), washed with brine, dried over $MgSO_4$, filtered, and concentrated under reduced pressure. Purification by column chromatography (ethyl acetate/petroleum ether, 1:20) afforded **2.51** (0.025 g, 13%) as a brown solid.

m.p.209-211 °C.

Rf: 0.6 (ethyl acetate/petroleum ether, 4:6).

^{1}H NMR (400 MHz, $CDCl_3$) δ 8.93 (dd, J = 8.4, 1.2 Hz, 1H), 8.69 (d, J = 9.2 Hz, 1H), 8.63 (dd, J = 7.5, 1.2 Hz, 1H), 7.94 (dd, J = 8.2, 7.5 Hz, 1H), 7.88 (d, J = 8.3 Hz, 2H), 7.60 (d, J = 10.0 Hz, 1H), 7.40 (dd, J = 9.2, 2.6 Hz, 1H), 7.05 (d, J = 2.6 Hz, 1H), 6.93 (d, J = 8.6 Hz, 2H), 6.66 (d, J = 10.0 Hz, 1H), 3.87 (s, 3H), 3.77 (s, 3H).

^{13}C NMR (101 MHz, $CDCl_3$) δ 196.55, 185.31, 164.83, 159.03, 141.58, 138.54, 132.58, 130.69, 130.33, 130.25, 129.69, 129.64, 128.17, 128.04, 127.95, 125.78, 125.51, 124.87, 123.45, 119.92, 114.41, 108.31, 55.66, 55.46.

IR (thin film) ν (cm^{-1}): 2935, 2839, 1639, 1595, 1258, 1165.

MS (MALDI-TOF): m/z = 395.25 $[M+H]^+$.

HRMS (ESI^+-TOF) m/z: $[M+H]^+$ calcd for $C_{26}H_{19}O_4$ 395.1283, found 395.1280.

UV-Vis (DCM): λ max (nm) (Ɛ ($M^{-1}.cm^{-1}$)) = 384 (1.65·104), 298 (3.30·104).

Fluorescence (CH_2Cl_2, Excitation at 384 nm): 513 nm.

3.8.3 Synthesis of spiro compound **2.50**

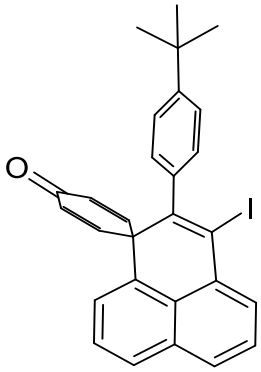

2.50

Compound **2.31** (0.10 g, 0.256 mmol, 1.0 eq) was placed in a two-neck round-bottom flask and dissolved in dry DCM (20 mL) under N_2. The reaction mixture was cooled to -75 °C using an acetone/dry ice bath, and ICl (0.5 mL, 0.54 mmol, 2.1 eq, 1 M) was added dropwise by additional funnel. The mixture was stirred for 2 h 15 min, then quenched with saturated aqueous sodium thiosulfate solution and allowed to warm to room temperature. The reaction mixture was extracted with CH_2Cl_2 (2 × 20 mL), and the combined extracts were washed with brine, dried over $MgSO_4$, filtered, concentrated under reduced pressure. Purification by column chromatography (ethyl acetate/petroleum ether, 1:20) afforded **2.50** (0.122 g, 95%) as a white solid.

m.p.244-245 °C.

^{1}H NMR (500 MHz, $CDCl_3$) δ 7.93 (dd, J = 7.4, 1.1 Hz, 1H), 7.81 (ddd, J = 8.3, 5.6, 1.1 Hz, 2H), 7.49 (quintet, J = 7.9 Hz, 2H), 7.30 (d, J = 8.4 Hz, 2H), 7.27 (d, J = 1.2 Hz, 1H), 7.03 (d, 2H), 6.97 (d, 2H), 6.10 (d, 2H), 1.32 (s, 9H).

^{13}C NMR (126 MHz, $CDCl_3$) δ 185.49, 151.21, 151.19, 143.47, 141.07, 133.36, 132.30, 130.92, 130.49, 129.46, 128.36, 127.69, 126.68, 126.61, 126.60, 126.37, 126.00, 124.58, 108.32, 53.90, 34.65, 31.32.

IR (thin film) ν (cm^{-1}): 2954, 1663, 853, 829, 775.

HRMS (ESI-TOF) m/z: $[M+H]^+$ calcd for $C_{28}H_{24}IO$ 503.0872, found 503.0874.

UV-Vis (DCM): λ max (nm) (Ɛ ($M^{-1}.cm^{-1}$)) = 349 ($6.43\cdot10^3$), 329 ($9.55\cdot10^3$), 316 ($8.55\cdot10^3$), 235 ($4.23\cdot10^4$).

Fluorescence (CH_2Cl_2, Excitation at 349 nm): 473 nm.

3.8.4 Synthesis of spiro-seven membered compound **2.53**

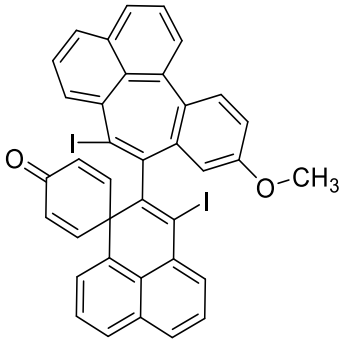

2.53

Homocoupling product **2.34** (0.08 g, 0.155 mmol, 1.0 eq) was placed in a two-neck round-bottom flask and dissolved in dry DCM (20 mL) under N_2. The reaction mixture was cooled to -75 °C using an acetone/liquid N_2 bath, and ICl (0.6 mL, 0.638 mmol, 4.1 eq, 1 M) was added dropwise by additional funnel. The mixture was stirred for 2 h 30 min, then quenched with saturated aqueous sodium thiosulfate solution and allowed to warm to room temperature. The reaction mixture was extracted with CH_2Cl_2 (2 × 20 mL), washed with brine, dried over $MgSO_4$, filtered, and concentrated under reduced pressure. Purification by column chromatography (ethyl acetate/petroleum ether, 1:20) afforded **2.53** (0.099 g, 84%) as an orange solid.

m.p.195.4-198.5 °C.

Rf: 0.2 (ethyl acetate/petroleum ether, 2:8).

^{1}H NMR (500 MHz, CD_2Cl_2) δ 8.10 (dd, J = 7.4, 1.1 Hz, 1H), 7.91 (dd, J = 7.4, 1.0 Hz, 1H), 7.86 (d, J = 8.0 Hz, 1H), 7.81 (dd, J = 8.2, 1.2 Hz, 1H), 7.67 (dt, J = 7.6, 3.8 Hz, 1H), 7.62 (d, J = 1.0 Hz, 1H), 7.62 – 7.60 (m, 1H), 7.60 – 7.59 (m, 1H), 7.59 – 7.57 (m, 1H), 7.56 – 7.53 (m, 2H), 7.43 (t, J = 7.7 Hz, 1H), 7.39 (t, J = 7.7 Hz, 1H), 7.27 (d, J = 2.7 Hz, 1H), 7.22 – 7.18 (m, 1H), 6.88 (dd, J = 8.8, 2.8 Hz, 1H), 6.80 (d, J = 8.8 Hz, 1H), 6.46 (dd, J = 9.8, 3.1 Hz, 1H), 6.10 – 6.03 (m, 1H), 3.76 (s, 3H).

^{13}C NMR (126 MHz, CD_2Cl_2) δ 184.82, 158.24, 151.83, 150.18, 148.45, 147.60, 137.62, 136.85, 136.18, 135.95, 135.10, 133.96, 133.30, 132.94, 132.16, 130.19, 130.01, 128.29, 127.61, 126.76, 126.66, 126.60, 126.52, 126.24, 125.67, 125.37,124.72 ,122.42 ,116.24 ,115.40 ,112.10, 109.50, 55.41, 54.17.

IR (thin film) ν (cm^{-1}): 3051, 1661, 1498, 1223, 852, 827, 767.

HRMS (ESI-TOF) m/z: $[M+H]^+$ calcd for $C_{37}H_{23}I_2O_2$ 752.9788, found 752.9785.

UV-Vis (DCM): λ max (nm) (Ɛ ($M^{-1}.cm^{-1}$)) = 400 ($2.2\cdot10^4$), 359 ($5.48\cdot10^4$), 340 ($5.63\cdot10^4$), 323 ($5.37\cdot10^4$).

Fluorescence (CH_2Cl_2, Excitation at 400 nm): 498 nm.

3.9 Isomerization of spiro compound **2.49** into seven-membered ring by acid and alcohol.

3.9.1 Synthesis of compound **2.56**

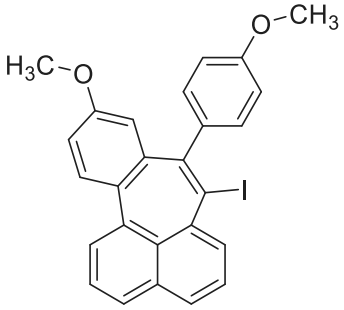

2.56

Compound **2.49** (0.10 g, 0.21 mmol, 1.0 eq) was dissolved in a 1:1 mixture of DCM/MeOH (10 mL, v/v) in a two-neck round-bottom flask equipped with a reflux condenser. Concentrated H_2SO_4 (8 drops) was added, and the reaction mixture was heated to 65 °C and refluxed for 71 h. The mixture was quenched with water and extracted with CH_2Cl_2 (3 × 30 mL), dried over $MgSO_4$, filtered, and concentrated under reduced pressure. Purification by column chromatography (ethyl acetate/petroleum ether, 1:10) afforded **2.56** (0.0138 g, 27%) as a yellow solid.

m.p.178.8-182.6 °C.

Rf: 0.6 (ethyl acetate/petroleum ether, 1:9).

^{1}H NMR (400 MHz, CD_2Cl_2) δ 7.99 (dd, J = 7.3, 1.1 Hz, 1H), 7.75 – 7.67 (m, 2H), 7.61 (dd, J = 8.0, 1.1 Hz, 1H), 7.54 (dd, J = 8.1, 7.1 Hz, 1H), 7.41 (dd, J = 8.1, 7.3 Hz, 1H), 7.25 (s, 2H), 6.96 (d, J = 8.3 Hz, 2H), 6.91 (d, J = 8.7 Hz, 1H), 6.83 (dd, J = 8.8, 2.7 Hz, 1H), 6.47 (d, J = 2.7 Hz, 1H), 3.85 (s, 3H), 3.62 (s, 3H).

^{13}C NMR (126 MHz, CD_2Cl_2) δ 158.97, 158.22, 148.16, 143.08, 137.73, 137.64, 136.84, 136.77, 136.73, 135.08, 134.21, 132.13, 127.75, 126.71, 126.43, 126.35, 124.66, 117.24, 114.60, 113.49, 106.35, 55.22, 55.11.

HRMS (ESI-TOF) m/z: $[M]^+$ calcd for $C_{26}H_{20}IO_2$ 491.0508, found 491.0511.

UV-Vis (DCM): λ max (nm) (Ɛ ($M^{-1}.cm^{-1}$)) = 366 ($6.19\cdot10^3$), 293 ($1.02\cdot10^4$), 251 ($3.02\cdot10^4$).

Fluorescence (CH_2Cl_2, Excitation at 366 nm): 491 nm.

3.9.2 Synthesis of compound **2.57**

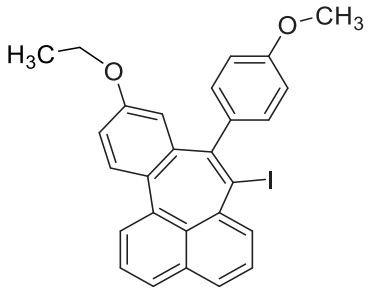

2.57

Compound **2.49** (0.10 g, 0.21 mmol, 1.0 eq) was dissolved in a 1:1 mixture of DCM/EtOH (10 mL, v/v) in a two-neck round-bottom flask equipped with a reflux condenser. Concentrated H_2SO_4 (8 drops) was added, and the reaction mixture was heated to 80 °C and refluxed for 96 h. The mixture was quenched with water and extracted with CH_2Cl_2 (3 × 30 mL). The combined organic extracts were dried over $MgSO_4$, filtered, and concentrated under reduced pressure. Purification by column chromatography (ethyl acetate/petroleum ether, 1:10) afforded **2.57**(0.022 g, 20%) as a yellow solid.

m.p.135.2-137.8 °C.

Rf: 0.6 (ethyl acetate/petroleum ether, 1:9).

^{1}H NMR (400 MHz, CD_2Cl_2) δ 7.99 (dd, J = 7.3, 1.1 Hz, 1H), 7.70 (ddd, J = 8.3, 4.8, 1.2 Hz, 2H), 7.61 (dd, J = 8.1, 1.1 Hz, 1H), 7.53 (dd, J = 8.1, 7.1 Hz, 1H), 7.41 (dd, J = 8.1, 7.3 Hz, 1H), 7.25 (s, 2H), 6.97 (d, J = 8.3 Hz, 2H), 6.89 (d, J = 8.8 Hz, 1H), 6.81 (dd, J = 8.7, 2.7 Hz, 1H), 6.46 (d, J = 2.7 Hz, 1H), 3.85 (s, 3H), 3.85 – 3.79 (m, 2H), 1.27 (t, J = 7.0 Hz, 3H).

^{13}C NMR (101 MHz, CD_2Cl_2) δ 158.96, 157.57, 148.21, 143.13, 137.71, 137.66, 136.82, 136.81, 136.70, 135.06, 134.05, 132.13, 127.73, 126.67, 126.38, 126.35, 124.64, 117.74, 115.13, 113.48, 106.27, 63.41, 55.22, 14.40.

HRMS (ESI-TOF) m/z: $[M+H]^+$ calcd for $C_{27}H_{22}IO_2$ 505.0664, found 505.0672.

UV-Vis (DCM): λ max (nm) (Ɛ ($M^{-1}.cm^{-1}$)) = 368 ($6.04\cdot10^3$), 292 ($1.05\cdot10^4$), 252 ($3.08\cdot10^4$).

Fluorescence (CH_2Cl_2, Excitation at 368 nm): 473 nm.

3.9.3 Synthesis of compound **2.58**

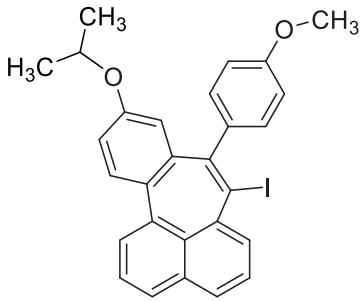

2.58

Compound **2.49** (0.10 g, 0.21 mmol, 1.0 eq) was dissolved in a 1:1 mixture of DCM/isopropanol (10 mL, v/v) in a two-neck round-bottom flask equipped with a reflux condenser. Concentrated H_2SO_4 (8 drops) was added, and the reaction mixture was heated to 83 °C and refluxed for 96 h. The mixture was quenched with water and extracted with CH_2Cl_2 (3 × 30 mL), dried over $MgSO_4$, filtered, and concentrated under reduced pressure. Purification by column chromatography (ethyl acetate/petroleum ether, 1:10), afforded **2.58** (0.0169 g, 16%) as yellow solid.

m.p.133.2–135.2 °C.

Rf: 0.3 (ethyl acetate/petroleum ether, 2:8).

^{1}H NMR (400 MHz, CD_2Cl_2) δ 7.98 (dd, J = 7.3, 1.1 Hz, 1H), 7.74 – 7.66 (m, 2H), 7.61 (dd, J = 8.1, 1.1 Hz, 1H), 7.53 (dd, J = 8.1, 7.1 Hz, 1H), 7.40 (dd, J = 8.1, 7.3 Hz, 1H), 7.25 (s, 2H), 6.97 (d, J = 8.3 Hz, 2H), 6.88 (d, J = 8.7 Hz, 1H), 6.79 (dd, J = 8.8, 2.7 Hz, 1H), 6.43 (d, J = 2.7 Hz, 1H), 4.33 (hept, J = 6.0 Hz, 1H), 3.85 (s, 3H), 1.17 (d, J = 6.0 Hz, 6H).

^{13}C NMR (101 MHz, CD_2Cl_2) δ 158.95, 156.48, 148.40, 143.15, 137.80, 136.79, 135.03, 127.72, 126.62, 126.35, 124.63, 118.92, 116.36, 113.47, 69.73, 55.23, 21.52.

HRMS (ESI-TOF) m/z: $[M+H]^+$ calcd for $C_{28}H_{24}IO_2$ 519.0821, found 519.0820.

UV-Vis (DCM): λ max (nm) (Ɛ ($M^{-1}.cm^{-1}$)) = 368 ($7.61\cdot10^3$), 294 ($1.25\cdot10^4$), 251 ($3.66\cdot10^4$).

Fluorescence (CH_2Cl_2, Excitation at 368 nm): 473 nm.

3.10 Synthesis of compound **2.61**

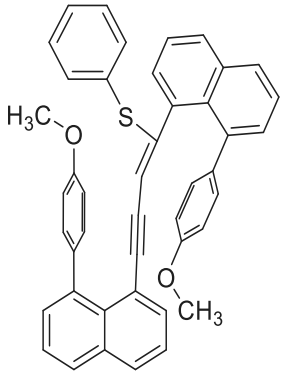

2.61

A mixture of **2.34** (0.11 g, 0.214 mmol, 1 eq), and K_2CO_3 (0.148 g, 1.1 mmol, 5 eq), were placed in microwave vial and stirred in DMF (6 ml) under N_2 for 10 min. Thiophenol (0.13 ml, 1.3 mmol, 6 eq) was added and the reaction heated at 120 °C for 23h. After cooling, the mixture was diluted with EtOAc (20 ml), washed with 1M HCl (40 ml), H_2O, and brine. It was dried over $MgSO_4$, and concentrated under vacuum, subjected to column chromatography by using a system of (DCM/petroleum ether) => 1:1, yielding **2.61** as a yellow solid (0.072 g, 54%).

m.p.125.6-128.1°C.

^{1}H NMR (400 MHz, Methylene Chloride-d_2) δ 7.88 (ddd, J = 8.0, 6.4, 1.4 Hz, 2H), 7.70 (ddd, J = 7.8, 6.3, 1.4 Hz, 2H), 7.58 (s, 1H), 7.55 – 7.48 (m, 2H), 7.45 (m, 2H), 7.42 (m, 2H), 7.37 (dd, J = 6.9, 1.4 Hz, 3H), 7.29 (dd, J = 8.2, 7.0 Hz, 2H), 7.13 (dd, J = 7.0, 1.4 Hz, 1H), 7.04 – 6.83 (m, 7H), 6.87 – 6.77 (m, 2H), 6.75 (s, 1H), 5.47 (s, 1H), 3.81 (s, 3H), 3.67 (s, 3H).

^{13}C NMR (126 MHz, CD_2Cl_2) δ 158.90, 158.83, 148.90, 140.35, 140.30, 137.07, 135.29, 135.00, 134.69 134.41, 134.30, 134.13, 133.24, 132.40, 130.83, 130.39, 130.27, 129.64, 129.41, 129.25, 129.05, 128.28, 127.67, 127.64, 126.80, 125.29, 125.19, 125.09, 124.36, 120.91, 113.98, 112.58, 97.78, 95.47, 55.18, 55.14.

HRMS (ESI$^+$-TOF) m/z: $[M+H]^+$ calcd for $C_{44}H_{33}O_2S$ 625.2202, found 625.2202

References

1. Menichini, E.; Bocca, B. Polycyclic Aromatic Hydrocarbons. In Encyclopedia of Food Sciences and Nutrition, 2nd ed, **2003**; pp 4616–4625.
2. Boehm, H., Setton, R. & Stumpp, E. Nomenclature and terminology of graphite intercalation compounds. *Pure and Applied Chemistry*. **1994**, 66, 1893-1901.
3. Dabestani, R. & Ivanov, I. N. A compilation of physical, spectroscopic and photophysical properties of polycyclic aromatic hydrocarbons. *Photochemistry and Photobiology*, **1999**, 10-34.
4. Novoselov, K. S. et al. Electric field in atomically thin carbon films. *Science***. 2004**, 306, 666–669.
5. Brodie, B. C. XIII. On the Atomic Weight of Graphite. *Philos. Trans. R. Soc.* **1859**, 149, 249–259.
6. Rozpp, F., Patyk, J. & Stankowski, J. Graphenes Bonding Forces in Graphite. *Acta Physica Polonica A*. **2007**, 112.
7. Wan, X., Huang, Y. I. & Chen, Y. Focusing on Energy and Optoelectronic Applications: A Journey for Graphene and Graphene Oxide at Large Scale. *Acc. Chem. Res*. **2012**, 45, 598–607.
8. Narita, A., Chen, Z., Chen, Q. & Müllen, K. Solution and on-surface synthesis of structurally defined graphene nanoribbons as a new family of semiconductors. *Chem. Sci*. **2019**, 10, 964–975.
9. Chen, L., Hernandez, Y., Feng, X. & Müllen, K. From nanographene and graphene nanoribbons to graphene sheets: Chemical synthesis. *Angew. Chem. Int. Ed*., **2012**, 51, 7640–7654.
10. Schwierz, F. Graphene transistors. *Nature Nanotechnology*. **2010**, 5, 487–496.
11. Wang, X. Y., Narita, A. & Müllen, K. Precision synthesis versus bulk-scale fabrication of graphenes. *Nat Rev*. **2018**, 2, 1-9.
12. Wang, X. Y., Yao, X. & Müllen, K. Polycyclic aromatic hydrocarbons in the graphene era. *Science China Chemistry*, **2019**, 62, 1099–1144.
13. Carrell, C. J. et al. Bay- and fjord-region distortions in dibenz[a,j]anthracene and tetrabenzo[de,hi,mn,qr]naphthacene. *Carcinogenesis*, **1994**, 15, 2931–2936.
14. Chen, T. A. & Liu, R. S. Synthesis of large polycyclic aromatic hydrocarbons from bis(biaryl)acetylenes: Large planar PAHs with low π-sextets. *Org. Lett*. **2011**, 13, 4644–4647.
15. Fort, E. H., Donovan, P. M. & Scott, L. T. Diels-Alder reactivity of polycyclic aromatic hydrocarbon bay regions: Implications for metal-free growth of single-chirality carbon nanotubes. *J. Am. Chem. Soc*. **2009**, 131, 16006–16007.
16. Hauptmann, S. The Aromatic Sextet. *Zeitschrift für Chemie*. **1973**. 5, pp 200.
17. Solà, M. Forty years of Clar's aromatic π-sextet rule. *Front. Chem*. **2013**. 1, 22.
18. Chou, C.-P. & Witek, H. A. An Algorithm and FORTRAN Program for Automatic Computation of the Zhang-Zhang Polynomial of Benzenoids. MATCH Communications in Mathematical and in Computer Chemistry MATCH Commun. Math. Comput. Chem. **2012**, 68.
19. Platt, J. R. Classification of spectra of cata-condensed hydrocarbons. J. Chem. Phys., **1949**, 17, 484–495.
20. Mondal, R., Adhikari, R. M., Shah, B. K. & Neckers, D. C. Revisiting the stability of hexacenes. Org. Lett. **2007**, 9, 2505–2508.
21. Biermann, D. & Schmidt, W. Diels-Alder Reactivity of Polycyclic Aromatic Hydrocarbons. 1. Acenes and Benzologs. **1980**, 3163–3173.
22. Payne, M. M., Parkin, S. R. & Anthony, J. E. Functionalized higher acenes: Hexacene and heptacene. J. Am. Chem. Soc. **2005**, 127, 8028–8029.
23. Suresh, C. H. & Gadre, S. R. Clar's aromatic sextet theory revisited via molecular electrostatic potential topography. Journal of Organic Chemistry, **1999**. 64, 2505–2512.
24. E. Clar, M. Zander. 11-Tribenzoperylene. *J. Chem. Soc*. **1958**. 161, 1861–1865.

25. Mughal, E. U., Naeem, N., Kainat, S. F., Sadiq, A. & Ogaly, H. A. Nanographene horizons: the emerging role of hexa-peri-hexabenzocoronene in functional material design. RSC Advances. **2025**, 15, 30490–30551.
26. Heravi, M. M. & Mohammad khani, L. Recent applications of Stille reaction in total synthesis of natural products: An update. *Journal of Organometallic Chemistry*. **2018**, 869, 106–200.
27. Stille, J. K. The Palladium-Catalyzed Cross-Coupling Reactions of Organotin Reagents with Organic Electrophiles. *Angew. Chem. Int. Ed. Engl*. **1986**, 25, 508–524.
28. Huo, S., Mroz, R. & Carroll, J. Negishi coupling in the synthesis of advanced electronic, optical, electrochemical, and magnetic materials. *Organic Chemistry Frontiers*. **2015**, 2, 416–445.
29. Jonas W. Meringdal, D. M. Suzuki–Miyaura (hetero-)aryl cross-coupling: recent findings and recommendations. *Chem. Soc. Rev.* **2025**, 54, 5746-5765.
30. Sonogashira, K. Development of Pd–Cu catalyzed cross-coupling of terminal acetylenes with sp^2-carbon halides. *J. Organomet. Chem.* **2002**, 653, 46–49.
31. Alberico, D., Scott, M. E. & Lautens, M. Aryl-aryl bond formation by transition-metal-catalyzed direct arylation. *Chem Rev*. **2007**, 107, 174–238.
32. Campeau, L. C. & Fagnou, K. Palladium-catalyzed direct arylation of simple arenes in synthesis of biaryl molecules. *Chem Commun (Camb)*. **2006**, 1253–1264.
33. Davidson, J. M. & Triggs, C. Reaction of metal ion complexes with hydrocarbons. Part I. 'Palladation' and some other new electrophilic substitution reactions. The preparation of palladium(I). Journal of the Chemical Society A: Inorganic, Physical, Theoretical. **1968**, 5, 1324–1330.
34. Dahlgren, M. K., Schyman, P., Tirado-Rives, J. & Jorgensen, W. L. Characterization of Biaryl Torsional Energetics and its Treatment in OPLS All-Atom Force Fields. J. Chem. Inf. Model. **2013**, 53, 1191–1199.
35. Omae, I. Intramolecular five-membered ring compounds and their applications. *Coord. Chem. Rev*. **2004**, 248, 995–1023.
36. Kleiman, J. P. & Dubeck, M. The Preparation of Cyclopentadienyl [o-(Phenylazo)Phenyl]Nickel. J. Am. Chem. Soc. **1963**, 85, 1544–1545.
37. Satoh, T. et al. Regioselective Arylation Reactions of Biphenyl-2-ols, Naphthols, and Benzylic Compounds with Aryl Halides under Palladium Catalysis. *Bull. Chem. Soc. Jpn*. **1998**, 71, 2239–2246.
38. Bedford, R.B., Coles, S.J., Hursthouse, M.B. and Limmert, M.E. , The Catalytic Intermolecular Orthoarylation of Phenols. *Angew. Chem. Int. Ed*. **2003**, 42, 112-114.
39. Izumi, T.; Watabe, H.; Kasahara, A. The σ-Bonded Palladium(II) Complexes of 2-Aryl-4,4-dimethyl-2-oxazolines. *Bull. Chem. Soc. Jpn*. **1981**, 54, 1711-1714.
40. Oi S, Ogino Y, Fukita S & Inoue Y. Ruthenium complex catalyzed direct ortho arylation and alkenylation of aromatic imines with organic halides. Org. Lett. **2002**, 4, 1783–1785.
41. He, Y. Q. & Zhong, Y. W. The synthesis of 2- and 2,7-functionalized pyrene derivatives through Ru(ii)-catalyzed C-H activation. *Chem. Commun*. **2015**, 51, 3411–3414.
42. Sire, C.; Cattey, H.; Tsivery, A.; Hierso, J.-C.; Roger, J. Phosphorus-Directed Rhodium-Catalyzed C–H Arylation of 1-Pyrenylphosphines Selective at the K-Region. *Adv. Synth. Catal*. **2022**, 364, 440.
43. Satoh, T., Kawamura, Y., Miura, M. and Nomura, M., Palladium-Catalyzed Regioselective Mono- and Diarylation Reactions of 2-Phenylphenols and Naphthols with Aryl Halides. *Angew. Chem. Int. Ed*. Engl., **1997**, 36, 1740-1742.
44. Rice, J. E. & Cai, Z.-W. An Intramolecular Arene-Triflate Coupling Reaction for the Regiospecific Synthesis of Substituted Benzofluoranthenesl. *J. Org. Chem*. **1993**,58, 1415-1424.
45. Campo, M. A. & Larock, R. C. Novel 1,4-Palladium Migration in Organopalladium Intermediates Derived from o-Iodobiaryls. *J. Am. Chem. Soc*. **2002**, 124, 14326–14327.

46. Campo, M. A., Huang, Q., Yao, T., Tian, Q. & Larock, R. C. 1,4-Palladium migration via C-H activation, followed by arylation: Synthesis of fused polycycles. *J. Am. Chem. Soc*. **2003**, 125, 11506–11507.
47. Rice, J. E. & Cai, Z. W. A palladium-catalyzed intramolecular arene-triflate coupling for the synthesis of fluoranthenes and benzofluoranthenes. *Tetrahedron Lett*. **1992**, 33, 1675–1678.
48. Mohammad-Pour, G. S. et al. Modular Design of Fluorescent Dibenzo- and Naphtho-Fluoranthenes: Structural Rearrangements and Electronic Properties. *J. Org. Chem*. **2018**, 83, 8036–8053.
49. Clar, E. and Furnari, F., Über die Konstitution des Benzanthrons und seiner Reduktionsprodukte (Mehrkernige Kohlenwasserstoffe, 16. Mitteil.). *Ber. dtsch. Chem. Ges*. **1932**, 65, 1420-1425.
50. Clar, E. Synthesis of ovalene. *Nature*, **1948**, 161, 238–239.
51. Clar, E.; Zander, M. Syntheses of Coronene and 1:2-7:8-Dibenzocoronene. *J. Chem. Soc*. **1957**, 4616–4619.
52. Mochida, K., Kawasumi, K., Segawa, Y. & Itami, K. Direct arylation of polycyclic aromatic hydrocarbons through palladium catalysis. *J. Am. Chem. Soc*. **2011**, 133, 28, 10716–10719.
53. Kawasumi K, Mochida K, Kajino T, Segawa Y, Itami K. Pd(OAc)2/o-chloranil/M(OTf)n: a catalyst for the direct C-H arylation of polycyclic aromatic hydrocarbons with boryl-, silyl-, and unfunctionalized arenes. *Org Lett*. **2012**, 14, 418-421.
54. Matsuoka W, Ito H, Itami K. Rapid Access to Nanographenes and Fused Heteroaromatics by Palladium-Catalyzed Annulative π-Extension Reaction of Unfunctionalized Aromatics with Diiodobiaryls. *Angew. Chem. Int. Ed.* **2017**, 129, 12392–12396.
55. Scholl, R.; Mansfeld, J. meso-Benzdianthron (Helianthron), meso-Naphthodianthron. *Ber. Dtsch. Chem. Ges.* **1910**, 43, 1734–1746.
56. Narita, A. et al. Synthesis of structurally well-defined and liquid-phase-processable graphene nanoribbons. *Nat. Chem*. **2014**, 6, 126–132.
57. Zhang, Y., Pun, S. H. & Miao, Q. The Scholl Reaction as a Powerful Tool for Synthesis of Curved Polycyclic Aromatics. *Chem. Rev*. **2022**, 122, 14554–14593.
58. Vingiello, F. A. & Youssef, A. K. The Isomerisation of 12-Phenylbenz[a]Anthracene. *Chem. Commun*. **1967**, 863-864.
59. Lavit-Lamy, D.; Buu-Hoï, N. P. The True Nature of "Dibenzo[a,l]pyrene" and Its Known Derivatives. *Chem. Commun*. **1966**, 92–94.
60. Clar, E.; Stewart, D. 147. Aromatic hydrocarbons. Part LIX. 1:2–3:4-Dibenzpyrene. *J. Chem. Soc*. **1951**, 687–690.
61. Yang, X., Rominger, F. & Mastalerz, M. Contorted Polycyclic Aromatic Hydrocarbons with Two Embedded Azulene Units. *Angew. Chem. Int. Ed*. **2019**, 58, 17577–17582.
62. Seyler, H., Purushothaman, B., Jones, D. J., Holmes, A. B. & Wong, W. W. H. Hexa-peri-hexabenzocoronene in organic electronics. *Pure Appl. Chem*. **2012**, 84, 1047–1067.
63. Ito, S., Wehmeier, M., Brand, J.D., Kübel, C., Epsch, R., Rabe, J.P. and Müllen, K., Synthesis and Self-Assembly of Functionalized Hexa-peri-hexabenzocoronenes. *Chem. Eur. J*. **2000**, 6, 4327-4342.
64. Wehmeier, M., Wagner, M. and Müllen, K., Novel Perylene Chromophores Obtained by a Facile Oxidative Cyclodehydrogenation Route. *Chem. Eur. J.* **2001**, 7, 2197-2205.
65. Zhang, Q., Kawasumi, K., Segawa, Y., Itami, K. & Scott, L. T. Palladium-catalyzed C-H activation taken to the limit. Flattening an aromatic bowl by total arylation. *J. Am. Chem. Soc*. **2012**, 134, 15664–15667.
66. Kawasumi, K., Zhang, Q., Segawa, Y., Scott, L. T. & Itami, K. A grossly warped nanographene and the consequences of multiple odd-membered-ring defects. *Nat. Chem*. **2013**, 5, 739–744.
67. Misselwitz, E. et al. Naphthyl-Separated Stone–Wales Defect-Type Nanographene via Scholl Cyclization of Tetra(1-naphthyl)naphthalene. *Org. Lett*. **2025**, 27, 9019–9023.
68. Narita, A., Wang, X. Y., Feng, X. & Müllen, K. New advances in nanographene chemistry. *Chem. Soc. Rev*. **2015**, 44, 6616–6643.

69. Ono, S., Minder, N., Chen, Z., Facchetti, A. & Morpurgo, A. F. High-performance n-type organic field-effect transistors with ionic liquid gates. *Appl. Phys. Lett*. **2010**, 97, 143307.
70. Zhou, X. & Yu, G. Modified Engineering of Graphene Nanoribbons Prepared via On-Surface Synthesis. *Adv. Mater*. **2020**, 32, 1905957.
71. Zhang, C., Li, S., Dong, X. Y. & Zang, S. Q. Circularly polarized luminescence of agglomerate emitters. *Aggregate*. **2021**, 2, e48.
72. Yang, W. et al. Carbon nanomaterials in biosensors: Should you use nanotubes or graphene. *Angew. Chem. Int. Ed*. **2010**, 49, 2114–2138.
73. Robinson, J. T. et al. Ultrasmall Reduced Graphene Oxide with High Near-Infrared Absorbance for Photothermal Therapy. *J. Am. Chem. Soc*. **2011**, 133, 6825–6831.
74. Dar, M. S., Tabish, T. A., Thorat, N. D., Swati, G. & Sahu, N. K. Photothermal therapy using graphene quantum dots. *APL Bioeng*. **2023**, 7, 031502.
75. Wu, J., Pisula, W. & Müllen, K. Graphenes as Potential Material for Electronics. *Chem. Rev*. **2007**, 107, 718–747.
76. Raccichini, R., Varzi, A., Passerini, S. & Scrosati, B. The role of graphene for electrochemical energy storage. *Nat. Mater*. **2014**, 14, 271–279.
77. Gu, Y., Qiu, Z. & Müllen, K. Nanographenes and Graphene Nanoribbons as Multitalents of Present and Future Materials Science. *J. Am. Chem. Soc*. **2022**, 144, 11499–11524.
78. Wang, X. Y., Yao, X., Narita, A. & Müllen, K. Heteroatom-Doped Nanographenes with Structural Precision. *Acc. Chem. Res*. **2019**, 52, 2491–2505.
79. Slota, M. et al. Magnetic edge states and coherent manipulation of graphene nanoribbons. *Nature*. 2018, **557**, 691–695.
80. Yamaguchi, M., Higuchi, M., Tazawa, K. & Manabe, K. Three-Step Synthesis of Fluoranthenes through Pd-Catalyzed Inter- and Intramolecular C-H Arylation. *J. Org. Chem*. **2016**, 81, 3967–3974.
81. Corey, E. J. & Tian, Y. Selective 4-arylation of pyridines by a nonmetalloorganic process. *Org. Lett*. **2005**, 7, 5535–5537.
82. Boyle, B. T., Levy, J. N., de Lescure, L., Paton, R. S. & McNally, A. Halogenation of the 3-position of pyridines through Zincke imine intermediates. *Science*. **2022**, **378**, 773–779.
83. Ahmadli, D., Sahin, Y., Calikyilmaz, E., Şahin, O. & Türkmen, Y. E. Rapid Access to Hydroxyfluoranthenes via a Domino Suzuki-Miyaura/Intramolecular Diels-Alder/Ring-Opening Reactions Sequence. *J. Org. Chem*. **2022**, 87, 6336–6346.
84. Natalia Chernyak, Vladimir Gevorgyan; Exclusive 5-exo-dig Hydroarylation of o-Alkynyl Biaryls Proceeding via C−H Activation Pathway. *Journal American Chemical Society*, **2008**, 130, 5636–5637.
85. Kwon, Y., Cho, H. & Kim, S. Expedient synthesis of phenanthrenes via In(III)-catalyzed 6-exo-dig cycloisomerization. *Org. Lett*. **2013**, 15, 920–923.
86. Bam, R. et al. Four-Fold Alkyne Benzannulation: Synthesis, Properties, and Structure of Pyreno[a]pyrene-Based Helicene Hybrids. *Org. Lett*. **2019**, 21, 8652–8656.
87. Zhang, M. et al. Palladium-catalyzed C8–H arylation and annulation of 1-naphthalene carboxylic acid derivatives with aryl iodides. *Org. Chem. Front*. **2021**, 8, 3274–3279.
88. Yan, J., Rahman, M. S. & Yoshikai, N. Pd-Catalyzed Annulation of 1-Halo-8-arylnaphthalenes and Alkynes Leading to Heptagon-Embedded Aromatic Systems. *Chem. Eur. J*. **2019**, 25, 9395–9399.
89. Zhen, C. J. et al. Singlet Biradical Versus Triplet Biradical/Zwitterion Characteristics in Isomers of C6−C5−C6−C7−C6-Fused Pentacyclic Aromatic Hydrocarbons Revealed through Reactivity Patterns. *Chem. Eur. J*. **2021**, 27, 16682–16689.
90. Li CW, Wang CI, Liao HY, Chaudhuri R, Liu RS. Synthesis of dibenzo[g,p]chrysenes from bis(biaryl)acetylenes via sequential ICl-induced cyclization and Mizoroki-Heck coupling. *J Org Chem*. **2007**, 72, 9203–9207.

91. Elsinger, F., Schreiber, J. & Eschenmoser, A. Cleavage of Alkyl Aryl Ethers with Lithium Iodide. *J. Chem. Soc. D*, **1969**, 616a-616a.
92. Chae, J. Practical demethylation of aryl methyl ethers using an odorless thiol reagent. *Arch. Pharm. Res.* **2008** 31, 305–309.
93. Zschunke, A., Mügge, C., Hintzsche, E. & Schroth, W. Zur Regio- und Stereoselektivität nucleophiler Thiol additionen an Polyine. *J. Prakt. Chem./Chem.-Ztg*. **1992**, 334, 141–146.
94. Díaz-Moscoso, A., Tizzard, G.J., Coles, S.J. and Cammidge, A.N., Synthesis of meso-Substituted Tetrabenzotriazaporphyrins: Easy Access to Hybrid Macrocycles. *Angew. Chem. Int. Ed*. **2013**, 52, 10784-10787.

5.0. Appendix

2.8

Crystal structure analysis of C_8H_6-OSO_2CF_3-1,-C_6H_4OMe-8

Crystal data: $C_{18}H_{13}F_3O4S$, M = 382.34. Orthorhombic, space group $Pna2_1$ (no. 33), a = 5.89336(13), b = 16.7513(3), c = 17.3269(4) Å, V = 1710.55(6) $Å^3$. Z = 4, Dc = 1.438 g cm^{-3}, F(000) = 784, T = 295.69(10) K, μ(Cu-Kα) = 21.8 cm^{-1}, λ(Cu-Kα) = 1.54184 Å.

The crystal was a colourless shard. From a sample under oil, one, *ca* 0. x 0. x 0. mm, was mounted on a small loop and fixed on a Rigaku Oxford Diffraction XtaLAB Synergy diffractometer, equipped with Cu-Kα radiation, HyPix detector and mirror monochromator. Intensity data were measured by thin-slice ω-scans. Total no. of reflections recorded, to θ_{max} = *ca* 72.2°, was 6238 of which 2622 were unique (Rint = 0.031); 2417 were 'observed' with $I > 2\sigma_I$.

Data were processed using the CrysAlisPro-CCD and -RED (1) programs. The structure was determined by the intrinsic phasing routines in the SHELXT program (2A) and refined by full-matrix least-squares methods, on F^2's, in SHELXL (2B). The non-hydrogen atoms were refined with anisotropic thermal parameters. The hydrogen atoms were included in idealised positions and their Uiso values were set to ride on the Ueq values of the parent carbon atoms. At the conclusion of the refinement, wR_2 = 0.107 and R_1 = 0.041 (2B) for all 2622 reflections weighted w = $[\sigma^2(F_o^2) + (0.0643 P)^2]^{-1}$ with P = $(F_o^2 + 2F_c^2)/3$; for the 'observed' data only, R_1 = 0.039.

In the final difference map, the highest peak (*ca* 0.14 $eÅ^{-3}$) was near H(4).

Scattering factors for neutral atoms were taken from reference (3). Computer programs used in this analysis have been noted above, and were run through WinGX (4) on a Dell Optiplex 780 PC at the University of East Anglia.

Legends for Figures

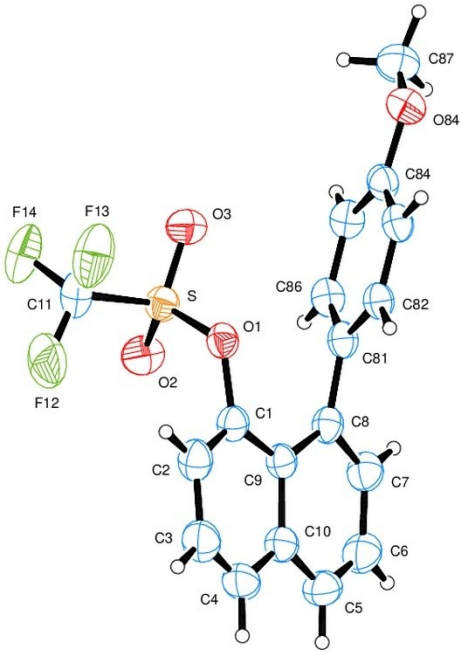

Figure 1. View of a molecule of C_8H_6-OSO_2CF_3-1,-C_6H_4OMe-8, indicating the atom numbering scheme. Thermal ellipsoids are drawn at the 20% probability level.

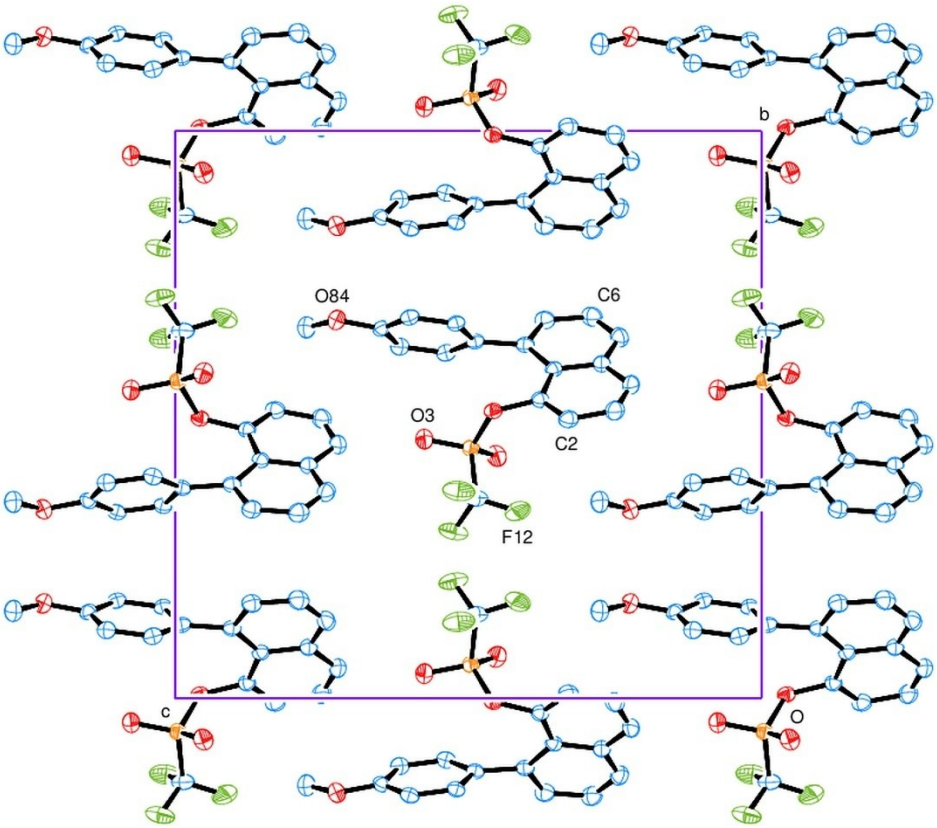

Figure 2. View of the packing of molecules, along the *a* axis.

Notes on the structure

Figure 1 shows the naphthalene ring and its two substituent groups of the title compound. There is a slight twist about the central bond, C(9)-C(10), of the naphthalene system, with the normals to the two six-membered rings 4.6(2) ° apart. The phenyl ring is rotated *ca* 59.14 ° from the plane of the C(5-10) ring; this brings O(3) to lie over the phenyl ring at a perpendicular distance of 3.178(4) Å.

We are surprised to find, in a molecule with two distinct planar groups, no extensive parallel plane (π–π) alignments between molecules; there is. however, peripheral overlap of the C(2)-C(3) bond by the bond C(6')-C(7') and on the other side, H(87a") points toward the centre of the C(5-10) ring with C…H distances 3.16-3.40 Å. Other intermolecular contacts are at distances close to van der Waals' values.

2.9

Crystal structure analysis of $C_{10}H_6$-C_6H_4OMe-1,-CC-C_6H_4OMe-8

Crystal data: $C_{26}H_{20}O_2$, M = 364.42. Monoclinic, space group $P2_1/c$ (no. 14), a = 12.3073(3), b = 9.3747(3), c = 17.4821(7) Å, β = 101.917(4) °, V = 1973.56(13) Å^3. Z = 4, Dc = 1.226 g cm^{-3}, F(000) = 768, T = 296(2) K, μ(Cu-Kα) = 6.0 cm^{-1}, λ(Cu-Kα) = 1.54184 Å.

The crystal was a yellow block. From a sample under oil, one, *ca* 0.17 x 0.31 x 0.46 mm, was mounted on a small loop and fixed in the cold nitrogen stream on a Rigaku Oxford Diffraction XtaLAB Synergy diffractometer, equipped with Cu-Kα radiation, HyPix detector and mirror monochromator. Intensity data were measured by thin-slice ω-scans. Total no. of reflections recorded, to θ_{max} = 72.5°, was 14,165 of which 3830 were unique (Rint = 0.064); 3197 were 'observed' with $I > 2\sigma_I$.

Data were processed using the CrysAlisPro-CCD and -RED (1) programs. The structure was determined by the intrinsic phasing routines in the SHELXT program (2A) and refined by full-matrix least-squares methods, on F^2's, in SHELXL (2B). The non-hydrogen atoms were refined with anisotropic thermal parameters. Hydrogen atoms were included in idealised positions and their Uiso values were set to ride on the Ueq values of the parent carbon atoms. At the conclusion of the refinement, wR_2 = 0.161 and R_1 = 0.066 (2B) for all 3830 reflections weighted $w = [\sigma^2(F_o^2) + (0.0938 P)^2 + 0.1577 P]^{-1}$ with $P = (F_o^2 + 2F_c^2)/3$; for the 'observed' data only, R_1 = 0.059.

In the final difference map, the highest peak (*ca* 0.2 eÅ^{-3}) was near C(84).

Scattering factors for neutral atoms were taken from reference (3). Computer programs used in this analysis have been noted above, and were run through WinGX (4) on a Dell Optiplex 780 PC at the University of East Anglia.

Legends for Figures

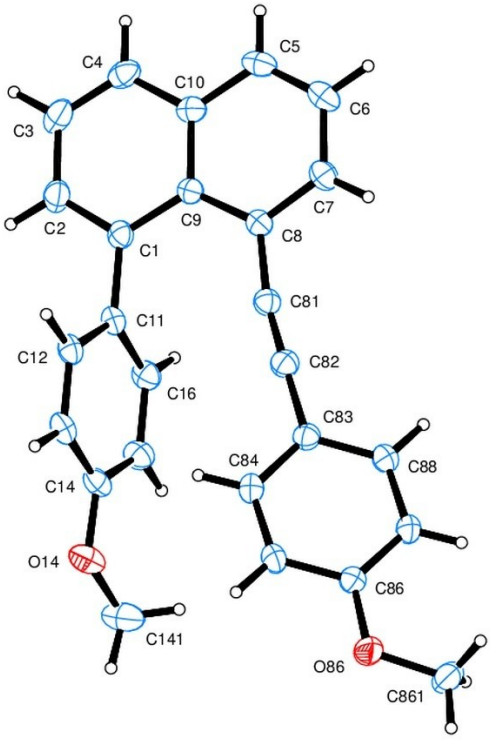

Figure 1. View of the naphthalene derivative, indicating the atom numbering scheme. Thermal ellipsoids are drawn at the 20% probability level.

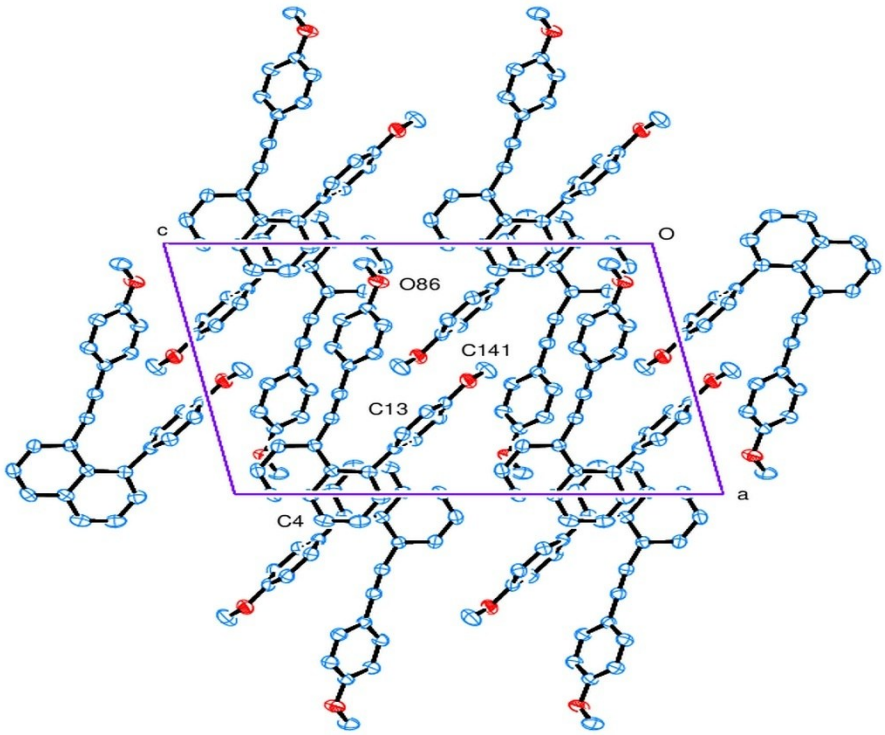

Figure 2. View along the *b* axis of the packing of molecules.

Notes on the structure

In this room-temperature study, the planar naphthyl group has a methoxyphenol group at C(1) and a methoxyphenyl acetylenyl group at C(8); the C(1)-C(11) and C(8)-C(81) bonds diverge slightly, 14.09(8)°, and the two phenyl rings are rotated *ca* 78.0° and 28.2° from the naphthyl ring plane.

There is no evidence of π…π interactions between any of the aromatic rings in the cell, and very few short C-H…π contacts, the shortest of which seems to be H(7)…C(14') at 2.85 Å. There are, however, some slightly shorter intramolecular contacts between the neighbouring methoxy-phenyl groups, e.g. C(13)…H(84) at 2.82 Å and C(16)…C(81) at 3.127 Å.

2.34

Crystal structure analysis of (MeO-C_6H_4-$C_{10}H_6$-CC-)$_2$

Crystal data: $C_{38}H_{26}O_2$, M = 514.59. Monoclinic, space group $P2_1/n$ (as no. 14), a = 7.10697(15), b = 11.4033(2), c = 16.4645(3) Å, β = 99.522(2) °, V = 1315.95(4) Å^3. Z = 2, Dc = 1.299 g cm^{-3}, F(000) = 540, T = 100(2) K, μ(Cu-Kα) = 6.14 cm^{-1}, λ(Cu-Kα) = 1.54184 Å.

The crystal was a pale yellow parallelogram. From a sample under oil, one, *ca* 0.51 x 0.12 x 0.03 mm, was mounted on a small loop and fixed in the cold nitrogen stream on a Rigaku Oxford Diffraction XtaLAB Synergy diffractometer, equipped with Cu-Kα radiation, HyPix detector and mirror monochromator. Intensity data were measured by thin-slice ω-scans. Total no. of reflections recorded, to θ_{max} = 72.5°, was 8685 of which 2496 were unique (Rint = 0.056); 2098 were 'observed' with $I > 2\sigma_I$.

Data were processed using the CrysAlisPro-CCD and -RED (1) programs. The structure was determined by the intrinsic phasing routines in the SHELXT program (2A) and refined by full-matrix least-squares methods, on F^2's, in SHELXL (2B). The non-hydrogen atoms were refined with anisotropic thermal parameters. Hydrogen atoms were included in idealised positions and their Uiso values were set to ride on the Ueq values of the parent carbon atoms. At the conclusion of the refinement, wR_2 = 0.115 and R_1 = 0.052 (2B) for all 2496 reflections weighted $w = [\sigma^2(F_o^2) + (0.0588 P)^2 + 0.1986 P]^{-1}$ with $P = (F_o^2 + 2F_c^2)/3$; for the 'observed' data only, R_1 = 0.044.

In the final difference map, the highest peak (*ca* 0.17 eÅ^{-3}) was near C(1).

Scattering factors for neutral atoms were taken from reference (3). Computer programs used in this analysis have been noted above, and were run through WinGX (4) on a Dell Optiplex 780 PC at the University of East Anglia.

Legends for Figures

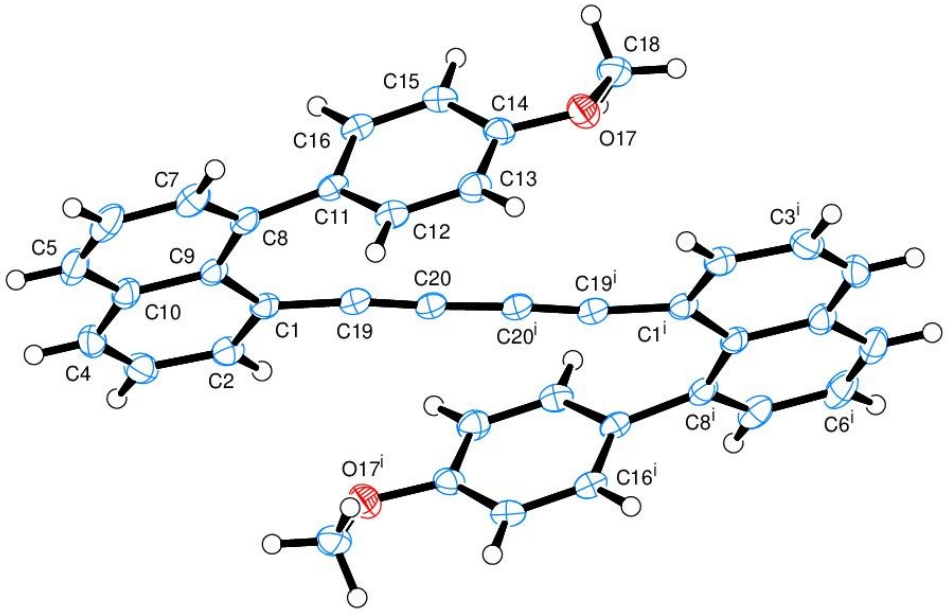

Figure 1. View of a molecule of the di-ynyl molecule, indicating the atom numbering scheme. Thermal ellipsoids are drawn at the 50% probability level.

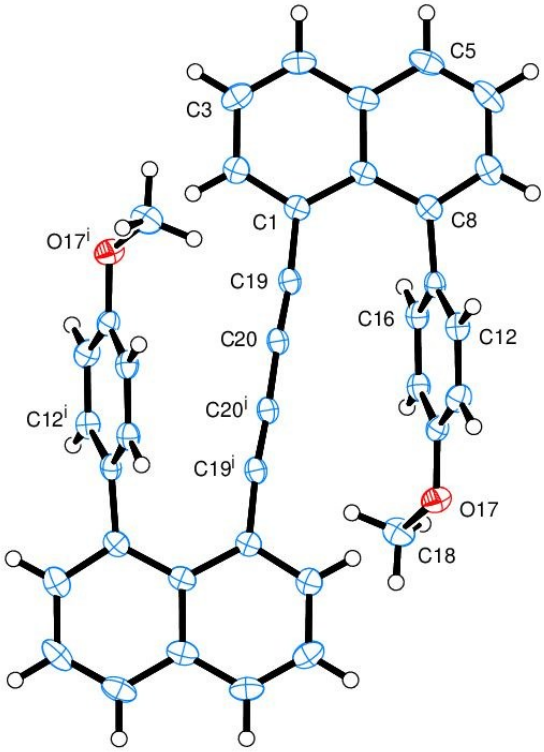

Figure 2. The molecule, viewed along the normal to the naphthalene rings.

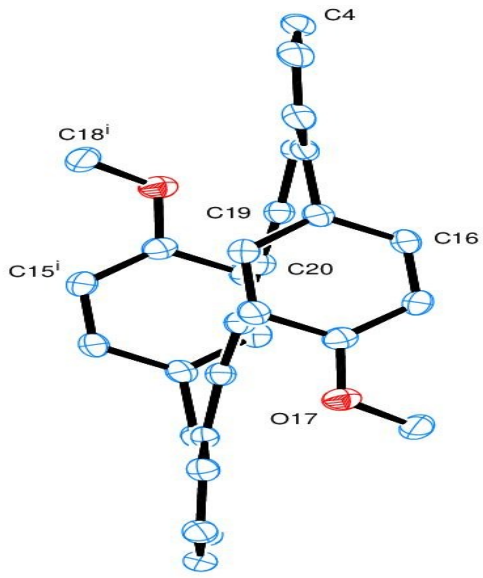

Figure 3. The molecule, viewed with the normal to the naphthalene rings horizontal in the page.

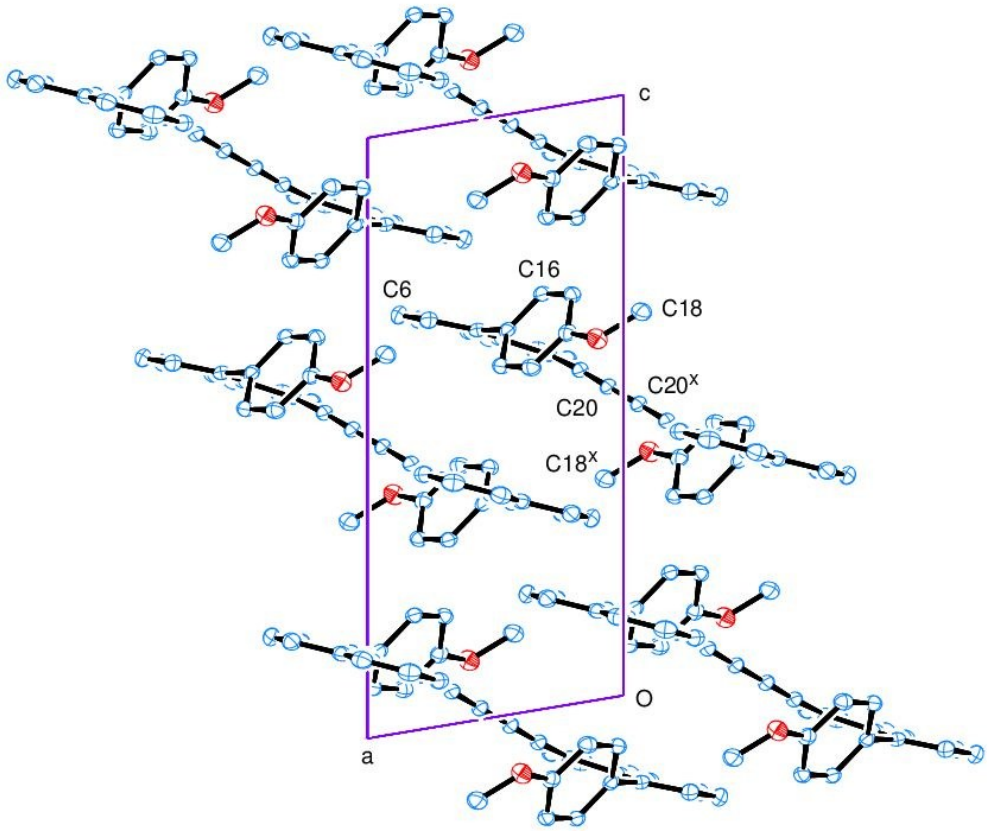

Figure 4. The packing of molecules, viewed along the *b* axis.

Notes on the structure

The molecular structure closely resembles the ChemDraw diagram for the compound; there is a centre of symmetry at the centre of the diagram and the molecule. The atom numbering scheme is shown in Figure 1. The di-ynyl group, from C(1) to C(1'), is essentially linear, Figure 1; the two naphthalene rings are parallel and bent only slightly from coplanarity; the phenyl rings are rotated *ca* 67 ° about the C(8)-C(11) bond, away from the naphthalene rings and lie close on either side of the di-ynyl chain, with the C(11)…C(19) contact distances at 2.820 Å, Figures 2 and 3. The packing of molecules is shown in Figure 4; most of the shortest intermolecular contacts are of the C-H…π type, as H(18c)…C(8) at 2.79 Å.

2.18

Crystal structure analysis of 1-OSO_2-CF_3, 4-C_5H_4N, 8-C_6H_4OMe-naphthalene, MeOH

Crystal data: $C_{23}\,H_{16}\,F_3\,N\,O_4\,S$, MeOH, M = 491.47. Orthorhombic, space group $Pna2_1$ (no. 33), a = 20.5849(4), b = 5.80954(9), c = 37.6791(7) Å, V = 4505.97(14) $Å^3$. Z = 8, Dc = 1.449 g cm^{-3}, F(000) = 2032, T = 100(2) K, μ(Cu-Kα) = 18.34 cm^{-1}, λ(Cu-Kα) = 1.54184 Å.

The crystal was a colourless needle. From a sample under oil, one, *ca* 0.91 x 0.12 x 0.07 mm, was mounted on a small loop and fixed in the cold nitrogen stream on a Rigaku Oxford Diffraction XtaLAB Synergy diffractometer, equipped with Cu-Kα radiation, HyPix detector and mirror monochromator. Intensity data were measured by thin-slice ω-scans. Total no. of reflections recorded, to θ_{max} = 72.5°, was 14,414 of which 6,666 were unique (Rint = 0.029); 6,365 were 'observed' with $I > 2\sigma_I$.

Data were processed using the CrysAlisPro-CCD and -RED (1) programs. The structure was determined by the intrinsic phasing routines in the SHELXT program (2A) and refined by full-matrix least-squares methods, on F^2's, in SHELXL (2B). There are two almost identical molecules in the unit cell. The non-hydrogen atoms were refined with anisotropic thermal parameters. The hydrogen atoms of the methanol solvent molecules were located in difference maps and were refined freely. The remaining hydrogen atoms were included in idealised positions and their Uiso values were set to ride on the Ueq values of the parent carbon atoms. At the conclusion of the refinement, wR_2 = 0.122 and R_1 = 0.048 (2B) for all 6,666 reflections weighted $w = [\sigma^2(F_o^2) + (0.0642\ P)^2 + 3.695\ P]^{-1}$ with $P = (F_o^2 + 2F_c^2)/3$; for the 'observed' data only, R_1 = 0.046.

In the final difference map, the highest peak (*ca* 0.3 $eÅ^{-3}$) was near O(111).

Scattering factors for neutral atoms were taken from reference (3). Computer programs used in this analysis have been noted above, and were run through WinGX (4) on a Dell Optiplex 780 PC at the University of East Anglia.

Legends for Figures

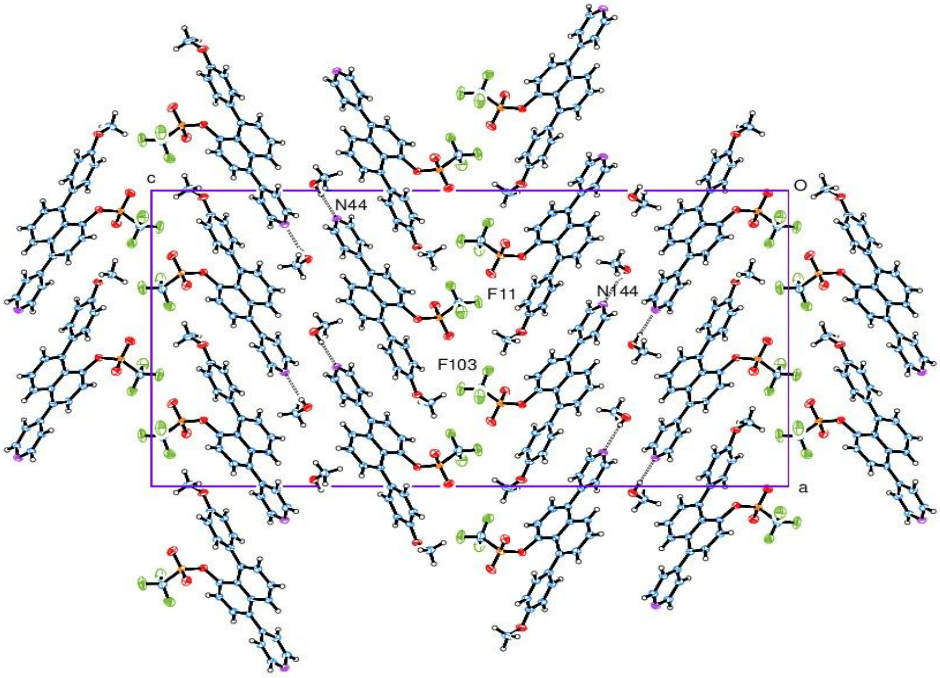

Figure 1. View of the two independent molecules of the naphthalene derivative, with the associated methanol solvent molecules, indicating the atom numbering scheme. Thermal ellipsoids are drawn at the 50% probability level.

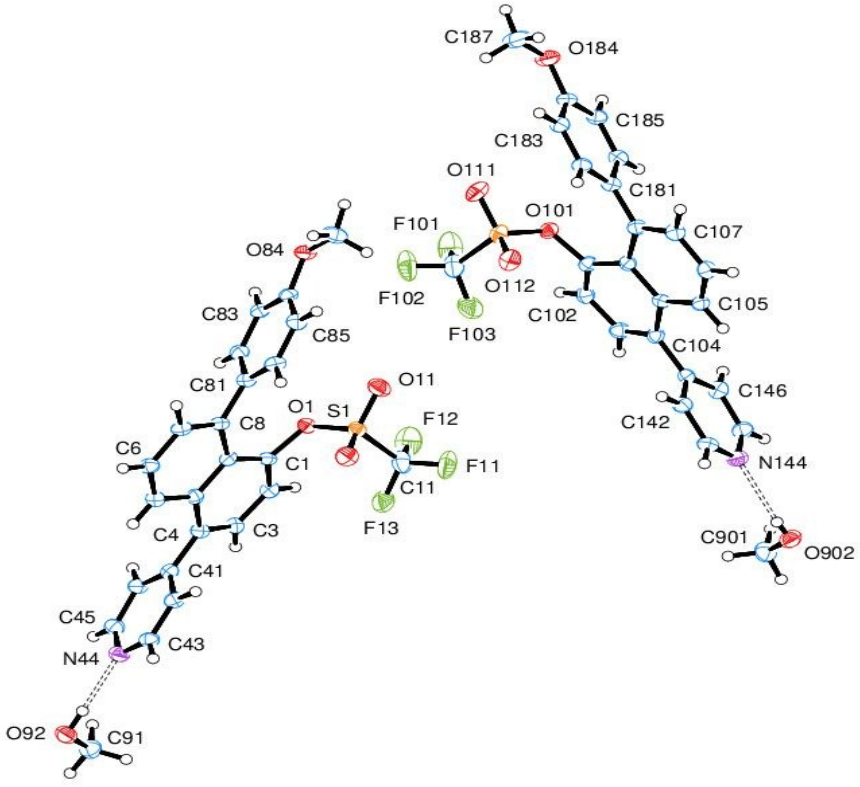

Figure 2 .The packing of molecules, viewed along the *b* axis.

Notes on the structure

The two independent molecules are essentially identical in shape and orientation and are related by a *pseudo*-glide plane at *z*=0.5 with a shift parallel to the *a* axis of *ca* 0.289. The intermolecular contacts are also very similar, except around the -CF_3 groups where the shortest contacts are F(11)…H(183') 2.49 Å and …C(3') 3.196 Å, and F(102)…H(87c) 2.71 Å and …C(87) 3.128 Å.

In each molecule, the central naphthalene group shows a slight twist, presumably caused by interactions between adjacent derivative groups, e.g. O(1)…C(81) and the corresponding O(11)…C(181). There are rotations of *ca* 60° about the C(4)–C(41) and C(8)–C(81) bonds in both molecules so that the pyridine and phenyl rings are almost parallel in each molecule.

2.41

Crystal structure analysis of ($C_{17}H_9O$)-OMe, isopropanol

Crystal data: $C_{18}H_{12}O_2$, $C_3H_8O_4$, M = 368.37. Triclinic, space group P-1 (no. 2), a = 7.257543(14), b = 10.9313(2), c = 11.6212(2) Å, α = 108.1627(19), β = 96.1065(17), γ = 96.2493(17) °, V = 863.28(3) $Å^3$. Z = 2, Dc = 1.417 g cm^{-3}, F(000) = 388, T = 100(2) K, μ(Cu-Kα) = 8.63 cm^{-1}, λ(Cu-Kα) = 1.54184 Å.

The crystal was a yellow block. From a sample under oil, one, *ca* 0.22 x 0.48 x 0.57 mm, was mounted on a small loop and fixed in the cold nitrogen stream on a Rigaku Oxford Diffraction XtaLAB Synergy diffractometer, equipped with Cu-Kα radiation, HyPix detector and mirror monochromator. Intensity data were measured by thin-slice ω-scans. Total no. of reflections recorded, to θ_{max} = 72.5°, was 9769 of which 3275 were unique (Rint = 0.029); 3071 were 'observed' with $I > 2\sigma_I$.

Data were processed using the CrysAlisPro-CCD and -RED (1) programs. The structure was determined by the intrinsic phasing routines in the SHELXT program (2A) and refined by full-matrix least-squares methods, on F^2's, in SHELXL (2B). The principal molecule, methoxy-benzanthrone, is well-defined and was refined smoothly. The solvent molecule, isopropanol, appears to be disordered and remains unresolved; the three-carbon skeleton of the 'isopropanol' unit is well defined, but there are four other atoms, which refine best as fully occupied oxygen atoms; difference peaks on O(25) and O(27) refine well as hydrogen atoms forming good hydrogen bonds to O(1).

The non-hydrogen atoms were refined with anisotropic thermal parameters. The hydrogen atoms of the methoxy group and of the two solvent methyl groups were located in difference maps and were refined freely. The aromatic hydrogen atoms were included in idealised positions and their Uiso values were set to ride on the Ueq values of the parent carbon atoms. The refinement was completed with inclusion of an extinction correction. At the conclusion of the refinement, wR_2 = 0.110 and R_1 = 0.041 (2B) for all 3275 reflections, weighted $w = [\sigma^2(F_o^2) + (0.0667\ P)^2 + 0.2682\ P]^{-1}$ with $P = (F_o^2 + 2F_c^2)/3$; for the 'observed' data only, R_1 = 0.040.

In the final difference map, the highest peak (*ca* 0.29 $eÅ^{-3}$) was near C(5).

Scattering factors for neutral atoms were taken from reference (3). Computer programs used in this analysis have been noted above, and were run through WinGX (4) on a Dell Optiplex 780 PC at the University of East Anglia.

Legends for Figures

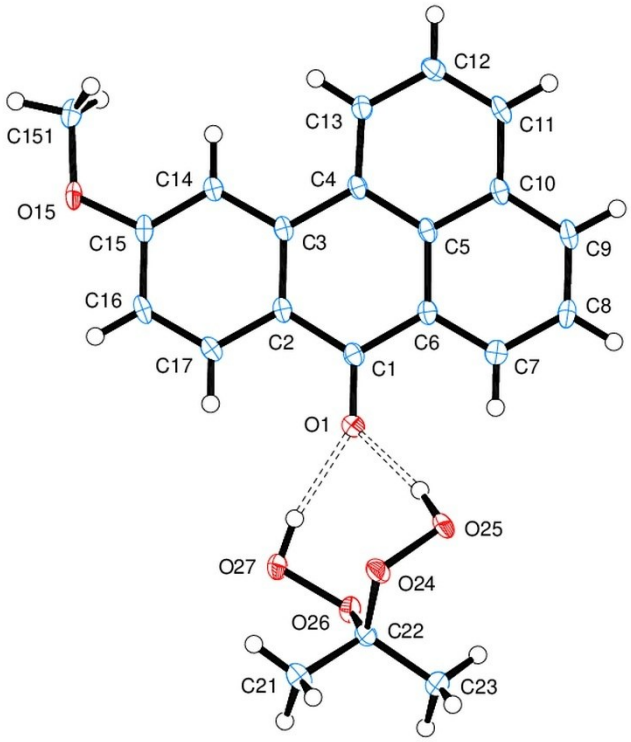

Figure 1. View of the methoxy-benzanthrone crystal, with an associated 'propanol' solvent molecule, indicating the atom numbering scheme. Thermal ellipsoids are drawn at the 50% probability level.

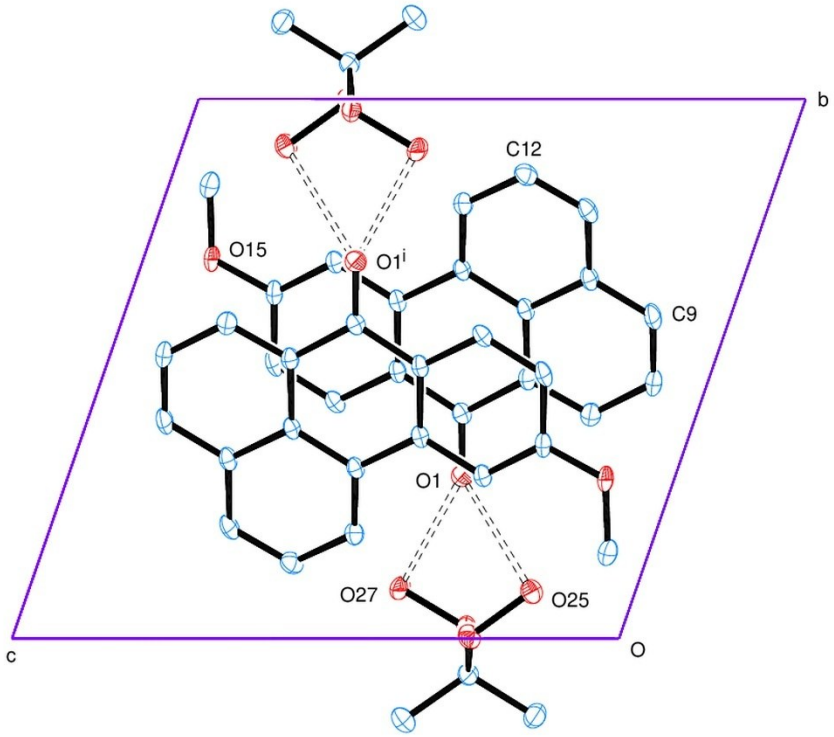

Figure 2. The packing of molecules, viewed along the *a* axis.

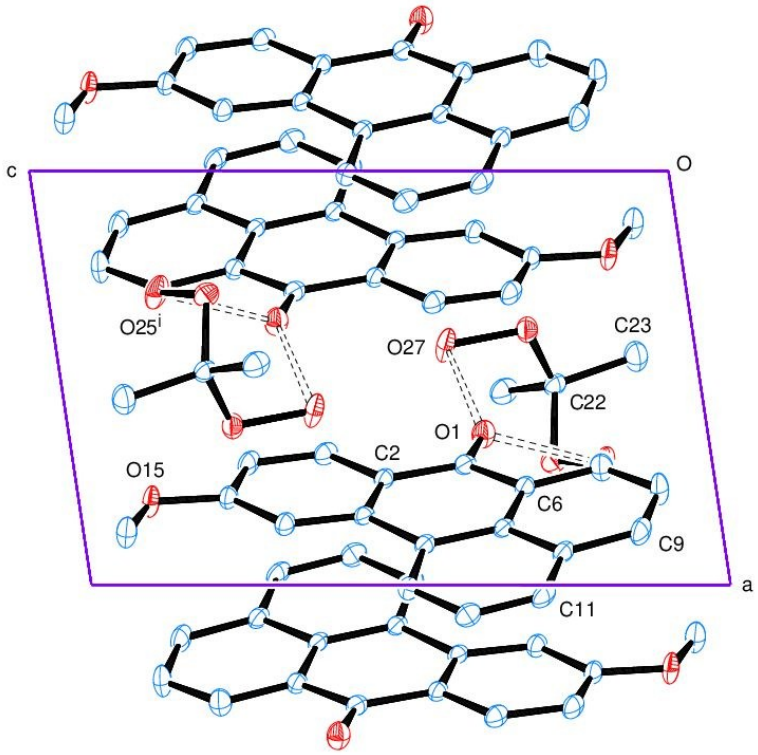

Figure 3. The packing of molecules, viewed along the *b* axis.

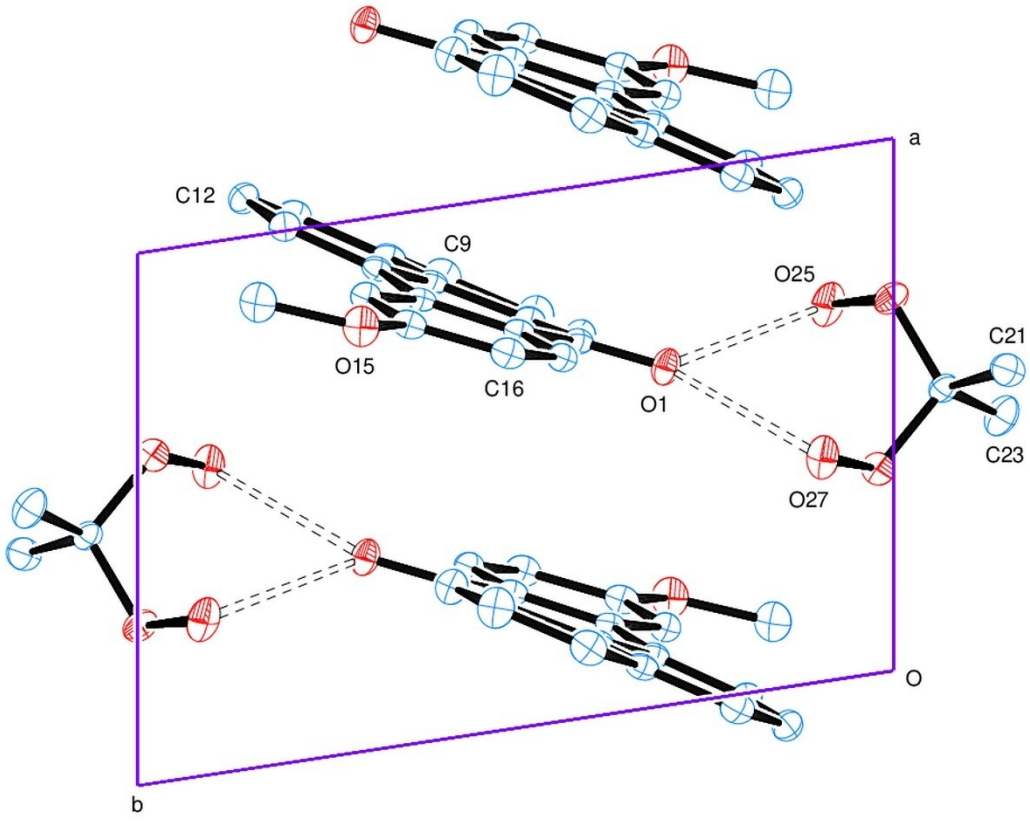

Figure 4. The packing of molecules, viewed along the *c* axis.

Notes on the structure

The benzanthrone moiety is close to planar, Figure 1. There is slight twisting and turning about the central ring of C(1-6), so that the angle between the normals to the outer rings, C(2-3, 14-17) and C(5-10) is 7.98(4) °. The carbonyl O atom, O(1), is the recipient of two hydrogen bonds, from the 'water' molecules, O(25) and O(27), but there is no indication of other H atoms on either of these atoms.

The benzanthrone molecules are stacked along the *a* axis, Figure 2. The central ring, C(1-6), is bounded by inverted rings at *ca* 3.356 Å either side (with shifts from total overlap). Alternative views of the packing are in Figures 3 and 4.

2.44

Crystal structure analysis of methoxyphenyl-$C_{17}H_8$-O,OMe

Crystal data: C_{25} H_{18} $O_{3.}$, M = 366.39. Monoclinic, space group $P2_1/c$ (no. 14), a = 12.4971(3), b = 12.3638(3), c = 11.6551(3) Å, β = 102.282(2) °, V = 1759.53(8) $Å^3$. Z = 4, Dc = 1.383 g cm^{-3}, F(000) = 768, T = 100(2) K, μ(Cu-Kα) = 7.21 cm^{-1}, λ(Cu-Kα) = 1.54184 Å.

The crystal was a yellow block. From a sample under oil, one, *ca* 0.04 x 0.15 x 0.18 mm, was mounted on a small loop and fixed in the cold nitrogen stream on a Rigaku Oxford Diffraction XtaLAB Synergy diffractometer, equipped with Cu-Kα radiation, HyPix detector and mirror monochromator. Intensity data were measured by thin-slice ω-scans. Total no. of reflections recorded, to θ_{max} = 72.5°, was 11,872 of which 3,388 were unique (Rint = 0.034); 2,853 were 'observed' with $I > 2\sigma_I$.

Data were processed using the CrysAlisPro-CCD and -RED (1) programs. The structure was determined by the intrinsic phasing routines in the SHELXT program (2A) and refined by full-matrix least-squares methods, on F^2's, in SHELXL (2B). The non-hydrogen atoms were refined with anisotropic thermal parameters. The hydrogen atoms were included in idealised positions and their Uiso values were set to ride on the Ueq values of the parent carbon atoms. At the conclusion of the refinement, wR_2 = 0.111 and R_1 = 0.048 (2B) for all 3,388 reflections weighted $w = [\sigma^2(F_o^2) + (0.0548 P)^2 + 0.4072 P]^{-1}$ with $P = (F_o^2 + 2F_c^2)/3$; for the 'observed' data only, R_1 = 0.040.

In the final difference map, the highest peak (*ca* 0.2 $eÅ^{-3}$) was near C(15).

Scattering factors for neutral atoms were taken from reference (3). Computer programs used in this analysis have been noted above, and were run through WinGX (4) on a Dell Optiplex 780 PC at the University of East Anglia.

Legends for Figures

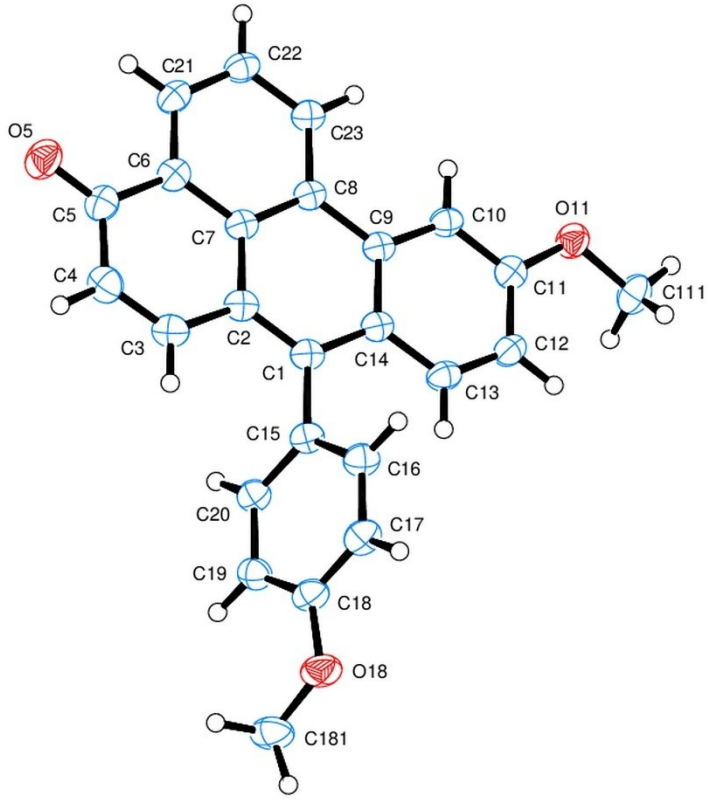

Figure 1. View of the title molecule, indicating the atom numbering scheme. Thermal ellipsoids are drawn at the 50% probability level.

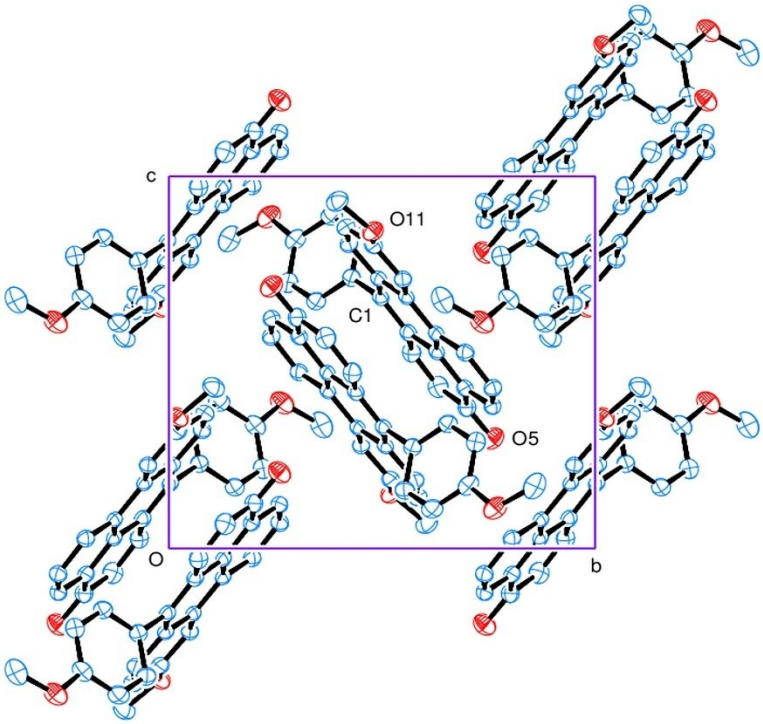

Figure 2. The packing of molecules, viewed along the *a* axis.

Notes on the structure

This polycyclic aromatic hydrocarbon (PAH) has a $C_{17}H_{10}$ benzo-phenalene core which is essentially planar. The plane of the phenyl group is rotated 61.4 ° about the C(1)-C(15) bond from the benzo-phenalene plane, Figure 1.

Pairs of these molecules lie overlapping about a centre of symmetry close to the C(8) atom, approximately 3.40 Å apart, as seen in Figure 2. Other short intermolecular contacts are 'weak hydrogen bonds', such as C(181)-H18a)…O(5), where the H…O distance is 2.36 Å and the C-H…O angle is 146.8 °.

2.49

Crystal structure analysis of spiro-(methoxyphenyl-phenalenone)-(C_6H_4=O)

Crystal data: $C_{23}H_{17}IO_2$, M = 476.28. Monoclinic, space group $P2_1/n$ (as no. 14), a = 10.20217(13), b = 17.4446(2), c = 11.34658(14) Å, β = 109.5169(14) °, V = 1903.36(4) $Å^3$. Z = 4, Dc = 1.662 g cm^{-3}, F(000) = 944, T = 100(2) K, μ(Cu-Kα) = 133.59 cm^{-1}, λ(Cu-Kα) = 1.54184 Å.

The crystal was a yellow block. From a sample under oil, one, *ca* 0.30 x 0.26 x 0.13 mm, was mounted on a small loop and fixed in the cold nitrogen stream on a Rigaku Oxford Diffraction XtaLAB Synergy diffractometer, equipped with Cu-Kα radiation, HyPix detector and mirror monochromator. Intensity data were measured by thin-slice ω-scans. Total no. of reflections recorded, to θ_{max} = 72.5°, was 13,549 of which 3633 were unique (Rint = 0.055); 3524 were 'observed' with $I > 2\sigma_I$.

Data were processed using the CrysAlisPro-CCD and -RED (1) programs. The structure was determined by the intrinsic phasing routines in the SHELXT program (2A) and refined by full-matrix least-squares methods, on F^2's, in SHELXL (2B). The non-hydrogen atoms were refined with anisotropic thermal parameters. Hydrogen atoms were included in idealised positions and their Uiso values were set to ride on the Ueq values of the parent carbon atoms. At the conclusion of the refinement, wR_2 = 0.103 and R_1 = 0.040 (2B) for all 3633 reflections weighted $w = [\sigma^2(F_o^2) + (0.0664 P)^2 + 1.8354 P]^{-1}$ with $P = (F_o^2 + 2F_c^2)/3$; for the 'observed' data only, R_1 = 0.040.

In the final difference map, the highest peak (*ca* 0.9 $eÅ^{-3}$) was near I(3).

Scattering factors for neutral atoms were taken from reference (3). Computer programs used in this analysis have been noted above, and were run through WinGX (4) on a Dell Optiplex 780 PC at the University of East Anglia.

Legends for Figures

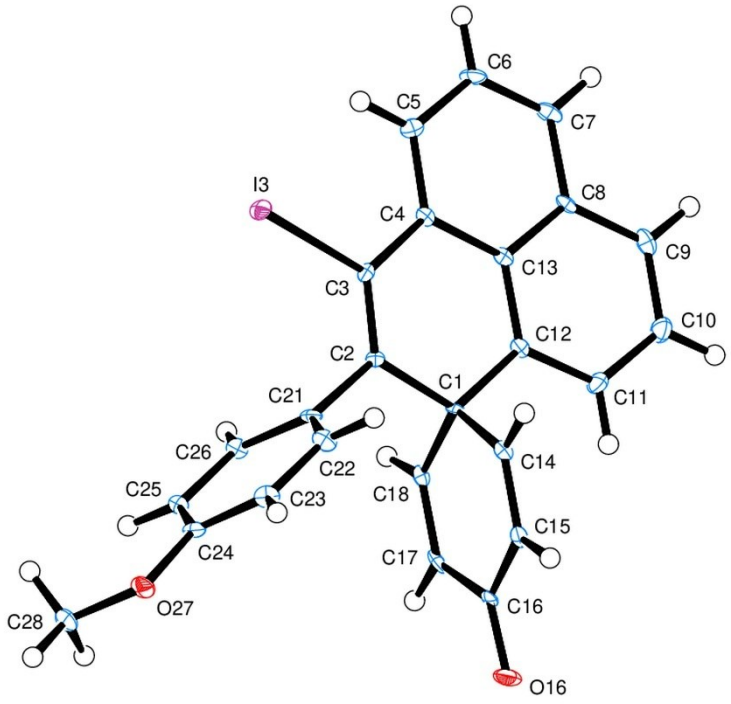

Figure 1. View of the spiro-phenalene derivative, indicating the atom numbering scheme. Thermal ellipsoids are drawn at the 50% probability level.

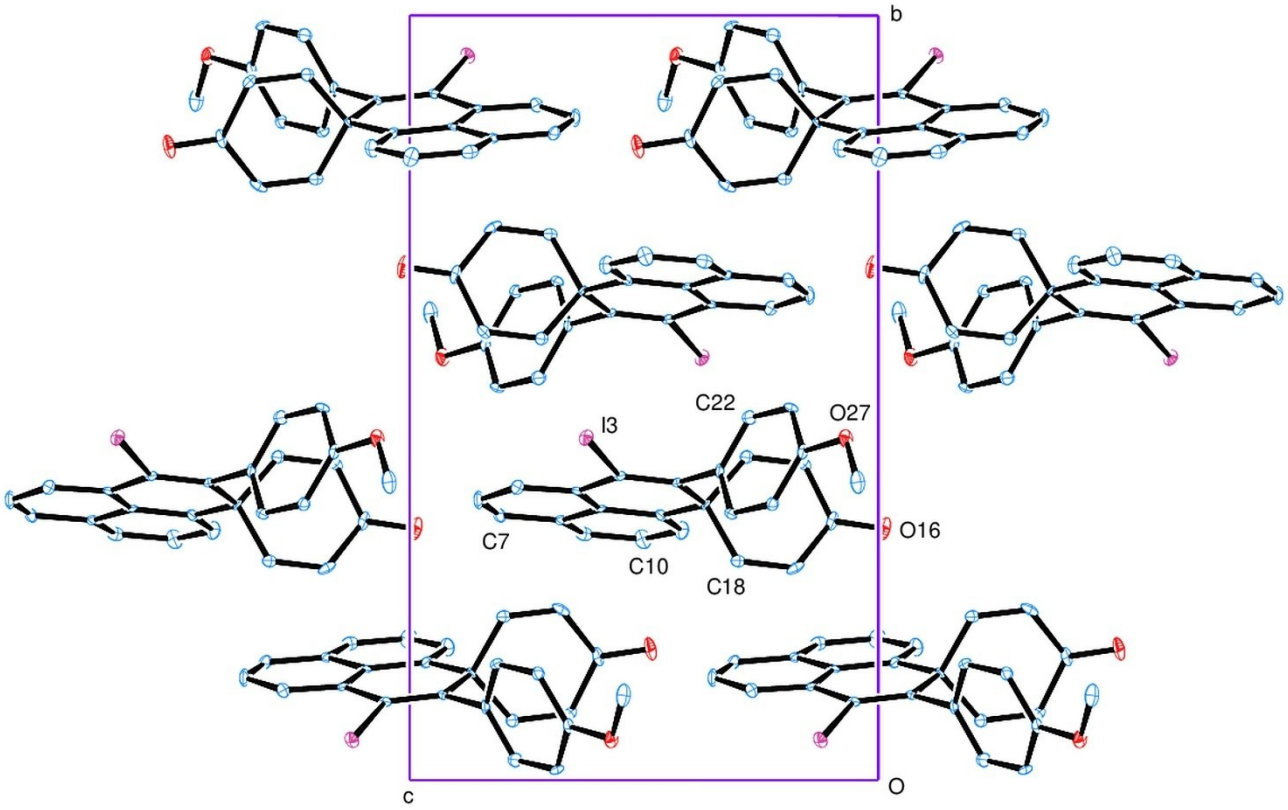

Figure 2 .The packing of molecules, viewed along the *a* axis.

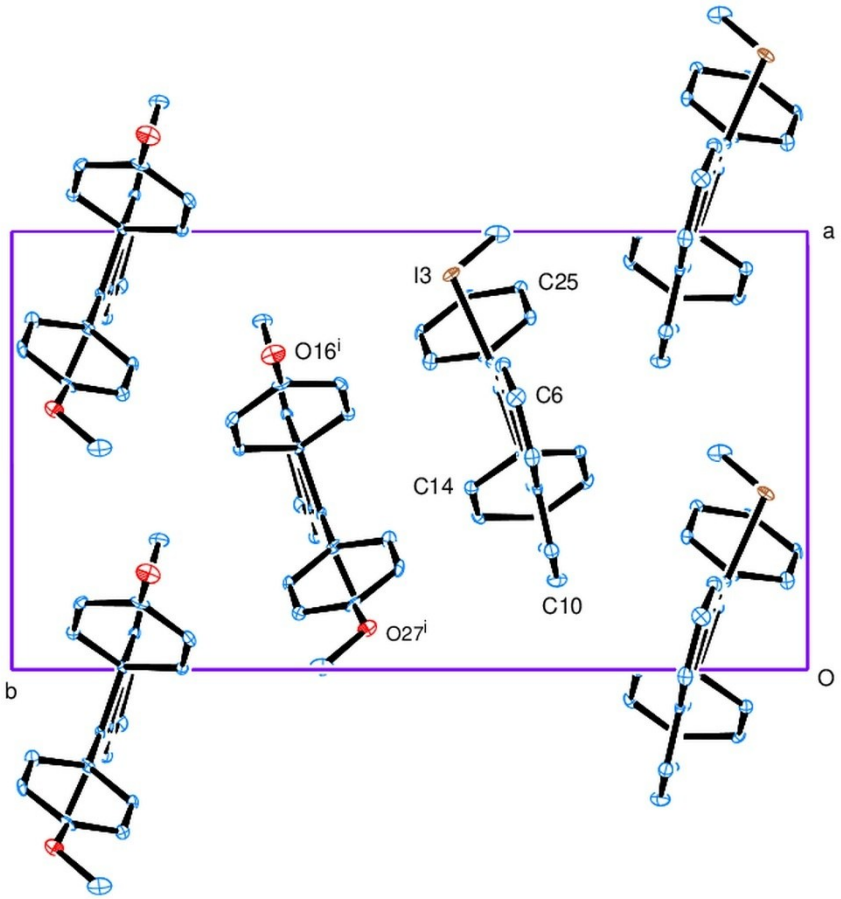

Figure 3. The packing of molecules, viewed along the *c* axis.

Notes on the structure

The spiro-phenalene derivative molecule is a molecule of three planes, viz. the fused system of benzene rings of the phenalene group, the phenyl ring (with the methoxy group not far removed from this plane), and spiro-linked cyclohexadienone ring at C(1). The bond dimensions in the last ring confirm the conjugated arrangement here.

Despite of abundance of aromatic rings in this structure, there is no evidence of π…π stacking interactions; the principal intermolecular contacts are of the C-H…π type, e.g. C(22)-H(22)…C(8') where H(22)…C(8') is 2.70 Å and the angle H-C…O is 153.6 °. The nearest contact of I(3) is also directed towards an aromatic ring with I(3)…C(23') at 3.521 Å with the C-I…C angle at 165.61 °.

The packing arrangements, viewed along the *a* and *c* axes are shown in Figures 2 and 3.

2.16

Crystal structure analysis of 1-hydroxy,-2,4-(C_5H_5N-SO_2CF_3)$_2$,8-methoxyphenyl-naphthalene

Crystal data: $C_{29}H_{22}F_6N_2O_6S_2$., M = 672.60. Triclinic, space group P-1 (no. 2), a = 9.8792(2), b = 10.69866(17), c = 14.0549(3) Å, α = 98.0332(14), β = 91.6632(16), γ = 99.1854(16) °, V = 1450.09(5) Å^3. Z = 2, Dc = 1.540 g cm^{-3}, F(000) = 688, T = 100(2) K, μ(Cu-Kα) = cm^{-1}, λ(Cu-Kα) = 1.54184 Å.

The crystal was a colourless plate. From a sample under oil, one, *ca* 0.06 x 0.25 x 0.42 mm, was mounted on a small loop and fixed in the cold nitrogen stream on a Rigaku Oxford Diffraction XtaLAB Synergy diffractometer, equipped with Cu-Kα radiation, HyPix detector and mirror monochromator. Intensity data were measured by thin-slice ω-scans. Total no. of reflections recorded, to θ_{max} = 70.0°, was 17,947 of which 5,378 were unique (Rint = 0.051); 4,771 were 'observed' with $I > 2\sigma_I$.

Data were processed using the CrysAlisPro-CCD and -RED (1) programs. The structure was determined by the intrinsic phasing routines in the SHELXT program (2A) and refined by full-matrix least-squares methods, on F^2's, in SHELXL (2B). The non-hydrogen atoms were refined with anisotropic thermal parameters. The hydrogen atoms were included in idealised positions and their Uiso values were set to ride on the Ueq values of the parent carbon atoms. At the conclusion of the refinement, wR_2 = 0.128 and R_1 = 0.051 (2B) for all 5,378 reflections weighted $w = [\sigma^2(F_o^2) + (0.0651P)^2 + 0.7604P]^{-1}$ with $P = (F_o^2 + 2F_c^2)/3$; for the 'observed' data only, R_1 = 0.047.

In the final difference map, the highest peak (*ca* 0.46 eÅ^{-3}) was near F(983).

Scattering factors for neutral atoms were taken from reference (3). Computer programs used in this analysis have been noted above, and were run through WinGX (4) on a Dell Optiplex 780 PC at the University of East Anglia.

Legends for Figures

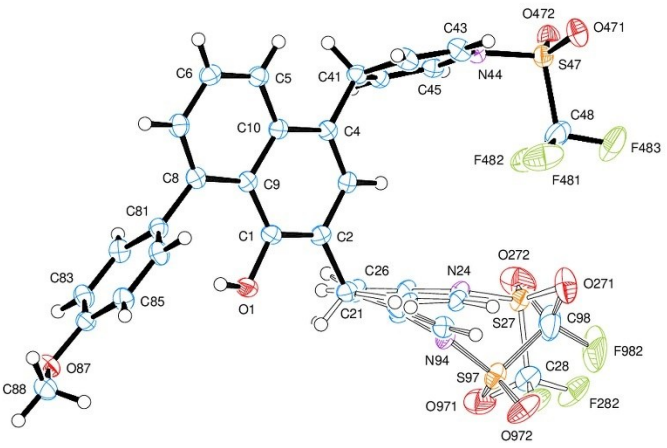

Figure 1. (a) The formula and (b) a view of a molecule of the naphthalene derivative, indicating the atom numbering scheme. Thermal ellipsoids are drawn at the 50% probability level.

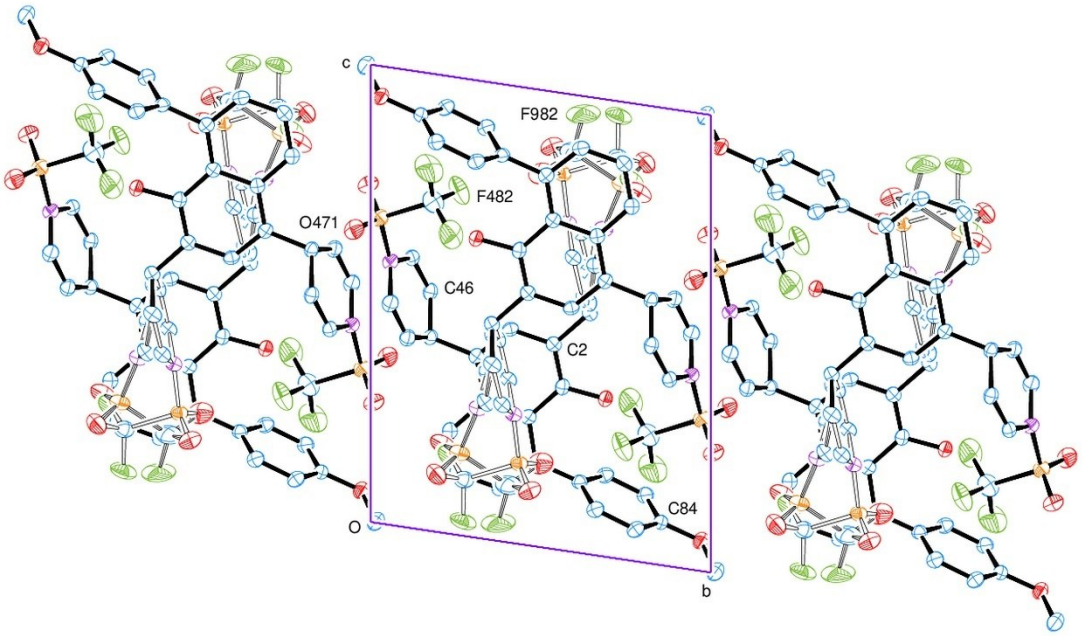

Figure 2. The packing of molecules, viewed along the *a* axis.

Notes on the structure

The formula and structure of the naphthalene derivative molecule are shown in Figure 1.

During the refinement process, one of the 'triflyl-pyridinyl' groups was found to be disordered in two distinct conformations. In Figure 1, the major component is drawn with 'open' bonds, and the minor component with 'one-line-filled' bonds. Most atom sites in the disordered region are clear with single atom occupancies; some sites, however, have shared occupancy, with atoms of both components given equivalent coordinates and thermal parameters; the paired atoms are C(21)/C(91), C(26)/C(96), O(271)/F(981), O(272)/F(983) and F(281)/O(71). The second 'triflyl-pyridinyl' group appears perfectly ordered. In both these groups, the opposing C(.2)–C(.3) and C(.5)–C(.6) bonds in the 'pyridinyl' rings are short and shown as double-bonds in Figure 1a. Correspondingly, the C(.1) atoms linking the 'triflyl-pyridinyl' groups to the naphthalene ring are tetrahedral, four-coordinate, sp^3 type atoms with a hydrogen atom in the fourth site.

The naphthalene unit is essentially planar. The hydroxyl group at C(1) lies in this plane and H(1o) points directly towards C(81) with the H…O distance of 2.12 Å, forming a good hydrogen bond. There is rotation about the C(8)-C(81) bond so that the normal to the phenyl ring plane is 77.03(5)° from that to the naphthalene ring plane. Around the non-planar C(.1) atoms of the 'triflyl-pyridinyl' groups, the rotation calculations are different, but the normals to the 'pyridinyl' planes of the N(24), N(94) and N(44) rings are 86.22(9), 80.81(11) and 70.00(5)°, respectively, from the normal to the naphthalene ring.

The shortest intermolecular contacts are H(26')…C(4) and …C(10) at 2.60 and 2.64 Å, with the C–H bond pointing into the naphthalene plane, and C(45)…C(46') at 3.473 Å with the partial overlap of N(44) 'pyridinyl' rings, Figure 2.

2.20

Crystal structure analysis of an $MeOC_6H_4$-1-naphthalene derivative

Crystal data: $C_{26}\,H_{20}\,F_3\,N\,O_4\,S$, M = 499.49. Triclinic, space group P-1 (no. 2), a = 5.7002(3), b = 13.3940(5), c = 14.8674(6) Å, α = 91.616(3), β = 100.635(4), γ = 96.549(4) °, V = 96.549(4) $Å^3$. Z = 2, Dc = 1.499 g cm^{-3}, F(000) = 516, T = 100(2) K, μ(Cu-Kα) = 18.4 cm^{-1}, λ(Cu-Kα) = 1.54184 Å.

The crystal was a red needle. From a sample under oil, one, *ca* 0.02 x 0.04 x 0.37 mm, was mounted on a small loop and fixed in the cold nitrogen stream on a Rigaku Oxford Diffraction XtaLAB Synergy diffractometer, equipped with Cu-Kα radiation, HyPix detector and mirror monochromator. Intensity data were measured by thin-slice ω-scans. Total no. of reflections recorded, to θ_{max} = 72.41°, was 12,452 of which 4221 were unique (Rint = 0.055); 3310 were 'observed' with $I > 2\sigma_I$.

Data were processed using the CrysAlisPro-CCD and -RED (1) programs. The structure was determined by the intrinsic phasing routines in the SHELXT program (2A) and refined by full-matrix least-squares methods, on F^2's, in SHELXL (2B). The non-hydrogen atoms were refined with anisotropic thermal parameters. Hydrogen atoms were included in idealised positions and their Uiso values were set to ride on the Ueq values of the parent carbon atoms. At the conclusion of the refinement, wR_2 = 0.144 and R_1 = 0.065 (2B) for all 4221 reflections weighted $w = [\sigma^2(F_o^2) + (0.0914\,P)^2]^{-1}$ with $P = (F_o^2 + 2F_c^2)/3$; for the 'observed' data only, R_1 = 0.051.

In the final difference map, the highest peak (*ca* 0.74 $eÅ^{-3}$) was near S(77).

Scattering factors for neutral atoms were taken from reference (3). Computer programs used in this analysis have been noted above, and were run through WinGX (4) on a Dell Optiplex 780 PC at the University of East Anglia.

Legends for Figures

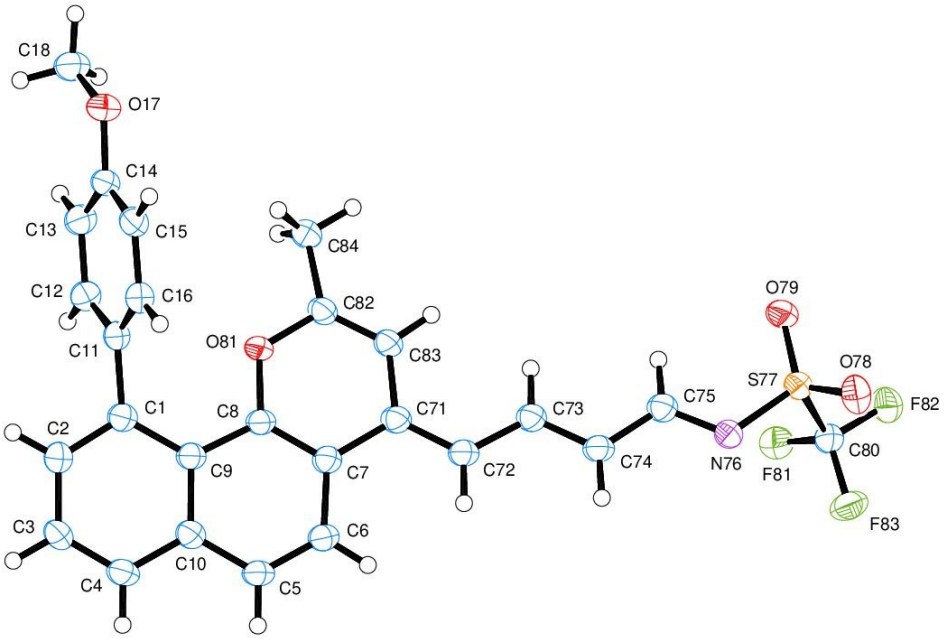

Figure 1. View of the molecule of the naphthalene derivative, indicating the atom numbering scheme. Thermal ellipsoids are drawn at the 50% probability level.

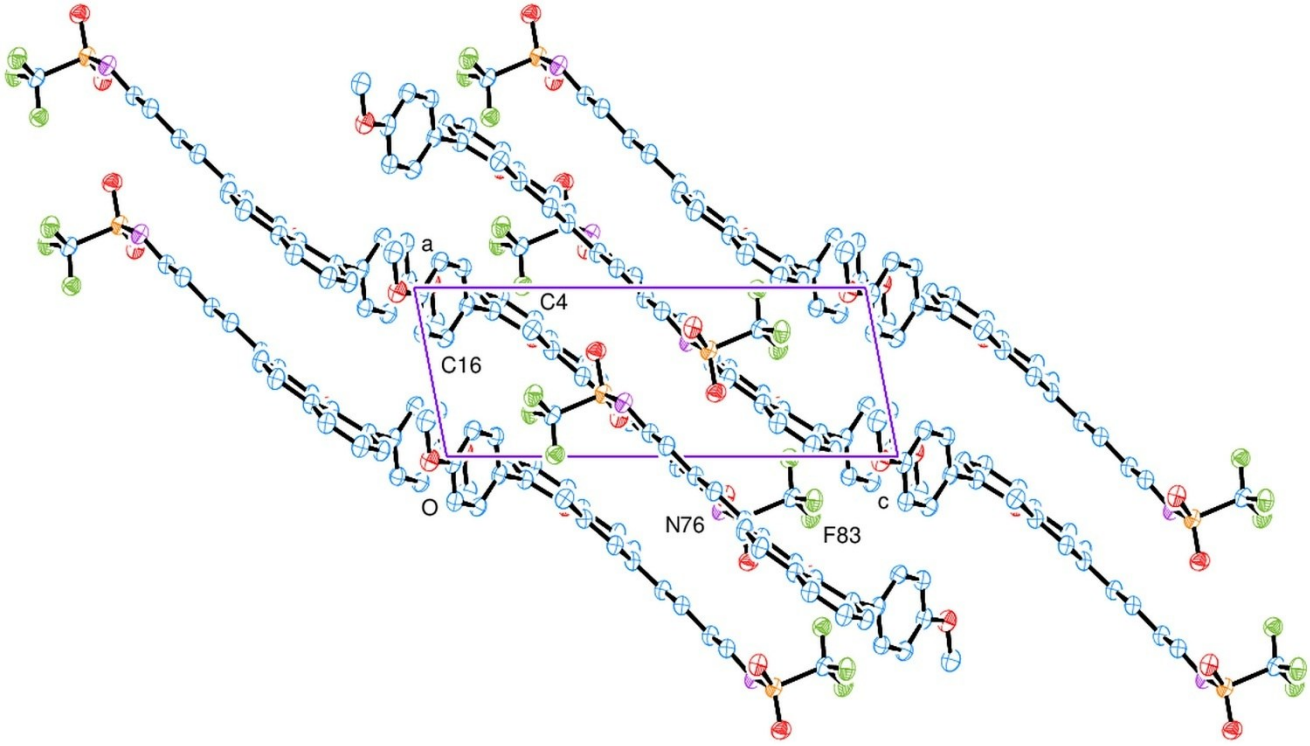

Figure 2. The packing/stacking of molecules, viewed along the *b* axis.

Notes on the structure

1. The X-ray data are good, SHELXT gave a single, good result, and SHELXL refined the structure well. Figure 1.
2. The naphthalene moiety is planar. The phenyl ring is rotated 67.6 ° about the C(1)-C(11) bond and the OMe group lies in the plane of the phenyl ring.
3. The six-membered ring of O(81) is essentially planar.
4. The six-membered chain, C(71)…N(76), also forms a good plane., leading into the tetrahedral S(77) and C(80) groups. The C(71)…N(76) chain shows conjugated double-bonding, with the C(73)-C(74) and C(75)-N(76) bonds shorter than the others in this chain.
5. The molecules are stacked along the *a* axis.

2.21

Crystal structure analysis of 1-methoxyphenyl,-5-bromo,-8-hydroxy-naphthalene

Crystal data: $C_{17}.H_{13}\,Br\,O_2$, M = 329.18. Monoclinic, space group $P2_1/c$ (no. 14), a = 12.8622(3), b = 5.79436(12), c = 18.8672(4) Å,β = 107.654(2) °, V = 1339.93(5) $Å^3$. Z = 4, Dc = 1.632 g cm^{-3}, F(000) = 664, T = 100(2) K, μ(Cu-Kα) = 41.6 cm^{-1}, λ(Cu-Kα) = 1.54184 Å.

The crystal was an orange block. From a sample under oil, one, *ca* 0.26 x 0.73 x 0.78 mm, was mounted on a small loop and fixed in the cold nitrogen stream on a Rigaku Oxford Diffraction XtaLAB Synergy diffractometer, equipped with Cu-Kα radiation, HyPix detector and mirror monochromator. Intensity data were measured by thin-slice ω-scans. Total no. of reflections recorded, to θ_{max} = 72.5°, was 8464 of which 2580 were unique (Rint = 0.063); 2472 were 'observed' with $I > 2\sigma_I$.

Data were processed using the CrysAlisPro-CCD and -RED (1) programs. The structure was determined by the intrinsic phasing routines in the SHELXT program (2A) and refined by full-matrix least-squares methods, on F^2's, in SHELXL (2B). The non-hydrogen atoms were refined with anisotropic thermal parameters. The hydroxy hydrogen atom was located in a difference maps and was refined freely. The remaining hydrogen atoms were included in idealised positions and their Uiso values were set to ride on the Ueq values of the parent carbon atoms. At the conclusion of the refinement, wR_2 = 0.180 and R_1 = 0.069 (2B) for all 2580 reflections weighted $w = [\sigma^2(F_o^2) + (0.1164\,P)^2 + 5.221\,P]^{-1}$ with $P = (F_o^2 + 2F_c^2)/3$; for the 'observed' data only, R_1 = 0.068.

In the final difference map, the highest peak (*ca* 2.2 $eÅ^{-3}$) was near the bromine atom.

Scattering factors for neutral atoms were taken from reference (3). Computer programs used in this analysis have been noted above, and were run through WinGX (4) on a Dell Optiplex 780 PC at the University of East Anglia.

Legends for Figures

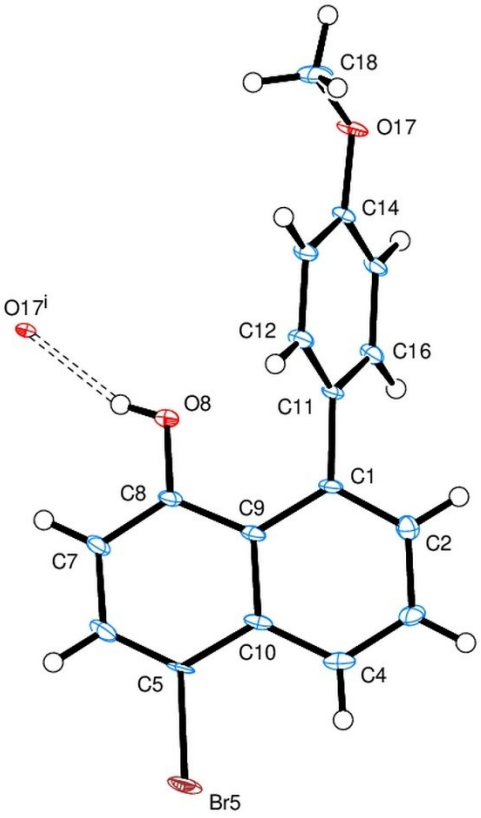

Figure 1. View of the naphthalene derivative with the hydrogen bond contact to a neighbouring molecule, indicating the atom numbering scheme. Thermal ellipsoids are drawn at the 50% probability level.

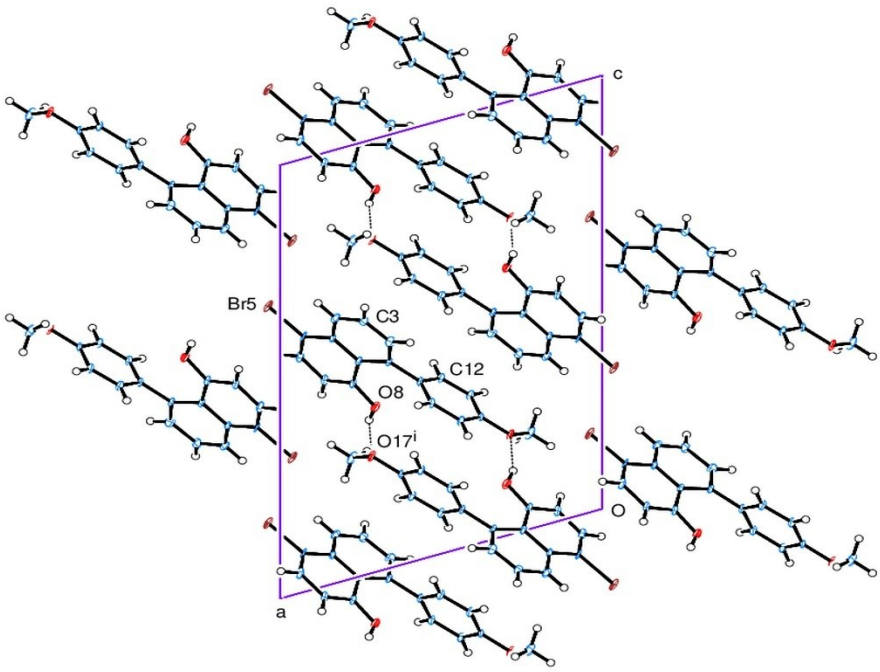

Figure 2. The packing of molecules, viewed along the *b* axis.

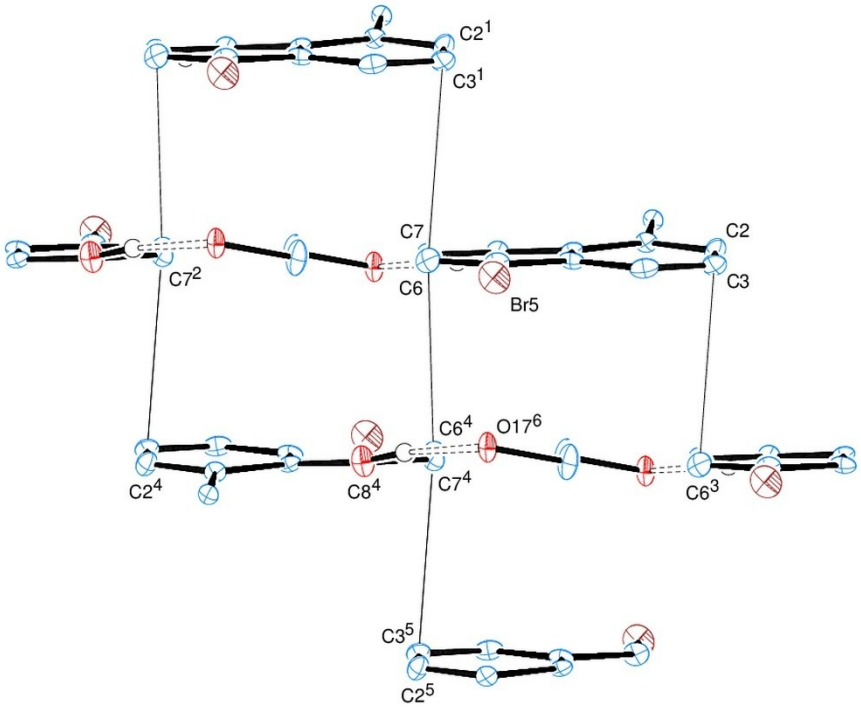

Figure 3. View of the stacking of naphthalene groups. The vertical line bonds show the inter-layer π…π contacts.

Notes on the structure

The naphthalene group, Figure 1, is almost planar – there is a small twist about the central C(9)-C(10) bond so that the normals to the two C_6 rings are 4.4(3) ° apart. The phenyl ring is rotated *ca* 61.95(12) ° about the C(1)-C(11) bond away from the C(1-4, 9-10) ring, and the –OMe group lies close to the plane of the phenyl group. The hydrogen of the phenolic oxygen, O(8), was clear in a difference map and forms a good hydrogen bond with O(17) of a neighbouring molecule; this is part of a chain of bonded molecules spiralling around a twofold screw axis parallel to the *b* axis, Figure 2.

The closest neighbours of the bromine atom are C(18) of the methoxy groups above and below Br(5) in an adjacent spiral chain. The shortest Br…H contact is 3.04 Å to H(4) on another spiral chain.

The planar naphthalene ring systems appear likely stacking units, but it is only the outermost bonds that form π…π bonds – the C(2)-C(3) bond overlaps a C(6)-C(7) bond, C(6) overlaps C(6') about an inversion centre, and the C(6')-C(7') bond overlaps a C(2')-C(3') bond; thus making a four level stack, Figure 3. The C(6)-C(6') distances are 3.335 Å and the C(3)…C(6) and …C(7) distances are 3.440 and 3-442 Å respectively.

2.22

Crystal structure analysis of a bromo-naphthoquinone derivative

Crystal data: $C_{17}H_{10}Br_2O_3$., M = 422.07. Monoclinic, space group $P2_1/n$ (no. 14), a = 8.1471(2), b = 21.3954(6), c = 8.3718(2) Å, β = 92.935(3) °, V = 1457.38(6) $Å^3$. Z = 4, Dc = 1.924 g cm^{-3}, F(000) = 824, T = 100(2) K, μ(Cu-Kα) = 0.715 cm^{-1}, λ(Cu-Kα) = 1.54184 Å.

The crystal was an orange block. From a sample under oil, one, *ca* 0.16 x 0.16 x 0.22 mm, was mounted on a small loop and fixed in the cold nitrogen stream on a Rigaku Oxford Diffraction XtaLAB Synergy diffractometer, equipped with Cu-Kα radiation, HyPix detector and mirror monochromator. Intensity data were measured by thin-slice ω-scans. Total no. of reflections recorded, to θ_{max} = 72.5°, was 9679 of which 2792 were unique (Rint = 0.076); 2615 were 'observed' with $I > 2\sigma_I$.

Data were processed using the CrysAlisPro-CCD and -RED (1) programs. The structure was determined by the intrinsic phasing routines in the SHELXT program (2A) and refined by full-matrix least-squares methods, on F^2's, in SHELXL (2B). The non-hydrogen atoms were refined with anisotropic thermal parameters. Hydrogen atoms were included in idealised positions and their Uiso values were set to ride on the Ueq values of the parent carbon atoms. At the conclusion of the refinement, wR_2 = 0.170 and R_1 = 0.065 (2B) for all 2792 reflections weighted $w = [\sigma^2(F_o^2) + (0.0915 P)^2 + 5.4019 P]^{-1}$ with $P = (F_o^2 + 2F_c^2)/3$; for the 'observed' data only, R_1 = 0.062.

In the final difference map, the highest peak (*ca* 1.4 $eÅ^{-3}$) was near H(2).

Scattering factors for neutral atoms were taken from reference (3). Computer programs used in this analysis have been noted above, and were run through WinGX (4) on a Dell Optiplex 780 PC at the University of East Anglia.

Legends for Figures

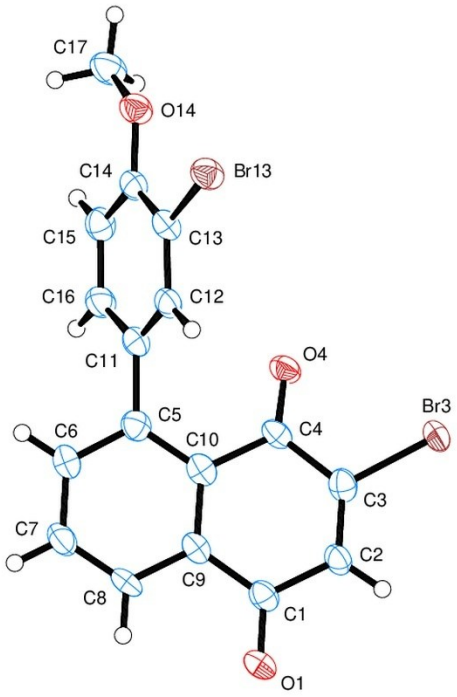

Figure 1. View of the bromo-naphthoquinone derivative. Thermal ellipsoids are drawn at the 50% probability level.

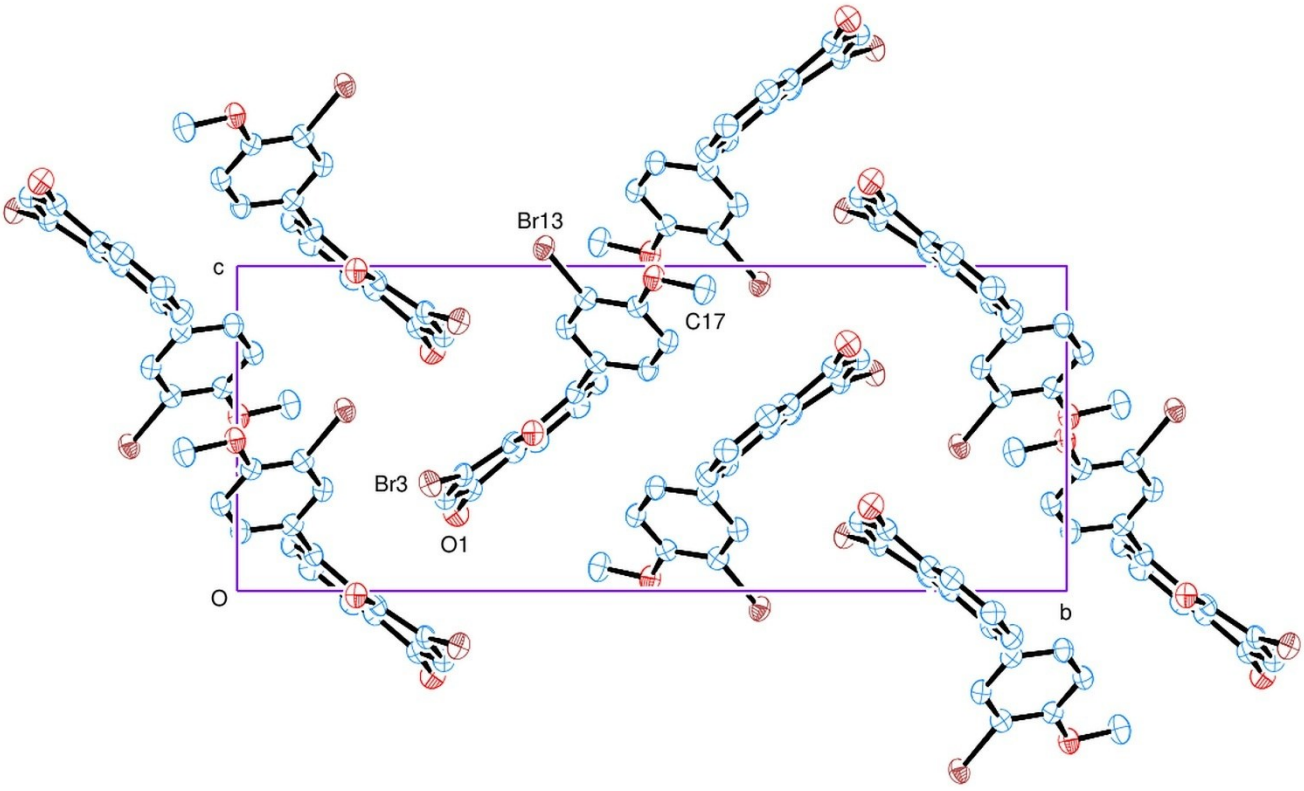

Figure 2. The packing of molecules, viewed along the *a* axis.

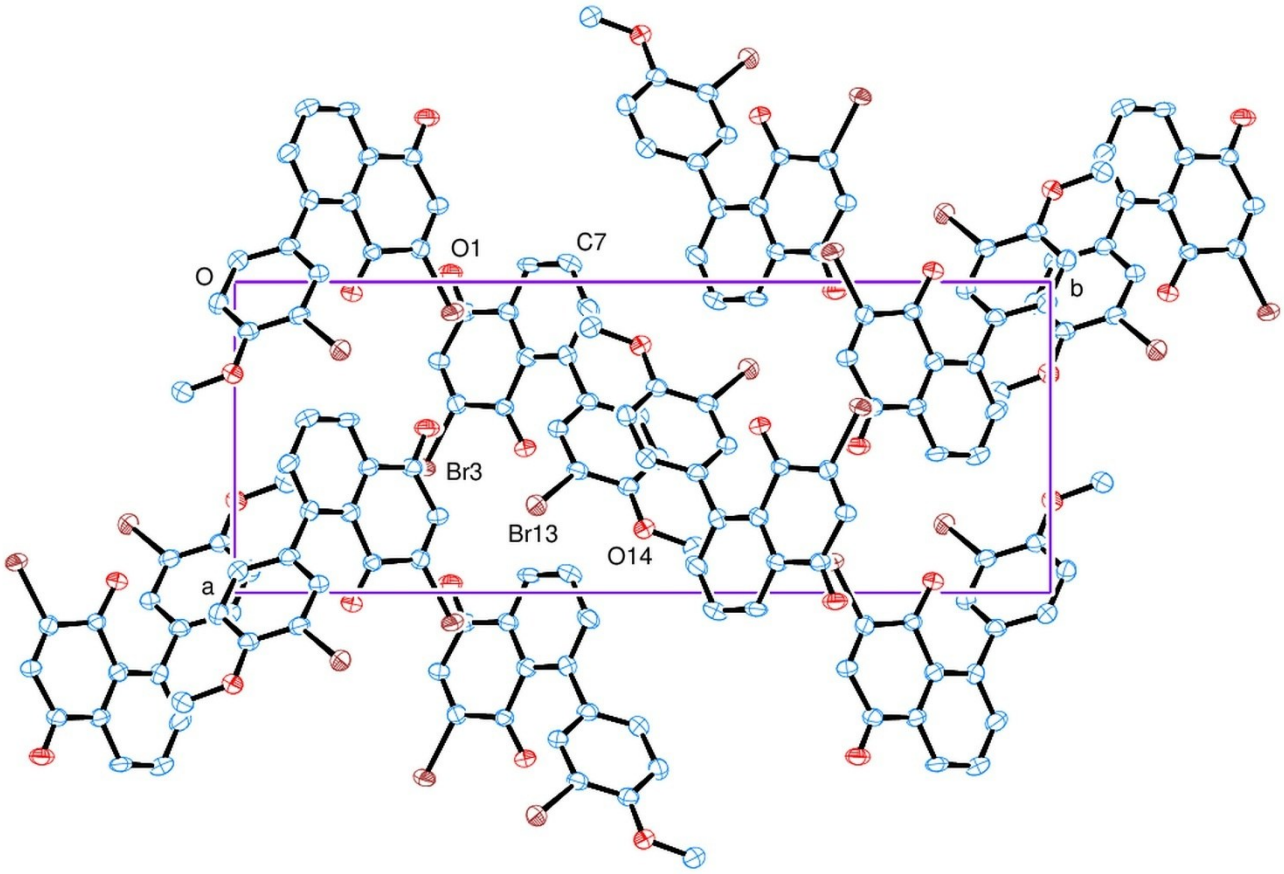

Figure 3. The packing of molecules, viewed along the *c* axis.

Notes on the structure

The dimensions in the quinone ring are as expected, e.g. the double bonds for C(1)-O(1), C(4)-O(4) and C(2)-C(3) are 1.231(7), 1.219(7) and 1.332(9) Å, respectively. The atoms of the benzene ring of C(5-10) form a good plane, but those of the quinone ring are less regular with deviations from the mean-plane of up to 0.076(4) Å. The plane of the phenyl group is rotated 64.7(2) ° from the benzene ring plane around the C(5)-C(11) bond.

The C(13-15) group of the phenyl ring contacts its related group in an off-set overlap arrangement. The bromine atoms make contact through van der Waals' interactions with each other, with a methyl group, and as Br…π interactions.

2.51

Crystal structure analysis of a benzanthracene derivative

Crystal data: $C_{26}H_{18}O_{4.}$, M = 394.40. Triclinic, space group P-1 (no. 2), a = 8.8485(4), b = 8.9728(5), c = 12.4229(5) Å, α = 82.967(4), β = 75.726(4), γ = 76.787(4) °, V = 928.29(8) $Å^3$. Z = 2, Dc = 1.411 g cm^{-3}, F(000) = 412, T = 100(2) K, μ(Cu-Kα) = 7.68 cm^{-1}, λ(Cu-Kα) = 1.54184 Å.

The crystal was an orange block. From a sample under oil, one, *ca* 0.15 x 0.19 x 0.24 mm, was mounted on a small loop and fixed in the cold nitrogen stream on a Rigaku Oxford Diffraction XtaLAB Synergy diffractometer, equipped with Cu-Kα radiation, HyPix detector and mirror monochromator. Intensity data were measured by thin-slice ω-scans. Total no. of reflections recorded, to θ_{max} = 70.0 °, was 10,609 of which 3,455 were unique (Rint = 0.032); 3,075 were 'observed' with $I > 2\sigma_I$.

Data were processed using the CrysAlisPro-CCD and -RED (1) programs. The structure was determined by the intrinsic phasing routines in the SHELXT program (2A) and refined by full-matrix least-squares methods, on F^2's, in SHELXL (2B). The non-hydrogen atoms were refined with anisotropic thermal parameters. The hydrogen atoms were included in idealised positions and their Uiso values were set to ride on the Ueq values of the parent carbon atoms. At the conclusion of the refinement, wR_2 = 0.111 and R_1 = 0.044 (2B) for all 3,455 reflections weighted $w = [\sigma^2(F_o^2) + (0.0616 P)^2 + 0.1720 P]^{-1}$ with $P = (F_o^2 + 2F_c^2)/3$; for the 'observed' data only, R_1 = 0.040.

In the final difference map, the highest peak (*ca* 0.36 $eÅ^{-3}$) was clos to H(10).

Scattering factors for neutral atoms were taken from reference (3). Computer programs used in this analysis have been noted above, and were run through WinGX (4) on a Dell Optiplex 780 PC at the University of East Anglia.

Legends for Figures

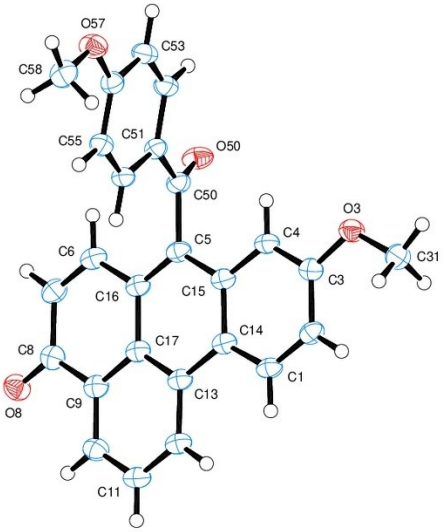

Figure 1. View of the benzanthracene derivative molecule, indicating the atom numbering scheme. Thermal ellipsoids are drawn at the 50% probability level.

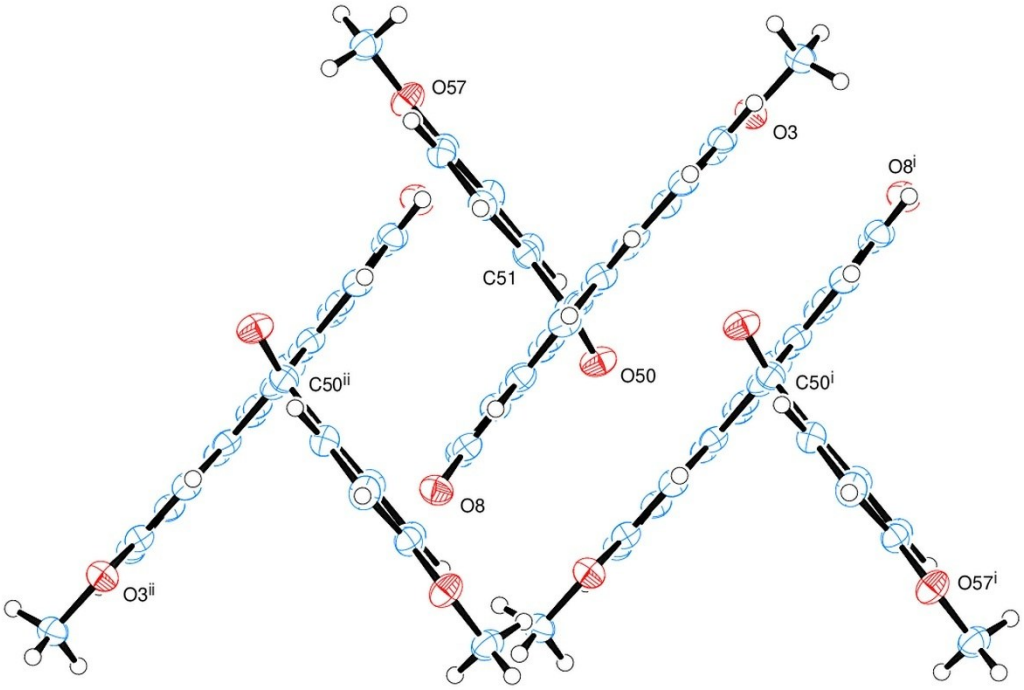

Figure 2. View along the C(50)–C(5) bond (approximately) between the benzanthracene and benzaldehyde groups.

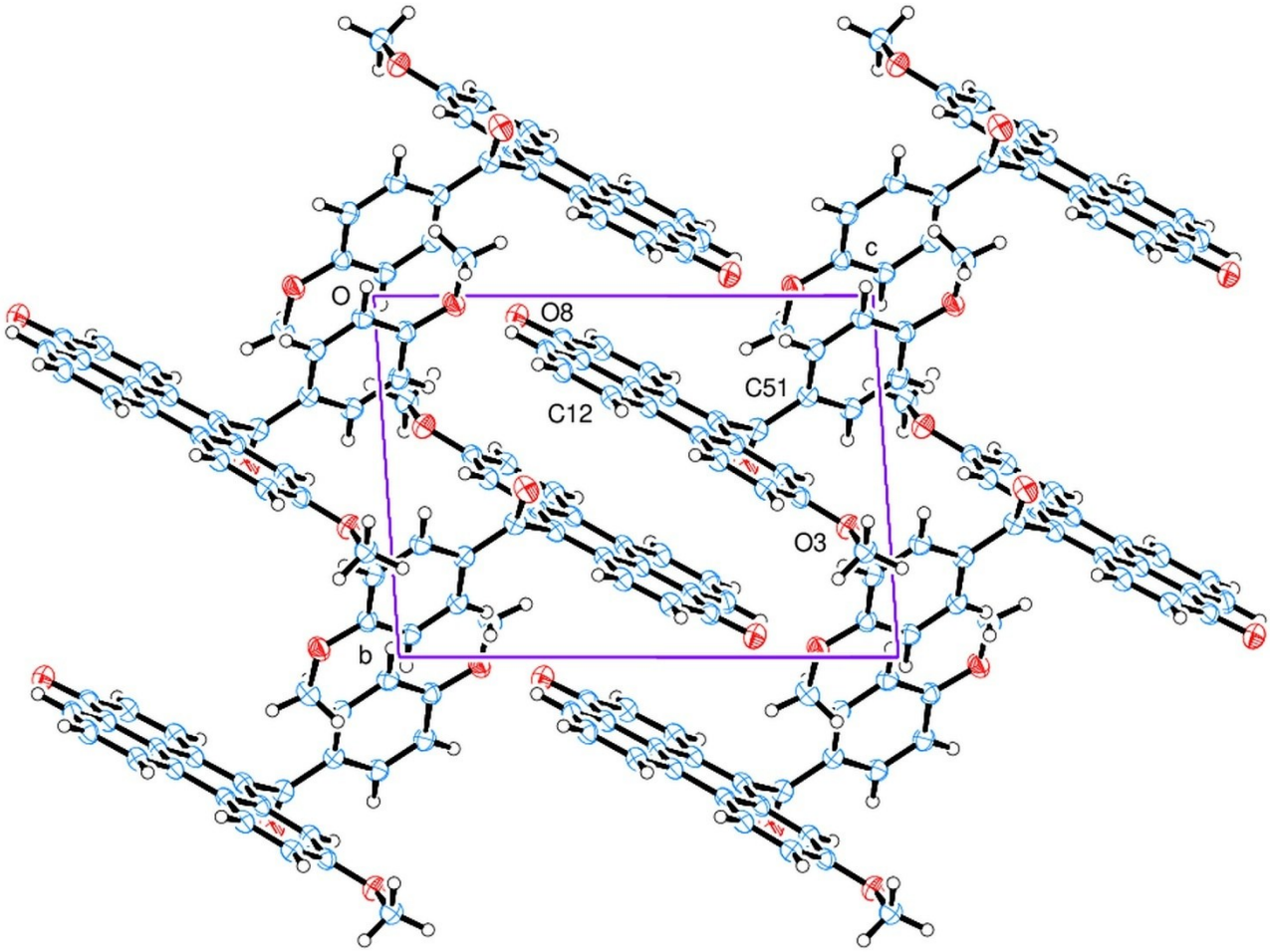

Figure 3. The packing of molecules, viewed along the *a* axis.

Notes on the structure

The determination of the molecular structure and the refinement process were both straightforward and trouble-free! The resulting molecule is shown in Figure 1 and comprises, principally, two planes, viz the benzanthracene ring system and the phenyl ring of the benzaldehyde group. The angle between the normals to these two planes is 79.64(3)°, Figure 2.

In the benzanthracene system, the C(6)–C(7) bond is short, at 1.340(2) Å, in conjugation with the C(8)=O(8) double-bond, 1.233(2) Å; the six-membered ring involving these atoms is not greatly distorted from the planarity of the benzanthracene ring system.

The packing diagram, Figure 3, shows the stacking of the benzanthracene units in columns parallel to the *b* axis; adjacent units are related by centres of symmetry, and are *ca* 3.45 Å apart.

2.31

Crystal structure analysis of naphthalene-(C≡C-C_6H_4-Bu^t)-1,-(C_6H_4-OMe)-8

Crystal data: $C_{29}H_{26}O$, M = 390.50. Triclinic, space group B-1 (as no. 2), a = 11.7807(3), b = 12.1901(2), c = 15.5838(3) Å, α = 79.465(2), β = 89.976(2), γ = 79.377(2) °, V = 2161.24(8) $Å^3$. Z = 4, Dc = 1.200 g cm^{-3}, F(000) = 832, T = 100(2) K, μ(Cu-Kα) = 5.42 cm^{-1}, λ(Cu-Kα) = 1.54184 Å.

The crystal was a yellow cuboid. From a sample under oil, one, *ca* 0.07 x 0.11 x 0.55 mm, was mounted on a small loop and fixed in the cold nitrogen stream on a Rigaku Oxford Diffraction XtaLAB Synergy diffractometer, equipped with Cu-Kα radiation, HyPix detector and mirror monochromator. Intensity data were measured by thin-slice ω-scans. Total no. of reflections recorded, to θ_{max} = 70.0°, was 16,897 of which 4,080 were unique (Rint = 0.022); 3,885 were 'observed' with $I > 2\sigma_I$.

Data were processed using the CrysAlisPro-CCD and -RED (1) programs. The structure was determined by the intrinsic phasing routines in the SHELXT program (2A) and refined by full-matrix least-squares methods, on F^2's, in SHELXL (2B. The non-hydrogen atoms were refined with anisotropic thermal parameters. The hydrogen atoms were included in idealised positions and their Uiso values were set to ride on the Ueq values of the parent carbon atoms. At the conclusion of the refinement, wR_2 = 0.098 and R_1 = 0.039 (2B) for all 4080 reflections weighted w = $[\sigma^2(F_o^2) + (0.0443 P)^2 + 1.3268 P]^{-1}$ with P = $(F_o^2 + 2F_c^2)/3$; for the 'observed' data only, R_1 = 0.037.

In the final difference map, the highest peak (*ca* 0.2 $eÅ^{-3}$) was near C(19).

Scattering factors for neutral atoms were taken from reference (3). Computer programs used in this analysis have been noted above, and were run through WinGX (4) on a Dell Optiplex 780 PC at the University of East Anglia.

Legends for Figures

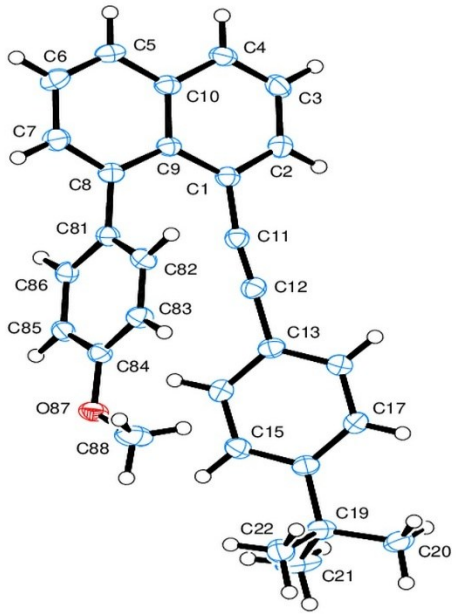

Figure 1. View of the naphthalene derivative molecule, indicating the atom numbering scheme. Thermal ellipsoids are drawn at the 50% probability level.

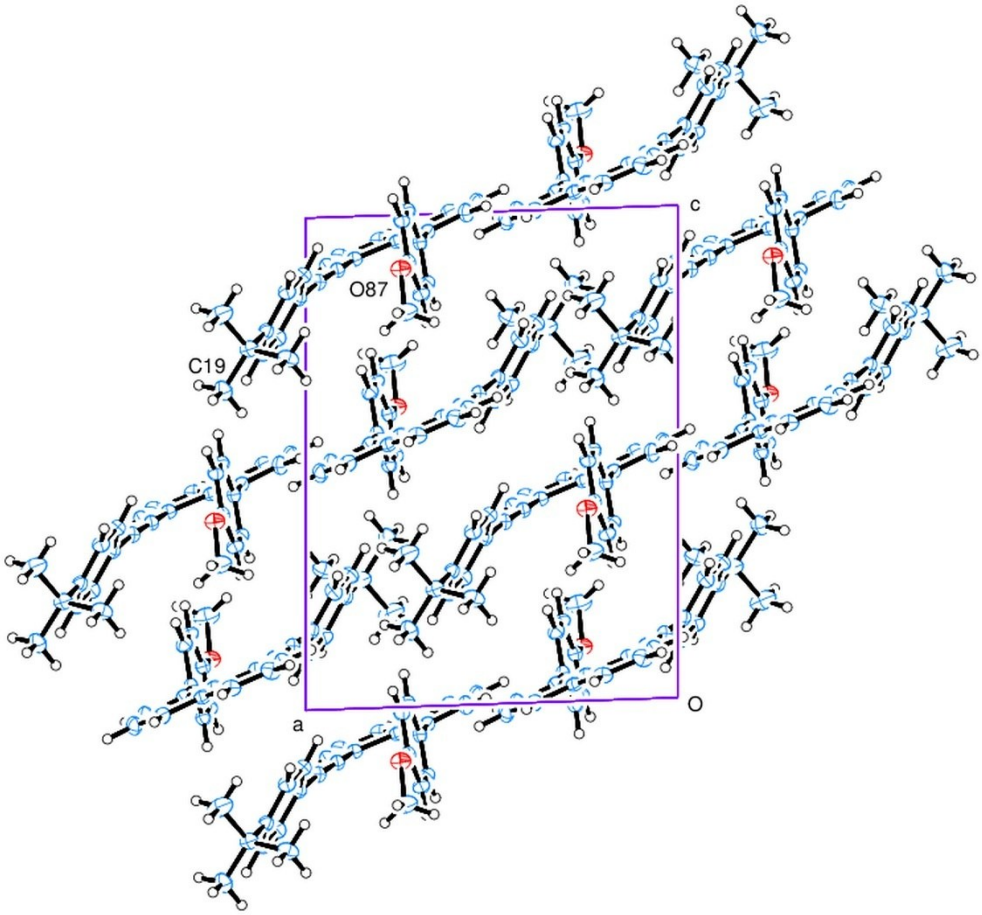

Figure 2. The packing of molecules, viewed along the *b* axis.

Notes on the structure

This crystal gave a good set of diffraction intensities, good refinement and good results.

The naphthalene rings are essentially planar, with substituent groups on C(1) and C(8), Figure 1. There is rotation about C(8)-C(81) so that the normals to the C(5-10) and C(81-86) rings are 79.68° apart; O(87) and C(88) lie close to the phenyl ring plane. There is slight divergence of the C(1) and C(8) groups along the C(1)…C(13) alkynyl group, and a rotation about this group so that the normals to the C(1-4,9,10) and C(13-18) rings are 41.71° apart. The closest interaction between these substituent groups is 2.76 Å between C(85) and H(14).

There are few close intermolecular contacts, the closest between non-hydrogen atoms being C(3)…C(3') at 3.292 Å, in an offset, peripheral π…π contact.

2.61

Crystal structure analysis of MeO-C_6H_4-naphth-CC-CHC(SPh)-naphth-C_6H_4-OMe

Crystal data: $C_{44}\,H_{32}\,O_2\,S$, M = 624.75. Triclinic, space group P-1 (no. 2), a = 8.18267(13), b = 11.6814(2), c = 18.0646(3) Å, α = 103.1954(16), β = 99.5251(15), γ = 95.8071(14) °, V = 1640.49(5) $Å^3$. Z = 2, Dc = 1.265 g cm^{-3}, F(000) = 656, T = 100(2) K, μ(Cu-Kα) = 11.65 cm^{-1}, λ(Cu-Kα) = 1.54184 Å.

The crystal was a pale yellow block From a sample under oil, one, *ca* 0.06 x 0.11 x 0.33 mm, was mounted on a small loop and fixed in the cold nitrogen stream on a Rigaku Oxford Diffraction XtaLAB Synergy diffractometer, equipped with Cu-Kα radiation, HyPix detector and mirror monochromator. Intensity data were measured by thin-slice ω-scans. Total no. of reflections recorded, to θ_{max} = 72.5°, was 21,302 of which 6,304 were unique (Rint = 0.045); 5,447 were 'observed' with $I > 2\sigma_I$.

Data were processed using the CrysAlisPro-CCD and -RED (1) programs. The structure was determined by the intrinsic phasing routines in the SHELXT program (2A) and refined by full-matrix least-squares methods, on F^2's, in SHELXL (2B). The non-hydrogen atoms were refined with anisotropic thermal parameters. The hydrogen atoms hydrogen atoms were included in idealised positions and their Uiso values were set to ride on the Ueq values of the parent carbon atoms. At the conclusion of the refinement, wR_2 = 0.105 and R_1 = 0.046 (2B) for all 6304 reflections weighted $w = [\sigma^2(F_o^2) + (0.0498\ P)^2 + 0.4129\ P]^{-1}$ with $P = (F_o^2 + 2F_c^2)/3$; for the 'observed' data only, R_1 = 0.039.

In the final difference map, the highest peak (*ca* 0.29 $eÅ^{-3}$) was near C(81).

Scattering factors for neutral atoms were taken from reference (3). Computer programs used in this analysis have been noted above, and were run through WinGX (4) on a Dell Optiplex 780 PC at the University of East Anglia.

Legends for Figures

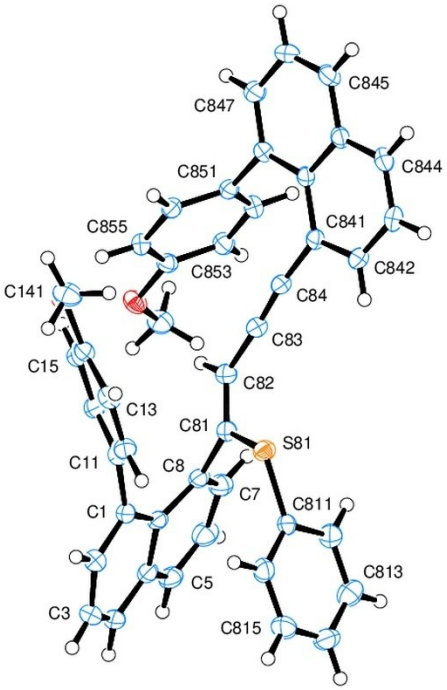

Figure 1. View of the bis-naphthalene alkyne derivative, indicating the atom numbering scheme. Thermal ellipsoids are drawn at the 50% probability level.

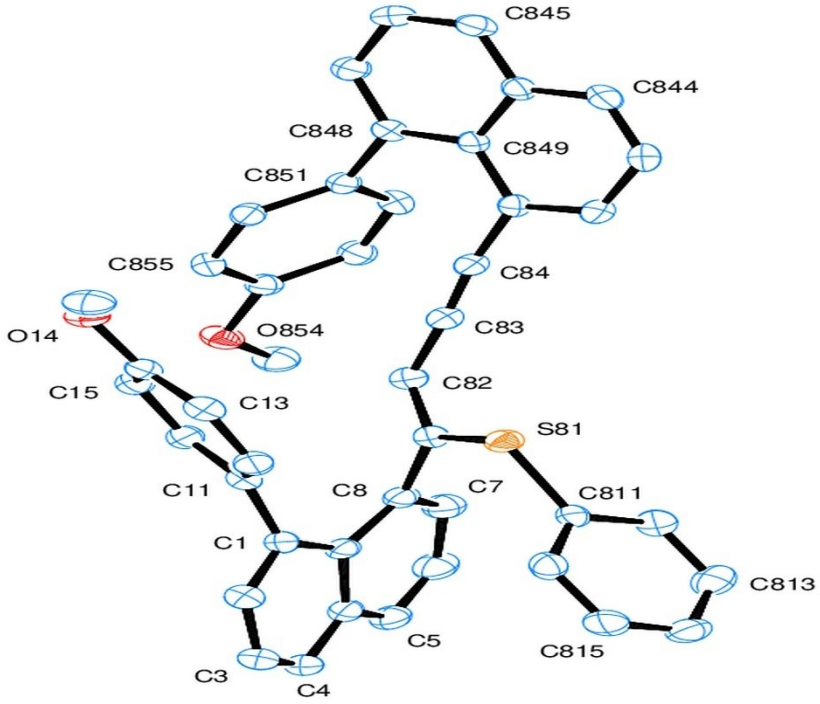

Figure 2. As Figure 1, but with all hydrogen atoms removed, for clarity.

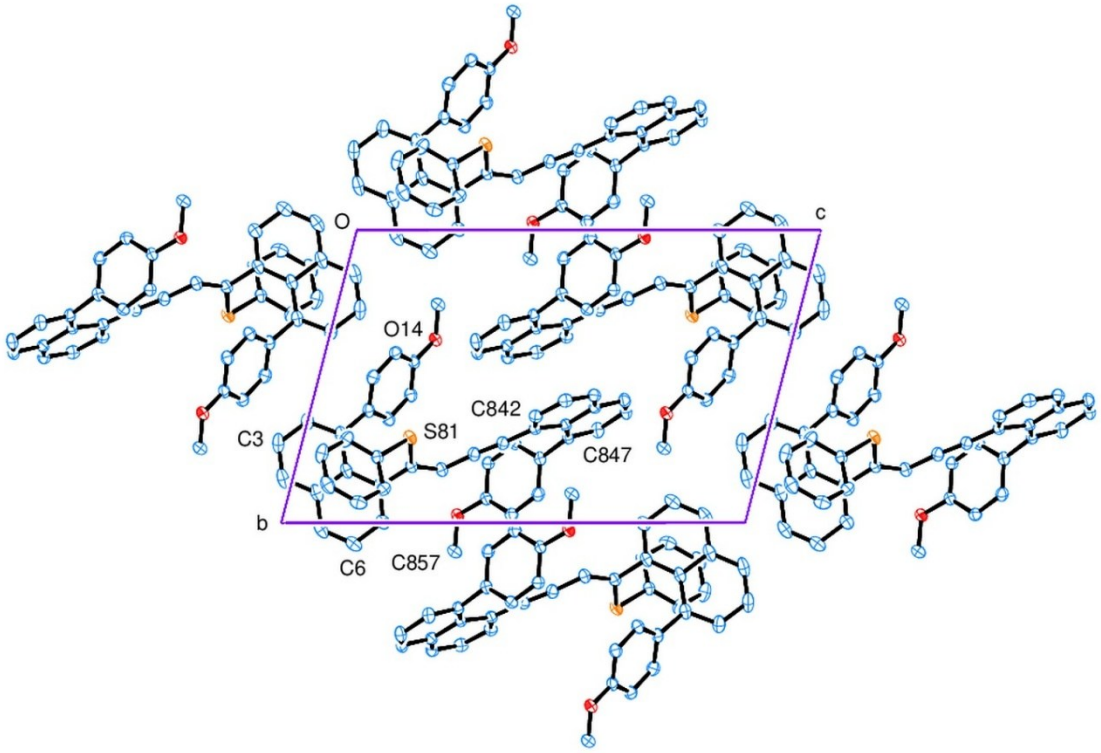

Figure 3. The packing of molecules, viewed along the *a* axis.

Notes on the structure

The bis-naphthalene alkyne molecule is shown in Figure 1 and, more clearly after removal of the hydrogen atoms, in Figure 2.

At the heart of the molecule, the alkynyl group shows the C(82)–C(83) and C(83)≡C(84) bonds at 1.421(2) and 1.205(2) Å, and the close-to-linear angles at C(83) and C(84) of 173.82(15) and 171.59(15) °. The bonding arrangement at C(82) is trigonal planar, with a double-bond C(81)=C(82) at 1.346(2) Å. The two MeO-1,8-C_6H_4-naphthalenyl groups are attached to the central section through C(8) and C(841). Both naphthyl groups show slight twisting about their central bonds, by 7.84(2) about the C(9)-C(10) bond and 3.39(10) ° about C(849)-C(850), these twists resulting from the spatial requirements of the different substituent groups at C(8) and C(841). The packing arrangements are shown in Figure 3. Pairs of aromatic rings are overlapped, to a greater or lesser degree, around two of the four unique centres of symmetry in the cell; the best overlapping is that of the six-membered ring of C(841-844, 850, 849) and its inverted ring about the centre at (½, ½, ½). The alkynyl group lies over the ring of C(851-856), with C(84)…C(851) at 2.823 Å, C(83)…C(852 and 856) at 3.477 and 3.383 Å, and H(82)…C(854) at 2.70 Å.